STRAIGHT STEEL I-GIRDER BRIDGES WITH SKEW INDEX APPROACHING 0.3

Final Report

FDOT Contract No: BE535

Submitted to:

Florida Department of Transportation

Tallahassee, Florida

Project Manager: Vickie Young, PE

Submitted by:

Donald W. White and Ajit Kamath

Georgia Institute of Technology

John A Heath, PE, Brian K. Adams, PE, and Amrithraj Anand

Heath & Lineback Engineers, Inc.

November 2020

DISCLAIMER

The opinions, findings, and conclusions expressed in this publication are those of the authors and are not necessarily those of the State of Florida Department of Transportation.

METRIC CONVERSION CHART

SI* (MODERN METRIC) CONVERSION FACTORS

APPROXIMATE CONVERSIONS TO SI UNITS

SYMBOL	WHEN YOU KNOW	MULTIPLY BY	TO FIND	SYMBOL
		LENGTH		
in	inches	25.4	millimeters	mm
ft	feet	0.305	meters	m
yd	yards	0.914	meters	m
mi	miles	1.61	kilometers	km
		AREA		
in^2	square inches	645.2	square millimeters	mm^2
ft^2	square feet	0.093	square meters	m^2
yd^2	square yard	0.836	square meters	m^2
ac	acres	0.405	hectares	ha
mi^2	square miles	2.59	square kilometers	km^2
		VOLUME		
fl oz	fluid ounces	29.57	milliliters	mL
gal	gallons	3.785	liters	L
ft^3	cubic feet	0.028	cubic meters	m^3
yd^3	cubic yards	0.765	cubic meters	m^3
		NOTE: volumes greater than 1000 L shall be shown in m^3		
		MASS		
oz	ounces	28.35	grams	g
lb	pounds	0.454	kilograms	kg
T	short tons (2000 lb)	0.907	megagrams (or “metric ton”)	Mg (or “t”)
		TEMPERATURE (exact degrees)		
°F	Fahrenheit	5(F-32)/9 or (F-32/1.8)	Celsius	°C
		ILLUMINATION		
fc	foot-candles	10.76	lux	lx
fl	foot-Lamberts	3.426	$candela/m^2$	cd/m^2
		FORCE and PRESSURE or STRESS		
lbf	poundforce	4.45	newtons	N
lbf/in^2	poundforce per square inch	6.89	kilopascals	kPa
K	Kips	4.45	kilonewtons	kN

APPROXIMATE CONVERSIONS FROM SI UNITS

SYMBOL	WHEN YOU KNOW	MULTIPLY BY	TO FIND	SYMBOL
		LENGTH		
mm	millimeters	0.039	inches	in
m	meters	3.28	feet	ft
m	meters	1.09	yards	yd
km	kilometers	0.621	miles	mi
		AREA		
mm^2	square millimeters	0.0016	inches	in
m^2	square meters	10.764	square feet	ft^2
m^2	square meters	1.195	square yards	yd^2
ha	hectares	2.47	acres	ac
km^2	square kilometers	0.386	square miles	mi^2
		VOLUME		
mL	milliliters	0.034	fluid ounces	fl oz
L	liters	0.264	gallons	gal
m^3	cubic meters	35.314	cubic feet	ft^3
m^3	cubic meters	1.307	cubic yards	yd^3
		MASS		
g	grams	0.035	ounces	oz
kg	kilograms	2.202	pounds	lb
Mg (or “t”)	megagrams (or “metric ton”)	1.103	short tons (2000 lb)	T
		TEMPERATURE (exact degrees)		
°C	Celsius	1.8C+32	Fahrenheit	°F
		ILLUMINATION		
lx	lux	0.0929	foot-candles	fc
cd/m^2	$candela/m^2$	0.2919	foot-Lamberts	fl
		FORCE and PRESSURE or STRESS		
N	newtons	0.225	poundforce	lbf
kPa	kilopascals	0.145	poundforce per square inch	lbf/in^2
kN	kilonewtons	0.225	Kips	K

TECHNICAL REPORT DOCUMENTATION PAGE

1. Report No.	2. Government Accession No.	3. Recipient's Catalog No.
4. Title and Subtitle Straight Steel I-Girder Bridges with Skew Index Approaching 0.3		**5. Report Date** November 2020
		6. Performing Organization Code
7. Author(s) Donald W. White, Ajit M. Kamath, John A. Heath, Brian K. Adams, and Amrithraj Anand		**8. Performing Organization Report No.**
9. Performing Organization Name and Address Heath and Lineback Engineers, Inc. 2390 Canton Road, Bldg. 200 Marietta, GA 30066 USA		**10. Work Unit No.**
		11. Contract or Grant No. **FDOT BE535**
12. Sponsoring Agency Name and Address Florida Department of Transportation 605 Suwannee Street, MS 33 Tallahassee, FL 32399-0450 USA		**13. Type of Report and Period Covered** Final Report March 2018 – April 2020.
		14. Sponsoring Agency Code
15. Supplementary Notes		

16. Abstract

To maximize engineering effectiveness, appropriate tools must be matched to the task. Straight skewed steel I-girder bridges have been designed traditionally using simplified 1D line girder analysis (LGA) methods. Modern 2D grid and 3D finite element analysis (3D FEA) procedures can capture the component and system response of these types of structures at a -higher resolution than the traditional approach. However, these refined analysis tools require more expensive software and greater time to execute and interpret the higher resolution analysis models. It is broadly recognized that LGA is appropriate and sufficient for the design of straight non-skewed girder bridges. The objectives of this research were to better understand the behavior of straight steel I-girder bridges with small to moderate skew, and to define and potentially extend the limits at which LGA provides an effective structural engineering solution for these bridge types. Comparative parametric 3D FEA and LGA studies were conducted on 26 bridges having a skew index $I_s = w_g \tan\theta / L_s$ up to and slightly larger than 0.3, where w_g is the framing width between the fascia girders, θ is the angle of the bearing lines measured from an axis perpendicular to the girders, and L_s is the span length. The results showed that routine LGA models using equal distribution of dead loads to the girders and established AASHTO live load distribution factors provide a fast and sufficient solution for straight steel I-girder bridges with I_s up to 0.45 and θ up to 50 degrees within certain qualifications. Recommendations were provided for improved design calculation of girder flange lateral bending stresses and cross-frame and diaphragm forces for designs using LGA.

17. Key Words	18. Distribution Statement
Skew, Girder bridge design, Structural steel, Line girder analysis, Finite element analysis	No restrictions.

19. Security Classif. (of this report)	20. Security Classif. (of this page)	21. No. of Pages	22. Price
Unclassified	Unclassified	4294	

Form DOT F 1700.7 (8-72) Reproduction of completed page authorized

ACKNOWLEDGEMENTS

The project team would like to acknowledge the valuable feedback and advice provided by the Florida Department of Transportation steering group for the project – Vickie Young (project manager), Dennis Golabek, Ben Goldsberry, Christina Freeman, and Scott Arnold.

EXECUTIVE SUMMARY

The skew index, $I_s = w_g \tan \theta / L_s$, is often used to quantify the extent of skew of girder bridges, where w_g is the framing width between the fascia girders, θ is the maximum angle of skew, and L_s is the span length under consideration. Many straight skewed I-girder bridges have skew indices less than or equal to 0.3 or only slightly larger. Prior research has shown that transverse load path effects can start to become relatively significant for $I_s > 0.3$. It is understood that bridge owners and consultants are increasingly using refined methods of analysis – 2D grid, plate and eccentric beam, or 3D finite element analysis (3D FEA) – for certain I-girder bridge geometries. However, traditionally, many straight skewed I-girder bridges have been designed using 1D line girder analysis (LGA). Refined methods of analysis require more expensive software, time to develop a working finite element model, and staff that have adequate knowledge of structural analysis modeling and its nuances.

The FDOT Structures Design Guidelines currently require a refined method of analysis for straight steel I-girder bridges with a skew index greater than 0.2 and less than or equal to 0.6. They require a 3D FEA if the skew index is greater than 0.6. Based on current FDOT design policy, a significant number of new bridges with a skew index less than 0.3 would therefore require a refined analysis for design, when line girder models may suffice. Application of LGA in lieu of 3D FEA for such bridges has the potential to simplify the workflow and allow concentration of resources on other important matters, if it can be understood that LGA provides acceptable designs for a wider range of straight skewed I-girder bridges.

This research sought to improve the understanding of the behavior of straight steel I-girder skewed bridges having skew indices up to and slightly larger than 0.3 and to evaluate the applicability of simplified methods of analysis. To achieve this goal, comparative parametric 3D FEA and LGA studies were conducted on a suite of 26 bridges with skew indices up to and slightly exceeding 0.3. These bridges were configured from a suite of 57 bridges sampled from the Florida DOT bridge inventory. Key response quantities studied included:

1. Girder positive and negative Strength I (STR I) major-axis bending moments,
2. Girder STR I vertical shear forces,
3. Girder HL-93 live load shear forces, focusing in particular on the live load shear forces at the obtuse corners of the bridge spans,
4. Girder STR I bearing reactions at span obtuse corners at end abutments and on the exterior girders at the piers in continuous-span bridges,
5. Girder total dead load vertical displacements, necessary for cambering of the girders, including consideration of the effects of steel dead load fit (SDLF) detailing of the cross-frames,
6. Girder concrete dead load vertical displacements, considering both staged and unstaged deck placement,
7. Girder layovers under the total dead load, which for SDLF detailing of the cross-frames are equal to the girder layovers under the concrete dead load,
8. Girder fatigue live load vertical shear forces,
9. Girder fatigue live load flexural stresses,
10. Girder flange lateral bending stresses,

11. Cross-frame and diaphragm forces,
12. Exterior girder live load distribution factors, considering the conservatism of lever rule and rigid cross-section analysis procedures, and
13. Girder live load deflections.

The suite of 26 bridges represents a gamut of skewed bridges having simple- and continuous-span designs, parallel and nonparallel skew, cross-frames parallel to the skew or perpendicular to the girders, contiguous and staggered cross-frame layouts, uniform and nonuniform girder spacing, and girder splay. The parametric study evaluated the extent to which LGA can adequately calculate the response quantities for straight steel I-girder bridges with small to moderate skew.

It was found that the accuracy of LGA procedures with respect to 3D FEA methods depends on a complex combination of structural attributes. Three of the predominant attributes are:

- The skew index,
- The skew angle of the bearing lines, and
- The framing arrangement of the cross-frames or diaphragms.

Regarding the framing arrangement of the cross-frames and diaphragms, some of the factors involved are:

1. Contiguous cross-frame arrangements tend to result in larger cross-frame forces and smaller girder flange lateral bending. However, if a contiguous cross-frame line is discontinued with a relatively short offset between this line and a bearing line or another intermediate cross-frame line, substantial girder flange lateral bending can be introduced at the location where the line is discontinued.
2. Generous use of staggers and offsets tends to reduce the cross-frame forces at the expense of some additional girder flange lateral bending.
3. Intermediate cross-frame lines framed across interior bearings tend to exhibit significant transverse cantilever action, resulting in large cross-frame forces. Any discontinuities at the ends of these types of cross-frames tend to attract large girder flange lateral bending.
4. Cross-frames framed directly into, or relatively close to, bearing locations often attract excessive forces. These forces can be mitigated by leaving the diagonals out of that specific cross-frame. Large girder flange lateral bending stress can occur at locations where these types of cross-frames are discontinued.

The comparative studies conducted in this research showed that routine LGA estimates of girder maximum STR I bending moments and shear forces are less than 10% unconservative for all the bridges studied. However, the accuracy of total dead load vertical displacements used for camber calculations is not adequate for bridges having larger skew and/or cross-frame arrangements exhibiting significant transverse load path effects. In addition, transverse load path effects have a significant impact on the accuracy of LGA estimates of vertical reactions, fatigue live load forces, and cross-frame forces when the skew index and the skew angle become larger.

The results showed that routine LGA models using equal distribution of dead loads to the girders and established AASHTO live load distribution factors provide a fast and sufficient

solution for straight steel I-girder bridges with I_s up to 0.45 and θ up to 50 degrees within certain qualifications. Three bridge categories were recommended to account for a progression of design requirements:

Category 1 – Parallel skew bridges with $\theta \leq 20$ degrees, and with contiguous intermediate cross-frame lines oriented parallel to the skew. For bridges in this category:

- The girder design demands are calculated directly from the recommended LGA procedures without application of any further adjustment factors.
- The estimated girder flange lateral bending stresses due to skew effects are taken equal to zero.
- The force demands on the intermediate cross-frame lines are relatively large due to their contiguous attribute; however, the force demands on the bearing line cross-frames are relatively small.

Category 2 – Parallel skew bridges with $\theta \leq 50$ degrees and $I_s \leq 0.3$, cross-frames oriented perpendicular to the girders. For bridges in this category:

- An additional multiplicative adjustment factor of 1.10 is recommended for calculation of the fascia girder bearing reactions at obtuse corners of the spans at end abutments and at the piers in continuous-span bridges. This is in addition to the application of the AASHTO LRFD skew correction factor for the girder shears to the bearing reactions.
- Estimated non-zero girder flange lateral bending stresses due to skew effects are applied at offsets and staggers in the cross-frame framing arrangements. Different estimates are applied for interior and exterior girders, and the estimated stresses are smaller for ample offsets (larger than $4b_f$) versus smaller offsets.
- The cross-frame force demands are influenced significantly by the cross-frame framing arrangements. The attributes of the framing arrangements include: (1) whether the intermediate cross-frames are contiguous or staggered, (2) the magnitude of the offsets provided between adjacent intermediate cross-frames and (3) the magnitude of the offsets provided between intermediate cross-frames and bearing lines containing cross-frames.

Category 3 – Parallel skew bridges with $\theta \leq 50$ degrees and $0.30 < I_s \leq 0.40$, or with $\theta \leq 30$ degrees and $0.40 < I_s \leq 0.45$.

It was found that the above design requirements could also be applied for the Category 3 bridges. The primary reason for the separate Category 3 was that the LGA results tend to be slightly less accurate for the bridges in this category compared to those for the bridges in Categories 1 and 2.

The research showed that the limits of applicability of LGA for bridges with nonparallel skew (differences in skew between the bearing lines larger than 10^o) would need to be more restrictive; however, the scope of the studies is insufficient to identify these limits. Recommendations were provided for consideration of minor girder splay and minor differences in girder stiffnesses. Various additional limits of applicability of the routine LGA procedures, starting with the limits stated in the AASHTO LRFD Specifications, were clarified.

For load combinations other than STR I involving HL-93 loading, and where LGA would be employed, namely Service II and Strength V, the ratio of the factored live load to the factored dead load is smaller than for STR I. The need for the above correction factor is primarily due to the demands from the HL-93 live load. Therefore, the above multiplicative correction factor of 1.10 may also be applied to the live load portion of the Service II and Strength V load combinations as a sufficient approximation. For load combinations other than STR I, it was recommended that the 1.10 correction factor may be applied only to the live load reaction for the fascia girder at the obtuse corners at end abutments and at piers in continuous span bridges, for bridges that fall within Categories 2 and 3.

Recommendations were provided for improved design calculation of girder flange lateral bending stresses and cross-frame and diaphragm forces. The current guidance in the AASHTO LRFD Article C6.10.1, providing coarse upper-bound estimates of girder flange lateral bending stresses due to skewed geometry effects, is refined. The refinements consider the influence of cross-frame offsets or staggers greater than or less than $4b_f$, where b_f is the largest flange width within the unbraced lengths on either side of a given cross-frame. The value $4b_f$ is a current AASHTO LRFD recommended minimum stagger or offset value. Offsets or staggers smaller than $4b_f$ are allowed, but lead to larger estimates of the flange lateral bending stresses. The current onerous Article C6.10.1 requirement, which states that the estimated nominal flange lateral bending stresses should be proportioned to the dead and live load in the same proportion as the unfactored major-axis dead and live load stresses at the cross-section under consideration, was replaced by recommended weighted-average load factors for different load combinations. This recognizes that the coarseness of the flange lateral bending estimates does not merit an elaborate manual calculation.

Comparable coarse upper-bound estimates of bridge cross-frame and diaphragm forces due to skewed geometry effects were recommended to be calculated as percentages of the maximum girder moments and shears obtained from LGA. The lowest percentages correspond to common stability bracing strength requirements. Larger percentage estimates are provided as a function of the cross-frame/diaphragm framing arrangements, keyed to the recommended $4b_f$ offset or stagger distance discussed above.

The synthesized results from this research provide detailed insight into various structural attributes influencing the behavior of straight skewed I-girder bridges. The research findings allow for potential new design guidance that can simplify design processes and eliminate the unnecessary application of more complex and expensive methods of analysis for a wide range of straight skewed I-girder bridges.

TABLE OF CONTENTS

LIST OF FIGURES

LIST OF TABLES

1. INTRODUCTION

1.1 Background

Line girder analysis (LGA) is the simplest and most basic method used in the analysis and design of girder bridges. With LGA, bridge girders are analyzed individually, and the interaction between the girders via the cross-frames, diaphragms, and bridge deck is ignored or accounted for only in a coarse approximate fashion. In contrast, refined methods of analysis involve the direct modeling of the interactions between the girders, cross-frames, and bridge deck to various degrees of rigor. 3D finite element analysis (3D FEA) is the most rigorous refined method and commonly involves a detailed three-dimensional representation of the bridge deck, girders, cross-frames, diaphragms, and bearings and potentially other substructure elements, capturing their collaboration and interaction in resisting the loads. In 3D FEA methods, the girders, cross-frames, diaphragms, bridge deck, bearings, and other structural components typically are modeled at their specific locations in three-dimensional space. Other refined methods of analysis include 2D grid and plate-eccentric beam analysis models. In 2D grid analysis methods, the girders, cross-frames, and potentially various longitudinal and transverse widths of the deck are modeled as line elements in a single horizontal plane. In the final composite constructed condition, the bridge deck is typically modeled by using the composite properties of the girders in these procedures. Refined methods of analysis are typically specified to be used for bridges that are expected to exhibit interaction between the girders, bridge deck and the cross-frames that cannot be captured by LGA.

The Florida DOT Structures Design Guidelines (FDOT, 2019a) currently limit the use of line girder analysis methods for straight steel I-girder bridges based on the value of the skew index,

$$I_s = \frac{w_g \tan\theta}{L_s} \tag{1}$$

where

w_g = width of the bridge measured between fascia girders

θ = skew angle at a support defined as the difference between the alignment of the support and a line perpendicular to the longitudinal axis of the bridge

L_s = length of the span under consideration.

The skew index for a bridge is generally taken as the maximum value from Equation 1, calculated considering each of the bearing lines and each of the spans. FDOT requires a refined method of analysis for straight steel I-girder bridges when the skew index is greater than 0.2 and less than or equal to 0.6 (FDOT, 2019a). They require a 3D FEA when the skew index is greater than 0.6. Approximately 250 steel I-girder bridges were constructed in Florida from the years 2000 to 2014, with over 90% having a skew index of less than 0.3 (FDOT, 2017). NCHRP Report 725 (White et al., 2012) indicates that LGA is capable of predicting girder noncomposite major-axis bending stresses and vertical displacements with a worst-case mean normalized error

less than or equal to 12 % when the skew index is less than or equal to 0.3. Based on current FDOT design policy, over one-third of the above bridges with a skew index less than 0.3 would require a 2D grid or 3D FEA for design, when line girder models may have sufficed.

Skew of the bearing lines in a straight bridge, i.e., non-perpendicular orientation of the bearing lines relative to the straight girders, introduces the potential for relatively complex transverse load path effects. In "significantly skewed" girder bridges, the bridge deck, diaphragms and cross-frames can transfer significant forces in the transverse direction between the bearing lines, or at least between positions along the girder lengths that are relatively close to the bearing lines. That is, in delivering the loads to the bearing lines, the combined bridge deck, girders, diaphragms and cross-frames can behave to some extent as a transversely and longitudinally stiffened orthotropic plate of parallelogram or trapezoidal shape within the bridge plan. The cross-frames and diaphragms can act effectively as "stiffening ribs" in the transverse direction, attracting loads and distributing them transversely to the bearing lines and to locations along other girders closer to the bearing lines than the point of application of a given load. These transverse "stiffening ribs" can attract large forces. This is especially true when the corresponding cross-frames or diaphragms connect directly to bearing locations or to locations on the girders that are close to the bearings.

In a "significantly skewed" girder bridge, the girders do not interact solely with the above transverse load path effects by accepting transverse loads and then transferring these loads to the bearing lines via major-axis bending and shear. The girders also participate in the transverse load path via their torsional stiffness. In steel I-girders, the predominant torsional stiffness comes from the girder resistance to warping, or cross-lateral bending, of their flanges. For composite I-girders in the bridge final constructed condition, the predominant girder torsional action comes from the lateral bending restraint provided to the top flange by the bridge deck, the lateral bending of the bottom flange, and the distortional stiffness of the girder web combined with any web stiffening via the frame action of intermediate transverse web stiffeners between the bottom flange and the deck.

Clearly, at some limit of the skew of the bridge bearing lines, the complex three-dimensional effects described above will tend to become relatively minor and it should be possible to execute a sufficient design of the bridge superstructure using a line girder analysis idealization. The challenge in this research is the identification of when this is the case. Most of the prior research on skewed steel I-girder bridges has focused predominantly on more heavily skewed geometries rather than geometries that reflect the majority of FDOT's steel I-girder bridge inventory. Moreover, a detailed study focused on the application of LGA for moderately skewed bridges is lacking in the literature.

1.2 Objectives of This Research

The objective of this research is to understand more fully the behavior of steel I-girder bridges with skew indices up to and slightly above 0.3, and to determine when, for these types of bridges, Line Girder Analysis (LGA) will yield results that are very similar to those obtained from 3D FEA. This includes the direct estimation of major-axis bending stresses and vertical displacements from the LGA, nearly direct estimation of girder layover at the bearings, and indirect estimation of girder flange lateral bending stresses and cross-frame forces. Guidance on

sufficient application of LGA to bridges with skew indices up to and potentially beyond 0.3 will allow for potential revisions to the current FDOT (2019a) requirements for use of refined analysis in design.

1.3 Research Approach

The above objectives are addressed via six major project tasks:

Task 1 – Literature Review. A literature review was conducted to investigate the existence of prior research and/or guidelines for the use of LGA for straight skewed steel I-girder bridges that would be of potential benefit to this study. This included a search for information accounting for the effects of skew and limiting factors for application of LGA.

Task 2 – Bridge Inventory Matrix. A matrix of variables was developed that reflect FDOT's inventory of steel I-girder bridges built from the years 2000 to present with skew indices ranging up to and slightly beyond 0.3. In coordination with the Project Manager and the FDOT steering group for the research, the project team developed a matrix of variables including but not limited to bridge span lengths, bridge articulation (simple- or continuous-span, and number of continuous spans), framing width, number of girders, girder spacing, skew angle, cross-frame spacing and framing arrangement (staggered, continuous, and combinations of the two).

Task 3 – Comparative LGA and 3D FEA Parametric Studies. LGA and 3D FEA parametric studies were conducted on 26 straight skewed steel I-girder bridges selected from Task 2, to determine the extent that LGA adequately calculates girder major-axis bending moments and vertical displacements when compared to 3D FEA results. The results of the analyses were evaluated to ascertain the key effects of the different considerations in the matrix of variables developed in Task 2. The comparative parametric studies included noncomposite responses associated with the steel erection and the concrete deck placement, as well as the detailed evaluation of live load effects on the bridges in their final composite condition.

Task 4 – Recommended Design Guidelines and Details. The results from Task 3 were analyzed to develop design guidance for the use of LGA, including the estimation of girder flange lateral bending stresses as well as estimation of force demands for design of cross-frames and diaphragms accounting for skew effects. Included in the Task 4 evaluations were the evaluation of the efficacy of a simplified method for prediction of girder layovers developed by FDOT. The extent of the calculated layover displacements was evaluated at the abutments of the study bridges.

Task 5 – Draft Final Report and Closeout Teleconference. A draft final report was developed presenting all the executed research tasks and findings.

Task 6 – Final Report. Upon approval of the draft final report, the project team has completed and submitted a final report (this report) to the FDOT research center.

1.4 Organization of This Report

This report is organized in five main chapters. Chapter 2 provides a broad review of prior research and guidelines, i.e., Task 1 of the project. The objectives of the research are addressed by a comparative parametric 3D FEA and LGA studies on a suite of 26 bridges that have skew indices up to and slightly exceeding 0.3. The 26 bridges are selected from a set of 57 bridges sampled from the FDOT inventory, which was Task 2 of the project. Chapter 3 presents the Task 2 data analysis of these bridges and outlines the development of the suite of 26 bridges for the parametric studies. Chapter 4 discusses key LGA and 3D FEA modeling idealizations and identifies key bridge responses that constitute the behavior of skewed I-girder bridges. In addition, considerations related to the load and response calculations for the parametric studies are explained in this chapter. These discussions provide a detailed explanation of the processes and procedures used in Task 3 of the project. Chapter 5 focuses on detailed comparisons of the LGA and 3D FEA results, considering each of the key bridge responses, that is, the results from the Task 4 efforts. Chapter 6 summarizes the specific findings and recommendations from this research, emphasizing the contributions of this research to the state-of-the-art of straight skewed I-girder bridge design. Appendix 1 provides a synthesis of the data pertaining to the 57 straight-skewed steel I-girder bridges sampled from the FDOT inventory. Appendix 2 shows the plan geometry of the FDOT bridges that were not selected for further study in this research. The plan geometry of the selected bridges is shown in Section 3.3 of the report. Appendix 3 presents concise summary data plus detailed plots and tables showing all the 3D FEA and LGA results for each of the 26 parametric study bridges considered in this research, as well as detailed LGA calculations for each of these bridges. Appendix 4 provides detailed presentations of staged deck placement analysis results for four cases selected from the parametric study bridges. Appendix 5 shows various comparison plots of bridge responses from the 3D FEA software employed in this research to results from a separate 3D FEA software system for two of the 26 parametric study bridges. Lastly, Appendix 6 lists detailed results for cross-frame forces for specific load cases and load combinations other than Strength I, obtained from the 3D FEA studies conducted in this research. These comparisons serve as quality control documentation, confirming that the data and results are correct. Appendices 3 through 6 are provided in a separate volume due to their substantial size.

2. LITERATURE REVIEW

This chapter reviews the present knowledge within the literature regarding the behavior of skewed I-girder bridges subjected to dead and live gravity loads, the influence of cross-frame arrangements and cross-frame detailing on bridge responses, as well as bridge behavior during deck placement. The chapter concludes with a summary of current guidance regarding the limits of applicability of line girder analysis for the design of straight skewed I-girder bridges.

2.1 Behavior of Skewed Bridges

Geometrically, a skewed bridge is one in which one or more lines of support are not oriented perpendicular to the longitudinal axis of the bridge. The effects of skew on structural behavior depend largely on the magnitude of the skew, quantified by the skew angle θ and the skew index I_s (see Equation 1), and the layout of cross-frames in the structure. The behavior of straight skewed I-girder bridges becomes increasingly three-dimensional with increasing skew. Sanchez (2011) shows that the skew index, I_s, is a coarse indicator of the sensitivity of steel I-girder bridges to skew.

The structural behavior of a skewed bridge is influenced both by the end bearing-line and intermediate cross-frames. End bearing-line cross-frames oriented along the skew twist the girders to maintain continuity between the skewed bearing-line cross-frames and the girders (NSBA, 2016). Figure 1 illustrates the behavior for two girders connected along a skewed bearing line. The bearings are assumed to be fixed (laterally and longitudinally restrained) for simplicity of the discussion. The major-axis bending rotation of the girders induces a longitudinal displacement Δ_z of the top flange relative to the bottom flange. However, since the girders are attached to the skewed bearing-line cross-frames, which have relatively high in-plane stiffness, the cross-frames can only achieve this longitudinal displacement by rotating about the axis tangent to the bearing line. This induces a relative lateral displacement between the top and bottom flange, Δ_x, and a twist rotation of the girders at the bearing line. Correspondingly, girder torsional moments are developed. These moments increase the vertical reactions at the obtuse corner and reduce the vertical reactions at the acute corner.

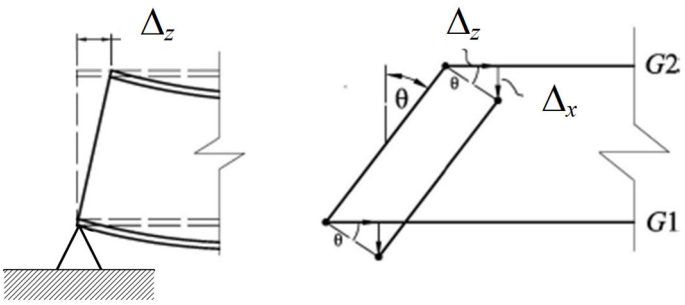

Figure 1. Relative flange displacement in a skewed bridge, adapted from Sanchez (2011).

Figure 2, from White et al. (2012), illustrates the above girder end rotations at the specific bearing on Girder G2. The girder web and the bearing-line cross-frame are assumed to be plumb in the current configuration shown in this figure. The double arrow perpendicular to the girder web represents the major-axis bending rotation of the girder, ϕ_x, about the fixed point. This rotation induces the longitudinal displacement Δ_z at the top flange of the girder. However, since the girder is attached to the skewed bearing line cross-frame, the top flange can only displace significantly in the direction normal to the plane of the cross-frame. This is indicated by the vector labeled Δ. The cross-frame deflects essentially only by rotating about its longitudinal axis through the fixed point. This is shown by the double-arrow vector ϕ. To maintain compatibility between the girder and the cross-frame, the top flange of the girder must deflect by the vector component labeled Δ_x in the figure, in addition to the deflection Δ_z. Therefore, the girder web lays over by the deflection Δ_x relative to the fixed point. This deflection, divided by the height h, gives the girder twist rotation ϕ_z.

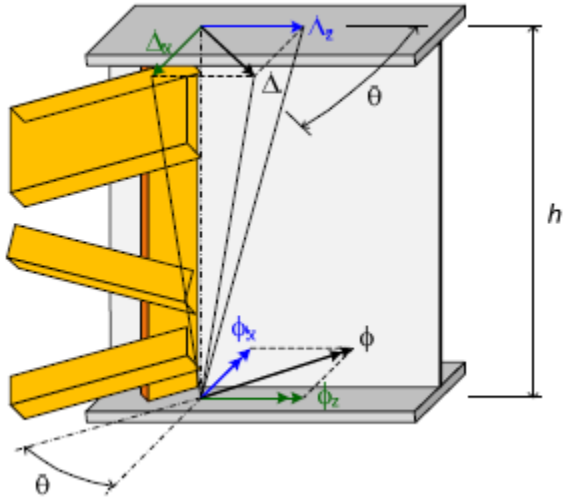

Figure 2. Illustration of the girder major-axis bending and twist rotations required for compatibility at a skewed bearing cross-frame (White et al., 2012).

Based on Figures 1 and 2, the girder layover at the bearing locations can be calculated as follows:

$$\Delta = \phi_x h \tan\theta \tag{2}$$

where

θ = skew angle at the bearing line and

ϕ_x = the girder major-axis bending rotation relative to the ideally plumb position associated with the dead load condition targeted for the cross-frame detailing.

h = girder depth.

When the intermediate cross-frames are perpendicular to the girders, twisting occurs because of the differential vertical deflections between the girders at each of the intermediate cross-frames (NSBA, 2016). The differential vertical deflections are due to the fact that the cross-frames connect to different positions within the span of each of the girders (NSBA, 2016). Due to the large in-plane rigidities of typical cross-frames, intermediate cross-frames that are perpendicular to the girders force them to have approximately the same twist and layover at the bracing points (Sanchez, 2011). The AASHTO LRFD Bridge Specifications (AASHTO, 2017) allow intermediate cross-frames to be oriented parallel to the skew if the skew angle is less than 20°, and it mandates the orientation of cross-frames to be perpendicular to the girders if the skew angle is greater than 20°. If the intermediate cross-frames are oriented parallel to the skew, the differential vertical deflections at the ends of cross-frames are essentially zero in straight bridges with parallel skew. However, the cross-frames still induce a twisting of the girders at these points when there is any major-axis bending rotation of the girders there, due to compatibility of deformations.

Florida DOT and various other states follow the AASHTO (2017) requirements for bridges having a skew angle up to 20°. Kansas DOT extends this limit up to 40° to reduce potential differential deflection and distortion induced fatigue (Zhou et al., 2017)). It should be noted that this may create a more critical detail for evaluation of load-induced fatigue at connection plates turned parallel to the cross-frames and welded to the girder flanges. Wisconsin DOT limits the use of cross-frames parallel to the skewed bearing lines to bridges with a skew angle of less than 15° (WisDOT, 2019). Ohio DOT mandates all intermediate cross-frames to be perpendicular to the girder regardless of the skew angle (ODOT, 2007).

Figures 3 and 4 show representative skewed bridge deflected shapes for the case where the cross-frames are oriented perpendicular to the girders, by focusing on two girders unconnected and then interconnected by cross-frames.

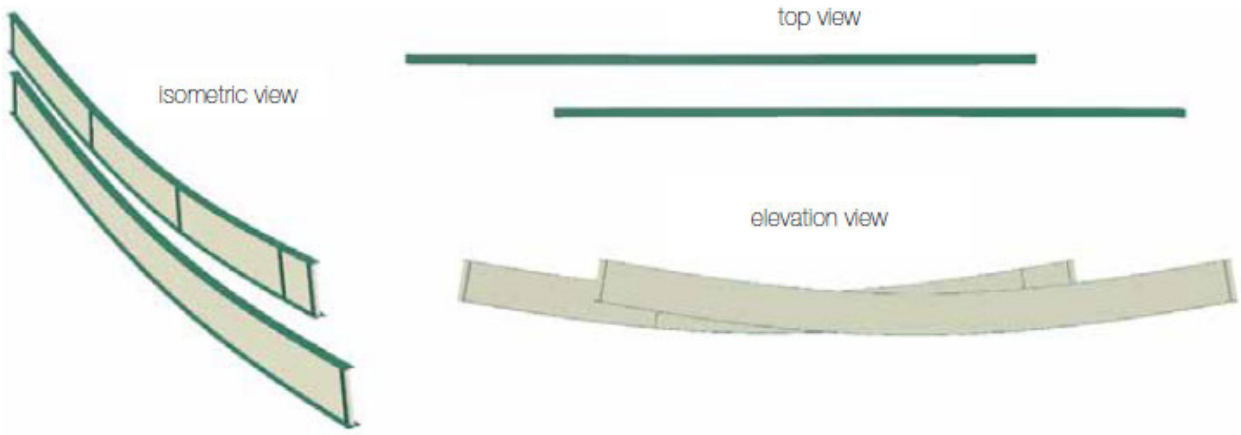

Figure 3. Girder deflections for two simple-span I-girders on parallel skewed supports, subjected to steel dead load prior to connecting the cross-frames (NSBA, 2016).

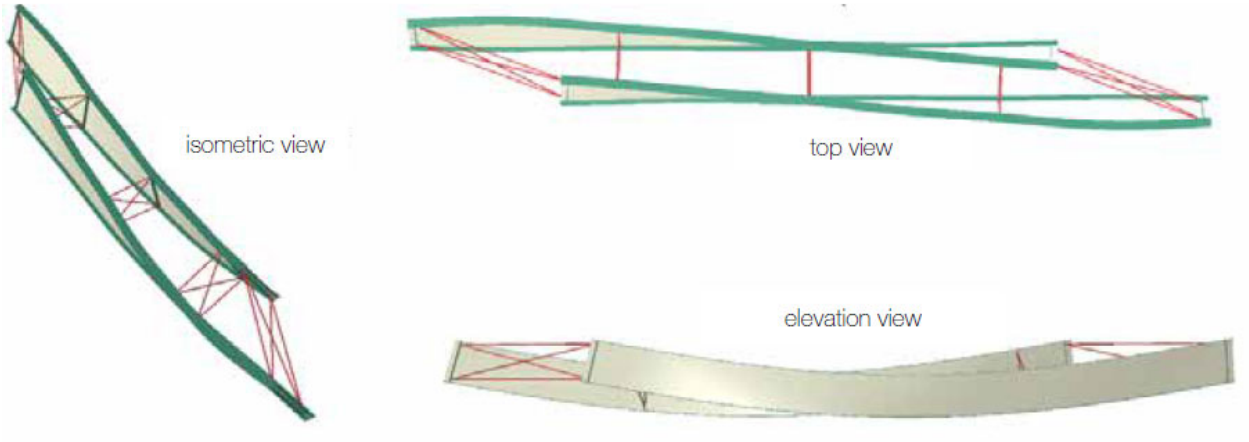

Figure 4. Girder deflections and twist for two simple-span I-girders on parallel skewed supports, subjected to steel dead load, after connecting the cross-frames (NSBA, 2016).

Figure 5 shows a sketch from (Sanchez, 2011) that illustrates the enforcement of compatibility of layover between adjacent girders by an intermediate cross-frame. Figure 5a shows the twist and vertical deflections of the two girders when only the end-bearing cross-frames are connected to the girders. Figure 5b shows the twist and vertical deflections of the two girders when all the cross-frames – end bearing and intermediate, are connected to the girders.

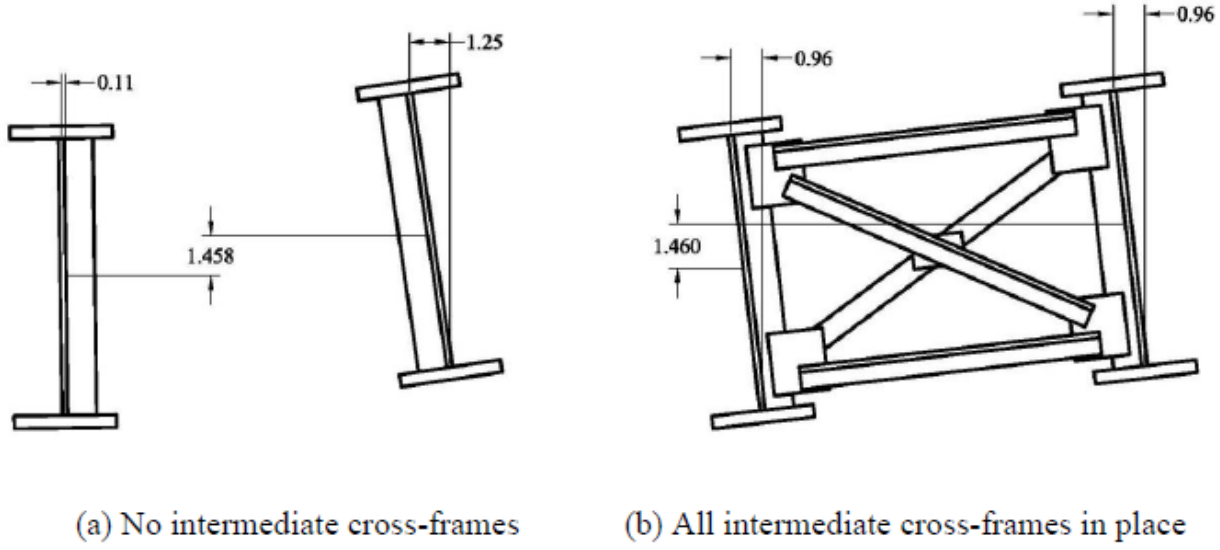

Figure 5. Layover compatibility between adjacent girders enforced by an intermediate cross-frame (Sanchez, 2011).

2.2 Forces in Cross-Frames of a Skewed Bridge

It is shown in Section 2.1 that intermediate cross-frames impart twist and lateral displacement such that the girders have approximately equal layovers at all the bracing points.

Compatibility of displacements and rotations develops forces at the connection points of the cross-frames to the girders as shown in Figure 6 (Sanchez, 2011). This also induces lateral bending of girder flanges. Furthermore, intermediate cross-frames provide a load path for transfer of vertical forces to the bridge supports. These forces depend on the overall transverse stiffness of the system formed by the grid of girders and cross-frames within the spans.

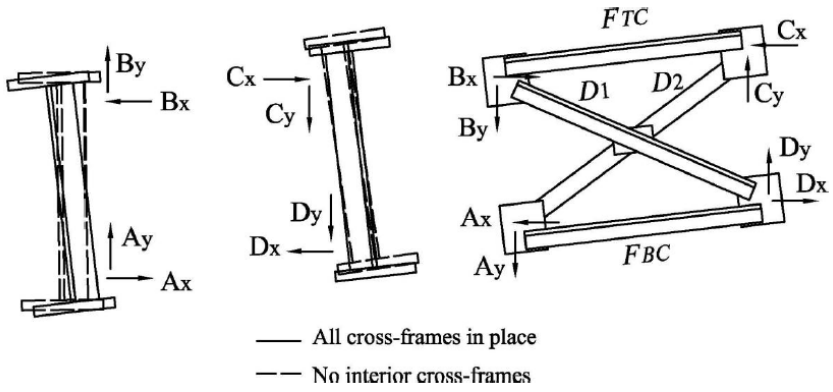

Figure 6. Internal forces in girders and cross-frames due to skew effects (Sanchez, 2011).

Due to larger stiffness of the system of girders and cross-frames along the shorter diagonal direction connecting the obtuse corners of a parallel skew bridge, a significant transverse load path can develop between the supports with large forces being observed near the obtuse corners of the bridge span (White et al., 2015). Kupricka and Poellot (1993) describe this behavior as nuisance stiffness. At contiguous cross-frame lines, the horizontal forces developed in the girder flanges are approximately balanced by the cross-frames connected to the girder from both sides of the girder. Therefore, the girder flange lateral bending stresses tend to be smaller in these situations, although significant flange lateral bending can occur where a contiguous cross-frame line is discontinued.

Conversely, when staggers and offsets in the cross-frame layout are used to mitigate the stiff transverse path, discussed subsequently in Section 2.3, the cross-frame forces tend to be reduced at the expense of the girder flange lateral bending stresses tending to be increased. This needs to be accounted in the proportioning of the girder flanges. The AASHTO LRFD Specifications (AASHTO, 2017) advise that, in such cases, flange lateral bending stresses are best determined by direct structural analysis. However, in many situations, these lateral bending stresses have a relatively minor influence on the girder design. Furthermore, offsets and staggers can provide a desirable reduction in the cross-frame/diaphragm forces (Grubb et al., 2010; NSBA, 2016; AASHTO, 2017). The AASHTO LRFD Specifications (AASHTO, 2017) indicate that, in some cases, the flange lateral bending stresses are reduced due to this decrease in the cross-frame forces.

The next section discusses a few strategies for mitigating the stiff transverse load path effects.

2.3 Strategies for Mitigating Transverse Load Path Effects

It is explained in Section 2.1 that intermediate cross-frames impart twist and lateral displacement such that the girders have approximately equal layovers at the bracing points. Compatibility of displacements and rotations develops forces at the connection points of the cross-frames to the girders as shown in Figure 6. This induces lateral bending of the girder flanges when there are offsets, staggers or general discontinuities in the cross-frame lines. Furthermore, intermediate cross-frames provide a load path for transfer of vertical forces to the bridge supports. These forces depend on the overall transverse stiffness of the system formed by the grid of girders and cross-frames within the spans.

If the first intermediate cross-frame within a span is connected too close to a bearing, high internal forces should be expected (Sanchez, 2011). Therefore, a strategy for mitigating the nuisance stiffness is to offset the intermediate cross-frames from the bearings in the vicinity of the skewed supports.

White et al. (2015) and NSBA (2016) recommend that, where support lines are skewed more than 20° from normal and cross-frames or diaphragms are provided along the skewed support line, the first intermediate cross-frames or diaphragms placed normal to the girders adjacent to the skewed support ideally should be offset, where practicable, by a minimum of the larger of $4b_f$ or $0.4L_b$ from the support, where b_f is the largest girder flange width within the unbraced length on either side of the first cross-frame or diaphragm, and L_b is the unbraced length between the first and the second intermediate cross-frame or diaphragm from the support along the girder under consideration. The AASHTO LRFD Specifications (AASHTO, 2017) have adopted these recommendations. Figure 7 shows an illustration of the application of this concept from NCHRP 20-07/Task 355 (White et al., 2015). In this example, staggering of the cross-frames is achieved by omitting alternate cross-frames within the bays between the interior girders.

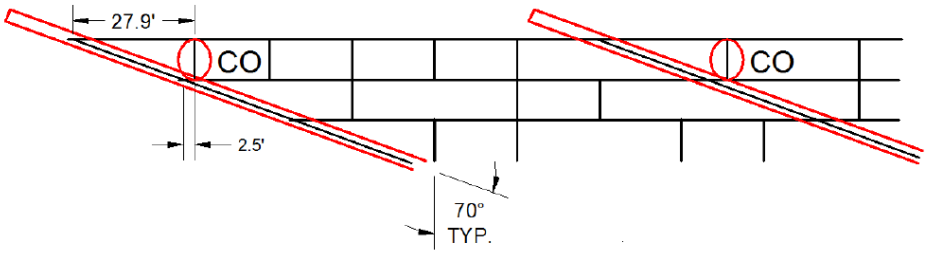

Figure 7. Use of a staggered cross-frame layout plus a single chord-only (CO) cross-frame at the acute corners of the bridge spans (White et al., 2015).

The above practice helps to alleviate the introduction of a stiff load path that will attract and transfer large transverse forces to the skewed support lines, particularly at the obtuse corners of a parallel skewed span. At the acute corners of severely skewed bridge spans, the above offset requirements may result in an excessive unbraced length on the fascia girder as can be observed in Figure 7. In this case, a single chord-only (CO) cross-frame containing only top and bottom chords (no diagonal members) can be framed from the first interior girder to the fascia girder at a small offset from the support, perpendicular to the girders, to avoid inducing a large transverse stiffness while also providing adequate lateral support to the fascia girder (White et al., 2015).

The use of unbraced lengths smaller than $4b_f$ or $0.4L_b$ often tends to result in the associated cross-frames working more like a contiguous cross-frame line rather than a discontinuous one.

Figure 8, from (White et al., 2015), illustrates the above concept on a bridge with an extreme nonparallel skew. NSBA (2016) explains that a cross-frame must be provided on at least one side of a girder at each bracing location to provide the required lateral bracing. In some situations, additional cross-frames may be required to provide sufficient lateral bracing stiffness. However, the alternate removal of intermediate cross-frames is usually structurally sufficient (White et al., 2015).

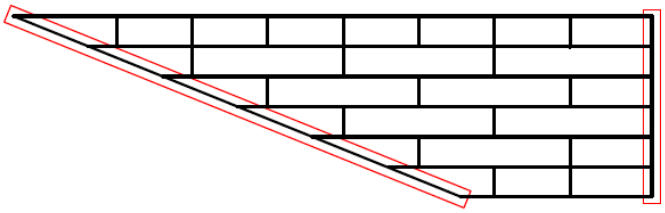

Figure 8. Use of staggered cross-frame layout for a bridge with extreme nonparallel skew (White, et al. 2015; NSBA, 2016).

For continuous-span bridges, the AASHTO LRFD 7th Edition (AASHTO, 2015) Article 6.7.4.2 states that at the discretion of the Owner, cross-frames and diaphragms need not be provided along skewed interior support lines if cross-frames or diaphragms normal to the girders are provided at bearings that resist lateral forces. Figure 9 provides an example of this type of framing arrangement from the bridges sampled from the FDOT inventory for this research. This framing arrangement causes substantial nuisance stiffness effects, since the cross-frames join points of zero vertical displacement on the bearing line and finite non-zero displacement on the other side of the cross-frame. A cantilever-type action occurs for these cross-frames when they are framed across a bearing line. Framing of an intermediate cross-frame perpendicular to the girders and into or near a bearing location along a skewed support is highly discouraged unless the cross-frames diagonals are omitted (NSBA, 2016). The AASHTO LRFD 8th Edition (AASHTO, 2017) has revised its recommendations to indicate a preference for offsets of the intermediate cross-frames from the bearing lines, and the provision of cross-frames between the girders along all bearing lines.

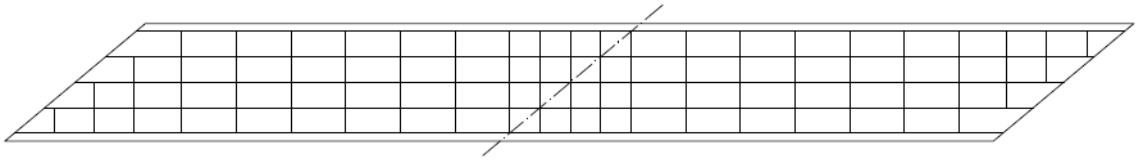

Figure 9. Example bridge with cross-frames removed from the pier bearing line, FDOT Bridge F31.

The NHI (Grubb et al., 2010) and NCHRP 20-07/Task 355 (White et al., 2015) reports find that transverse stiffness effects are alleviated most effectively by placing diaphragms or cross-frames along the bearing lines, and locating perpendicular intermediate diaphragms or cross-frames at greater than or equal to the minimum offset from skewed bearing lines as discussed

above (in the context of bridges with skew angle $\theta > 20°$). Figure 10 shows an example of this type of framing arrangement. NSBA (2016) explains that the lines through the work-points at the mid-length of the intermediate cross-frames are all parallel to the bearing lines in this bridge. However, given the skew angle in the bridge, the stagger distances between the intermediate cross-frame locations within the span are both greater than $4b_f$ and $0.4L_{b,adj}$, where b_f is the largest girder flange width within the unbraced length on either side of the intermediate cross-frame, and $L_{b,adj}$ is the unbraced length between intermediate cross-frame under consideration and the adjacent cross-frames.

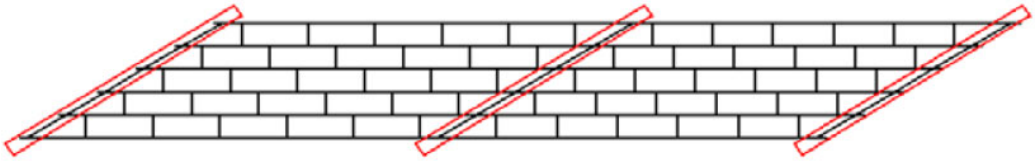

Figure 10. Recommended staggered framing arrangement for straight skewed bridges with parallel skew angles at bearing lines (NSBA, 2016).

The NCHRP 20-07/Task 355 report also suggests an arrangement that places the cross-frames perpendicular to the girders in a staggered arrangement (with skews greater than 20°), but positions a common "work point" on the different cross-frames at locations parallel to the skew. That is, the work points are "fanned" approximately between the skew angles at the ends of the span. Such an arrangement is shown in Figure 11.

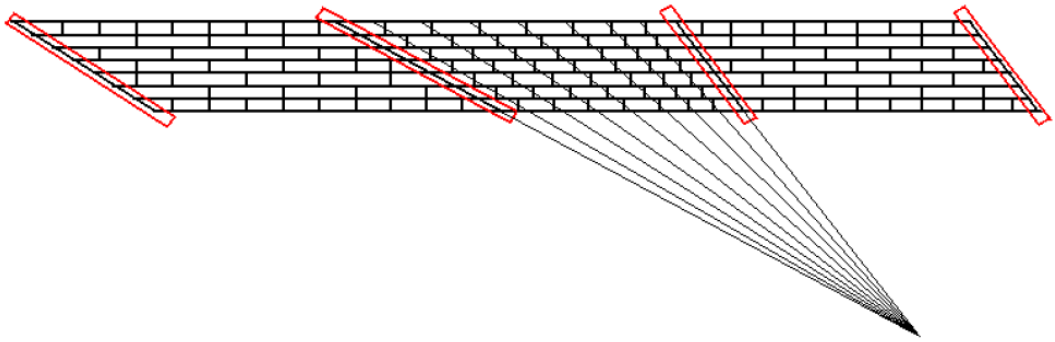

Figure 11. Sketch of an alternative staggered "fanned" cross-frame layout for a nonparallel skewed bridge (White et al., 2015).

Furthermore, generally diaphragms or cross-frames can be omitted to alleviate uplift considerations at certain bearings, as well as potentially to relieve excessive diaphragm or cross-frame forces due to transverse stiffness effects if the skew is significant (White et. al., 2015; AASHTO, 2017).

Another approach to mitigate significant transverse load path effects is to use a lean-on cross-frame system arrangement in parallel skew bridges, as shown in Figure 12 (Romage, 2008; Zhou, 2006; Helwig and Yura, 2015). In this structural system, the diagonals are left out of a large number of the cross-frames. Only the top and bottom chords are installed, providing a load path to resist the torsional rotation of all the girders connected along contiguous cross-frame

lines by one or only a few cross-frames on each line (Helwig and Yura, 2015). This basically provides a "shear release," removing the restraint of the differential displacements between the girders throughout much of the bridge plan. However, the top and bottom chords connect the girders together such that equal layover is enforced among the girders connected at the lean-on bracing location.

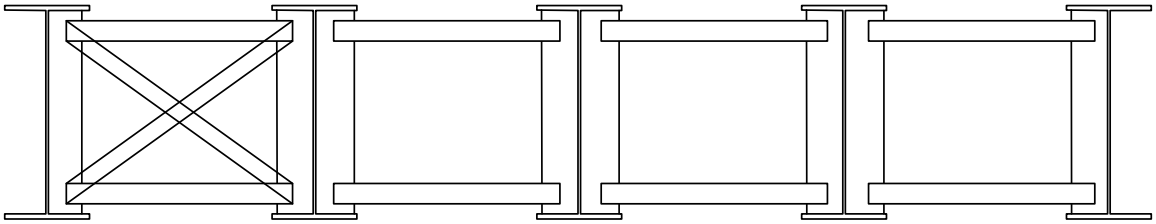

Figure 12. Lean-on bracing system for bridge girders.

The NCHRP 20-07/Task 355 research (White et al., 2015) studied a bridge with a lean-on cross-frame system, also studied extensively by Romage (2008). The Task 355 research showed that a staggered cross-frame arrangement gives lower average maximum cross-frame forces for all cross-frame detailing methods (NLF, SDLF and TDLF) than the lean-on-bracing arrangement. It should also be noted that the shear release provided by the lean-on framing arrangement can allow excessive differential vertical deflections between the girders, resulting in large deviations in the final elevations. In some cases, this attribute must be considered when designing lean-on systems. Furthermore, the use of a lean-on bracing system also requires attention to the sequence of erection of the structural steel, since until the cross-frame containing the diagonal members is installed, the girders are not braced at the corresponding bridge cross-section illustrated in Figure 12.

The Task 355 research concludes that the lean-on and the recommended staggered cross-frame framing systems are comparable in terms of achieving the desired results of mitigating nuisance transverse stiffness effects. The use of staggered cross-frames provides greater overall continuity between the girders throughout the span, and a staggered arrangement in which every other intermediate cross-frame is removed within the span results in a substantial reduction in the number of cross-frames within the overall bridge system (White et al., 2015).

It should be noted that the above recommendations were developed focusing on a wide range of skewed bridge geometries, with the bridge skew in many of the cases being relatively large. These concepts should be beneficial for bridges with less severely skewed geometry as well, but the impact of these changes in the cross-frame framing arrangement will not be as dramatic. The softening of the transverse load path obtained using staggered cross-frame arrangements can potentially increase the range of applicability of line girder analysis for straight skewed bridges.

The AASHTO LRFD Bridge Specifications (AASHTO, 2017) allow intermediate cross-frames to be oriented parallel to the skew for bridges if the skew angle is less than 20°, and they mandate the orientation of cross-frames to be perpendicular to the girders if the skew angle is greater than 20°. Kansas DOT extends this limit up to 40° as discussed above in Section 2.1. Although cross-frames oriented parallel to the skewed bearing lines can be effective with skew angles larger than 20°, the influence of bent plate connection flexibilities can become an issue

(Wang and Helwig, 2008). Wang and Helwig (2008) further state that when a brace is oriented parallel to the skewed supports, the stiffness and strength of the brace can be significantly reduced. The stiffness reduction is due to the fact that the full stiffness of the brace is not engaged in resisting twist of the girder cross-section due to the angled orientation of the brace. In addition, the orientation of the brace parallel to the skew results in longer lengths in the brace member, which reduces the stiffness of the bracing in restraining girder torsional rotations. However, this reduction in stiffness also can be beneficial, potentially, by reducing the tendency of the cross-frames to attract force within the statically indeterminate bridge structural system.

Zhou et al. (2017) studied the behavior of straight skewed I-girder bridges having skew angles of 0°, 20° and 40°, for a staggered cross-frame arrangement and a contiguous cross-frame arrangement where cross-frames are placed parallel to skew. Each of these bridges were investigated for different types of cross-frame connections that included a half-pipe stiffener, bent-plate and transverse stiffeners. Cross-frames oriented parallel to skew often are connected to the girder via a bent plate. The bent plate connection provided excessive flexibility into the system. This can be eliminated by using a half-pipe stiffener connection (Quadrato, 2010). Girders in bridges that employed half-pipe stiffeners resulted in smaller lateral displacements in the study by Zhou et al. (2017). The bridge models that include the half-pipe stiffeners produced higher compression axial stresses near the connection ends. However, the stress magnitudes at locations away from the connection were similar in all the bridge models. The cross-frame forces in a bridge with a half-pipe connection were generally observed to be lower than with other types of connection.

2.4 Fit Considerations for Skewed Bridges

Skewed I-girder bridges undergo torsional displacements of the individual girders, as discussed in the previous sections. As a result, the girder webs can be plumb only under one loading condition. To achieve approximately plumb girder geometries for a given dead load condition (e.g., steel dead load or total dead load), the cross-frames and diaphragms are detailed to "fit" to the conceptually plumb girders once they are vertically deflected (from their initial cambered geometry) under this load condition. Thus, a "fit" condition can be defined as the deflected or undeflected girder geometry under which the cross-frames or diaphragms are detailed to connect to theoretically plumb girders (NSBA, 2016). A fit condition is selected to offset, or compensate for (to different extents), the twisting of the I-girders under dead load. According to NSBA (2016), the detailer accomplishes an I-girder bridge fit by setting the "drops" between the girders for the fabrication of the cross-frames and connection plates. Drops are calculated as the difference in the vertical elevation between the tops of the girder webs at the cross-frame connections to the girders under the targeted dead load condition (initial cambered elevations minus the estimated vertical deflections of the girders under the targeted dead load condition).

Table 1 (NSBA, 2016) summarizes the three most common fit conditions considered in steel I-girder bridge construction. SDLF gives approximately plumb girder webs after the erection of all the steel components, and TDLF gives approximately plumb girder webs after the bridge is subjected to its total dead load (NSBA, 2016). In this context, total dead load typically refers to loads that include the weight of the steel components and the concrete deck. The cross-frames are erected before the deck is cast. The girders are fabricated with a camber calculated on the

basis of total dead loads. Therefore, for both SDLF and TDLF detailing, a lack-of-fit force is developed in the cross-frames that can be calculated based on the changes in the ideal plumb girder geometry between the initial no-load cambered positions and the idealized plumb girder positions under the targeted dead load.

Table 1. Common fit conditions (NSBA, 2016).

Loading Condition Fit	Construction Stage Fit	Description	Practice
No-Load Fit (NLF)	Fully-Cambered Fit	The cross-frames are detailed to fit to the girders in their fabricated, plumb, fully-cambered position under zero dead load	The fabricator (detailer) sets the drops using the no-load elevations of the girders (i.e., the fully cambered girder profiles)
Steel Dead Load Fit (SDLF)	Erected Fit	The cross-frames are detailed to fit to the girders in their ideally plumb as-deflected positions under the bridge steel dead load at the completion of the erection.	The fabricator (detailer) sets the drops using the girder vertical elevations at steel dead load, calculated as the fully cambered girder profiles minus the steel dead load deflections.
Total Dead Load Fit (TDLF)	Final Fit	The cross-frames are detailed to fit to the girders in their ideally plumb as-deflected positions under the bridge total dead load.	The fabricator (detailer) sets the drops using the girder vertical elevations at total dead load, which are equal to the fully cambered girder profiles minus the total dead load deflections.

The FDOT Structures Design Guidelines Section 5.1 mandate the use of SDLF. No Load Fit (NLF) and steel dead load fit (SDLF) may be used where appropriate (NLF can be acceptable when the bearings are at a small skew angle; however, NLF detailing leads to girder layovers at end bearings that are larger than they really need to be when the end bearing line is skewed (NSBA, 2016).) Total Dead Load Fit (TDLF) is not permitted by FDOT without Structures Design Office (SDO) approval.

NCHRP 20-07/Task 355 (White et al., 2015) report that in straight skewed bridges, SDLF using Line Girder Analysis (LGA) cambers results theoretically in zero cross-frame forces, zero flange lateral bending stresses and perfectly plumb girders in the SDL condition. Similarly, TDLF using LGA cambers results theoretically in zero cross-frame forces, zero flange lateral bending stresses and perfectly plumb girders in the TDL condition. This is based on the

idealization that the deck forms and the bridge deck in the early condition during concrete placement do not provide any interconnection between the girders in resisting TDL, i.e., the concrete deck is assumed to not have any setup that would resist the girder displacements under subsequent concrete placement. The above behavior for SDLF and TDLF is the same regardless of whether the bridge has parallel or nonparallel skew of its bearing lines.

White et al. (2015) further report that, for straight skewed bridges, theoretically the most accurate girder cambers, which should be fabricated into the girders to achieve the targeted elevations under the TDL (when the cross-frames are detailed based on the LGA cambers), are:

- For TDLF, the negative of the girder TDL vertical deflections obtained from the LGA.
- For SDLF, the negative of the girder SDL vertical deflections obtained from the LGA plus the negative of the Concrete Dead Load (CDL) vertical deflections obtained from a NLF 3D Refined Analysis (RA). This solution considers the fact that the behavior of the bridge subjected to the steel dead load, where the SDLF detailing effects offset the SDL twist rotations of the girders, is different than the behavior of the bridge for the CDL, where the bridge deflects as a three-dimensional system in resisting the weight of the concrete. For SDLF using the theoretical girder elevations obtained by subtracting the LGA steel dead load deflections from the above cambers, the girders will be theoretically plumb and the cross-frame forces will be theoretically zero under the steel dead load.

It is important to include the lack-of-fit effects associated with the fit condition in refined analysis to obtain accurate cross-frame forces (White et al. 2015, Gull and Azizinamini 2014a. That is, for SDLF or TDLF detailing, the cross-frames do not fit to the girders in their initial cambered no-load geometry, and this lack-of-fit in the initial no-load condition has a significant impact on the bridge internal forces. Gull and Azizinamini (2014a and 2014b) achieve this in ANSYS (2019) by using the "Element Birth and Death" feature of this software. For SDLF, the cross-frames can be modeled as inactive until the erection of steel and this is achieved by using the "Death" command. After girder erection, the unstressed cross-frames can be incorporated into the subsequent 3D refined analysis model, at the current deformed configuration of the structure, using the "Birth" command.

SDLF can be simulated in CSiBridge (CSi, 2019) using its staged construction capabilities and appropriate stiffness modifiers. A very small number such as 1E-20 is used to make the cross-frames conceptually inactive during the stage involving application of the steel dead load. This stage consists of the steel girders and the cross-frames deflecting under their self-weight. At this stage in the analysis, it is essential to ensure lateral stability of the girders. The easiest way to ensure this is to support the girders laterally using fictitious supports. The subsequent stage of the analysis includes activating the cross-frames in the deflected configuration of the girders, by resetting the cross-frame members to their actual stiffness, and applying the wet concrete loads to the noncomposite bridge structure composed of the girders and cross-frames.

NCHRP 20-07/Task 355 (White et al., 2015) uses initial strains to simulate lack-of-fit effects in refined analysis. The initial strains are calculated based on a position vector analysis between the initial locations of the connection workpoints in the initial no-load geometry of the girders and the final position of the connection workpoints in the targeted dead load condition. The

corresponding strains associated with the deflections between these configurations can be inserted as temperature loads in the FEA model if the software does not directly allow for insertion of initial strains from this lack-of-fit in the targeted girder geometry. This type of approach is recommended to address the lack-of-fit effects in curved bridges. This is because curved bridge girders are often not stable, or would deflect excessively if the cross-frame systems are theoretically removed. RA cambers (i.e., cambers calculated entirely from refined analysis of the connected three-dimensional bridge structural system) are recommended for the position vector analysis since it becomes difficult to use LGA for such bridges to determine the deflection profiles (White et al., 2015). Additionally, RA better accommodates the consideration of staged concrete deck placement, its influence on the CDL deflections and the resulting appropriate cambers. White et al. (2015) discusses these aspects in detail.

Both of the above approaches can be useful, depending on the context and depending on the capabilities of the software system being employed for the structural analysis.

2.5 Distribution of Girder Dead and Live Loads for Line Girder Analysis

The accuracy of line girder analysis is influenced directly by the assumed distribution of the loads from the physical three-dimensional structural system to the individual girders. The following sections discuss common assumptions for the distribution of the dead loads, and calculations for the distribution of the live loads.

2.5.1 Dead Loads

There are numerous approaches for distributing dead loads to bridge girders for a line girder analysis. The following is a sample of recommendations:

- In steel bridges, the action of the cross-frames tends to distribute the weight of the wet concrete deck so that the girders deflect nearly equally on a straight bridge with right supports. As such, if all the girders are of equal or nearly equal stiffness, the deck weight will be carried nearly equally by all the girders via the restoring forces in the cross-frames. That is, although the loads applied directly to the girders from the formwork will be essentially based on the tributary width of the deck associated with each girder, the cross-frames (if they are essentially rigid compared to the girders) force the girders to deflect equally. Therefore, if the girders have equal stiffness, the restoring forces from the girders will be equal in resisting the loads. Shear forces are developed in the cross-frames that distribute the loads directly applied to the girders such that the internal forces are approximately the same in all the girders. AASHTO LRFD Article 4.6.2.2.1 (AASHTO, 2017) recognizes this fact by stating that for multi-girder bridges satisfying certain conditions (constant deck width, parallel girders having approximately the same stiffness, and at least four girders in the bridge cross-section), the permanent loads “of and on the deck” may be distributed equally to each of the girders for approximate line-girder analyses. However, in the case of more significantly skewed steel-girder bridges, the precise distribution of the deck weight is rather complex and strictly can only be ascertained by refined analysis. An important question in the context of the present research is whether the skew effects in bridges with a skew index up to and slightly above 0.3 are sufficiently small such that the assumption of uniform distribution of the loads still works well. In addition, the commentary to Article 4.6.2.2.1 discusses

recommended extensions for handling of live loads in bridges with splayed girders. The implications are that the uniform distribution of dead loads also may be sufficient for these types of bridges, possibly within certain limits.

- As noted above, AASHTO LRFD Article 4.6.2.2.1 also indicates that for bridges satisfying the above stated conditions, permanent loads applied "on" the deck after the deck is made composite may also be distributed equally to each girder. The permanent loads applied to the composite deck can include the weight of parapets, barriers, sidewalks, wearing surface loads, utility loads, etc. It is apparent that the simple statement in AASHTO LRFD Article 4.6.2.2.1 will likely become invalid for some types of loadings, particularly concentrated loadings near the edges of the bridge deck. However, clearly if concentrated loads are small enough, the coarse approximation of distributing them equally to all the girders may be sufficient. Additional considerations for the application of composite dead loads to the bridge girders are discussed below.

- Heavier superimposed dead loads such as parapets, barriers, sidewalks or sound walls should not be distributed equally to all the girders for the analysis (Grubb et al., 2015). Engineering judgment should be applied in distributing these loads for approximate line-girder analyses. Usually the largest portion of the parapet load on an overhang is assigned to the fascia girder, or to the fascia girder and the first interior girder. In fact, in some cases, the exterior girder may receive more than the weight of a heavy parapet, sound wall, etc. on the extreme deck overhang due to cantilever effects, with resulting uplift of one or more interior girders. These superimposed dead loads are applied to the long-term composite section for the analysis to account in an approximate fashion for long-term creep effects. The Iowa DOT Bridge Design Manual (IOWA DOT, 2018) recommends that the weight of deck (part of DC1 loads) shall be distributed to each girder assuming the slab between girders is simply supported and all of the deck weight from an overhang is distributed to the exterior girder.

- For wearing surface loads and deck overlays, the assumption of an equal distribution of the load to each girder for approximate line-girder analyses is reasonable and has been the customary practice.

- Regarding distribution of weight of railing and sidewalks (DC2) and a future wearing surface (DW), the Iowa DOT Bridge Design Manual (IOWA DOT, 2018) recommends that for superstructures with roadway widths not greater than 44 feet, DC2 and DW be distributed equally to all girders. Further, it recommends that for superstructures with roadway widths greater than 44 feet, the future wearing surface shall be distributed equally to all girders. However, it indicates that each railing and raised sidewalk cast after the deck along the edge of the superstructure shall be distributed one-half to the exterior girder, one-quarter to the first interior girder, and one-quarter to the second interior girder.

- For the DC2 loads for very wide bridges (total width > 70 ft), the Georgia DOT Bridge Manual (GDOT, 2019) recommends distributing the sidewalk, barrier and parapet loads to the four exterior girders on each side, and the median loads to the girders under the median.

In a slightly more specific context, Sumner et al. (2006) developed an empirical method, using field testing and FEA predictions, to predict the noncomposite deflections in steel I-girder simply supported skewed bridges. The method involves an initial calculation of the girder deflections using tributary loads followed by the application of an empirical correction factor based on the bridge characteristics. X- and K-type intermediate cross-frames without top chords were considered in the study. In addition, axial stiffness of the deck forms was considered in the studies. The interaction of these stiffnesses with the other bridge components provides a mechanism for lateral load transfer between girders.

2.5.2 Live Loads

Determining the value of the maximum moments and shears in girders due to live load is a three-dimensional system analysis problem. The load transfer from the concrete bridge deck and cross-frames to the steel girders is quite complex, depending generally on numerous aspects. Live load distribution factors (LLDF) are used to estimate the live load effects on individual girders. AASHTO Articles 4.6.2.2.2 and 4.6.2.2.3 recommend various distribution factor equations to calculate the amount of live load resisted by each girder in different types of bridges. The LLDFs account for the differences between interior and exterior girders, as well as the differences between simple and continuous spans (Grubb et al., 2010). The NCHRP Project 12-26 report (Zokaie et al., 1991) explains the development of the base empirical equations in detail. These LLDF equations are significantly more accurate—specifically, less conservative—than the traditional *S*/5.5 rule on the wheel in the AASHTO Standard Specifications (AASHTO, 2002).

It should be noted that the NCHRP 12-26 study (Zokaie et al., 1991) was carried out for bridges without cross-frames or diaphragms. Cross-frames and diaphragms tend to increase the moments in exterior girders and decrease the moments in interior girders; that is, they further tie the girders together such that the girders and cross-frames act as a three-dimensional unit. The stiffness of concrete parapets (also commonly referred to as barriers, or rails) was also neglected in the primary studies. These rails, when they act structurally, increase the load in the outer two girders due to the additional stiffness. The effect of flange-level lateral bracing in steel I-girder bridges was not considered and is not addressed by the LLDF equations. To assure conservative results, the constants in the formulas were adjusted so that the ratio of the value computed using the approximate LLDF to the more accurate distribution factor obtained using 3D FEA methods would in most cases be greater than 1.0 (Grubb et al., 2015).

AASHTO LRFD Article 4.6.2.2.2d (AASHTO, 2017) mandates that in steel beam-slab bridge cross-sections with cross-frames or diaphragms, the LLDF for the exterior girder, beam, or stringer is not to be taken to be less than that which would be obtained by assuming the cross-section deflects and rotates as a rigid cross-section. This rigid cross-section analysis (RCA) is needed since the LLDFs were developed without taking the effect of cross-frames and diaphragms into consideration. Therefore, the RCA ensures that this deficiency is addressed, albeit with some potential conservatism.

In addition, AASHTO (2017) Article 4.6.2.2.2 generally requires the calculation of LLDFs for both single-lane and multiple-lane application of live load to the bridge deck. For interior girders, the single-lane empirical formulas never govern relative to the corresponding multiple

lane equations within their limits of applicability for steel beam – concrete slab bridges. However, for the exterior (i.e., fascia) girders, Article 4.6.2.2.2d employs the lever rule for the calculation of the single-lane LLDF. The lever rule idealizes the bridge deck as a basic planar beam simply-supported at the first interior girder, not considering any of the continuity of the deck across the top of the first interior girder, and with a cantilever overhang with continuity of the deck across the top of the exterior or fascia girder. This rule tends give a conservative representation of the true live load distribution to the exterior girders. Generally, since a multiple-lane bridge must accommodate traffic in both multiple lanes as well as any single lane, conceptually the single-lane LLDF must be employed if it is larger than the multiple-lane LLDF. As such, the LLDF from the lever rule for the single-lane loading case often governs relative to both the LLDF from RCA and from the empirical multiple-lane equations.

The AASHTO (2017) Article 4.6.2.2 equations for the beam-slab bridge LLDFs, applicable for distribution of the AASHTO lane loads (in contrast to the distribution of wheel loads in former AASHTO Specifications, e.g., AASHTO (2002)), are as follows:

For calculation of the live load moment in interior girders for single-lane loading

$$g_{mint} = 0.06 + \left(\frac{S}{14\ \text{ft}}\right)^{0.4}\left(\frac{S}{L}\right)^{0.3}\left(\frac{K_g}{12Lt_s^{\,3}}\right)^{0.1} \tag{3}$$

For calculation of the live load moment in interior girders for multiple-lane loading

$$g_{mint} = 0.075 + \left(\frac{S}{9.5\ \text{ft}}\right)^{0.6}\left(\frac{S}{L}\right)^{0.2}\left(\frac{K_g}{12Lt_s^{\,3}}\right)^{0.1} \tag{4}$$

where

S = girder spacing, ft $(3.5\ \text{ft} \le S \le 16\ \text{ft})$

L = span length, ft $(20\ \text{ft} \le L \le 240\ \text{ft})$

K_g = longitudinal stiffness parameter, in^4 $(10{,}000\ \text{in}^4 \le K_g \le\ 7x10^6\ \text{in}^4)$

$$K_g = n\left(I + Ae^2\right) \tag{5}$$

n = modular ratio of girder material to slab material

I = girder moment of inertia, in^4

e = distance between the centroids of the girder and the bridge deck, in

t_s = slab thickness, in $(4.5\ \text{in} \le t_s \le 12\ \text{in})$

For calculation of the live load moment in exterior girders, the empirical distribution factor (used for multiple-lane cases) is determined as

$$g_{mext} = g_{mint} e_m \tag{6}$$

$$e_m = 0.77 + \frac{d_e}{9.1 \text{ ft}} \tag{7}$$

where

d_e = distance from the center of the exterior girder to the edge of the inside edge the curb or traffic barrier in ft (-1.0 ft $\leq d_e \leq$ 5.5 ft)

AASHTO (2017) Article 4.6.2.2.2e provides an empirical correction factor for the moment LLDF to account for the effects of skewed supports. This can be written as

$$f_m = 1 - c_{1m} \left(\tan \theta \right)^{1.5} \tag{8}$$

where

$$c_{1m} = 0.25 \left(\frac{K_g}{12 L t_s^{\,3}} \right)^{0.25} \left(\frac{S}{L} \right)^{0.5} \tag{9}$$

with K_g, L, and t_s as defined above, applicable when the girders are "sufficiently connected to act as a unit" and when the difference between skew angles of two adjacent lines of support does not exceed 10 degrees. The parameter c_{1m} is taken equal to zero if θ is less than 30°, and θ is taken as 60° when $\theta > 60°$.

The application of the AASHTO (2017) LLDF provisions can be quite complex when it comes to the consideration of various specific aspects of common steel I-girder bridge structures, specifically handling of continuous spans involving I-girders with variable cross-sections along their length. Furthermore, although the stated assumption at the beginning of Article 4.6.2.2.1 is that the "beams are parallel and have approximately the same stiffness," some variation in I-girder stiffnesses can commonly occur for numerous reasons (e.g., concentrated loads on individual girders from walls, sidewalks or heavy appurtenances, and/or differences in girder length due to nonparallel skew). The girders generally may be framed with unequal spacing. Therefore, accommodation of unequal girder stiffness, unequal spacing and splay is needed for the general practical application of the provisions. The following are salient features pertaining to the application of the AASHTO (2017) Article 4.6.2.2 provisions for the moment LLDF in this research:

1. Moment LLDF for interior girders
   a) Use the span length for which the moment is being calculated, for calculation of positive moments.

b) For calculation of positive moments, use the weighted average value of K_g, weighted by the ratio of the lengths of the prismatic segments corresponding to each of the cross-sections along the girder length within each span to the span length. For applications with unequal girders, use the largest weighted average K_g of all the girders, interior and exterior, in the calculation of the empirical LLDF values.
c) For calculation of negative moments, use the average of the adjacent span lengths.
d) For calculation of negative moments, use the average of the above weighted average K_g values from the adjacent spans.
e) Use the maximum S at 2/3 of the span length with all of the girder calculations, for bridge spans with unequal girder spacing and/or splayed girders.
f) For the fatigue LLDF, divide the empirical value from Equation 3 by 1.2 to remove the implicit multiple presence factor from the equation (the AASHTO LRFD multiple presence factor (mpf) values are included implicitly within the above empirical formulas, but the single-lane fatigue truck loading does not include any mpf). LRFD Simon (NSBA, 2019) presumes the inclusion of the multiple presence factor in its input user-defined LLDFs; therefore, one should not divide by the above 1.2 factor when calculating the input values for Simon.
g) The skew correction factor for moment is often not applied. It is not applied in this research. This factor (Equations 8 and 9) basically accounts for reductions in the major-axis bending moments of parallel skew bridges due to the load path that develops via the vertical bending stiffness of the bridge deck in the short diagonal direction of the parallel skew, acting in concert with the major-axis bending stiffness of the bridge girders. These formulas do not consider any contribution from the cross-frames and diaphragms. Given that it can be beneficial to design cross-frame framing arrangements that aim to soften the bridge transverse stiffness, and given that the values of K_g can be on the larger end of the intended range of application of the empirical equations, leading to smaller values of this correction factor, this factor is mainly an additional complication that is not worth the trouble.
h) For multiple-span bridges, once the governing single- and multiple-lane LLDFs have been calculated for each span, apply the larger of each these factors from all of the spans. LRFD Simon (NSBA, 2019) allows for the external definition of only one single-lane and one multiple-lane moment LLDF within its user interface.

2. Moment LLDF for exterior girders
a) For two or more lanes, use the above interior LLDF equations with the adjustment factor e_m from Equation 7, using the spacing between the exterior and first interior girder at 2/3 of the span length (for splay).
b) Use the lever rule for single-lane cases, using the spacing between the exterior and first interior girder at 2/3 of the span length (for splay).
c) The LLDF is never to be taken smaller than the value obtained from rigid cross-section analysis (RCA). However, the lever rule (multiplied by the multiple presence factor of 1.2) controls relative to RCA for single-lane cases. For multiple-lane cases, the RCA LLDF for each number of lanes considered is multiplied by the corresponding multiple presence factor to determine the applicable LLDF value.
d) For the fatigue LLDF, no multiple presence factor is included in the calculation. The lever rule, without any multiple presence factor, governs relative to RCA (without any multiple presence factor, applied for a single lane) in many situations.

e) The skew correction factor for moment is often not applied. It is not applied in this research.
i) For multiple-span bridges, once the governing single- and multiple-lane LLDFs have been calculated for each span, apply the larger of each of these factors from all of the spans. LRFD Simon (NSBA, 2019) allows for the external definition of only one single-lane and one multiple-lane moment LLDF within its user interface.

For calculation of the live load shear in interior girders and single-lane loading,

$$g_{sint} = 0.36 + \left(\frac{S}{25\ \text{ft}} \right) \tag{10}$$

For calculation of the live load shear in interior girders and multiple-lane loading,

$$g_{sint} = 0.2 + \left(\frac{S}{12\ \text{ft}} \right) - \left(\frac{S}{35\ \text{ft}} \right)^2 \tag{11}$$

and for calculation of the live load shear in exterior girders, the empirical LLDF (used for multiple-lane cases) is determined as

$$g_{sext} = g_{sint} e_s \tag{12}$$

where

$$e_s = 0.6 + \frac{d_e}{10\ \text{ft}} \tag{13}$$

AASHTO (2017) gives the following correction factor for the shear LLDF at the obtuse corners of skewed bridges:

$$f_s = 1 + c_{1s} \left(\tan \theta \right) \tag{14}$$

where

$$c_{1s} = 0.2 \left(\frac{L t_s}{12 K_g} \right)^{0.3} \tag{15}$$

and K_g, t_s and L are as defined previously. This factor accounts for the tendency to develop larger live load shear forces in the girders at the obtuse corners of the span, due to vertical bending stiffness of the bridge deck in the short diagonal direction of a parallel skew, acting in concert with the major-axis bending stiffness of the bridge girders. These formulas do not consider any contribution from the cross-frames and diaphragms. Therefore, as skewed geometries become more severe, these equations can easily under-estimate these live load effects.

The following are salient features for the application of these equations:

1. Shear LLDF for interior girders
   a) Use the span length corresponding to the location for which the shear is being calculated.
   j) Use the K_g value from the above flexure calculations corresponding to the span for which the shear is being calculated (the variables L and K_g enter the calculation of the shear LLDF only via the skew correction factor in Equation 15). For applications with unequal girders, use the smallest weighted average K_g of all the girders, interior and exterior, in the calculation of the empirical LLDF values. This gives a larger estimate of the skew correction factor.
   b) For multiple-span bridges, conservatively use the larger value of the skew correction factors determined for each span (LRFD Simon (NSBA, 2019) allows for the external definition of only one user-defined skew correction factor within its user interface).
   c) Use the maximum S at 2/3 of the span length, for simple-span bridges with unequal girder spacing and/or splayed girders
   d) To obtain the fatigue LLDF, the result from the empirical equation is divided by 1.2 to remove the multiple presence factor (the AASHTO LRFD multiple presence factor (mpf) values are included implicitly within the empirical formulas, but the single-lane fatigue truck loading does not include any mpf).
   e) The skew correction factor is applied conservatively throughout the length of the exterior girder and the first interior girder adjacent to the obtuse corner (similar to the above, this allowed for the external definition and application of one user-defined skew correction factor within the LRFD Simon user interface; SIMON does not provide for definition of which end of the girder corresponds to the obtuse corner of the span in its user interface). It is not applied to the other girders. More precisely, the skew correction factor may be varied from its value at the bearings at and adjacent to the obtuse corner of the span to 1.0 at the mid-span of these girders, and taken as 1.0 for the remainder of the length of these girders. This can be accomplished with SIMON by not defining any skew correction factor at all in its user interface, but rather applying the skew correction factor manually and externally to the live load internal shear forces output from SIMON; this type of application would not accommodate the calculation of design shear requirements and design of the girders in SIMON though.
   k) For multiple-span bridges, once the governing single- and multiple-lane LLDFs have been calculated for each span, apply the larger of each these factors for all of the spans. LRFD Simon (NSBA, 2019) allows for the external definition of only one single-lane and one multiple-lane moment LLDF within its user interface.

2. Shear LLDF for exterior girders
   a) For single-lane loaded cases, the lever rule calculation of the shear LLDF required by AASHTO governs relative to RCA for the majority the bridges considered in this research. However, generally, in following the AASHTO rules, both of these calculations should be checked and the larger value used.
   b) For the fatigue LLDF, there is no division by the multiple presence factor for the lever rule and the RCA (the AASHTO LRFD multiple presence factor values are included implicitly within the empirical formulas, and the 1.2 factor needs to be divided out for interior girders, as explained above; the multiple presence factor simply is not included when using the direct analysis calculations such as the lever rule and the RCA).

c) For multiple-lane loaded cases, the LLDF is calculated by applying the adjustment factor e_s to the interior LLDF; however, this value is not allowed to be smaller than value obtained from a rigid cross-section analysis (RCA). Furthermore, although the single-lane shear LLDF is always smaller than the corresponding multiple-lane factor for interior girders with $S > 4$ ft, the required lever rule for single-lane cases can easily give a larger shear LLDF than the AASHTO empirical multiple-lane equation. Since the bridge with multiple traffic lanes still should accommodate single lanes, conceptually the larger LLDF from the single- and multiple-lane cases should govern. Therefore, in designing for the HL-93 live load, the larger LLDF from the single-lane (lever rule) calculation and the multiple-lane empirical factor equation should be used.
d) Apply the skew correction factor to the exterior girders in the manner described above for the first interior girders. Note that the skew correction factor is applied to the distribution factor obtained from RCA as well as from the lever rule in this research.
l) For multiple-span bridges, once the governing single- and multiple-lane LLDFs have been calculated for each span, apply the larger of each these factors for all of the spans. LRFD Simon (NSBA, 2019) allows for the external definition of only one single-lane and one multiple-lane shear LLDF within its user interface.

2.6 Deck Placement Considerations in Skewed Bridges

The most economical construction of steel bridges is unshored (Grubb et al., 2010). In this case, the bare steel structure consisting of I-girders and cross-frames have to resist their own weight and the weight of the wet concrete deck slab, deck forms and construction equipment. The deck becomes composite with the steel I-girders once the deck hardens. Depending on the length of the bridge, casting of the deck in stages may be required. If the deck is cast in stages, some portions of the deck becomes composite with the girder before other portions. As a result, the behavior of the bridge changes during staged deck casting. This aspect generally needs to be considered in analysis and design of a bridge. For continuous-span bridges, the deck in the positive moment regions is cast before the negative moment regions over the support in order to minimize cracking at the top of the slab as illustrated in Figure 13 for a parallel skew two-span continuous bridge (Grubb et al., 2010).

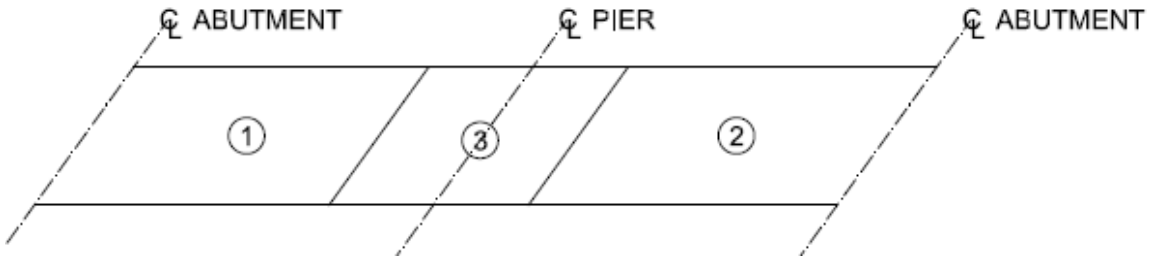

Figure 13. Typical sequence of casting concrete in decks for continuous-span bridges.

For skewed bridges, it becomes important to ensure deck placement is reasonably symmetrical laterally to minimize eccentric or unbalanced loading (Grubb et al., 2010). This reduces differential deflections between adjacent girders. It is preferable on skewed bridges where the differential deflection between girders are reasonably small to keep the finishing

machine normal to the bridge as it reduces the length required for the machine. In bridges with significant skew, the bridge may twist due to differential deflections during casting due to differential loads on the girders due to the skew. Therefore, in cases with severe skews leading to large differential deflections, it may become necessary to consider skewing the finishing machine to avoid casting significantly more concrete than needed to meet the specified bridge minimum deck thickness or roadway elevations and achieve proper bridge geometry (Grubb et al., 2010). This is illustrated in Figure 14.

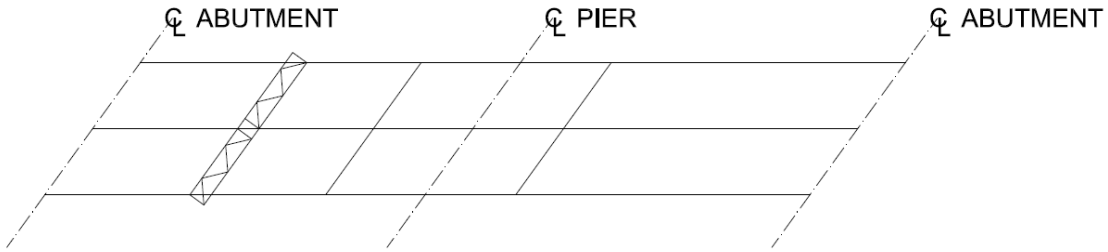

Figure 14. Orientation of screed machine for multispan continuous bridges having parallel skew.

The twisting of girders due to differential vertical deflections is explained in Section 2.1. One of the sources of differential vertical deflections may be the inaccuracy in camber calculations using LGA vertical displacement estimates. This can potentially result in twist of girders when the cross-frames are erected, if the accuracy of the predictions is different on different girders. The differential vertical deflections may cause the finished deck thicknesses to be incorrect. This is shown in Figure 15, in which δ_{deck} indicates the loss of deck thickness due to the differential vertical deflections and the twist of the girders. Hence, accuracy of the camber calculations is important in ensuring deck placement within tolerances.

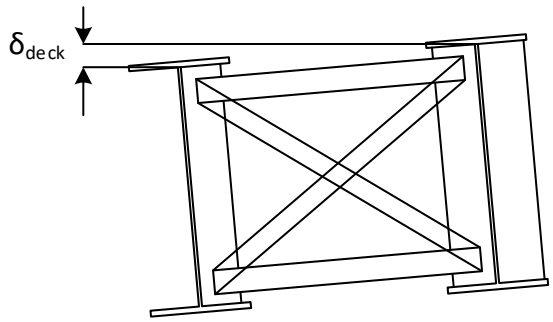

Figure 15. Loss of deck thickness due to twist of girders.

Another aspect to be considered in analysis is that the actual composite stiffness during deck placement depends on whether the concrete has hardened or not before the next pour. Grubb et al. (2010) indicate that the stiffness of previously cast portions of the concrete deck when computing deflections considering deck staging should be based on a modular ratio closer to the short-term modular ratio since the concrete does not have enough time to creep between casts.

FDOT Structures Design Guidelines Article 5.2 mandates the design of structures including consideration of the deck casting sequence. Camber diagrams are to be developed accounting for

the casting sequence. A grid, 3-D or finite element analysis currently is required by FDOT to determine girder deflections and required camber for bridges with skews greater than 20°.

2.7 State DOT Restrictions on Use of LGA or Requirements for Use of Refined Analysis

A number of states have specified explicit requirements regarding refined analysis for skewed bridges, or limits on the use of LGA. Sample requirements from a several states are as follows:

1. Florida DOT (FDOT, 2019a):
   a) Use a refined analysis method if the bridge skew index satisfies $0.2 < I_s \leq 0.6$.
   b) Use a 3D FEA if the bridge skew index, I_s, is greater than 0.6.

2. Pennsylvania DOT (PennDOT, 2015):
   a) Simple and continuous-span straight steel girder bridges with skew index $I_s \geq 0.3$ require consideration of uplift potential at acute and obtuse corners by conducting a refined analysis.
   b) Steel structures with skew angles, $\theta \geq 20°$, require a special cross-frame design and the cross-frame members must be considered as main load carrying members.
   c) The design of bearings for bridges with skew angles, $\theta \geq 20°$, require consideration of out-of-plane rotations.
   d) PennDOT does not take advantage of reductions in the LLDF for moment due to skew effects.

3. Ohio DOT (ODOT, 2007): When site conditions require the use of a superstructure type that exceeds the recommended limits set forth by AASHTO LRFD and/or this manual, a special design method may be required using a two-dimensional or three-dimensional model and some type of numerical analysis to solve the model. Examples of special design methods include grillage, finite element, finite strip and classical plate solutions.

3. DEVELOPMENT OF BRIDGE MATRIX

This chapter documents the development of a matrix of bridges for the parametric study targeted in this research. Section 3.1 summarizes a preliminary data screening of Florida bridges. Section 3.2 identifies key variables that can influence the behavior of skewed bridges, and discusses the characteristics of 57 bridges sampled from the Florida DOT inventory. Section 3.3 identifies 20 bridges selected from this group for parametric study. The bridges selected for the parametric study address the most common geometries in Florida, and provide a broad representation of bridges having skew index up to and slightly larger than 0.3. The bridges with skew indices larger than 0.3 are expected to exhibit more substantial three-dimensional behavior, but are considered important in understanding the behavior of skewed bridges and investigating the potential boundaries of when line girder analysis (LGA) gives acceptable results.

The cross-frame layout heavily influences the structural behavior of skewed bridges via transverse load path effects. Hence, six of the above 20 selected bridges are studied using an alternative cross-frame arrangement that mitigates the transverse load path effects. Section 3.3 summarizes the design of the alternative cross-frame arrangements and also explains the order in which the 26 bridges are studied. Lastly, this section explains the selection of several bridges studied to investigate the impact of staged deck placement.

3.1 Preliminary Screening of Bridges by FDOT

The parametric study plans were initiated by identification of 255 steel I-girder bridges by Florida DOT from their inventory. Of these bridges, 145 qualified as skewed bridges. Out of these 145, 33 bridges were eliminated since they were either curved structures or bridge plans were not available. Of the remaining bridges, 40% were simple-span bridges, 35% were two-span continuous bridges and the remaining 25% were either three or four-span continuous bridges. As described in Chapter 1, the focus of this research is on bridges that have a skew index up to and slightly exceeding 0.3. However, it is also prudent to study a limited number of bridges with more extreme skew to provide some testing of implications of exceeding the targeted range of skew indices. Therefore, to this end, a total of 51 bridges (23 simple-span, 24 two-span continuous, two three-span continuous bridges and two four-span continuous bridges) were selected with skew indices between 0.05 to 0.4, and an additional six bridges (three simple-span and three two-span continuous) were selected as outliers having a skew index of less than 0.05 (three bridges) or greater than 0.4 (three bridges). Therefore, the total number of bridges for further consideration was 57. These 57 bridges include two bridges (one three-span unit and another two-span unit), which were designed in the early 90s when software tools were not as advanced. These bridges were intended to provide basic sanity checks of the modern design calculations. These 57 bridges are a larger representative set of Florida DOT bridges, from which 20 were selected for the parametric study.

3.2 Data Analysis of 57 Representative Florida DOT Bridges

Based on the literature review in Chapter 2, and also recognizing the fact that design specifications are constantly updated to represent the state-of-the-art, the following variables are identified as the most pertinent for developing a Bridge Inventory Matrix:

1. Date of design
2. Applicable specifications, for the Design of Bridge
3. Bridge articulation (simple-span or continuous)
4. Span lengths (measured along the centerline of the deck)
5. Bridge framing width (between fascia girders)
6. Number of girders
7. Maximum spacing between girders
8. Minimum spacing between girders
9. Support skew angles
10. Support skew indices
11. Cross-frame layout (contiguous or staggered)
12. Cross-frame type (X, K, with or without top chord, etc.)
13. Maximum cross-frame spacing
14. Minimum cross-frame spacing
15. Averaged cross-frame spacing
16. Cross-frame fit detailing
17. Type of deck forms
18. Deck thickness
19. Deck concrete strength
20. Number of stages of deck placement
21. The ratio of the maximum girder spacing to the deck thickness
22. Girder span-to-depth ratio
23. Type of bearings

The characteristics of the 57 bridges sampled by FDOT are summarized below. Given the focus of this research, the most important variables are considered to be the bridge articulation (simple- or continuous- span construction), the skew index, the skew angles of the bearing lines, and the cross-frame type and layout. Table 2 summarizes the bridge articulation for these structures, that is, whether the bridge units are simple-span or continuous-span, and the number of spans for the continuous-span bridges.

Tables 3 through 6 list the skew angles, skew indices, span lengths and framing widths between the fascia girders for each of the above four sets of bridges, organized based on the bridge articulation. Tables 7 through 10 show, for each bridge articulation, the position of each of the bridges within a matrix composed of five ranges of the skew index, I_s, for the columns and three ranges of skew angle, θ, for the rows. The footnotes to the cells in these tables summarize noteworthy characteristics of the cross-frame framing arrangements for a number of the bridges. Additional summary tables of various other bridge parameters are presented in Appendix 1.

Table 2. Bridge articulation.

Bridge Articulation	Number of Bridges
Simple-Span	26
Two-Span Continuous	27
Three-Span Continuous	2
Four-Span Continuous	2

Table 3. Geometric properties of simple-span bridges.

	Skew Angle at supports		Skew Index at supports		Span	Framing
Identifier	Left	Right	Left	Right	Length (ft)	Width (ft)
F1	-41.5	-41.5	0.276	0.276	202	63.0
F2	-30.0	-30.0	0.062	0.062	195	21.0
F3	-35.9	-35.9	0.185	0.185	202	51.7
F4	-39.7	-39.7	0.202	0.202	212	51.7
F5	-16.5	-16.5	0.108	0.108	202	73.5
F6	21.3	21.3	0.098	0.098	191	48.0
F7	21.3	21.3	0.098	0.098	191	48.0
F8	42.0	42.0	0.183	0.183	165	33.5
F9	11.2	11.2	0.137	0.137	165	114.6
F10	-16.2	-16.2	0.154	0.154	241	128.1
F11	42.1	42.1	0.189	0.189	172	36.0
F12	-8.0	-8.0	0.027	0.027	174	33.8
F13	-29.4	-29.4	0.422	0.422	144	108.3
F14	-15.9	-15.9	0.084	0.084	183	54.0
F15	-20.6	-20.6	0.050	0.050	175	23.2
F16	-18.0	-19.0	0.064	0.068	172	34.0
F17	-43.9	-42.9	0.159	0.154	218	36.0
F18	-36.8	-36.8	0.138	0.138	195	36.0
F19	23.7	23.7	0.124	0.124	198	55.8
F20	23.7	23.7	0.149	0.149	198	66.9
F21	-43.7	-43.7	0.133	0.133	243	33.9
F22	-43.7	-43.7	0.177	0.177	243	45.1
F23	35.5	35.5	0.334	0.334	96	45.1
F24*	52.2	52.2	0.364	0.448	190	55.5, 66.2
F25	-49.4	-49.4	0.462	0.462	208	82.5
F26	7.0	7.0	0.034	0.034	172	48.0

* This is a splayed girder bridge; the widths at each end, measured between the actual or projected fascia girder tangent lines at the centerline of the bridge cross-section at the end abutments, are reported.

Table 4. Geometric properties of two-span continuous bridges.

	Skew Angle at supports*		Skew Index at supports		Span	Framing
Identifier	Left	Right	Left	Right	Length (ft)*	Width (ft)
F27	-36.1	-32.1	0.299	0.258	208.1	85.5
F28	52.9	54.3	0.190	0.200	250.5	36.0
F29	-25.6	-25.6	0.110	0.110	175.9	40.3
F30	-50.3	-50.3	0.281	0.281	250.2	58.3
F31	-50.2	-50.2	0.246	0.246	248.2	51.0
F32	-50.7	-50.7	0.372	0.372	251.8	76.6
F33	-23.4	-23.4	0.274	0.274	147.7	93.3
F34	-17.5	-17.5	0.076	0.076	166.7	40.3
F35	26.0	26.0	0.242	0.242	168.9	83.9
F36	-8.5	-8.5	0.028	0.028	128.8	24.0
F37	-9.0	-9.0	0.059	0.059	128.8	48.0
F38	-9.0	-9.0	0.054	0.054	128.8	44.0
F39	-35.9	-35.9	0.225	0.225	205.2	63.6
F40	-35.9	-35.9	0.187	0.187	205.2	52.9
F41	-17.5	-17.5	0.080	0.080	114.5	29.0
F42	52.7	52.7	0.372	0.372	169.8	48.3
F43	54.5	54.5	0.251	0.251	196.4	35.3
F44	57.2	57.2	0.460	0.460	160.0	47.5
F45	-23.0	-23.0	0.105	0.105	121.7	30.0
F46	-39.8	-39.8	0.184	0.184	216.5	48.0
F47	-38.9	-42.4	0.209	0.237	231.7	60.0
F48	-38.2	-38.2	0.386	0.386	185.2	91.0
F49	13.9	13.9	0.029	0.029	183.7	21.7
F50	15.1	15.1	0.144	0.144	171.8	91.9
F51	13.9	13.9	0.032	0.032	168.5	21.7
F52	-20.7	-20.7	0.345	0.345	115.8	106.0
F53	-10.0	-10.0	0.150	0.150	79.4	67.5

* The skew angles, skew indices at the supports, and the span lengths are reported for the span having the largest skew index.

Table 5. Geometric properties of three-span continuous bridges.

	Skew Angle at supports*		Skew Index at supports		Span	Framing
Identifier	Left	Right	Left	Right	Length (ft)*	Width (ft)
F54	58.7	58.7	0.317	0.317	182.0	35.0
F55	-38.1	-38.1	0.258	0.258	184.8	61.0

* The skew angles, skew indices at the supports, and the span lengths are reported for the span having the largest skew index.

Table 6. Geometric properties of four-span continuous bridges.

	Skew Angle at supports*		Skew Index at supports		Span	Framing
Identifier	Left	Right	Left	Right	Length (ft)*	Width (ft)
F56	0.0	50.1	0.000	0.233	184.5	36.0
F57	-53.4	-36.2	0.352	0.191	188.2	49.2

* The skew angles, skew indices at the supports, and the span lengths are reported for the span having the largest skew index.

Table 7. Classification of simple-span bridges.

		Skew Index, I_s				
		<0.1	0.1-0.2	0.2-0.3	0.3-0.4	>0.4
Maximum Skew Angle, θ (degrees)	<20	F12, F14, F16, F26	F5, F9, *F10*[+]			
	20-30	F6, F7, F15,	F19, F20			*F13*
	30-60	F2	F3, F8, F11, F17, F18, F21, F22	*F1*, *F4**	*F23(S), F24*[&]	*F25*

[+]Cross-frames parallel to skew, *Staggered cross-frame arrangement, [@]Cross-frames framing into the bearing line, [&]Splayed girder bridge.

Table 8. Classification of two-span continuous bridges.

		Skew Index, I_s				
		<0.1	0.1-0.2	0.2-0.3	0.3-0.4	>0.4
Maximum Skew Angle, θ (degrees)	<20	F34, F36, F37, F38, F41[+], F49, F51	F50, *F53*[+]			
	20-30		F29, F45[@]	*F33**, F35	*F52*	
	30-60		F28, F29, F39, F46	F30[@], F31[@], F40, *F43*[@], F47	*F27, F32*[@]*, F42, F48*	*F44*[@]

[+]Cross-frames parallel to skew, *Staggered cross-frame arrangement, [@]Cross-frames framing into the bearing line, [&]Splayed girder bridge.

Table 9. Classification of three-span continuous bridges.

		Skew Index, I_s				
		<0.1	0.1-0.2	0.2-0.3	0.3-0.4	>0.4
Maximum Skew Angle, θ (degrees)	<20					
	20-30					
	30-60				F54, F55	

Table 10. Classification of four-span continuous bridges.

		Skew Index, I_s				
		<0.1	0.1-0.2	0.2-0.3	0.3-0.4	>0.4
Maximum Skew Angle, θ (degrees)	<20					
	20-30					
	30-60			F56	F57	

A thorough review of the drawings and attributes of the above 57 bridges leads to the following principal observations:

- The bridges have been designed in the early 2000s, and therefore the specifications followed for bridge design are also those of the late 90s and early 2000s.
- The deck width of the bridges varies from a minimum of 30 ft to a maximum of 135 ft.
- Eight bridges out of the 57 have been constructed in phases (deck placed in different phases transversely). These bridges have special design considerations for the cross-frames between girders at the location of the closure pours.
- Bridge F24 is a splayed girder bridge, and has a maximum total width of 64.1 ft.
- The skew angles of the bridge bearing lines vary from a minimum of 8° to a maximum of 58°. Skew angle is important in the consideration of local "skew" effects (e.g., layover at the end bearing lines), and is an important parameter in the development of bridge matrix as is discussed later. The two-span continuous bridge F27, three-span continuous bridge F54, two four-span continuous bridges F56 and F57 have nonparallel skew at the ends and at intermediate supports. All the other bridges have parallel skew at the ends and at intermediate supports.
- The skew indices of the bridges vary from 0.03 to 0.47. Tables 3 through 6 show the maximum skew index identified at the bearings lines for all the bridges. The skew index is considered to be the principal parameter typically used for estimating potential nuisance stiffness effects associated with the development of a stiff transverse load path, and is considered to be the most important parameter in the development of bridge matrix. However, it is well known that the cross-frame framing arrangement is also a key factor in determining the magnitude of the skew effects.
- The span-to-depth ratios (span along the centerline of the bridge divided by the web depth) of the bridges varies from 19 to 40. (This data for each of the specific bridges is detailed in Appendix 1.) Most of the bridges have span-depth ratios between 25 and 35. Bridge F25 (simple-span bridge) has a span-to-depth ratio of 40. Five additional bridges (all two-span continuous bridges) have a span-to-depth ratio greater than 35. Three bridges have a span-to-depth ratio less than 25.
- The cross-frame layout of all the bridges, with the exception of a few, is contiguous with intermediate cross-frames framing perpendicular to the girders. In bridges F10, F41 and F53, where the skew angle is less than 20°, the cross-frames are parallel to the skew. In bridges

F3, F4 and F33 the cross-frames are staggered, although the stagger does not meet current recommendations in commentary of the AASHTO LRFD Specifications (AASHTO, 2017). In Bridge F33, the cross-frames are staggered although the start-points of the cross-frames are aligned along the skew. As a result, the offsets of the intermediate cross-frames are relatively small and thus the cross-frame behavior is closer to a contiguous layout than one with the recommended staggered layout.

- In continuous- span bridges F30, F31, F32, F43, F44 and F45, the cross-frames frame into the skewed bearing line at the bearings and at the pier locations, while the cross-frames or diaphragms are omitted along the skewed pier bearing line. This practice has been suggested as one option in NHI course guidance (Grubb et al., 2010), but has been found in the NHI course guidance and in the NCHRP 20-07/355 (White et al., 2015) studies to not work as well as providing cross-frames along the skewed bearing line combined with offsetting of the cross-frames within the span from the bearing locations.
- The cross-frame detailing is NLF for Bridge F43, SDLF for bridges F14, F21, F22, F24, F27, F43 and F47, and TDLF for all the other bridges. The requirement that "girder flanges and/or webs and/or stiffeners should be vertical after construction of bridge" was interpreted as Total Dead Load Fit.
- Stay-in-place metal deck forms have been used in all the bridges, in all cases where the detailed deck information is available. The specific characteristics of the deck forms was not available for five of the bridges.
- The deck thickness varies from 8 in to 9.5 in for the bridges considered. The deck concrete strength is a standard of 4.5 ksi, except in Bridge F34 where concrete of strength 5.5 ksi is used.
- Six bridges (all two-span continuous) bridges use pot bearings. All other bridges use elastomeric bearings.

3.3 Selection of Bridges for Further Study

For a skewed bridge, as the skew index of a bridge increases, the structural behavior tends to become more three dimensional due to the development of a stiff transverse path in the short diagonal direction. The stiff transverse path can be mitigated by varying the cross-frame layout as discussed in Section 2.3. Also, the local effects of skew (e.g., layover at abutment bearing lines) increase with higher skew angles. Therefore, it is rational to select bridges with a high skew index and skew angle and at the same time cover the gamut of cross-frame arrangements. Thus the bridges are categorized based on skew indices and maximum skew angles of the bridges in Tables 7 to 10.

Tables 7 and 8 show the categorization of the screened simple-span and two-span continuous bridges, respectively, on the basis of skew index and skew angle. The bridges in the last two columns of Tables 7 and 8, which are italicized, are recommended for the research study (total of nine), since skew is expected to significantly affect the structural behavior of these bridges. Bridge F1 is representative of the most common skew bridges in Florida. Hence, Bridge F1, italicized in Table 7, is recommended for the study. Apart from these bridges, four additional bridges are selected in which the cross-frame arrangements are not contiguous. These are underlined in the above tables. In addition to the above 16 bridges, all the three- and four-span continuous bridges listed in Tables 9 and 10 are selected for further study. Therefore, a total of 20 bridges were selected for further study.

In addition, the cross-frame arrangement for the bridges was varied according to recommendations in AASHTO LRFD 8th edition (AASHTO, 2017) and NCHRP 20-07/355 (White et al., 2015) as discussed in the Section 2.3 considering the following key considerations:

- Stagger the cross-frames within the spans.
- Avoid framing cross-frames into bearing locations.
- Frame cross-frames or diaphragms along the bearing line at pier supports, and offset intermediate cross-frames relative to the bearing line.
- For continuous-span bridges, provide diaphragms/cross-frames along the bearing lines with no intermediate cross-frames framing into the bearing line.

Revising the cross-frame arrangements in this way should significantly relieve stiff "nuisance" load paths in the transverse direction, and maximize the applicability of line girder analysis. By having two sets of bridges for selected critical bridges, one with a cross-frame layout that tends to cause larger transverse load path effects and one with cross-frame layout that tends to relieve these effects to the maximum extent possible, the project should be able to provide guidance for what is inferred to be current FDOT practices, as well as gains that could be achieved if FDOT were to adopt practices that are more in the direction of the recommendations in the AASHTO LRFD Specifications. Hence, the six bridges F24, F25, F44, F48, F56 and F57 were studied with an alternate cross-frame arrangement.

Thus, a total of 26 bridges were selected for the parametric studies. The key characteristics of and the overall plan framing arrangement for these 26 bridges are shown in Figures 16 to 41. The figure captions list the bridge span lengths, L_s, framing widths between the fascia girders, w_g, skew angles, θ, skew indices, I_s, and minimum offsets between non-contiguous intermediate cross-frames, or between intermediate cross-frames and bearing lines, normalized by the largest flange width within the corresponding girder unbraced length, O_{min}/b_f. Where the girder spacing is unequal, that attribute is marked. Plan sketches of the other 31 bridges not selected from the set of the 57 bridges sampled by FDOT are shown in Appendix 2.

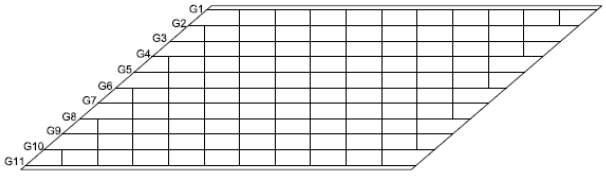

Figure 16. Bridge 1 (F25) (L_s = 208 ft; w_g = 82.5 ft; θ = 49.4°, 49.4°; I_s = 0.46; O_{min}/b_f = 4.20).

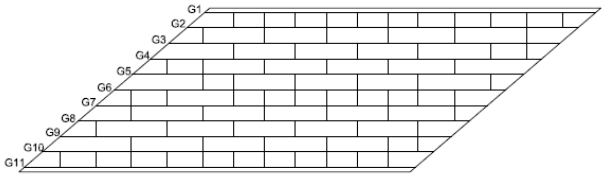

Figure 17. Bridge 2 (F25 Alt) (L_s = 208 ft; w_g = 82.5 ft; θ = 49.4°, 49.4°; I_s = 0.46; O_{min}/b_f = 4.00).

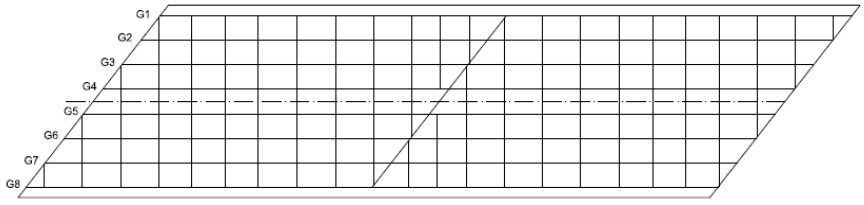

Figure 18. Bridge 3 (F48) (L_s = 185 ft, 185 ft; w_g = 91 ft; θ = 38.2°, 38.2, 38.2°; I_s = 0.39; O_{min}/b_f = 0.00).

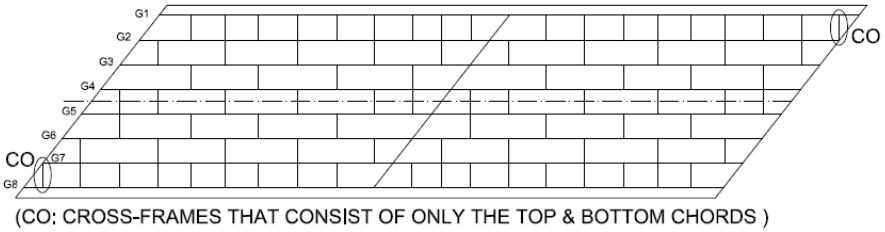

Figure 19. Bridge 4 (F48 Alt) (L_s = 185 ft, 185 ft; w_g = 91 ft; θ = 38.2°, 38.2, 38.2°; I_s = 0.39; O_{min}/b_f = 4.00).

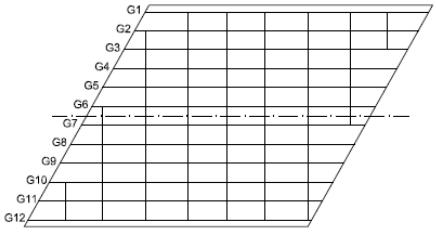

Figure 20. Bridge 5 (F13) (L_s = 144 ft; w_g = 108 ft; θ = 29.4°, 29.4°; I_s = 0.42; O_{min}/b_f =1.05).

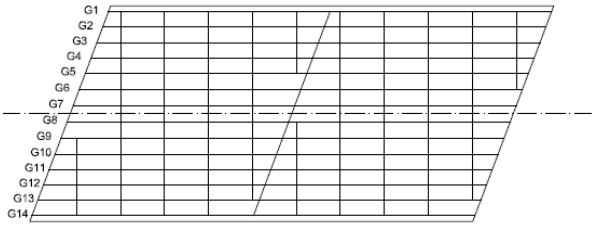

Figure 21. Bridge 6 (F52) (L_s = 116 ft, 116 ft; w_g = 106 ft; θ = 20.7°, 20.7°, 20.7°; I_s = 0.35; O_{min}/b_f = 1.73; unequal girder spacing).

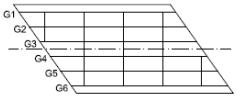

Figure 22. Bridge 7 (F23) (L_s = 96 ft; w_g = 45.1 ft; θ = 35.5°, 35.5°; I_s = 0.33; O_{min}/b_f = 2.18).

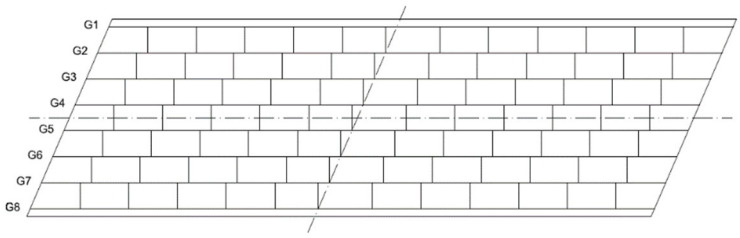

Figure 23. Bridge 8 (F33) (L_s = 148 ft, 173 ft; w_g = 93.3 ft; θ = 23.4°, 23.4°, 23.4°; I_s = 0.27; O_{min}/b_f = 3.15).

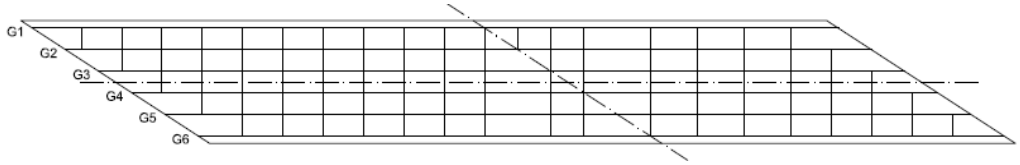

Figure 24. Bridge 9 (F44) (L_s = 202 ft, 158 ft; w_g = 57.5 ft; θ = 57.2°, 57.2°, 57.2°; I_s = 0.47; O_{min}/b_f = 0.00).

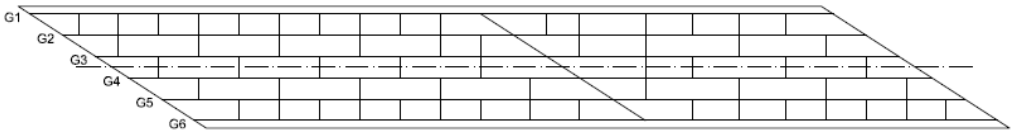

Figure 25. Bridge 10 (F44 Alt) (L_s = 202 ft, 158 ft; w_g = 57.5 ft; θ = 57.2°, 57.2°, 57.2°; I_s = 0.47; O_{min}/b_f = 4.00).

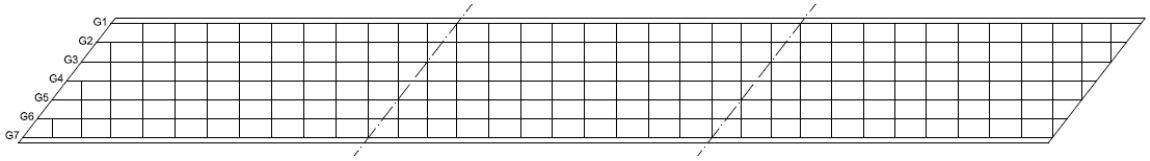

Figure 26. Bridge 11 (F55) (L_s = 188 ft, 186 ft, 185 ft; w_g = 61 ft; θ = 38.1°, 38.1°, 38.1°, 38.1°; I_s = 0.26; O_{min}/b_f = 0.00).

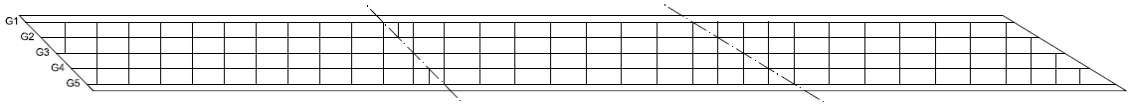

Figure 27. Bridge 12 (F54) (L_s = 202 ft, 187 ft, 182 ft; w_g = 35 ft; θ = 44.7°, 44.7°, 58.7°, 58.7°; I_s = 0.32; O_{min}/b_f = 0.00).

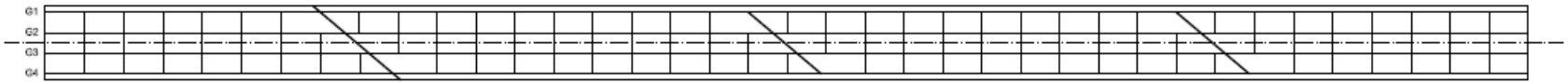

Figure 28. Bridge 13 (F56) (L_s = 185 ft, 253 ft, 253 ft, 186 ft; w_g = 36 ft; θ = 0°, 50.1°, 50.1°, 50.1°, 0°; I_s = 0.23; O_{min}/b_f = 2.40).

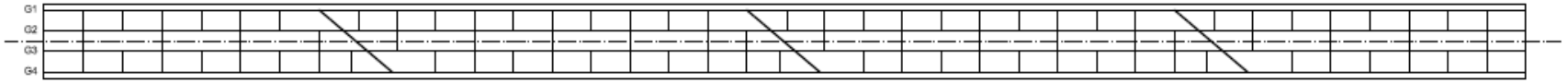

Figure 29. Bridge 14 (F56 Alt) (L_s = 185 ft, 253 ft, 253 ft, 186 ft; w_g = 36 ft; θ = 0°, 50.1°, 50.1°, 50.1°, 0°; I_s = 0.23; O_{min}/b_f = 4.00).

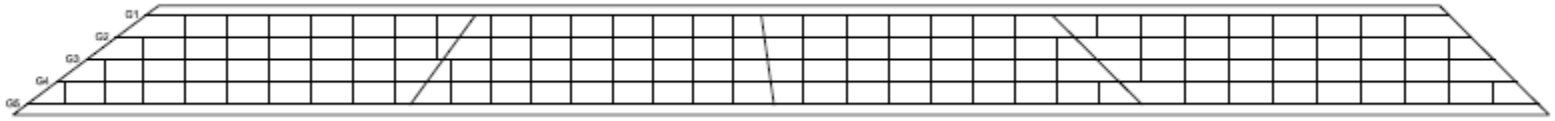

Figure 30. Bridge 15 (F57) (L_s = 188 ft, 156 ft, 159 ft, 226 ft; w_g = 49.2 ft; θ = 53.4°, 36.2°, 8°, 45.3°, 45.3°; I_s = 0.32; O_{min}/b_f = 1.45).

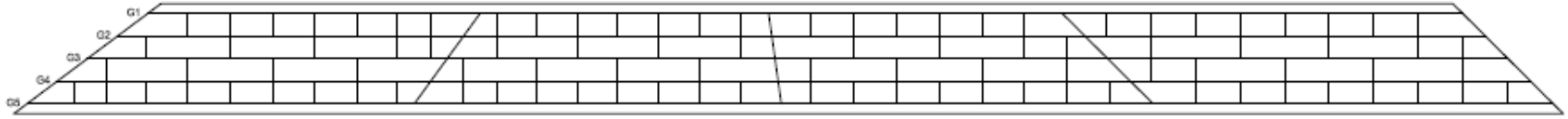

Figure 31. Bridge 16 (F57 Alt) (L_s = 188 ft, 156 ft, 159 ft, 226 ft; w_g = 49.2 ft; θ = 53.4°, 36.2°, 8°, 45.3°, 45.3°; I_s = 0.32; O_{min}/b_f = 4.00).

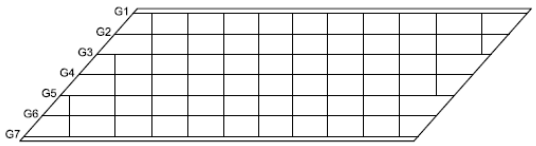

Figure 32. Bridge 17 (F1) (L_s = 202 ft; w_g = 63 ft; θ = 41.5°, 41.5°; I_s = 0.28; O_{min}/b_f = 2.15).

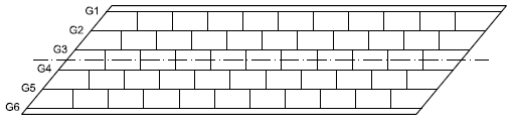

Figure 33. Bridge 18 (F4) (L_s = 212 ft; w_g = 51.7 ft; θ = 39.7°, 39.7°; I_s = 0.20; O_{min}/b_f = 3.23).

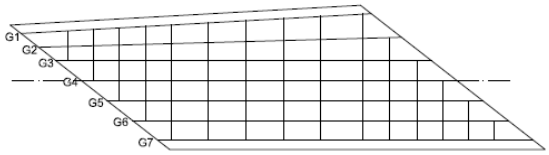

Figure 34. Bridge 19 (F24) (L_s = 196 ft; w_g = 55.5 to 66.2 ft; θ = 52.2°, 52.2°; I_s = 0.45; O_{min}/b_f = 2.30; unequal girder spacing).

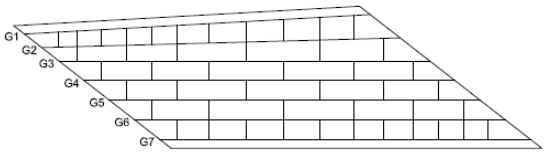

Figure 35. Bridge 20 (F24 Alt) (L_s = 196 ft; w_g = 55.5 to 66.2 ft; θ = 52.2°, 52.2°; I_s = 0.45; O_{min}/b_f = 4.00; unequal girder spacing).

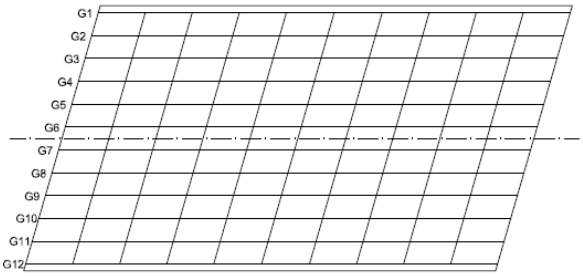

Figure 36. Bridge 21 (F10) (L_s = 241 ft; w_g = 128 ft; θ = 16.2°, 16.2°; I_s = 0.15; O_{min}/b_f = L_b/b_f).

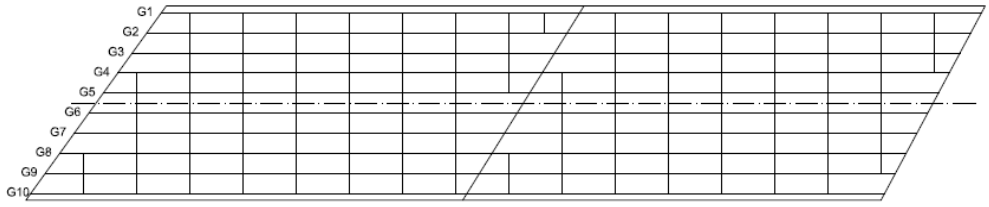

Figure 37. Bridge 22 (F27) (L_s = 204 ft, 195 ft; w_g = 85.5 ft; θ = 36.1°, 32.1°, 28.4°; I_s = 0.31; O_{min}/b_f = 2.63).

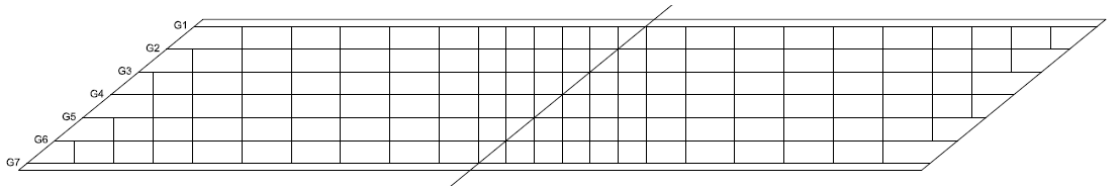

Figure 38. Bridge 23 (F32) (L_s = 252 ft, 252 ft; w_g = 84.2 ft; θ = 50.7°, 50.7°, 50.7°; I_s = 0.37; O_{min}/b_f = 0.00).

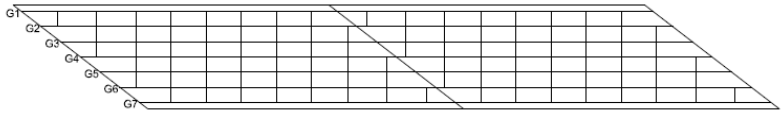

Figure 39. Bridge 24 (F42) (L_s = 170 ft, 170 ft; w_g = 48.3 ft; θ = 52.7°, 52.7°, 52.7°; I_s = 0.37; O_{min}/b_f = 2.31).

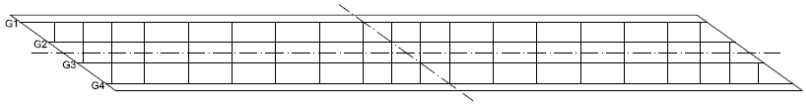

Figure 40. Bridge 25 (F43) (L_s = 196 ft, 196 ft; w_g = 35.3 ft; θ = 54.5°, 54.5°; I_s = 0.25; O_{min}/b_f = 0.00).

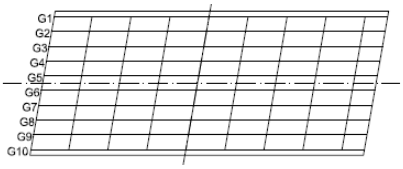

Figure 41. Bridge 26 (F53) (L_s = 79.4 ft, 92 ft; w_g = 67.5 ft; θ = 10°, 10°; I_s = 0.15; O_{min}/b_f = L_b/b_f).

Bridges F24, F25, F44 and F48 are parallel skew bridges. The modifications for these bridges included adding bearing-line cross-frames at the piers (in bridges which do not have bearing-line cross-frames, offsetting the intermediate cross-frames). The alternate cross-frame arrangements are shown in Figures 17, 19, 25 and 35. In addition, the intermediate cross-frames were staggered to soften the stiff transverse path that develops between the two obtuse corners of the spans. Bridges F56 and F57 are nonparallel skew bridges. The modifications for these bridges included staggering of intermediate cross-frames by positioning their work points in a "fanned" pattern between the skew angles at the ends of the span. The alternate cross-frame arrangements are shown in Figures 29 and 31.

In general, the bridges that were considered apt to cause the most difficulty were analyzed first, e.g., the bridges were studied largely in the order of decreasing skew indices and skew angles. These results were used to refine the focus in the study of other bridges. Therefore, findings about the behavior of the "difficult" bridges was able to potentially influence the identification of additional bridges to be studied. The results led to the consideration potentially to not study Bridges 21 and 26. However, in consultation with the research advisor group for the project, it was decided that these bridges would provide valuable insights regarding the behavior and design of bridges having the smallest skew angles and skew indices.

Furthermore, staged deck placement analysis was carried out for four bridges out of the 26 bridges, the two-span continuous bridges F48 and F48 with an alternative cross-frame arrangement, the three-span continuous bridge F55 and a four-span continuous bridge F57.

The 26 bridges were numbered 1 to 26 in the order they were studied. Figures 16 to 41 show the 26 bridges and provide a summary of its characteristics that include the skew angles at the bearing lines, span lengths, bridge framing width and the skew index. The bridge span lengths are denoted by L_s in the order of the spans, separated by commas. The variable w_g denotes the bridge framing width between the fascia girders. The skew angle magnitudes (θ) are reported at each bearing line, beginning from the left end abutment and moving towards the right end of the bridge. The direction of skew can be identified from the plan sketch. The skew index, I_s, is calculated as the maximum value from Equation 1 considering each bearing line and the adjacent span lengths.

As an example, consider Bridge 8 (Figure 23). This bridge is two-span continuous. The first and second spans of Bridge 8 have lengths of 148 and 173 ft. The bridge framing width is 93.3 ft. The skew angle magnitudes (23.4°) are reported at each bearing line, beginning from the left end abutment and moving towards the right end of the bridge. The direction of skew can be identified from the plan sketch. Considering a second example, the four-span continuous Bridge 15 (Figure 30) has five bearing lines, the skew angles of which are 53.4°, 36.2°, 8°, 45.3°, and 45.3° respectively. The first two of these bearing lines have a clockwise skew angle whereas the last three have a counterclockwise skew angle. This bridge has four spans with span lengths of 188, 156, 159 and 226 ft.

In summary, the selected bridges numbered according to the order of study and classified according to articulation are:

- Simple-span bridges 1(F25), 2(F25 Alt), 5(F13), 7(F23), 17(F1), 18(F4), 19(F24), 20(F24 Alt), 21(F10)
- Two-span continuous bridges 3(F48), 4(F48 Alt), 6(F52), 8(F33), 9(F44), 10(F44 Alt), 22(F27), 23(F32), 24(F42), 25(F43), 26(F53)
- Three-span continuous bridges 11(F55), 12(F54)
- Four-span continuous bridge 13(F56), 14(F56 Alt), 15(F57), 16(F57 Alt)

4. MODELING CONSIDERATIONS AND CALCULATION OF RESPONSES

In this research, the commercial software package CSiBridge V21.0.2 (CSi, 2019) was used for the 3D finite element analysis (3D FEA) and the AISC/NSBA LRFD Simon V10.3.0.0 software (NSBA, 2019) was used for the line girder analysis (LGA) of the bridges. The design of a parametric study includes numerous considerations related to definition of loads, creation and execution of the analysis models, and collection of responses. It is imperative that calculation of loads for LGA is consistent with the calculation of loads in 3D FEA. For example, the dead load reactions from the LGA models of the different girders ideally should sum to the total dead load reactions within the 3D FEA model. This chapter summarizes details regarding the modeling idealizations, calculation of loads and calculation of responses in CSiBridge and LRFD Simon. This is followed by an explanation of the procedures and processes developed for efficient execution of the parametric studies comparing LGA and 3D FEA for the suite of 26 bridges identified in Chapter 3.

4.1 Modeling Idealizations for 3D FEA and LGA

4.1.1 3D Finite Element Analysis

The following are key 3D FEA modeling idealizations employed in CSiBridge in the conduct of this research:

1. Frame and shell elements are used by CSiBridge in the modeling of various components of the bridge. “Mixed” frame and shell modeling of the girders is used, where the web is modeled by shell elements and the flanges are modeled using frame elements. The connection plates are modeled using frame elements. Cross-frames are modeled using frame elements with moment releases at the ends. The deck is modelled using shell elements.
2. To account for the reduced axial stiffness of single angle members in cross-frames due to the eccentricity at end connections, a stiffness reduction factor of 0.65 is used. This is based on the recommendations in AASHTO LRFD Article C4.6.3.3.4.
3. Cross-frames along skewed bearing lines are often connected to the girder connection plates by means of a bent gusset plate. The bent gusset plate provides additional flexibility to the end bearing-line cross-frames that potentially can be beneficial in reducing the skew effects. The bent-plate connection flexibility is not included in the 3D FEA models developed in this research. It is assumed that the connection detail to the girders is such that any additional deformations occurring at the connections are negligible.
4. CSiBridge has the capability to analyze a bridge construction sequence using a staged construction load case. This capability is used to study the effects of staged deck placement in this research. In addition, in this work, a staged construction load case is employed for analyzing noncomposite and composite dead load, as well as for modeling steel dead load fit (SDLF) detailing effects. These modeling procedures are described in detail in Section 4.5.
5. Live load effects are calculated by CSiBridge using “floating lanes” as explained in Section 4.2.5.
6. Elastomeric bearings are employed in all the bridges studied in this research. A nominal stiffness of 100 kip/ft is used in the lateral and longitudinal directions. It is assumed that the

lateral displacements at the elastomeric bearings are smaller than the tolerances necessary to engage with anchor bolts, guides or other restraining devices, and therefore the lateral displacements are restrained only by the lateral stiffness of the elastomeric bearing pads. As discussed by Grubb et al. (2010), rigid modeling of lateral restraint conditions the bearing locations commonly results in unrealistic large lateral forces that then must be equilibrated within the bridge system model.

4.1.2 Line Girder Analysis

Line girder analysis was set up based on the discussion in Section 2.5. Line girder analysis commonly was carried out for exterior girder(s) (see Section 4.4 for more details), the first interior girder and a "representative" central interior girder. In this project, LRFD Simon was used for line girder analysis of bridges. The following are the specifics of how the line girder analysis was conducted using LRFD Simon:

1. The aspects of calculation of dead loads are explained in Section 2.5.1. For all the bridges considered in these parametric studies, all the dead loads are distributed equally to all the girders.
2. Staged construction can be simulated in LRFD Simon using stage-wise partial uniformly distributed loads.
3. DC1, DC2 and DW loads are calculated for each girder as discussed in Section 4.2. LRFD Simon accepts the input of these loads as uniform loads.
4. Live load calculations are based on distribution factors calculated as per Section 2.5.2. However, the position of the HL-93 truck is based of influence line diagrams for both positive and negative moments. This is handled automatically in LRFD Simon.
5. LRFD Simon provides results for all the design and service load cases including the load case from the concrete deck placement. These can be readily used in the calculation of cambers.

4.2 Load Definitions and Their Calculations in CSiBridge and LRFD Simon

This section explains the details pertaining to the definition of loads in CSiBridge and LRFD Simon to maintain consistency in 3D FEA and LGA such that the overall results from each of these two analysis types can be compared within a broader context.

The bridge analyses in the parametric studies have been conducted for the following seven specific load cases:

1a. Steel Dead Load (SDL/SDLF), including the influence of steel dead load fit (SDLF) effects,

1b. Steel Dead Load (SDL/NLF), not including the influence of steel dead load fit (SLDF) effects, i.e., based on No-Load Fit,

2a. Concrete Dead Load (CDL), neglecting any influence of prior setup of the concrete during deck placement, or due to staged deck placement or phased construction,

2b. Concrete Dead Load (CDL/SDP), considering the influence of staged deck placement (staged deck placement effects will be studied only for four bridges, as discussed in Section 3.3),

3. Barrier Rail Load (RL),

4. Future Wearing Surface and Utilities Load (DW),

5. Vehicular Live Load (LL),

6a. Live Load with a derived HL-93 vehicle that consists of 25% truck load and 100 % of the lane load (LL Simon),

6b. Live Load with a derived HL-93 vehicle that consists of only the truck load (LL Truck Only),

7. Fatigue Live Load (Fatigue LL).

The bridges were analyzed for all of these loadings as unfactored loads. This facilitated the assessment of how the straight skewed bridges considered respond under the different load types. The responses for a given AASHTO LRFD Load Combination was obtained by superimposing the results from the appropriate load cases. All of the analyses were material linear elastic and geometrically linear (i.e., first-order linear elastic) analyses, for which superposition is valid.

The first three load cases provide information about the bridge responses in their noncomposite (DC1) condition. The fourth load case illustrates the influence of staged deck placement. In the fourth case (Case 2b), the concrete deck stiffness for the portions of the deck placed in previous stages is set to correspond to short-term composite loading (modular ratio of n) while the stiffness of the concrete deck is taken to be negligible for the new loading at a given stage. For the fifth and sixth load cases (RL and DW), the stiffness of the entire concrete deck is set to the long-term composite loading (modular ratio of 3n) value. Lastly, for the vehicular live load cases, the stiffness of the entire concrete deck is set to its short-term composite loading value. The vehicular live load analyses are conducted to determine the maximum and minimum envelope response values in all of the bridge components being assessed.

Load Case 1b is the predominant type of Steel Dead Load analysis performed in current 3D FEA and 2D Grid steel girder bridge design analysis calculations. On the other hand, Load Case 1a recognizes the correct analytical influence of the lack-of-fit of cross-frames relative to the initial no-load cambered geometry of the girders when the cross-frames are detailed for SDLF. For *straight* skewed I-girder bridges with the cross-frames detailed in this way, the girders are theoretically plumb under the steel dead load, and the corresponding steel dead load flange lateral bending stresses and cross-frame forces are zero. This matches with the steel dead load result obtained from LGA. The results from this analysis when contrasted with Load Case 1b, emphasizes that, for SDLF detailing of the cross-frames, refined 3D FEA and 2D Grid analyses generally do not provide the correct analytical steel dead load responses within the structure.

The effect of the SDLF detailing of the cross-frames on the bridge responses can be obtained by subtracting the results of Load Case 1a from the result of Load Case 1b. These results, while not generated in the parametric study, can be readily generated, given the Excel spreadsheets developed. However, it is more informative for bridge engineers to compare and scrutinize the results for SDL/SDLF and SDL/NLF (Load Cases 1a and 1b), than to study the effects of SDLF in isolation.

The following sections explain further details of the load calculations for each of the above load cases. Although the given loadings constitute the most basic load cases, setting up these basic load cases involves many "approximations" that are described in the next few sections.

4.2.1 Steel Dead Load

Steel dead load is basically the self-weight of the structural steel contained in the superstructure. This includes the steel girders, the cross-frames, and the various miscellaneous steel items including girder splice plates, girder connection plates at the cross-frame locations, girder transverse stiffeners, gusset plates and spacer plates within the cross-frames, bolts and weld material.

Calculation of steel dead load of the bridge superstructure in LRFD Simon LGA models can be summarized as:

- Within each constant-area girder segment (all the bridge girders are prismatic with stepped changes in the cross-section at field and/or shop splices in this work), the nominal steel self-weight of the girders is applied as a uniformly distributed load corresponding to the girder cross-section area times the weight density of steel (490 pcf). This load is calculated automatically in LRFD Simon.
- The total additional steel self-weight from a miscellaneous steel allowance of 5 % of the total self-weight of the girders, 130 % of any solid-web diaphragms, and 130 % of the cross-frame member self-weights, is calculated and divided by the total length along all of the steel girders. This uniformly distributed load is applied along all the girder lengths.
- The lengths of the cross-frame members and solid web diaphragms are taken as the lengths between workpoints at the centerline of the girder webs.
- The lengths of the girders are taken as the lengths between the centerline of the bearings. Girder overhangs beyond the bearing lines are neglected.

The applied loads are handled for the 3D FEA in the same manner as described for the LGA, with the following differences:

- The self-weight of the girders, diaphragms and cross-frame members is applied directly as a body load for each of these components based on the areas of the components at any given cross-section. The 5 % allowance for the steel self-weight of the girders, and the 30 % allowance corresponding to the steel self-weight of the cross-frames and solid-web diaphragms, is applied directly to the body load for all of the components. Similar to the calculations of the self-weight for the LGA, the length of all the components is determined using the distances between work points at the centerline of the girder webs. In this study, to streamline definition of diaphragms, a rectangular cross-section is specified for each of the cross-frame members composed of angle section or Tee sections. The area of the rectangular section will be the same as the area of the physical member. The height of the rectangular section will be taken as two times the distance from the top of the physical member cross-section to the centroid of the physical member cross-section. This ensures that the cross-frame chords will be modeled at the correct physical elevations in CSiBridge. The use of rectangular cross-sections for the cross-frame members does not have any impact on the

stiffnesses in the bridge model since CSiBridge uses frame elements with end releases to model the chords and diagonals.

- The girder connection plates at diaphragms and cross-frames are explicitly modelled in CSiBridge. Without modelling of the connection plates at these locations, the girder webs, represented by shell finite elements, tends to distort excessively due to the eccentricity of the cross-frame chords relative to the girder flanges. In this study, the weight density of the girder connection plates is set to zero. This simplifies the calculation of consistent self-weights (i.e., same total weight) in CSiBridge and LRFD Simon. The girder connection plate self-weights are assumed to be included within the 30 % miscellaneous steel for the cross-frames.

- Two different 3D FEA calculations are considered for the Steel Dead Load:

  (1a) Steel Dead Load, No Load Fit (SDL-NLF)

  (1b) Steel Dead Load, steel dead load fit (SDL-SDLF)

  The steel dead load (self-weight) is the same in both of these analyses. However, for SDL-NLF, the load is applied to the 3D FEA model of the bridge without considering the SDLF effects. That is, the 3D bridge model is constructed and these gravity loads are then simply "turned on." Conversely, SDL-SDLF accounts for the actual detailing of the cross-frames for SDLF. This is accomplished by using the staged construction feature in CSiBridge to analyze the bridge according to the idealization that the girders are initially stably supported on the vertical supports and the cross-frames are hung from the girders.

Regardless of how the steel self-weight is estimated, it is still largely just a basic *estimate*. The aspect of key importance for this research was that the total of the bearing vertical reactions obtained from the 3D FEA and obtained by summing all the reactions from the LGA idealizations should be the same value (within say 1 percent). This allows for us to state that the 3D FEA and LGA loadings are indeed "equivalent."

4.2.2 Concrete Dead Load

In this study, concrete dead load is taken as the total weight of the concrete bridge deck, including the weight of stay-in-place metal deck forms (and the concrete within the flutes of these forms), the concrete in the overhangs and the concrete within the haunches (i.e., bolsters) over the top of the steel girders.

For the majority of the cases studied, where staged-deck placement is not considered, the total weight of the wet concrete is calculated by considering:

- The weight density of concrete, taken as 150 pcf, times the area of the concrete within the bridge cross-section, obtained as the sum of:
  a) The area of the rectangular structural portion of the deck equal to the structural thickness multiplied by the overall width of the deck.
  b) The area of a sacrificial overlay thickness times the overall width of the deck. (In this work, based on guidance from the FDOT Structural Design Guidelines (FDOT, 2019a)

and from the FDOT steering group for the research, the sacrificial overlay thickness is taken as 0.5 inches for decks with a thickness greater than or equal to 8.5 inches. Furthermore, the sacrificial overlay thickness is taken equal to zero for decks with 8.0 inch thickness or less, and it is taken as the specified depth minus 8.0 inches for decks between 8.0 and 8.5 inches in thickness.)

c) The area of the concrete within the girder haunches, taken as the haunch depth minus the thickness of the girder top flange times the flange width for all the girders,
d) A tapered triangular shaped area of the concrete within the two deck overhangs, located below the structural thickness of the deck and varying from zero at the edge of the deck to the haunch depth minus the flange thickness at the tip of the fascia girder top flanges.

- The weight of stay-in-place metal deck forms between the girder flanges, including the weight of the concrete within the flutes of the forms, taken as 20 psf as specified in the FDOT SDG (FDOT, 2019a).

These loads are divided by the total number of girders, and then applied as equal line loads in LGA to each of the girders in the bridge cross-section.

As a simplification, the temporary bridge form loads on the deck overhangs are neglected. This simplification is applied both in the LGA and in the 3D FEA, so that the LGA and 3D FEA results can be compared on a consistent basis. No specific construction loads, such as screed rail loads, wheel loads from a screed machine, walkway and other related loads supported by the bridge during the deck placement, and loads from the construction operations, are considered in this work, either for the LGA or for the 3D FEA. In conclusion, the wet concrete loads on the overhangs, as modeled, are taken as a representative set of loads for comparison of the LGA and 3D FEA calculations.

Handling of the concrete dead load for staged deck placement is addressed in LRFD Simon by subdividing the girder into lengths corresponding to each stage. The sequence of the placement of these lengths is then specified. LRFD Simon analyzes these successive placements, modeling the concrete in the previously placed stages as composite.

In CSiBridge, the weight of the rectangular structural portion of the bridge deck is considered directly as a body load. All of the other contributions to the concrete dead load are determined in a similar fashion to that described for the LGA, then applied as a uniformly distributed load across the total area of the bridge deck.

It should be noted that this idealization gives a relatively simple approximation of the various torsional effects on the fascia girders from the deck overhangs. In CSiBridge 3D FEA models, the torsion from the overhang is applied entirely to the corresponding fascia girder. In the physical bridge, the above overhang loads, are applied to the corresponding fascia girder during the deck placement. However, when the overhang forms are removed, the direct torsion on the fascia girder from the overhang support brackets is released and the fascia girder exhibits an elastic rebound due to the release of this torsion. In the remaining structure, the concrete dead load on the overhangs is resisted predominantly by the cantilever action of the deck over the top of the fascia girder. Therefore, the torsional moments on the fascia girders, in their final constructed condition, are over-estimated by the “Wet Concrete Loading” procedure in CSiBridge.

The 3D FEA and LGA solutions can be compared consistently based on this approximation. The flange lateral bending stresses in the fascia girders are estimated using AASHTO LRFD Equation C6.10.3.4.1-2 for the purpose of a consistent comparison with 3D FEA estimates. This is explained in more detail in Section 5.5.10. Further, the total concrete dead load on the bridge is the same in the 3D FEA and LGA solutions.

4.2.3 Barrier Rail Load

Barriers composed of rails that serve as traffic barriers are placed near the edges of the bridge width and extends throughout the length of the bridge. Barrier rails are erected/installed after the deck hardens and hence the load is applied to the composite bridge section.

In this study, various aspects of calculation of barrier rail loads can be summarized as:

- The weight of the barrier rails is applied as a DC2 load, resisted by the long-term section of the girders. Consideration of barrier rail load in the bridge studies is useful to gage the ability of 1D LGA vs 3D FEA to evaluate the bridge response to a long-term composite superimposed dead load that is applied at concentrated positions across the bridge width. In this study, barrier rail load corresponding to 36 inch single-slope rail was applied in all the bridges. Referring to FDOT (2019a) SDG Table 2.2-1, the 36 inch single-slope rail weighs 430 plf.
- No other barrier loads, sidewalk loads, etc. that would typically be applied as DC2 loads are considered in this research.

In LGA, the total load from the barrier rails, assumed to be two rails, one on each side of the bridge deck, is divided by the total number of girders to obtain an equal line load applied to each of the girders in the bridge cross-section.

In the 3D FEA model, the barrier rail loads are applied to the concrete deck at the approximate centroid of the 36 inch single-slope rails. This is taken as nine inches from the edges of the deck.

4.2.4 Future Wearing Surface and Utilities Load

Weight of non-integral wearing surface and utilities supported by the bridge constitute the future wearing surface and utilities load.

In this study, various aspects of calculation of future wearing surface and utilities loads can be summarized as:

- A future wearing surface load of 15 psf = (150 pcf) (1.2 inches) is applied to the overall width of the deck. This is divided by the total number of girders in the bridge cross-section to obtain an equal nominal DW load applied to each of the bridge girders, using the long-term composite properties of the girders.
- No other utility loads are considered in the bridge studies conducted in this research.

In LGA, the total future wearing surface load on the bridge is divided by the total number of girders to obtain an equal line load applied to each of the girders in the bridge cross-section.

In 3D FEA, the future wearing surface loads are as specified for the LGA, but are applied directly as a 15 psf load to the full deck area in the CSiBridge models.

4.2.5 Vehicular Live Load

Analysis of live load involves determining the most critical locations of the AASHTO design vehicular live load to estimate the maximum critical responses for the various bridge components. The AASHTO LRFD Specifications require the consideration of *n* live load lanes for a given bridge, where *n* is the number of 12 ft wide lanes that can be placed between the curb lines on the deck. These lanes are to be moved or "floated" across the width of the bridge between the curbs disregarding the presence of medians and sidewalks, to obtain the most critical live load response. In this study, which utilizes a geometric linear and elastic analysis, the maximum responses are obtained using influence surfaces. For a line girder analysis, the maximum responses are obtained using live load distribution factors (LLDF) and influence line diagrams.

In the study, pedestrian live load or special vehicular live loads (e.g., permit loadings, etc.) is not considered. HL-93 vehicular live load defined in the AASHTO LRFD Specifications is used to evaluate the sufficiency of line girder analysis for the bridges to be studied. For the overall system analysis of the bridges studied, the tandem loading in the HL-93 load definitions will never govern. Therefore, the tandem loading is not considered in this project.

<u>Modeling Vehicular Live Load within CSiBridge:</u>

CSiBridge v21 provides very powerful features that greatly facilitate the definition and application of the AASHTO LRFD HL-93 live load model. The HL-93 live load definitions from AASHTO (2017) Article 3.6.1.3.1 are already included in CSiBridge. The application of this model to a bridge is defined in a succinct way by defining a floating lane set. The overall width of the bridge that is accessible to vehicular live load is taken as the width between the exterior barrier rails in this project. This is specified as the lane width for the floating lane set. Given the standard lane width of 12 ft, the total width of the floating lane set is divided by 12 ft, then rounded down to the closest integer, *n*. This is the number of live load lanes that the width of the bridge can accommodate. CSiBridge then "floats" the *n* lanes across the width of the bridge, i.e., it positions the lanes at various locations across the bridge width, to generate the maximum live load effects. Within each lane, the HL-93 loading rules apply (again, the tandem load is not included in our analyses). That is, the trucks are positioned such that their wheels are 2.0 ft or more from the lane longitudinal edges. The 10 ft wide lane loads are positioned against either edge of the 12 ft wide lanes. For negative moment between points of contraflexure under uniform loads on all spans and for the calculation of pier reactions, 90% of the effect of two design trucks spaced a minimum of 50 ft between the lead axle of one truck and the rear axle of the other truck, combined with 90% of effect of the design lane load is considered. The distance between the 32 kip axles of each truck is taken as 14 ft. Within the definition of the HL-93 vehicle loading, the dynamic load allowance factor of 1.33 is included in the definition of the "nominal" live load.

Within the floating lane set, CSiBridge considers 1, 2, 3, 4 and up to *n* lanes. For the case of one lane positioned within the width of the floating lane set for maximum effect, a multiple

presence factor of 1.2 was employed. For two and three lanes, multiple presence factors of 1.0 and 0.85 are employed. For four or more lanes, a multiple presence factor of 0.65 is used (following the AASHTO LRFD requirements). Floating lanes within a lane set are not allowed to cross or overlap each other. CSiBridge calculates the amount that the floating lanes are allowed to move transversely, based on the total width of the lane set, and the standard 12 ft lane width.

When positioning the floating lanes at a given station, the following possibilities are considered:

- All lanes adjacent in a single group with no intermediate gaps.
- A single gap between two groups of lanes, each group containing no gaps.

For N floating lanes in a lane set, this leads to N possible groupings. This is shown in Figure 42, from the CSiBridge Reference Manual (CSi, 2019) for the case where N = 4. For each case, the one or two groups are moved transversely to find the position that leads to the maximum response.

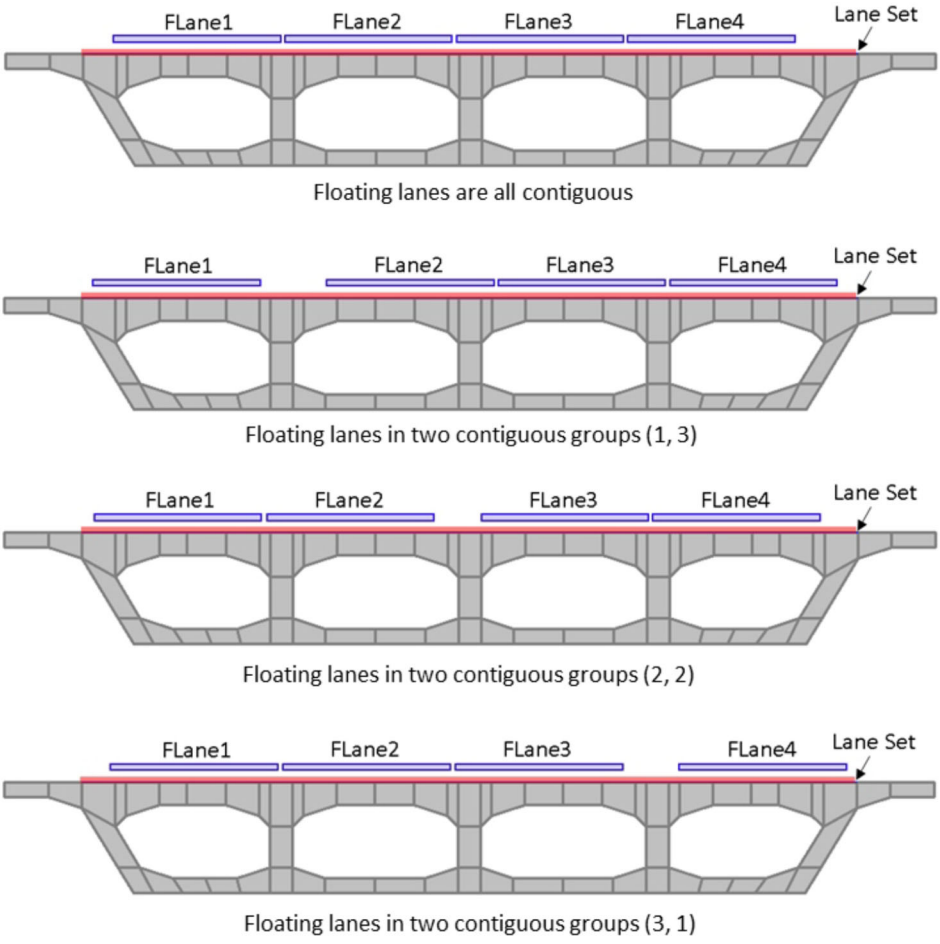

Figure 42. Transverse positioning of four floating lanes showing all possible grouping options from (CSi, 2019).

CsiBridge has lane discretization factors for moving the live loads. These are set to 10 ft in the longitudinal and transverse lane directions. That is, CSIBridge varies the positioning of the

loads in 10 ft increments, called lane-load points, to determine the influence surface ordinates of the lane. The influence surface is constructed through interpolation between the lane-load points, which is further used in determining maximum load effects. In addition, the discretization along the lane is set such that it is never greater than 1/10 of the span length. AASHTO LRFD requires consideration of wheel loads up to 1 ft from the barrier rail (curb) for design of the overhangs. However, the focus in our project was on the overall bridge system design. As such, both edges of all the lanes are considered as "interior edges," meaning that wheel loads do not need to be placed closer than 2 ft from the edge of the lane.

CSiBridge considers traffic moving in either direction within a given lane in obtaining the maximum live load effects. For the bridges considered in this study, the live load was defined by creating a single floating lane set.

Modeling Vehicular Live Load within LRFD Simon:

In LRFD Simon, live loads are applied to the girders based on AASHTO LRFD live load distribution factors (LLDF), as described in Section 2.5.2. Simon conducts structural analysis to obtain the maximum live load effects, using influence line diagrams to obtain the maximum and minimum envelopes for various response quantities.

4.2.6 Vehicular Live Load for Deflection Calculations

For optional live load deflection evaluation, AASHTO LRFD Specification (AASHTO, 2017) Article 3.6.1.3.2 states:

If the owner invokes the optional live load deflection criteria specified in Article 2.5.2.6.2, the deflection should be taken as the larger of:

1. That resulting from the design truck alone, or
2. That resulting from 25% of the design truck taken together with the design lane load

Further, AASHTO LRFD Specification (AASHTO, 2017) Article 2.5.2.6.2 states:

1. The vehicular load shall include the dynamic allowance.
2. When investigating the maximum absolute deflection for straight girder systems, all design lanes shall be loaded, and all supporting components should be assumed to deflect equally.
3. For composite design, the stiffness of the design cross-section used for the determination of deflection should include the entire width of the roadway and the structurally continuous portion of the railings, sidewalks and median barriers (we are assuming none of these are structurally continuous in our calculations).
4. For straight girder systems, the composite bending stiffness may be taken as the stiffness determined as specified above, divided by the number of girders.
5. The live load portion of Load Combination Service I of Table 3.4.1-1 should be used including the dynamic load allowance, IM. Basically, a live load multiplier of 1.0 times 1.33 should be used. In addition, the reference to Table 3.4.1-1 indirectly brings in the consideration of the multiple presence factor, since Article 3.4.1 indicates the use of the multiple presence factor with Table 3.4.1-1.

6. The live load shall be taken from Article 3.6.1.3.2, which brings in the requirement of 25 % of the HL-93 truck with the lane load, or the HL-93 truck alone.

Summarizing, all of the above gives the live load distribution factor of $m^*(N_L/N_g)$, applied with 25 % of the HL-93 truck plus the lane load, or the HL-93 truck alone, where, where m is the multiple presence factor, N_L is the maximum number of lanes that can be accommodated on the bridge and N_g is the number of girders in the bridge. The distribution factor obtained is used in calculating an average estimate of live load deflection.

However, Grubb et al. (2010) note that the assumption of equal deflections is not applicable for bridges that have a skew angle exceeding 20°. This is because the differential deflections that occur between girders is more important than an average estimate of live load deflection obtained from AASHTO optional live load deflection evaluation. Hence, in conclusion, live loading ranging from one to the maximum number of lanes that can be accommodated on the bridge should be employed in the calculation of live load deflection estimates.

Separate load cases 6a, which is composed of a derived HL-93 vehicle that consists of 25% truck load and 100 % of the lane load and 6b, which is composed of a derived HL-93 vehicle that consists of only the truck load were considered for the investigation of girder deflections under live load. An impact factor of 1.33 was applied to the truck load in both load cases 6a and 6b as recommended by AASHTO LRFD Specifications.

In order to simulate load cases 6a and 6b in CSiBridge, derived HL-93 vehicles pertaining to load cases 6a and 6b were defined from the base vehicle used in the general live load case 5. LRFD Simon automatically calculates the live load deflection for load cases 6a and 6b using the distribution factor m^*N_L/N_g and presents the maximum of the two deflections.

4.2.7 Fatigue Live Load

AASHTO (2017) Article 3.6.1.4.1 defines the vehicle for evaluation of fatigue as follows:

1. The fatigue load shall be one design truck or axle, but with a constant spacing of 30 ft between the 32 kip axles.
2. A dynamic load allowance of 15% (1.15) shall be applied to the static effects of the design truck.

Analysis for fatigue involves positioning the fatigue vehicle in a single lane that spans throughout the bridge length and the roadway width, to obtain the most critical effects. This was achieved in CSiBridge by defining a single lane for fatigue that spans throughout the length and between the rails in the transverse direction. The AASHTO LLDF calculation used in the evaluation of fatigue live load response in LGA is as described in Section 2.5.2.

4.3 Consideration of Girder Axial Forces Obtained from the CSiBridge 3D FEA Models

The elastic 3D behavior of a bridge depends on the relative stiffness of the composite concrete deck and the steel I-girders which in turn influences the distribution of forces between the concrete deck and the steel girders. When analyzing composite girders using the long-term elastic modulus of concrete, for sustained superimposed dead loads, and for short term elastic

modulus of concrete for vehicular live loads, the portion of slab that acts composite to each steel I-girder is calculated based on the tributary width of the slab for each girder. This assumption has been found to be reasonable and is commonly used in the design of composite bridge girders.

Ideally, in the absence of longitudinally applied axial loads (such as may occur in some cases due to the combination of the bridge skew and specifics of bridge bearing constraints), the axial forces in a composite girder should be zero. In other words, the portion of the slab acting compositely with each girder is such that the axial force on all the girders at a bridge cross-section is zero. This action is captured in a 3D FEA of the concrete deck and the steel I-girders.

The relative distribution of loads and thereby, the participation of the deck with each steel I-girder is also influenced by the type and location of the load. The deformed shape of the concrete deck around each steel I-girder provides an insight into the portion of deck that participates with the steel I-girder. For a uniform pressure load spread over the entire area of the bridge, the portion of deck acting with each steel girder is reasonably well approximated by the tributary widths. However, for a load such as the barrier rail load that is effectively a concentrated load applied at a particular position within the bridge cross-section, the 3D FEA can suggest that the portion of deck that participates with the different girders is different than the tributary width.

CSiBridge uses tributary width of the deck composite with each steel I-girder to report the internal forces of the composite girders. As a result, a measurable net axial force is observed on the composite section in some cases such as the above. It should be noted that the total axial force on the entire bridge system is zero (assuming negligible longitudinal constraints and negligible applied axial loading on the bridge cross-section, which are considered to be appropriate assumptions within the context of this study). However, due to the assumption of tributary widths of deck acting compositely with each steel I-girder, non-zero axial forces are calculated on the individual composite girders. The calculated axial forces on all composite girders of the bridge sum to zero.

Due to the presence of a net girder axial forces, the horizontal axis about which the girder bending moments is calculated becomes important. The neutral axis of the composite girders is at different depths for the non-composite, short term composite and long term composite section. The net effect is that the major axis bending moments and bending stresses are influenced by the presence of the girder axial forces. This effect is more significant for concentrated load cases such as the barrier rail load.

CSiBridge, by default reports the internal forces at a horizontal axis passing through the mid-web depth of each section. This entails that the bending moment due to the net axial force must be added to the bending moment resultants obtained from CSiBridge to obtain revised bending moments. The bending stress at the flanges can then be calculated using the revised bending moments and the axial stress due to the axial force can be added to obtain the correct estimates of stress. Of course, the stresses at different locations on the girders is calculated directly by the 3DFEA model and can be output directly, rather than calculating the resultant moments and the back-calculating the stresses from the resultant moments given the common girder design-analysis cross-section models. A study was conducted to evaluate the effects of axial force on bending moments for girders of Bridge 1. A maximum error of approximately 1 ksi was found for the barrier rail load case. For practical purposes, a maximum error of 1 ksi which is 2% of the

material yield strength of 50 ksi, is considered acceptable. Therefore, the effect of the above girder axial forces was ignored in the calculation of the girder major-axis bending moments. However, these axial forces are collected and catalogued in the excel spreadsheets developed in the study of each bridge.

4.4 Presentation of Results

In this research, results from LRFD Simon and CSiBridge are processed and compiled in a series of excel workbooks. Detailed plots and comparison tables, from these excel workbooks, have been compiled within appendix sections for each of the 26 bridges studied. These 26 sections are contained in Appendix 3. The presentation of the data from the parametric studies, in each Appendix 3 section, is organized so that the results can be readily inspected and understood for the individual bridges studied, as well as for the overall suite of bridges studied. The presentation is predominantly graphical, and organized in the same fashion for each bridge. In each individual appendix section, the most meaningful results addressing the project objectives are presented. Various other data can be examined in the excel worksheets. The workflow of building the analysis models, extracting the results and processing the results will be explained in detail in Section 4.5.

Each Appendix 3 section corresponds to an individual bridge studied, and begins with a summary of the bridge characteristics, girder details and cross-frame details. This is followed by a synthesis of comparisons between the results from the LGA and from 3D FEA solutions for the selected bridge. Lastly, various detailed plots and tables providing results comparisons are provided. Plots are presented for each of the key response quantities discussed below for each of the following load cases described in Section 4.1:

1a. Steel Dead Load (SDL/SDLF), including the influence of steel dead load fit (SDLF) effects.
1b. Steel Dead Load (SDL/NLF), not including the influence of steel dead load fit (SDLF) effects, i.e., based on No-Load Fit.
2a. Concrete Dead Load (CDL), neglecting any influence of prior setup of the concrete during deck placement.
3. Barrier Rail Load (RL).
4. Future Wearing Surface and Utilities Load (DW).
5. Vehicular Live Load (LL).
6. Vehicular Live load for Displacement
7. Fatigue Live Load

For four bridges, as explained in Section 3.5, the following additional load case is considered:

2b. Concrete Dead Load (CDL/SDP), considering the influence of staged deck placement.

These results are presented as sections of Appendix 4, separate from the responses presented in Appendix 3.

The numbering of the appendix sections, which is shown at the top of each of the appendix pages, is as follows:

- The first number corresponds to the Appendix number, i.e., number 3 for the detailed bridge-by-bridge data.
- The number for the second-level sections corresponds to the bridge being studied, 1 through 26.

The third-level sections focus on the different bridge characteristics, responses and contexts listed in Table 11.

Each of the 26 bridges studied are given a unique detailed name, which appears on the first page of each second-level section. For instance, Bridge 1 is named Bridge 1-49.4-0.462-C. Each of the parts of the name are separated by a dash, i.e., "-". The different parts of the names are defined as follows:

- The first part of the name is the bridge number.
- The second part of the name is the maximum skew angle.
- The third part of the name is the value of the skew index.
- The fourth part of the name is "C" for "contiguous" cross-frame framing arrangements or "S" for "staggered" cross-frame framing arrangements.

Some of the appendix sections have a fourth section level corresponding to attributes such as the girder number, in the sub-sections presenting the girder data, the specific cross-frame response in the sub-sections presenting the cross-frame data, etc.

For a number of the bridges studied, results are presented for three girders – one of the fascia girders, the first interior girder adjacent to this fascia girder, and the central interior girder closest to the mid-width of the bridge. These cases correspond to bridges having parallel skew of their bearing lines and in which there is a symmetry of the geometry about the mid-width of the bridge. In cases where the bearing lines are not parallel to one another, and/or where there is a lack of symmetry about the mid-width of the bridge, four girders are considered in the collection and presentation of the results. From the girders studied, Girder 1 refers to the fascia girder at the top of the plan view, Girder 2 refers to the interior girder adjacent to this fascia girder, and Girder 3 refers to the girder closest to or at the bridge mid-width. Girder 4, if studied, refers to the fascia girder at the bottom of the plan view. For Bridge 1, and for the other bridges where the results for four girders are presented, Girder 4 refers to the fascia girder at the bottom of the bridge plan. For instance, for Bridge 1, the results are presented for four girders, labeled 1 to 4, because one of the fascia girders has a slightly different bottom flange. Girders G1 and G2 correspond to Girders 1 and 2, Girder G6 corresponds to Girder 3, and Girder G11 is labeled as Girder 4. This is illustrated in Figure 43. Response quantities 1 to 9 (see Table 11) are reported for each of the girders considered. For the major-axis bending moments, vertical deflections and vertical shear forces, the responses obtained from 3D FEA and LGA are shown on the same plots. These comparison plots allow for a direct evaluation of the differences between the 3D FEA and LGA predictions.

For the live load vertical deflections, the results presented are based on the maximum values from (1) design truck alone, and (2) 25 % of the design truck taken together with the design lane load, as explained in Section 4.1.6.

Table 11. Organization of third-level section of Appendix 3.

Third Level Section Number	Focus	Context
1	Summary of bridge characteristics, and synthesis of comparisons between LGA and 3D FEA solutions	
2	Major-Axis bending moments, and fatigue stress range for the top and bottom flanges	Three or more girders
3	Vertical deflections	Three or more girders
4	Layover displacements	Three or more girders
5	Twist rotations	Three or more girders
6	Normalized twist rotations	Three or more girders
7	Vertical shear forces	Three or more girders
8	Top flange lateral bending stresses	Three or more girders (only for 3D FEA)
9	Bottom flange lateral bending stresses	Three or more girders (only for 3D FEA)
10	Cross-frame member axial forces	Cross-frame top chords, bottom chords and diagonal members (only for 3D FEA)
11	Overall cross-frame resultant moments and shears	Overall cross-frame units (only for 3D FEA)
12	Vertical reactions	Each of the individual bridge bearings
13	Lateral displacements	Bridge bearings (only for 3D FEA)
14	Live load distribution factor estimates	Three or more girders
15	Normalized mean differences	Major-axis bending moments, shear forces and vertical displacements for each of the girders considered
16	Detailed hand calculations	Various quantities

Regarding the calculation of girder layover displacements, two different values are presented on the same plot in the third-level 4 listed in Table 11:

1. Transverse displacement of the top flange and
2. Relative displacement of the top flange with respect to the bottom flange.

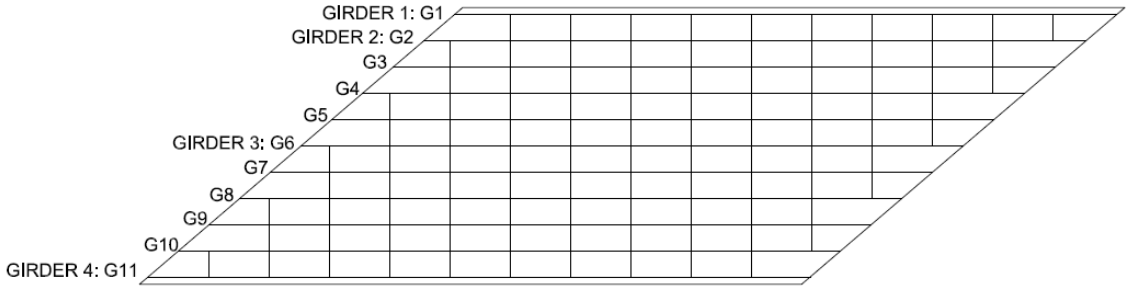

Figure 43. Illustration of Girders 1 to 4 in the presentation of results of Bridge 1.

The related twist rotations are presented in two different ways in the third-level Sections 5 and 6:

1. Twist rotations in radians in Section 5 and
2. Relative displacement of the top flange with respect to the bottom flange per foot depth of the web, i.e., the relative displacements from Section 4, divided by 12 inches, in Section 6.

A summary table is provided in the third-level Section 5, providing a comparison of the 3D FEA layovers at the supports to estimates from LGA using procedures recommended by FDOT. The procedure is explained in more detail in Section 5.1.2.

The cross-frame forces are reported as the axial forces in the component cross-frame members, as well as the resultant moments and shear forces on the overall cross-frames in the third-level Sections 10 and 11. Cross-frame member axial forces are reported separately for the top chords, the bottom chords and the diagonal members respectively on separate plots in the third-level Secton 10. In addition, the cross-frame resultant moment and resultant shear forces, at a transverse section at the mid-width of each cross-frame, are reported separately in the third-level Section 11. For loadings in which the bridge is composite, the resultant moments and shears include the contribution from the bridge deck to the cross-frame internal forces.

The cross-frame results are presented as bar charts showing the forces on a cross-frame-by-cross-frame basis moving along the length of the bridge within each “bay” between the girders. The plots start in Bay 1 between Girders 1 and 2 (at the top left of the plan drawing), move toward the top right corner of the plan, then progress downward to the next bay and from left to right again. This is explained in Figure 44 showing a plan view of Bridge 1 that illustrates the girder numbering G1 through G11 as well as the Bays 1 through 10 between these girders. In addition, the specific cross-frames are numbered from 1 to 12 in each bay as we move from left to right in this bridge. All the bays have the same total number of cross-frames in this bridge.

Figure 45 shows the corresponding plan for Bridge 2, which is the same as Bridge 1 but with an improved alternative cross-frame arrangement involving the use of ample staggers and offsets of the cross-frames throughout the bridge. The development of the alternative cross-frame arrangement was explained in Section 3.3.

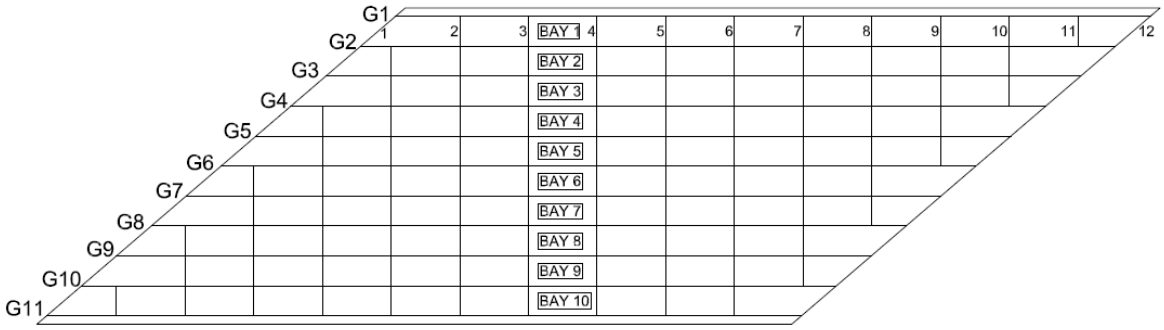

Figure 44. Girder, bay, and cross-frame numbering for Bridge 1.

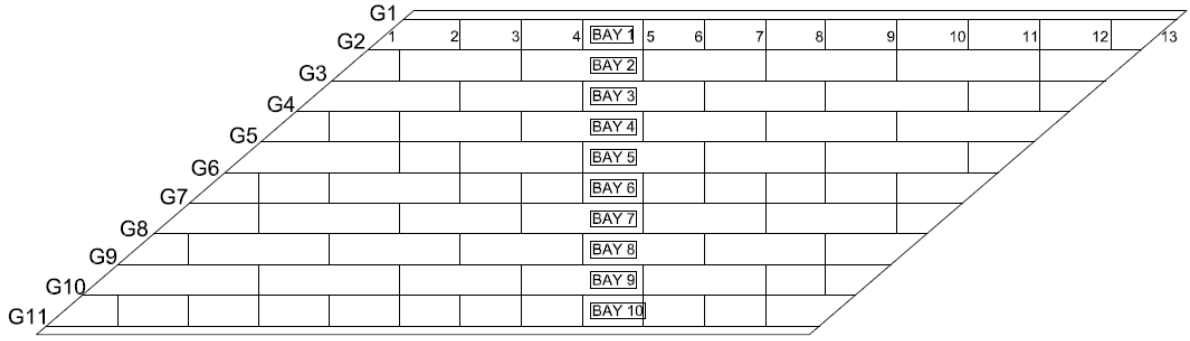

Figure 45. Girder, bay, and cross-frame numbering for Bridge 2.

Figures 46 and 47 show example cross-frame component force results for these two bridges. Specifically, these plots show the top chord forces from 3D FEA, corresponding to the nominal concrete dead load for these bridges. These plots provide a concise compilation of all the cross-frame component forces throughout these structures. The plots in Figures 46 and 47 are annotated to highlight the cross-frame component member forces corresponding to each of the bays. In Figure 46, 14 forces are shown for each of the bays. Two forces are plotted for the cross-frames at the abutment lines, i.e., for Bay 1, the abutment line cross-frames are labeled as 1 and 12 in Figure 44. These two forces are the forces on each side of the inverted-V attachment of the diagonals to the top chords in the cross-frames at the abutment lines. Otherwise, each bar in the leftmost portion of the graph corresponding to Bay 1 corresponds to cross-frames 2 through 12 in Figure 44. The bar graphs for the other bays are similar.

Figure 46 conveys all the CDL top-chord forces in Bridge 2. In this case, there are 15 bar values for Bays 1 and 10, since there are 13 cross-frames in these bays, and the forces on each side of the top chord are shown at the abutment lines. Most of the intermediate bays in Bridge 2 have only eight cross-frames, and therefore 10 bars are shown for each of these bays. Bay 6 has 12 cross-frames and 14 corresponding cross-frame top chord forces.

Given these plots various aspects of the cross-frame responses in the different bridges can be readily ascertained. For instance, the development of a transverse load path through the cross-frames in the short direction between the obtuse corners of each of these bridges can be observed. In addition, it's easier to compare the overall relative magnitudes of the cross-frame forces. For instance, comparing Figures 46 and 47, one can observe that the maximum cross-frame forces in Bridge 2 are approximately one-half those in Bridge 1. Bridge 2 has a smaller number of cross-frames, 94 in total, compared to 120 cross-frames in Bridge 1, and yet the cross-frames in Bridge 2 tend to have smaller internal forces. Potential economies may be gained by recognizing the influence of an alternative cross-frame arrangement with ample offsets and staggers.

It is known that theoretically (i.e., based on engineering idealization) the girder flange lateral bending stresses and the cross-frame forces are zero for steel dead load fit under steel dead load. Therefore, these plots are not included in the appendix sections. To maintain the same page locations for presentation of the different results, the space that would correspond to these plots is empty. This maintains all the plots at the same locations within all the presentations, making it easier to readily locate and compare the various responses.

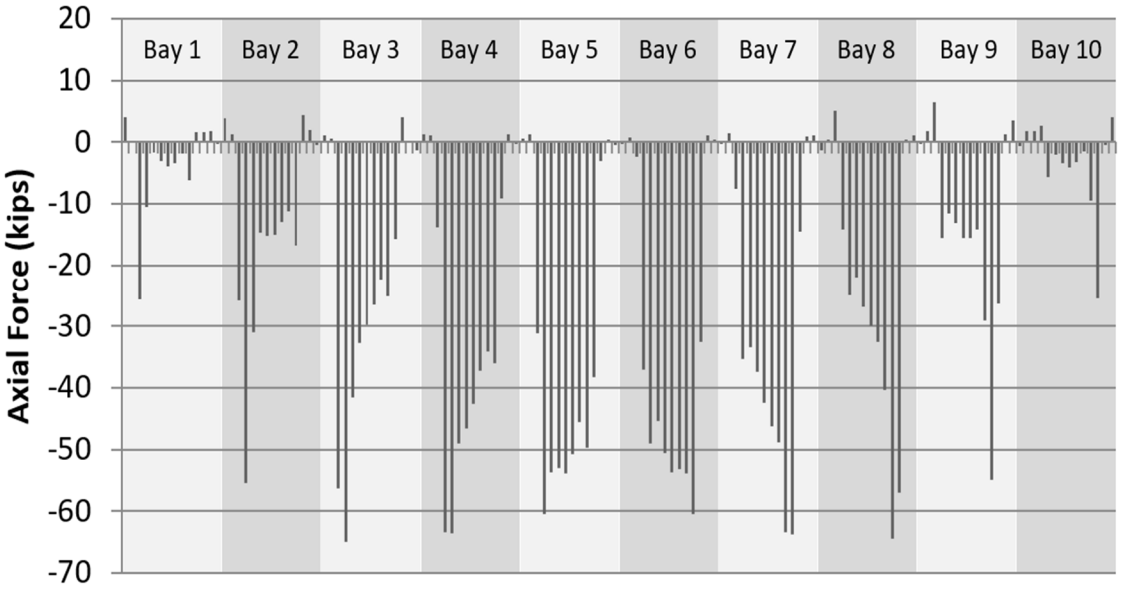

Figure 46. Example cross-frame component force plot (CDL top-chord forces), Bridge 1.

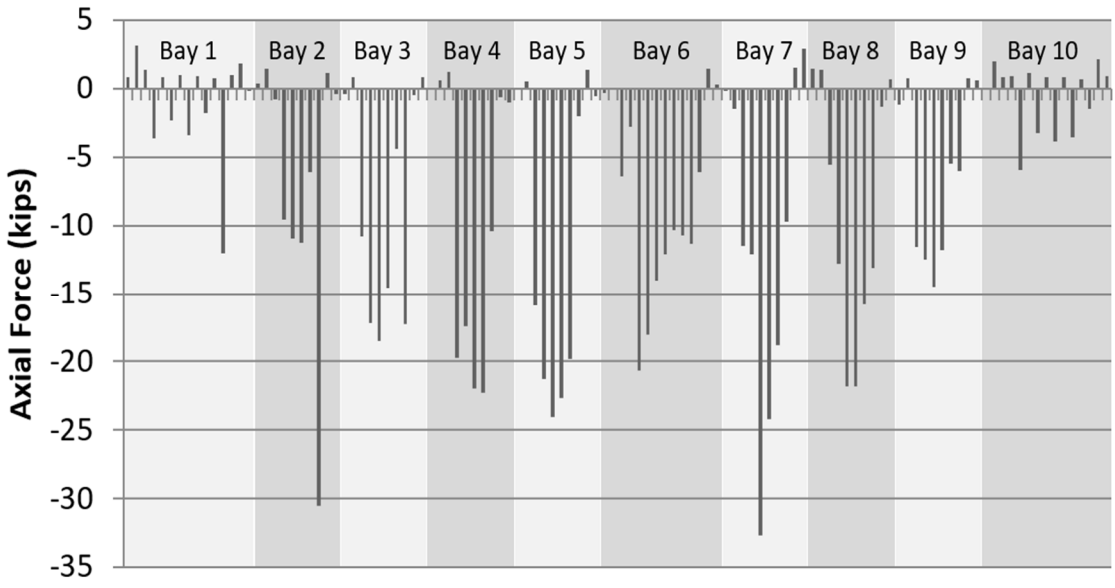

Figure 47. Example cross-frame component force plot (CDL top-chord forces), Bridge 2.

In the third-level Section 12 listed in Table 11, vertical reactions are reported at all the bearing locations using bar charts. These bar charts show the reactions for each bearing. For each support line, these quantities are reported for each bearing as one moves from the top to the bottom of the plan view (i.e., from girders G1 through Gn, where n is the fascia girder number at the bottom of the plan view). For the simple-span bridges, the results are listed starting from the leftmost support line and then moving to the rightmost support line in the plan view. For multispan continuous bridges, the vertical reactions are reported at the leftmost support line, then the rightmost support line, and finally at the intermediate pier supports. For three- and four-span continuous bridges, the bearing reactions at the pier supports are presented starting from the leftmost pier and progressing to the rightmost pier.

In addition, in the third-level Section 13 listed in Table 11, the 3D FEA lateral displacements perpendicular to the girders at all the bearing locations are presented using bar charts. The order of presentation of this data is the same as that described above for the girder vertical reactions. As mentioned in Section 4.1.1, a representative elastomeric bearing shear stiffness of 100 kip/ft is assumed at each of the bearing locations in the bridge models. The corresponding bearing lateral forces can be determined by multiplying the lateral displacements (presented in inches) by 100/12.

Significant differences are observed in the live load responses obtained from 3D FEA and LGA. This is readily apparent by comparison of the live load distribution factors (LLDFs) obtained from 3D FEA to the AASHTO LLDFs employed with LGA. In the third-level Section 14, the LLDFs obtained from 3D FEA are compared to the LGA values obtained based on the requirements of Section 4 of the AASHTO LRFD Specifications. LRFD Simon provides live load bending moment envelopes at every tenth point in the spans. If these moment values are divided by the AASHTO LLDF, an envelope of the bending moments corresponding to a LLDF

= 1.0 is obtained. The ratios of the 3D FEA live load envelope bending moments at the tenth points to the corresponding bending moments for LLDF = 1.0 obtained from LRFD Simon is presented as the 3D FEA LLDFs. 3D FEA LLDFs are presented for both the positive and negative moment envelopes. The negative moment LLDFs are taken as zero for simple-span bridges. Additionally, 3D FEA LLDF are presented for moments obtained from the fatigue live loading on the bridge.

Section 14 also provides plots of the 3D FEA based LLDFs for the moment and shear ranges obtained from analyses considering the AASHTO fatigue load vehicle. These 3D FEA LLDF are somewhat different from the above values. The fatigue shear range is required in the design of shear connectors. Hence, Section 14 also presents the 3D FEA LLDF for the fatigue shear range. Similar to the ordinary LLDF calculation for moments or shears, the LLDF for shear range is the ratio of 3D FEA fatigue shear live load shear range at the tenth points to the corresponding shear range for LLDF = 1.0 obtained from LRFD Simon.

For the comparison studies, the normalized mean difference and normalized difference of the maximums are used to quantify the differences between the 3D FEA and 1D LGA results. Additional measures of difference are employed in the evaluation of results from the parametric studies. The additional measures of differences are not presented in the appendix sections and are explained in detail in Section 5.2.3. The measures of differences quantified in the appendix sections are described below.

The normalized mean difference is defined as follows:

$$\varepsilon_{mean} = \frac{\sum_{i=1}^{n} \left| \text{LGA} - \text{3DFEA} \right|}{n \times \left| \text{3DFEA} \right|_{\max}} \tag{16}$$

where

n = number of data points along a given girder, throughout the length of the bridge (data sampled at the 10th points) for girder moments, shears and vertical displacements, or the total number of bearings, for the bridge vertical reactions

The normalized mean difference is useful as a broad measure of accuracy, particularly for quantities such as displacement, where both underestimating and overestimating may have negative consequences.

The normalized difference of the maximums is defined as

$$\varepsilon_{\max} = \frac{\left(\left| \text{LGA} \right|_{\max} - \left| \text{3DFEA} \right|_{\max} \right)}{\left| \text{3DFEA} \right|_{\max}} \tag{17}$$

The normalized difference of the maximums is a more demanding measure, indicating the worst-case conservative and unconservative differences, normalized by the corresponding maximum 3D FEA response. The normalized difference of the maximums is computed as the difference

between the maximum positive and maximum negative responses. This calculation is conducted without consideration of the specific locations of the responses.

The third-level Section 15 presents the summary ε_{mean} and ε_{max} values for the bending moments, vertical shear forces, vertical displacements and support reactions, for comparison of the 3D FEA and LGA responses. For the bending moments and shear forces, ε_{mean} and ε_{max} values are presented for all the load cases (including the fatigue live load case) for each of the considered bridge girders. Additionally, bending moment ε_{mean} and ε_{max} values are presented for the Strength I and Service II load combinations, and shear ε_{mean} and ε_{max} values are reported for Strength I. For the vertical displacements, ε_{mean} values are reported for SDL, CDL, RL, and DW, and ε_{max} values are reported for all the load cases. Additionally, ε_{mean} and ε_{max} values are reported for the Total Dead Load (steel dead load fit), TDL (SDLF), load combination. This constitutes the sum of the vertical displacements for the dead load cases SDL (SDLF), CDL, RL and DW. The TDL (SDLF) vertical displacement values are used to determine the camber for the girders.

For the bearing reactions, ε_{mean} values are presented for all the load cases and for the Strength I and Service II load combinations.

The Appendix 3 materials for each bridge conclude with a level-three Section 16 presenting the hand calculation of the composite and noncomposite loads, the AASHTO LLDFs, including the rigid cross-section analysis values for the fascia girders, and "exact" LLDFs to be applied to the results obtained from LRFD Simon to match the results from CSiBridge.

4.5 Workflow for Parametric Studies

The 26 bridges studied in the parametric studies are existing bridges, for which drawings are available. 3D FEA and LGA models are built from the data obtained from these drawings. Loads are calculated as described in Section 4.2. The process from obtaining data to analyzing the models can be summarized as follows:

1. Extract essential data from bridge drawings:
   a) Define geometry of the bridge: articulation, span lengths, bridge width, overhang lengths, parallel or nonparallel skew, skew angles at each bearing line.
   b) Cross-frame layout: arrangement of intermediate cross-frames – contiguous (perpendicular to girders or parallel to skew) or staggered, end cross-frames, intermediate pier cross-frames for continuous-span bridges, staggers near end and/or intermediate pier cross-frames.
   c) Girder sizes: number of girders, web depth, flange widths, flange and web thicknesses, locations of transition in flange widths and flange and/or web thickness
   d) Cross-frame sizes: types of end and intermediate cross-frames, number of cross-frames of each type, sizes of cross-frame members.
   e) Deck: structural thickness of deck, sacrificial thickness, haunch depths for girders, reinforcement layout and bar sizes.

2. Calculation of weights and its application in analysis models:
   a) The steel dead load is calculated as described in Section 4.2.1.
   b) The concrete dead load is calculated as described in Section 4.2.2.

c) For staged deck placement analyses, parts of the deck and the corresponding additional loads are calculated in stages, and the deck in each stage is made composite beginning from the corresponding succeeding stages. It follows that the CDL loads are applied successively in stages in both CSiBridge and LRFD Simon.
d) LRFD Simon internally calculates the weight of the modeled steel girders and applies it as a DC1 load. Additional DC1 load spread uniformly over the length of the bridge can be defined in the Simon user interface. Loads applied in CSiBridge and LRFD Simon must be equivalent. Total DC1 load includes the weights of steel girders, cross-frames, miscellaneous steel, concrete deck, overhang tapers, sacrificial thickness, haunches and SIP forms. Hence, additional DC1 load in LRFD Simon includes the weight of cross-frames, miscellaneous steel, concrete deck, overhang tapers, sacrificial thickness, haunches and SIP forms applied uniformly over the length of each girder.
e) LRFD Simon provides results for DC1 and "Other DC1" load described in part d). SDL comprises of weights of steel girders, cross-frames and miscellaneous. Adjustment factors for results of DC1 and "Other DC1" obtained from LRFD is modified using factors to obtain results for SDL and CDL cases.

   It should be noted that the weight of end cross-frames is not included in the calculations of the SDL and CDL factors. The weight of the end cross-frames are applied at the ends of the girders, which are the points of support for the girders. In LGA, the point loads applied at the support are directly transmitted to the supports. Hence, the weights of end cross-frames are directly added to the LGA support reactions for SDL. Tributary end cross-frame or intermediate pier cross-frame weights are calculated for each girder bearing support and are added to the SDL reactions.

3. Calculation of live load distribution factors (LLDF) for LGA:
   a) Calculation of the AASHTO (2017) LLDF for LGA is discussed in Section 2.5.2. The calculation of the longitudinal stiffness parameter K_g involves the use of moment of inertia, I, of the steel girder. A typical steel I-girder in a bridge has a number of section transitions within a span. It is therefore, necessary to obtain an "average" representative estimation of moment of inertia, I, to be used in the calculation of the longitudinal stiffness parameter. Hence, in the parametric studies, "average" moment of inertia, I, of a girder is obtained by averaging the moment of inertia of the steel section at each 20^{th} point in a given span. The length of the given span is used in estimation of moment LLDFs for positive bending. For the estimation of negative bending moment at an interior support of a multispan continuous bridge, AASHTO (2017) Table 4.6.2.2.1-2 recommends using the average lengths of the two adjacent spans for the estimation of moment LLDF. Similarly, an average moment of inertia, I, is calculated as the average of the "average" moment of inertia for the two adjacent spans. Thus, the positive moment LLDF is calculated for each span, and the negative moment LLDF is calculated for a set of adjacent spans. The LLDFs thus estimated are approximately equal to one another. Hence, the maximum of the LLDF estimates calculated is used as the bending moment LLDF in LGA.
   b) The shear LLDF, on the other hand, is only dependent on the spacing and hence, is a unique value for each girder.
   c) The fatigue LLDF for bending moment is calculated as the bending moment LLDF for a single lane in step (a) divided by the multiple presence factor of 1.2.

d) The fatigue shear LLDF is similarly calculated as the shear LLDF for a single lane in step (b) divided by the multiple presence factor of 1.2.

4. Building the 3D FEA analysis model:
   a) Aspects of 3D FEA modeling in CSiBridge are described in Section 4.1.1.
   b) Dead load cases are simulated in CSiBridge using its "Staged Construction" capabilities. The staged construction sequence in CSiBridge, in a way, simulates the sequence of construction of the bridge and the application of loads on it. For example, the noncomposite DC1 load case consists of the steel dead load and the wet concrete load applied to the steel superstructure. The definition of the DC1 (with SDL (NLF) load case in CSiBridge consists of the following two stages:
      i) Activate the steel superstructure comprising of steel girders and the cross-frames. The self-weight of the superstructure is then applied to the activated steel superstructure. This refers to the condition of SDL (NLF).
      ii) The wet concrete load is applied to the steel superstructure.
   c) The definition of SDL (SDLF) load case in CSiBridge consists of the following stages:
      i) Activate the steel superstructure comprising of steel girders and the cross-frames. Apply a stiffness modifier of 1E-20 to the cross-frames, to "deactivate" the stiffness of the cross-frames. The self-weight of the superstructure is then applied to the active steel I-girders, because the cross-frame stiffness has been deactivated. However, the self-weight of the cross-frames will be applied to the steel structure since the cross-frames are a part of the superstructure. This refers to the condition of SDL (SDLF). For SDL (SDLF), it is important to ensure lateral stability of the girders. Hence, the top flanges of all the girders are restrained at the bearing lines.
      ii) The self-weight of the superstructure is then applied to the active steel I-girders, because the cross-frame stiffness has been deactivated. However, the self-weight of the cross-frames will be applied to the steel structure since the cross-frames are a part of the superstructure. This refers to the condition of SDL (SDLF). For SDL (SDLF), it is important to ensure lateral stability of the girders. Hence, the top flanges of all the girders are restrained at the bearing lines. The results of this stage should theoretically match results from LGA, provided the loads are applied consistently in both LGA and 3D FEA.
   d) Staged construction of the bridge can be defined similar to the DC1 load case using the CSiBridge staged construction capabilities. For example, a bridge that is constructed in three stages of deck pour can be defined is CSiBridge using the following:
      i) Activate the steel superstructure comprising of steel girders and the cross-frames. The self-weight of the superstructure is then applied to the activated steel superstructure.
      ii) Apply the wet concrete load pertaining to the first stage of deck pour to the steel superstructure.
      iii) The concrete poured in the previous stage should be simulated to be composite with the steel superstructure. This is achieved by using the feature "Remove Forms". Removing the forms pertaining to the deck pour in the previous stage essentially activates the stiffness of the concrete deck poured in the previous stage. Apply the wet concrete load pertaining to the second stage of deck pour to the partially composite superstructure.

iv) Remove the forms pertaining to the deck pour in the second stage, and apply the wet concrete pertaining to the second stage of deck pour to the partially composite superstructure.

e) The definition of composite dead load cases in CSiBridge consists of one stage: Activate the bridge structure consisting of the steel superstructure and the concrete deck. Apply a stiffness reduction factor of 1/3 to the concrete deck, to simulate long-term stiffness of the composite bridge structure. Apply the dead load (barrier rail or wearing surface load) to the composite structure.

f) Aspects of live load modeling in CSiBridge are described in Section 4.2.5. The short-term stiffness of the concrete deck is used in live load analyses. To simulate short-term stiffness, the stiffness of the bridge structure does not need to be modified.

5. Building the LGA analysis model:
   a) Aspects of LGA modeling in LRFD Simon are described in Sections 4.1.2.
   b) Calculation of steel and concrete dead loads as described in Sections 4.2.1 and 4.2.2 are applied to the noncomposite girder by LRFD Simon.
   c) The barrier rail dead load and the wearing surface loads are distributed in the ratios of total lengths of each girder. These loads are applied to the composite girder. Tributary width is the effective width of each girder, as per AASHTO LRFD Specification. The long-term stiffness of the concrete deck is used in calculating the properties of the composite girder.
   d) The short-term stiffness is used in calculating the properties of the composite girder, for live load analysis.
   e) The distribution factors obtained from the empirical equations and RCA are calculated manually for the exterior girders each for single-lane moment, multi-lane moment, single lane shear and multi-lane shear. The larger of the two for each is input into LRFD Simon.
   f) Since RCA is not required for interior girders, LRFD Simon's capabilities are used for the calculations of LLDFs for interior girders. The skew angle for the central interior girder is set to zero so that the skew correction factor is not calculated for the central interior girder.

6. 3D FEA and LGA and extracting results:
   a) The 3D FEA model is analyzed and the following results are extracted:
      i) Bending moments and shear forces for each load case separately for all girders exported from the CSiBridge interface in the form of excel sheets.
      ii) Displacements and rotations for each load case separately for all girders exported from the CSiBridge interface in the form of excel sheets.
      iii) Bearing reactions for each load case exported from the CSiBridge interface in the form of excel sheets.
      iv) Bearing displacements for each load case exported from the CSiBridge interface in the form of excel sheets.
      v) Cross-frame forces from CSiBridge extracted using an excel VBA script. The excel file is named "VBA Code" and is used in generating bridge appendices as explained later.
   b) Girder LGA models for each bridge are analyzed and the following results are extracted: Bending moments, shear forces, vertical displacements and reactions obtained from LRFD Simon files and processed in an excel sheet for each girder.

c) An excel file named “Consolidated Results” assembles results of bending moments and shear forces from 3D FEA for all load cases, for the girders to be studied. Plots for stresses in the top and bottom flanges of each girder are generated. Additionally, fatigue results from LRFD Simon results are obtained and comparison plots for fatigue stress range for girders are plotted.
d) An excel file named “Consolidated Displacements” assembles results of vertical displacements, layover displacements, twist rotations and normalized twist rotations from 3D FEA for all load cases, for the girders to be studied.
e) An excel file named “Comparison 1D vs 3D” assembles LGA and 3D FEA results described in b), c) and d) above. Comparison plots for bending moments, vertical shear forces and vertical displacements are developed. Additionally, data from LGA and 3D FEA results is further processed to calculate ε_{mean}, ε_{max}, layovers and LLDFs.
f) An excel file named “Consolidated Reactions” assembles results of bearing reactions from 3D FEA and LGA. Comparison bar charts for vertical reactions, as well as bar charts showing lateral bearing displacements from 3D FEA are developed.
g) Finally, all of these plots are collected and organized in the order mentioned in Table 11, in a file named “Bridge Appendix”. A pdf developed from this excel file constitutes the appendix section for each bridge.

The processed results in the appendices are further evaluated to develop recommendations for application of LGA for straight skewed bridges having skew index approaching 0.3. Chapter 5 describes the synthesis and evaluation of these processed results from LGA and 3D FEA, to develop recommendations for application of LGA.

5. RECOMMENDED DESIGN GUIDELINES AND DISCUSSION OF PARAMETRIC STUDY RESULTS

This chapter presents the results from the evaluation and comparison of a wide range of LGA and 3D FEA calculations important to skewed steel I-girder bridge design.

Key responses discussed are:

1. The girder positive and negative STR I major-axis bending moments.
2. The girder STR I vertical shear forces.
3. The girder HL-93 live load shear forces, focusing in particular on the live load shear forces at the obtuse corners of the bridge spans.
4. The girder STR I bearing reactions at span obtuse corners, and on the fascia girders at the piers in continuous-span bridges.
5. The girder total dead load vertical displacements, including consideration of the effects of steel dead load fit (SDLF) detailing of the cross-frames.
6. The girder concrete dead load vertical displacements, considering both staged and unstaged deck placement.
7. The girder layovers under the total dead load, which for SDLF detailing of the cross-frames are equal to the girder layovers under the concrete dead load. This is because the layovers are approximately zero under the steel dead load when SDLF detailing is employed. (These responses are estimated indirectly from the LGA results using equations recommended by FDOT; since the calculations are relatively straightforward, simple, and based on mechanics, they are considered as a part of the LGA calculations.)
8. The girder fatigue live load vertical shear forces.
9. The girder fatigue live load flexural stresses.
10. Girder flange lateral bending stresses.
11. Cross-frame and diaphragm forces.
12. Fascia girder live load distribution factors (LLDFs), considering the conservatism of the lever rule and rigid cross-section analysis procedures.
13. Girder live load deflections.

The emphasis is on the comparison of these responses and on establishing limits within which LGA provides an estimate of the 3D FEA values considered sufficient for design.

Regarding key bridge responses not predicted directly by LGA, the report first evaluates the accuracy of the girder flange lateral bending stress estimates as recommended by AASHTO LRFD Article C6.10.1 with some minor recommended modifications. Lastly, the research study focuses on an estimation of cross-frame dead load (DC1 and DC2), wearing surface and utilities (DW), live load (LL), Strength I (STR I) and fatigue loading forces due to skew effects, which can be used to complete a bridge design based upon LGA modeling. These responses and their estimation are discussed separately from the above responses since they are based on synthesis of the bounds of the responses determined from the parametric 3D FEA studies.

Section 5.1 first summarizes the specific LGA calculation procedures recommended based on this research. Section 5.2 then discusses the bridge characteristics required for application of

these procedures (i.e., the limits of applicability of the recommended LGA procedures). Section 5.3 discusses the specific measurement of the differences between the LGA and 3D FEA results upon which the recommended procedures are based. Section 5.4 identifies the bridges from the Task 3 parametric study satisfying the stated requirements, and highlights the key attributes of these bridges. This section also highlights the bridges from the parametric study that do not satisfy the stated requirements and summarizes the requirements they violate.

5.1 Recommended LGA-Based Procedures

The LGA-based procedures recommended in this research involve routine LGA calculations, as implemented in the LRFD Simon software (NSBA, 2019), as well as the following specific practices and/or adjustments to obtain complete estimates of the forces necessary for design:

1. Distribute the miscellaneous steel dead loads, cross-frame steel dead loads, concrete dead load, rail loads (i.e., barrier loads), and wearing surface and utility loads equally as line loads to all the girders.
2. Employ the FDOT procedures for calculation of girder layovers. These procedures are summarized below in Section 5.1.2.
3. In certain cases, increase the calculated STR I girder vertical reactions at the obtuse corners of bridge simple spans, and at the fascia girders in continuous spans, by a multiplicative factor of 1.10. The background to this factor is summarized in Section 5.1.3.
4. Employ a form of the AASHTO LRFD Article C6.10.1 recommendations for estimating the girder flange lateral bending stresses, with recommended minor modifications/simplifications (see Section 5.1.4).
5. In addition to satisfying the base AASHTO LRFD requirements for design of cross-frames and diaphragms, including the consideration of wind load forces, forces from overhang loads during construction, etc., design for the DC1, construction, DC2, DW and LL cross-frame and diaphragm forces caused by the skewed geometry effects (see Section 5.1.5) using the appropriate LRFD load combinations. Also, evaluate the fatigue force ranges in the cross-frame members.
6. Calculate LLDFs as defined in AASHTO (2017) Article 4.6.2.2, with the exception that the moment reduction factors of Article 4.6.2.2.2e are not employed. The skew correction factors for shear defined in Article 4.6.2.2.3c are to be employed.
7. Estimate girder live load deflections using the AASHTO LRFD LLDFs for moment, rather than the AASHTO Article 2.5.2.6.2 factor based on the assumption of equal deflection of all the girders.

Three separate design categories are recommended for application of the above procedures:

Category 1 – Parallel skew bridges with $\theta \leq 20$ degrees, and with contiguous intermediate cross-frame lines oriented parallel to the skew. For bridges in this category:

- The girder design demands are calculated directly from the recommended LGA procedures without application of any adjustment factors.
- The estimated girder flange lateral bending stresses due to skew effects are taken equal to zero.

- The force demands on the intermediate cross-frame lines are relatively large due to their contiguous attribute; however, the force demands on the bearing line cross-frames are relatively small.

Category 2 – Parallel skew bridges with $\theta \leq 50$ degrees and $I_s \leq 0.3$, cross-frames oriented perpendicular to the girders. For bridges in this category:

- A multiplicative adjustment factor is recommended for calculation of bearing reactions at obtuse corners of the spans at end abutments. This is in addition to application of the AASHTO shear skew correction factor to the bearing reactions.
- Estimated non-zero girder flange lateral bending stresses due to skew effects are applied at offsets and staggers in the cross-frame framing arrangements. Different estimates are applied for interior and exterior girders, and the estimated stresses are smaller for ample offsets (larger than $4b_f$) versus smaller offsets.
- The cross-frame force demands are influenced significantly by the cross-frame framing arrangements. The attributes of the framing arrangements include: (1) whether the intermediate cross-frames are contiguous or staggered, (2) the magnitude of the offsets provided between adjacent intermediate cross-frames and (3) the magnitude of the offsets provided between intermediate cross-frames and bearing lines containing cross-frames.

Category 3 – Parallel skew bridges with $\theta \leq 50$ degrees and $0.30 < I_s \leq 0.40$, or with $\theta \leq 30$ degrees and $0.40 < I_s \leq 0.45$. For bridges in this category:

- A multiplicative adjustment factor is recommended for calculation of bearing reactions at obtuse corners of the spans at end abutments. This is in addition to application of the AASHTO shear skew correction factor to the bearing reactions.
- Estimated non-zero girder flange lateral bending stresses due to skew effects are applied at offsets and staggers in the cross-frame framing arrangements. The estimation of these stresses is the same as for Category 2.
- The cross-frame force demands are influenced significantly by the cross-frame framing arrangements. The estimation of these force demands is the same as for Category 2.

Two additional categories are employed in this report for discussion of the results:

Category 4 – Nonparallel skew bridges, and

Category 5 – Simple-span splayed girder bridges.

Although many of the design demands for the bridges in these last two categories can be estimated accurately to conservatively using LGA, the behavior of the bridges from the parametric study that fall within Categories 4 and 5 generally is such that 3D FEA should be considered for calculation of certain design demands, particularly girder shear forces, total dead load deflections, and cross-frame forces. These findings are likely influenced to some extent by the fact that all of the nonparallel skew and splayed girder bridges studied within this research have I_s and/or θ values that violate the above Category 2 and 3 limits.

One can observe that the specific recommended procedures are the same for both Categories 2 and 3. The primary reason for these separate categories are that the LGA results tend to be slightly less accurate for the bridges in Category 3.

It should be noted that for purposes of discussion, all of the parallel skew bridges from the parametric studies with $I_s < 0.30$ and cross-frames framed perpendicular to the girders are presented within Category 2, regardless of their θ values. In addition, for purposes of discussion, all of the parallel skew bridges with $I_s > 0.30$ are presented within Category 3, regardless of their θ values.

The detailed considerations associated with these calculations are discussed below.

5.1.1 Distribution of Dead Loads

The dead loads are calculated as described in Section 2.5.1. For all the bridges considered in the parametric studies, all the dead loads, with the exception of the steel girder self-weights, are distributed equally to all the girders. The steel girder self-weights are applied directly as distributed loads based on the distribution of the girder areas along their lengths.

5.1.2 Calculation of Girder Layovers

Florida DOT (FDOT, 2018) recommends estimation of the maximum girder layovers at simply-supported girder bearing lines based on the girder vertical deflections from LGA and a fundamental application of compatibility of deformations. The girder layover is defined as the lateral displacement of its top flange relative to its bottom flange as shown in Figure 48.

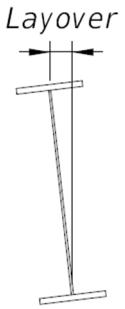

Figure 48. Definition of girder layover.

The steps of the FDOT procedure are as follows:

1. For bridges employing steel dead load fit (SDLF) detailing of the cross-frames, the layover under the full steel dead load is taken equal to zero. This recognizes that SDLF detailing results in the girder webs being approximately plumb under the full steel dead load.

2. The girder layover at the completion of the deck placement is of primary interest. This layover is calculated by first estimating the girder major-axis bending rotation α, due to the concrete dead load (CDL) associated with the bridge deck self-weight. If this rotation is provided directly by the LGA software, then it is recommended to use the provided value.

Alternatively, given the associated CDL vertical displacement at the girder 1/10th point within the span, $\delta_{0.1Ls}$, the girder major-axis bending rotation may be estimated as

$$\alpha = \frac{\delta_{0.1L_s}}{0.1L_s} \tag{18}$$

in radians, where L_s is the span length. This estimate is based on the assumption that α is sufficiently small such that $\alpha \cong \tan(\alpha) \cong \sin(\alpha)$, which is the case for any practical bridge girder end rotations. This estimate is employed with the 1/10 point deflections obtained from LRFD Simon in this research.

Another potential set of estimates is

$$\alpha = \frac{3.2\delta_{\max}}{L_s} \tag{19}$$

for simple spans and

$$\alpha = \frac{4.2\delta_{\max}}{L_s} \tag{20}$$

for continuous spans, where δ_{max} is the maximum CDL girder deflection within the span. Equation 19 is based on the assumption of a simply-supported prismatic girder loaded by a constant uniformly distributed load. This estimate is not recommended unless the prismatic simply-supported condition is approximately satisfied. Similarly, Equation 20 is an estimate of the rotation at the simply-supported end of a continuous-span bridge. The value from this equation is 16 % larger than the rotation at the simply-supported end of a three-span continuous girder with three equally-loaded equal-length spans. The value from Equation 18 is recommended as a reasonably accurate estimate for all cases.

3. Given the girder major-axis bending rotation, α, and the assumption that the cross-frame deformations are small enough such that the cross-frames may be modeled as rigid diaphragms within their own plane, compatibility of deformations between the girders and the cross-frames requires that the girders must twist by an angle

$$\phi = \alpha \tan(\theta) \tag{21}$$

in radians, where θ is the skew angle of the bearing line, equal to zero when the bearing line is perpendicular to the longitudinal axis of the girders.

4. Given the girder twist angle under the CDL, the corresponding layover at the top flange of the girder may be estimated as

$$Layover = D\phi \tag{22}$$

where D is the girder web depth. Similar to the above assumptions for α, this calculation is based on the assumption that ϕ is a small enough angle such that $\phi \cong \tan(\phi) \cong \sin(\phi)$.

5.1.3 Calculation of Strength I Girder Vertical Reactions

The STR I reactions from 3D FEA at the bearings on the fascia girders corresponding to obtuse corners at abutments, and all the pier bearings on the fascia girders of continuous-span bridges, tend to be measurably larger compared to the corresponding LGA reactions. This occurs both at end abutments and at pier bearing lines in continuous-span bridges, since the intermediate bearings correspond to an obtuse corner on one of the spans and an acute corner on the other span on both sides of the bridge cross-section. This is due to the tendency to develop a transverse load path in the short direction between the obtuse corners of the span in parallel skew bridges. In addition, the torsional moment induced in the girders by the bearing-line cross-frames forcing a twist (i.e., layover) into the fascia girder tends to increase the end reaction on the fascia girder at the obtuse corners at end abutments. Based on the bridges studied in this research, it is determined that within the Category 2 and 3 bridges, the STR I bearing reaction on the fascia girder can be predicted accurately to conservatively in all cases, where LGA is permitted, by multiplying the corresponding reaction from LGA, for the fascia girder at the obtuse corners at end abutments and at the piers in continuous-span bridges, by a correction factor of 1.10. This multiplicative factor is in addition to the application of the live load skew correction factor of AASHTO LRFD Article 4.6.2.2.3c to these reactions. No modifications are required for the girder reactions at other locations. In addition, it should be noted that even after multiplying the fascia girder reactions by this factor, the largest reaction may still occur at a location other than the fascia girder bearing. The multiplicative factor of 1.10 is not required for bridges that fall within Category 1.

For load combinations other than STR I involving HL-93 loading, and where LGA would be employed, namely Service II and Strength V, the ratio of the factored live load to the factored dead load is smaller than for STR I. The need for the above correction factor is primarily due to the demands from the HL-93 live load. Therefore, the above multiplicative correction factor of 1.10 may also be applied to the live load portion of the Service II and Strength V load combinations as a sufficient approximation. As such, for load combinations other than STR I, it is recommended that the 1.10 correction factor may be applied only to the live load reaction for the fascia girder at the obtuse corners at end abutments, and at piers in continuous span bridges, for bridges that fall within Categories 2 and 3.

5.1.4 Estimation of Girder Flange Lateral Bending Stresses

In straight skewed bridges, intermediate cross-frames framed perpendicular to the girders connect to the girders at different longitudinal positions within the span. This results in twisting of the girders to maintain compatibility of the girder and cross-frame displacements and rotations. This twisting of the girders produces cross-frame forces and girder flange lateral bending stresses.

AASHTO LRFD Article 6.7.4.2 recommends generous offsets between the intermediate cross-frames and the bearing lines, and generous staggers between the cross-frames within the span, to soften the transverse load path in skewed I-girder bridges. Generous offsets and staggers tend to increase the girder flange lateral bending stresses in most situations, while reducing the magnitude of the cross-frame forces due to the softening of the transverse load path. The cross-

frame staggers interrupt and reduce the stiffness of the transverse load path by forcing load transfer via girder flange lateral bending.

In steel girder bridges where the cross-frames are detailed for steel dead load fit (SDLF), the girder flange lateral bending stresses and the cross-frame forces are theoretically zero under the steel dead load. However, significant flange lateral bending stresses can be induced by other dead loads and by live load effects. The girder top flanges need to be checked considering flange lateral bending when the girders are in their noncomposite condition during construction; however, AASHTO LRFD does not require any further consideration of flange lateral bending in the top flanges once the bridge is in its final composite condition. This is because the composite bridge deck effectively prevents any significant additional bending of the top flange.

Significant girder flange lateral bending stresses may be caused generally by wind, and by torsion from eccentric concrete deck overhang loads acting on cantilever forming brackets placed along fascia girders during construction. In addition, significant girder flange lateral bending can be caused by the above interactions between the cross-frames and the girders in resisting the dead and live load effects. That is, significant girder flange lateral bending can be induced by the skewed geometry effects on the response to gravity loads.

Article C6.10.1 provides the following rules for a simple upper-bound estimate of the girder flange lateral bending stresses from the skew effects, when LGA is employed:

1. The total unfactored flange lateral bending stress in a girder flange at a cross-frame or diaphragm at or near supports, when discontinuous (e.g., staggered) cross-frames or diaphragms are used at these locations, may be taken as:
   a. 7.5 ksi for exterior girders.
   b. 10 ksi for interior girders.

   These values are intended as estimates of the flange lateral bending only at discontinuous cross-frame lines in the vicinity of supports. They are not intended as estimates at other locations within the span length. In addition, one should note that for all skewed bridges other than those that fall within the above Category 1, a “discontinuity” or “stagger” in the vicinity of the supports simply means that the cross-frame line is not framed directly into the support, but rather ends at a certain offset from the bearing line.

2. In regions of the girders where the cross-frames or diaphragms are contiguous, flange lateral bending from the skew effects need not be considered. That is, the flange lateral bending stresses may be taken equal to zero in these regions.

3. The total unfactored flange lateral bending stress in a girder flange at locations within a span other than at or near supports, when cross-frames or diaphragms are placed in discontinuous lines (e.g., staggered) throughout the bridge span, may be taken as:
   a. 2.0 ksi for exterior girders.
   b. 10 ksi for interior girders.

The 3D FEA girder flange lateral bending stresses determined in this research are reasonably consistent with the above coarse approximations. It is observed that measureable maximum STR I flange lateral bending stresses occur in the bottom flange at first intermediate cross-frames in

the vicinity of the obtuse corners of bridge spans (in the final constructed condition of the bridge), when the first intermediate cross-frame is offset from the bearing location. This occurs regardless of the stagger or continuity of the cross-frame lines within the spans, and is associated largely with the enforcement of continuity of deformations between the girders and the separate intermediate and bearing line cross-frames or diaphragms.

In addition, measurable flange lateral bending stresses are observed at discontinuous cross-frame locations within the middle of the spans and near the mid-width of the bridge cross-section. In certain cases, these stresses are somewhat larger than the AASHTO Article C6.10.1 estimates. In parallel skew bridges, these stresses are associated largely with the development of beam action by the cross-frames along the short diagonal direction between the obtuse corners of the span. The largest bending moments associated with this beam action are at the middle of the bridge spans and mid-width of the bridge cross-section. Discontinuities in the cross-frame lines, e.g., staggers between adjacent cross-frames, near these locations break up the transfer of the bending moments associated with the beam action along the short diagonal direction of the span. This results typically in a beneficial reduction in cross-frame forces by softening the transverse stiffness associated with the beam action along the short diagonal direction. However, this also results in concomitant lateral bending of the girder flanges at these locations. As noted in AASHTO Article C6.7.4.2, "Where the flange sizes are increased due to the additional flange lateral bending, this increase often is not significant. In fact, the increased cost resulting from the larger flange sizes is often offset by the reduced cost of providing fewer and smaller diaphragms or cross-frames and smaller diaphragm or cross-frame connections."

It is important to note that the above flange lateral bending stress estimates are highly simplified upper-bound estimates of the flange lateral bending stresses "based on a limited examination of refined analysis results for bridges with skews approaching 60 degrees from normal and an average D/b_f [web depth to flange width] ratio of approximately 4.0" (AASHTO 2017). The studies in this research show that the above stress estimates are somewhat sensitive to the lengths of the "offsets" or "staggers" at the cross-frame line discontinuities, and that discernable reductions in the girder flange lateral bending stresses occur when generous offset or stagger lengths are employed. The value of $4b_f$, the minimum offset or stagger length recommended by Article C6.7.4.2, is suggested as an appropriate discrete offset value at which a smaller estimate of the flange lateral bending stresses may be used.

Considering this "$4b_f$" offset refinement, it is suggested the AASHTO Article C6.10.1 recommendations may be modified to the following:

1. The total unfactored flange lateral bending stress in a girder flange at a cross-frame or diaphragm at or near supports, when discontinuous (e.g., staggered) cross-frames or diaphragms are used at these locations, may be taken as:
   a. 4 ksi for exterior girders, when the offsets relative to the supports at the location under consideration are greater than or equal to $4b_f$, where b_f is the largest flange width within the girder unbraced lengths on either side of the location being considered.
   b. 8 ksi for exterior girders with offsets relative to the supports at the location under consideration smaller than $4b_f$.
   c. 5 ksi for interior girders, when the offsets relative to the supports at the location under consideration are greater than or equal to $4b_f$.

d. 10 ksi for interior girders with offsets relative to the supports at the location under consideration smaller than $4b_f$.

2. In regions of the girders where the cross-frames or diaphragms are contiguous, flange lateral bending from the skew effects need not be considered. That is, the flange lateral bending stresses may be taken equal to zero in these regions.

3. The total unfactored flange lateral bending stress in a girder flange at locations within a span other than at or near supports, when cross-frames or diaphragms are placed in discontinuous lines (e.g., staggered) throughout the bridge span, may be taken as:
   a. 2 ksi for exterior girders, when the smallest offsets or stagger between adjacent cross-frames or diaphragms is greater than or equal to $4b_f$ throughout the bridge span.
   b. 3 ksi for exterior girders, when the offsets or staggers relative to the closest adjacent cross-frames or diaphragms are less than $4b_f$ at any location throughout the bridge span.
   c. 10 ksi for interior girders, when the smallest offsets or stagger between adjacent cross-frames or diaphragms is greater than or equal to $4b_f$ throughout the bridge span.
   d. 15 ksi for interior girders, when the offsets or staggers relative to the closest adjacent cross-frames or diaphragms are less than $4b_f$ at any location throughout the bridge span.

Clearly, the above values are simplistic estimates of the flange lateral bending stresses, given their discreet change at offset and stagger lengths of $4b_f$, and given that they are independent of the bridge skew index and skew angles. However, it should also be noted that the influences of the many different details of potential cross-frame framing arrangements are difficult to capture without actually conducting a structural analysis of the resulting framing systems of some sort. Fortunately, the impact on the design economy of using upper-bound flange lateral bending estimates such as the above tends to be relatively small for the types of bridges that are amenable to the recommended LGA methods for design.

Table 12 provides a summary comparison of the above recommendations to the current AASHTO LRFD Article C6.10 recommendations.

In all of the above cases, AASHTO LRFD Article C6.10.1 recommends that the unfactored values of the flange lateral bending stresses be apportioned to the dead and live load in the same proportion as the unfactored major-axis dead and live load stresses at the girder cross-section under consideration. In this research, it is recommended that a weighted average load factor of 1.6 be assumed in all cases when checking the STR I limit state. As such, the above values are multiplied by 1.6 to determine the upper-bound estimates of the factored flange lateral bending stresses due to the skew effects for the STR I load combinations. The above stress estimates are extremely coarse values. It is not appropriate to require the designer to perform large numbers of tedious calculations implying high precision with these estimates, or to imply that the apportionment of these stresses to the different load cases is somehow tied in some precise way to the flexural stresses in the girders at the cross-frame location. Table 13 lists the recommended weighted average load factors for the STR I load combination as well as other load combinations.

These estimated flange lateral bending stresses are to be combined with the factored flange lateral bending stresses due to other effects. That is, these factored stresses must be calculated separately and added to the appropriate factored stresses from wind, eccentric overhang bracket loads, etc. according to the AASHTO LRFD load combination rules. The recommendations provided in this section only address the calculation of the girder flange lateral bending stresses due to skew effects.

Table 12. Summary of recommended estimations of the unfactored flange lateral bending stresses, f_ℓ

Bridge Category	Cross-frame Framing Arrangement	Orientation of Intermediate Cross-frames	Girder	Location	f_ℓ (ksi)		
					O_{min}/b_f < 4	O_{min}/b_f ≥ 4	AASHTO C6.10
1	Contiguous	Parallel to skew	Exterior	All	0	0	0
			Interior		0	0	0
2/3	Contiguous	Perpendicular to girders	Exterior	At or near supports	8	4	7.5
				Throughout the span	0	0	0
		Perpendicular to girders	Interior	At or near supports	10	5	10
				Throughout the span	0	0	0
2/3	Staggered	Perpendicular to girders	Exterior	At or near supports	8	4	7.5
				Throughout the span	3	2	2
		Perpendicular to girders	Interior	At or near supports	10	5	10
				Throughout the span	15	10	10

Table 13. Recommended weighted average load factors for estimation of girder flange lateral bending stresses due to skew effects in straight I-girder bridges.

Load Combination Limit State	Weighted Average Load Factor Applied to Article C6.10.1 Coarse Estimate of f_ℓ
Strength I	1.6
Strength II	1.3
Strength III	1.3
Strength V	1.3
Additional load combination for DC + construction loads, Article 3.4.2.1	1.4
Service I	1.0
Service II	1.2
Fatigue I	1.75
Fatigue II	0.8

5.1.5 Estimation of Cross-Frame and Diaphragm Forces

Similar to the estimation of the girder flange lateral bending stresses, when LGA is employed, there is no direct way of estimating the cross-frame forces associated with the interactions between the cross-frames and the girders due to the skewed geometry effects in resisting the dead load effects. AASHTO (2017) LRFD presently does not provide any guidance for estimating the cross-frame forces considering these actions. AASHTO (2017) Article 6.6.1.3.1 does indicate that, "In the absence of better information, the welded or bolted connection[s] should be designed to resist a 20.0-kip lateral load for straight, nonskewed bridges." Therefore, it would be appropriate to always design the connections for a force that is greater than or equal to 20.0 kips. The estimation of the forces at cross-frame and diaphragm connections due to skew effects are discussed below.

Based on the research studies discussed subsequently in Section 5.5.11, it is recommended that intermediate and bearing line cross-frames should be designed for the estimated loads due to bridge skewed geometry effects shown in Table 14. The cross-frame forces in this table are expressed as fractions of the maximum shear and moment within any of the bridge girders as determined by LGA. Tying the cross-frame force estimates to the maximum girder shear and moment facilitates their general applicability. Furthermore, engineers familiar with stability bracing design will observe that the specified values are approximately equal to or somewhat greater than established stability bracing strength requirements. These forces should be added to the loads from other sources such as wind, eccentric overhang bracket loads, etc.

From Table 14, one can observe that the DC2 cross-frame forces expressed as fractions of the maximum shear and moment within any of the bridge girders as determined by LGA are larger than the fractions for the other load cases and load combinations. This can be attributed to the fact that a large portion of the DC2 loads, i.e., the barrier rail loads of 430 plf applied to each of

the overhangs in this research, is distributed between the exterior and first interior girders by the cross-frames in the bays between these girders. However, it is important to note that the barrier rail load effects are relatively small compared to the other load effects considered in this research. As discussed subsequently in Section 5.2, Item 7, if the concentrated loads from barriers, sidewalks, walls, etc. are larger than 625 plf, approximations other than the simple assumption of equal distribution of these loads between the girders should be considered. In addition, for larger DC2 loads, a more refined estimate of the corresponding DC2 cross-frame forces than provided in Table 14 should be beneficial.

Table 14. Cross-frame shears and chord level connection horizontal forces due to skew effects.

Cross-Frame Case	Load Effect	DC1 & Constr	DC2	DW	HL-93 LL	STR I & SER II	Fatigue LL*
(1i) Intermediate cross-frames using offsets and staggers greater than or equal to $4b_f$ throughout the span	$V_{max.ICF\text{-}}/V_{max.g}$	0.02	0.40	0.03	0.06	0.03	0.06
	$B_{max.cn.ICF}/(M_{max.g}/h_{cf})$	0.02	0.20	0.02	0.06	0.03	0.05
	$T_{max.cn.ICF}/(M_{max.g}/h_{cf})$	0.02	0.20	0.02	0.05	0.02	0.05
(2i) Contiguous intermediate cross-frames, or intermediate cross-frames with any offsets and staggers less than $4b_f$ within the span	$V_{max.ICF\text{-}}/V_{max.g}$	0.06	1.20	0.06	0.20	0.09	0.14
	$B_{max.cn.ICF}/(M_{max.g}/h_{cf})$	0.02	0.60	0.04	0.14	0.08	0.12
	$T_{max.cn.ICF}/(M_{max.g}/h_{cf})$	0.03	0.40	0.02	0.08	0.04	0.08
(1b) Bearing line cross-frames where the offset of intermediate cross-frames relative to the bearing line is greater than or equal to $4b_f$	$V_{max.BCF\text{-}}/V_{max.g}$	0.02	0.07	0.02	0.02	0.02	0.02
	$B_{max.cn.BCF}/(M_{max.g}/h_{cf})$	0.02	0.04	0.02	0.02	0.02	0.02
	$T_{max.cn.BCF}/(M_{max.g}/h_{cf})$	0.02	0.10	0.02	0.03	0.02	0.04
(2b) Bearing line cross-frames where the offset of intermediate cross-frames relative to the bearing line is smaller than $4b_f$	$V_{max.BCF\text{-}}/V_{max.g}$	0.04	0.12	0.06	0.06	0.04	0.06
	$B_{max.cn.BCF}/(M_{max.g}/h_{cf})$	0.02	0.14	0.02	0.08	0.05	0.07
	$T_{max.cn.BCF}/(M_{max.g}/h_{cf})$	0.02	0.14	0.02	0.03	0.02	0.05

* The fatigue live load calculation pertains to the force range and uses the corresponding maximum range of $V_{max.g}$ and $M_{max.g}$ from LGA.

The force quantities in Table 14 are defined as follows:

$V_{max.ICF}$ = maximum magnitude of the intermediate cross-frame shear force throughout the bridge span.

$V_{max.BCF}$ = maximum magnitude of the bearing line cross-frame shear force.

$B_{max.cn.ICF}$ = maximum magnitude of the intermediate cross-frame connection horizontal force at the level of the cross-frame bottom chord throughout the bridge span, equal to the maximum magnitude chord force at locations where no cross-frame diagonals frame into the connection plates, and equal to the sum of the maximum magnitude chord force plus the horizontal component of the maximum magnitude diagonal axial force at locations where cross-frame diagonals frame into the connection plates.

$T_{max.cn.ICF}$ = maximum magnitude of the intermediate cross-frame connection horizontal force at the level of the cross-frame top chord throughout the bridge span, equal the maximum magnitude chord force at locations where no cross-frame diagonals frame into the connection plates, and equal to the sum of the maximum magnitude chord force plus the horizontal component of the maximum magnitude diagonal axial force at locations where cross-frame diagonals frame into the connection plates.

$B_{max.cn.BCF}$ = maximum magnitude of the bearing line cross-frame connection horizontal force at the level of the cross-frame bottom chords, equal to the maximum magnitude chord force at locations where no cross-frame diagonals frame into the connection plates, and equal to the sum of the maximum magnitude chord force plus the horizontal component of the maximum magnitude diagonal axial force at locations where cross-frame diagonals frame into the connection plates.

$T_{max.cn.BCF}$ = maximum magnitude of the bearing line cross-frame connection horizontal force at the level of the cross-frame top chords, equal to the maximum magnitude chord force at locations where no cross-frame diagonals frame into the connection plates, and equal to the sum of the maximum magnitude chord force plus the horizontal component of the maximum magnitude diagonal axial force at locations where cross-frame diagonals frame into the connection plates.

$V_{max.g}$ = maximum magnitude of the girder vertical shear force throughout the bridge span or spans under consideration, due to the force effect under consideration. The shear is determined using LGA with the assumption that the dead loads are equally distributed to all girders. For force effects that include live loads, the LGA analysis is based on the AASHTO LLDF procedures, including the skew correction factor.

$M_{max.g}$ = maximum magnitude of the girder major-axis bending moments (positive or negative) throughout the bridge span or spans under consideration, due to the force effect under consideration. The moment is determined using LGA with the assumption that the dead loads are equally distributed to all girders. For force effects that include live loads, the LGA analysis is based on the AASHTO LLDF procedures (no skew reduction included).

h_{cf} = for the bridge in its composite condition, the distance between the mid-thickness of the bridge deck and the centroid of the cross-frame bottom chord; for the bridge in its noncomposite condition, the distance between the cross-frame chords.

It should be noted that the Table 14 values for the intermediate cross-frame bottom and top chord level connection forces are comparable to or somewhat greater than established values for design of I-girder torsional bracing. The bearing line cross-frame values are comparable to or somewhat greater than established values for design of I-girder lateral bracing (Yura, 2001). The cross-frame components should be designed to resist these forces either in tension or in compression. These values are determined in this research by the evaluation of 3D FEA results for the bridge system effects associated with skew. It is recommended that these maximum force estimates are sufficient without further amplification due to stability effects. It is emphasized that other force effects such as wind, seismic, etc. must be added to these effects for calculation of the total cross-frame forces for design.

Given the above maximum cross-frame shears and chord-level horizontal forces transferred from the connections to the girders, the cross-frame member force demands may be determined by an ordinary idealization of the cross-frames as trusses and use of the method of joints at the top and bottom corners of the cross-frames. For X-type cross-frames, the total cross-frame shear should be distributed half to the top and half to the bottom of the cross-frame. For V- and inverted-V type cross-frames, the full shear should be considered to be transferred by the connection at the corner of the cross-frame into which the corresponding diagonal member is framed.

For design of solid-web diaphragms, it is recommended that the diaphragm connections should be designed for the shear force plus the sum of the above cross-frame bottom and top connection forces applied as a concentric axial force to the diaphragm connections and members, and that h_{cf} should be taken as the distance between the mid-thickness of the bridge slab and the centroid of the solid-web diaphragm. This provides an estimate of the force effects induced in the diaphragm associated with its combined action with the composite bridge deck.

For design evaluation of solid-web diaphragms during construction, the diaphragms should be sized for the above shear forces plus the moments at the diaphragm connections equal to the values obtained by applying the factors in Table 14 directly to the girder moments.

In all cases, $V_{max.g}$ and $M_{max.g}$ are the maximum factored shears and moments in any one of the individual girders of the bridge system, determined by LGA.

In general, minimum stiffness requirements should be satisfied by the cross-frames and diaphragms. The base stiffness requirements for torsional and lateral bracing of I-girders are defined by Yura (2001).

Specific individual cross frames at acute corners of the bridge plan, where the diagonals are removed to mitigate the transfer of large forces while providing bracing to the fascia girder adjacent to the acute corner, should be designed for the above bottom and top level connection forces, but since the diagonals are removed, these cross-frames do not need to be designed for shear.

It should be emphasized that the above forces and moments are upper-bound values obtained considering the bridges evaluated in this research and for which LGA is permitted based on the limits for Categories 1 through 3 in Section 5.1, as well as the additional broad requirements listed in Section 5.2. The actual force demands in a large number of the cross-frames will tend to be significantly smaller than these values. This is the case in general for typical cross-frame design. That is, even if 3D FEA is employed to obtain the cross-frame force demands, one set of cross-frame member sizes will often be selected for the intermediate and the bearing line cross-frames. This provides the benefits of repetition of member sizes in the cross-frame fabrication. In addition, it should be noted that if the recommended design demands from DC1, DC2, DW and LL are combined directly from the values listed for the separate load cases, a value larger than that specified for Strength I or Service II can be obtained. This is because the maximum cross-frame forces for the separate load cases do not necessarily occur at the same location within the bridge.

It is intended that Table 14 be applied predominantly using the third and last two columns of the table, which give the cross-frame force ratios for DC1 plus construction loading, Strength I or Service II, and for the AASHTO fatigue truck loading. The ratios for Strength I and Service II also may be applied for estimating the cross-frame forces due to gravity loads and the skew effects for other load combinations such as Strength III and Strength V. It should be noted that the specific ratios for Strength I and Service II obtained from the research studies differ, but only slightly; therefore, Table 14 gives one set of ratios for estimation of the cross-frame forces for both of these load combinations. The values in the first column for DC1 and construction are based on the studies of DC1 loads in this research. It is recommended that the cross-frame forces due to construction loads may be approximated by using the same fractions as DC1 No specific construction load analyses were conducted in this research. Alternatively, it is expected that the fractions for DC2 can be applied as a conservative estimate of force effects such as those from a screed machine acting on screed rails supported by overhang brackets. The individual load case columns for DC2, DW, and HL-93 live load in Table 14 are intended primarily for reference purposes, to indicate the nature of the maximum cross-frame forces for these different load cases.

5.2 Bridge Characteristics Required for Application of the Recommended LGA Procedures

The recommended LGA procedures detailed in Section 5.1 are subject to the following requirements, or limits of applicability:

1. Broadly speaking, the general requirements of the AASHTO (2017) LRFD Specifications pertaining to the use of LGA must be satisfied. The following requirements provide additional restrictions and/or clarifications of the AASHTO LRFD limits.

2. The bridge should have parallel skew of the bearing lines. It is recommended that adjacent bearing lines may be considered to be parallel as long as their skew angles do not differ by more than 10°. One bridge, Bridge 22, with a difference in adjacent bearing line skew angles of up to 4° was studied in the current work. Although not directly related, AASHTO (2017) Article 4.6.1.2.4b indicates that curved I-girder bridges with bearing lines not skewed more than 10° from radial may be considered as straight bridges for determining their major-axis bending moments and shears. In addition, though also not directly related, Article 4.6.2.2.2e allows a reduction in the AASHTO moment live load distribution factors (LLDFs) when the skew angles of two adjacent support lines do not exceed 10°. Appendix B6.2 of AASHTO (2017) allows moment redistribution in continuous-span I-section members when the support lines are not skewed by more than 10°. Therefore, 10° deviation in skew from the ideal is allowed at several locations in the AASHTO LRFD Specifications. For bridges that have a deviation in their skew angle between adjacent bearing lines, the girders should still be analyzed using their actual lengths determined from the actual geometry of the bridge.

3. The maximum skew angle at any of the bearing lines, θ, is limited to values less than or equal to 50°. Based on the results from this research, bridges with skew angles larger than 50° may exhibit a number of significant (larger) deviations between the recommended LGA and corresponding 3D FEA solutions.

4. The skew index, I_s, must be less than or equal to 0.40, unless θ is less than or equal to 30°. In such a case, I_s up to 0.45 is permitted. Similar to the above statement 3, bridges violating these requirements may exhibit a number of significant (larger) deviations between the recommended LGA and corresponding 3D FEA solutions. As discussed in Section 5.1, three categories are specified in the recommended LGA procedures for bridges applicable within these limits, allowing for direct application of routine LGA procedures without adjustment for bridges with smaller skew angles and skew indices.

5. The bridge should have constant width and parallel orientation of the girders. However, consistent with the discussions in Articles 4.6.2.2.1 and C4.6.2.2.1 of AASHTO (2017), it is expected that minor deviations from constant deck width and/or parallel girders can exist. Two simple-span bridges studied in this research, Bridges 19 and 20, have non-constant deck width and splayed girders. Both of these bridges have a maximum girder splay angle of 3.12° and a 19 % change in the deck width along their length. These bridges violate a number of targeted goals for accuracy of the LGA calculations. However, they also violate the above maximum limits on I_s and θ for application of the recommended LGA-based procedures. Furthermore, the splayed fascia girder in these bridges has noncomposite moments of inertia that deviate from those of the other girders by more than 10 %. Therefore, these studies are not sufficient to clearly define limits on variation of the deck width or girder splay for use of the recommended LGA procedures. Based on inference from the solutions considered in this research, it is recommended that girder splay angles up to 3° and deviations in the deck width up to 15 % can be accommodated within any given span as long as the other restrictions on the applicability of the recommended LGA procedures are satisfied.

   The calculation of LLDFs using the girder spacing at the 2/3 point along the span toward the wider end, suggested in AASHTO (2017) Article 4.6.2.2.1, is employed for the calculation of the LLDFs in this work, and is found to provide an acceptable approximation. Furthermore, equal distribution of the bridge dead loads as uniformly distributed line loads to all the girders in these studies, with the exception of the steel girder self-weights (which are applied directly as self-weight distributed loads based on the girder cross-sectional areas throughout the bridge)

6. The girders should have approximately the same stiffness across the bridge cross-section. Based on the bridge solutions considered in this research, it is recommended that deviations in the noncomposite and short-term composite girder moments of inertia of up to 10 % can be accommodated using the recommended LGA procedures. This requirement accommodates some minor deviation between the steel I-girder section dimensions, spacing between the girders, and differences in tributary deck width of the fascia girders versus the interior girders within the bridge cross-section.

7. If concentrated loads from barriers, sidewalks, walls, etc. exceed 625 plf, approximations other than equal distribution of the dead load to the girders should be applied, or a refined analysis solution should be considered for these loadings. As noted in Section 4.2.3, the studies conducted in this research involved concentrated loads of only 430 plf applied near the edges of the bridge deck. The 3D FEA studies show that the assumption of equal distribution of these rail loads to all the girders is significantly in error; however, these loads are small enough such that the overall LGA solution accuracy is not significantly affected.

8. The ratio of the girder web depth to the girder flange width, D/b_f, should be less than or equal to 5.0. AASHTO (2017) Article 6.10.2.2 specifies a maximum limit on D/b_f of 6.0 for I-girders. However, the AASHTO Article C6.10.1 procedure for estimating girder flange lateral bending stresses due to skew effects in straight skewed I-girder bridges is based on "a limited examination of refined analysis results for bridges with skews approaching 60 degrees from normal and an average D/b_f ratio of approximately 4.0." Girders with larger D/b_f tend to be sensitive to flange lateral bending. The bridges studied in which LGA performed well in this research included bridges with D/b_f up to 5.0.

9. At I-girder flange transitions, the flange lateral moment of inertia of the smaller section should be equal to or larger than one-half of the corresponding value for the larger section. Similar to the above requirement, this rule is intended to ensure the integrity of the girder flange lateral bending estimates in the recommended LGA procedures. Also, this requirement is recommended in AASHTO (2017) Article C6.10.8.2.3. Two of the bridges studied in this research, Bridges 15 and 16, violated this requirement at one of the flange transitions. This resulted in a significant spike in the flange lateral bending stresses at the flange transition in Bridge 16.

10. All V-type cross-frames should have a top and bottom chord. The top chord can be omitted in X-type cross-frames. This requirement comes from White et al. (2012) and White et al. (2015). V-type cross-frames without a top chord have a substantially reduced stiffness prior to the bridge deck becoming composite, due to the lack of section depth at the V connection of the diagonals to the chord. X-type cross-frames have some reduction in stiffness in the noncomposite condition of the bridge; this reduction in stiffness typically provides some benefit by softening the transverse load paths in the bridge structural system. All cross-frames should have diagonals within the exception of cross-frames framed between a location at or close to an adjacent girder support bearing and the fascia girder at the acute corner of a bridge span, provided to reduce the fascia girder's unbraced length at the acute corner.

11. The cross-frames should be detailed for steel dead load fit (SDLF). In the conduct of the project studies, all of the bridges were assumed to have cross-frames detailed for steel dead load fit (SDLF). SDLF detailing is an appropriate option for skewed I-girder bridges. This practice results in girders that are approximately plumb at the completion of the steel erection. In addition, the girder flange lateral bending stresses and the cross-frame forces are effectively negligible under the steel self-weight when this detailing practice is employed. SDLF detailing effectively forces the bridge to respond in a manner close to the LGA approximation under the steel self-weight. No-load fit (NLF) detailing of the cross-frames is not recommended for bridges with significant skew of their bearing lines. This is because the girders will layover at these bearing lines under the steel dead load in a manner related to the Concrete Dead Load layovers discussed in Section 5.1.2. Also, the girder flange lateral bending stresses and the cross-frame forces are measureable under the steel dead load if the cross-frames are detailed for NLF.

    In some situations, Total Dead Load Fit (TDLF) may be specified, although TDLF is not permitted by FDOT without approval from the Structures Design Office (FDOT, 2019a). The recommended LGA procedures are considered applicable with TDLF detailing of the cross-

frames. The girder webs will be approximately plumb, and the total dead load girder flange lateral bending stresses and cross-frame forces will be relatively small when TDLF detailing is employed. Therefore, the girder flange lateral bending estimates discussed in Section 5.1.4 and the cross-frame force estimates discussed in Section 5.1.5 will tend to be more conservative in the final constructed condition if TDLF detailing is employed. It should be noted, however, that TDLF tends to increase the cross-frame forces, girder flange lateral bending stresses, and general fit-up forces within the bridge system during the steel erection stage, compared to SDLF (White et al., 2015; NSBA, 2016).

It is useful to list the additional broad requirements specified by AASHTO (2017) that are relevant to the applicability of the recommended LGA solutions. These requirements are as follows:

1. The following additional limits of applicability are specified in AASHTO (2017) Article 4.6.2.2:

    a. The roadway portion of the deck overhang width, d_e, must be less than or equal to 3.0 ft. In addition, d_e must be greater than or equal to -1.0 ft.

    b. The girder spacing, S, should satisfy, 3.5 ft < S < 16 ft. The smaller spacings within this range are considered somewhat unrealistic for straight skewed steel I-girder bridges; they are based on the underlying LLDF developments by Zokaie et al. (1991).

    c. The concrete deck structural thickness should satisfy 7 in < t_s < 12 in. The 7 inch minimum limit is specified in AASHTO Article 9.7.1.1 and is cited in Article C4.6.2.2.1.

    d. The span lengths should fall within the limits 20 ft < L_s < 240 ft. The lower limit in this expression of 20 ft is significantly smaller than typically expected for skewed steel I-girder bridges, but represents the lower limits of the studies by Zokaie et al. (1991).

    e. Number of bridge girders, $N_g \geq 4$.

    f. The composite girder longitudinal stiffness parameter should satisfy 10,000 < K_g < 7,000,000, where K_g is defined by AASHTO (2017) Equation 4.6.2.2.1-1. These limits tend to be easily satisfied by composite steel I-girders in bridges satisfying the span length limits in (d).

2. Article 6.7.4.2 states that "Diaphragms or cross-frames for rolled beams and plate girders should be as deep as practicable, but as a minimum should be at least 0.5 of the beam depth for rolled beams and 0.75 of the girder depth for plate girders." This requirement should be satisfied to help ensure the efficient action, and sufficient strength and stiffness, of the cross-frames and solid-web diaphragms.

3. Article 6.9.3 states that for primary members subjected to compression only, or to both tension and compression, the effective slenderness of the member, $K\ell/r$, shall be limited to 120. For secondary members, the effective slenderness is limited to140. As noted in Section 5.1.5, the cross-frame members in straight skewed bridges should be designed to

accommodate the estimated force effects from skew in both tension and compression. It is recommended that the intermediate and bearing line cross-frame members in straight skewed bridges designed by LGA may be considered as secondary members. When the girders are designed using LGA, without the use of any reductions in moment LLDFs due to skew, a load path has been provided for transfer of the applied loads to the bearing lines simply via the girders. It should be noted that to satisfy the strength requirements based on Section 5.1.5 most efficiently, the cross-frame members often will have Kℓ/r values close to or smaller than 120.

4. Article 6.7.3 states that the "Structural steel, including bracing, cross-frames, and all types of gusset plates… shall not be less than 0.3125 in.[5/16 in.] in thickness." This requirement, combined with the above minimum $K\ell/r$ requirement, can lead to an increase in the cross-frame member sizes in some situations, indirectly providing an additional margin of safety.

It should be noted that the recommended LGA procedures are considered applicable for evaluation of staged deck placement effects, that is, study of the influence of placement of the deck in separate stages along the bridge length, for bridges satisfying the limits detailed in the above. Software such as LRFD Simon (NSBA, 2019) provides automated capabilities for considering these effects. Limited studies were conducted in this research to provide some validation of these capabilities versus 3D FEA solutions. The recommended LGA procedures are also considered applicable for phased construction, i.e., construction of the bridge in parallel units that are ultimately connected together into one bridge system, when the individual phases are constructed in a manner in which they are independent of one another, and when the individual phases and the completed bridge meet the above requirements for applicability of the LGA.

5.3 Measurement of Differences between LGA and 3D FEA

The recommended LGA procedures discussed in Section 5.1, and the requirements that need to be satisfied for the use of these procedures discussed in Section 5.2 are based on the following measures of the differences between the calculation results:

1. Professional factor ρ_{max} no larger than 1.11 in all cases for the following responses:
   a. Girder STR I positive and negative major-axis bending moments
   b. Girder STR I shear forces
   c. Girder STR I bearing reactions
   d. Girder fatigue live load vertical shear ranges
   e. Girder fatigue live load flexural stress ranges at locations subjected to net tension stresses

   where the professional factor is defined as

$$\rho_{\max} = \frac{\left|3DFEA\right|_{\max}}{\left|LGA\right|_{\max}} \tag{23}$$

$\left|3DFEA\right|_{\max}$ = girder maximum 3D FEA response throughout the bridge length

$\left|LGA\right|_{\max}$ = corresponding girder maximum LGA response throughout the bridge length.

The professional factor is commonly employed in structural reliability analysis, where the numerator of this ratio is typically the measured strength of a structural component, and the denominator is the predicted strength using a selected engineering approximation. For cases where ρ_{max} is greater than 1.0, this factor gives the ratio by which the approximate calculation would need to be scaled to ensure an accurate prediction of the measured strength. In this work, $\left|3DFEA\right|_{\max}$ and $\left|LGA\right|_{\max}$ are the maximum calculated demands obtained from the benchmark 3D FEA calculations and the demands calculated by the selected LGA analysis approximation.

In the bridge appendices generated in the studies, the accuracy of the LGA solutions are provided for many of the above quantities in terms of the measure

$$\varepsilon_{\max 1} = \frac{\left|LGA\right|_{\max} - \left|3DFEA\right|_{\max}}{\left|3DFEA\right|_{\max}} \tag{24}$$

The above two difference measures are related as follows. Given a value for ρ_{max}, one can calculate

$$\varepsilon_{\max 1} = \frac{1}{\rho_{\max}} - 1 \tag{25}$$

Conversely, given a value for ε_{max1}, the professional factor may be calculated as

$$\rho_{\max} = \frac{1}{\varepsilon_{\max 1} + 1} \tag{26}$$

Therefore, $\rho_{max} = 1.11$ corresponds to an "unconservative" difference of LGA relative to 3D FEA of $\varepsilon_{max1} = -0.10$.

The selection of $\varepsilon_{max1} = -0.10$ as an acceptable tolerance for evaluation of the differences between the LGA and 3D FEA for the above responses is of course subjective. The fact of the matter is that finite differences between the LGA and 3D FEA responses, some being "unconservative," can occur even for a straight I-girder bridge with zero skew. The value of $\varepsilon_{max1} = -0.10$ is selected as a value for which the overall impact on any reduction in the bridge structural reliability is relatively small. Specifically, the influence of $\varepsilon_{max1} = -0.10$, or $\rho_{max} = 1.11$ is approximately two times the impact on the structural reliability by variations in the load modifier η_i in Article 1.3.2.1 of AASHTO LRFD.

Ultimately, for the bridges in Categories 1 and 2, the largest ρ_{max} values for all of the above response quantities are less than or equal to 1.05 with the exception of an exterior

girder reaction that is equal to 1.08 in one of the Category 1 bridges. Therefore, for the Category 1 and 2 bridges, the influence of the largest ρ_{max} values is approximately the same as the impact on the structural reliability by the variations in the load modifier η_i in Article 1.3.2.1 of AASHTO LRFD. One of the Category 3 bridges has a ρ_{max} equal to 1.16 for the Strength I shear on its fascia girders, indicating a somewhat larger impact on the structural reliability for this one bridge response quantity.

2. A normalized difference $|\varepsilon_{\max 2}| < 0.0005$ in all cases for the girder total dead load vertical displacements, including the consideration of the effects of steel dead load fit (SDLF) detailing of the cross-frames, where

$$\varepsilon_{\max 2} = \frac{(\Delta_{LGA})_{\max} - (\Delta_{3DFEA})_{\max}}{L_s} \tag{27}$$

$(\Delta_{LGA})_{\max}$ = girder maximum total dead load vertical deflection from LGA, downward deflections taken as negative

$(\Delta_{3DFEA})_{\max}$ = girder maximum total dead load vertical deflection from 3DFEA, downward deflections taken as negative

This normalized difference is considered to be a more appropriate measure than ρ_{max} when comparing the LGA total dead load vertical displacement predictions to corresponding 3D FEA values. This is because the ρ_{max} values for the LGA total dead load vertical displacement predictions can be larger than 1.11 and smaller than 0.91 (i.e., $\varepsilon_{max1} < -0.10$ or > 0.10). However, depending on the span length, these differences may be acceptable. The limit of 0.0005 on $\varepsilon_{\max 2}$ can be related indirectly to typical tolerances on the roadway smoothness, as discussed below.

The girder total dead load (TDL) displacements are used in setting girder cambers. A significant portion of the girder cambers is "taken out" by the girder vertical deflections during the casting of the deck. Thus, approximations in the TDL displacements can ultimately have some influence on the smoothness of the finished deck. Although the smoothness tolerances of the finished deck surface are not directly related to the differences between LGA and 3D FEA, the smoothness tolerances can be used as an assessment of the differences between LGA and 3D FEA in the prediction of the girder TDL displacements.

Deck smoothness tolerances are provided in Section 400-15.2.5.5 of the FDOT Specifications (FDOT, 2019b). This section states the following limit for deviations in the finished deck elevation, measured using a profilograph, longitudinally along the length of the bridge:

"Correct individual bumps or depressions exceeding a cutoff height of 0.3 inch from a chord of 25 feet (see ASTM E1274) on the profilograph trace."

A deviation of 0.3 inch per 25 feet comes out to a limit of 1/1000. Recognizing that the maximum displacement approximately occurs at the mid-span of the girders, and considering an extension of the deck smoothness limit to vertical deviations along the length of the girders due to approximations from the structural analysis, a similar longitudinal "tolerance" on the deviation between the LGA and 3D FEA vertical displacements can be set as $\frac{L_s/2}{1000} = \frac{L_s}{2000}$, where L_s is the span length.

The tolerance of 0.0005 on ε_{max2} can also be related to the positive camber tolerance of 1.5 inches on a welded girder given in Section 3.5.1.3 of (AWS, 2019). For a span length of 250 ft, 1.5 in / 250 ft / (12in/ft) = 0.0005. Therefore, $\left|\varepsilon_{\max 2}\right| < 0.0005$ ensures against deviations between the calculated LGA and 3D FEA deflections being larger than the positive girder camber tolerance for all values of span length for which the recommended LGA procedures can be applied.

3. A normalized difference $\varepsilon_{\max 3} < 0.001$ in all cases for the girder total dead load vertical displacements, including the consideration of the effects of steel dead load fit (SDLF) detailing of the cross-frame, where

$$\varepsilon_{\max 3} = \max\left\{\begin{array}{l} \dfrac{\left|\left[\left(\Delta_{LGA}\right)_{\max} - \left(\Delta_{3DFEA}\right)_{\max}\right]_{G3} - \left[\left(\Delta_{LGA}\right)_{\max} - \left(\Delta_{3DFEA}\right)_{\max}\right]_{G1}\right|}{w_g}, \\ \dfrac{\left|\left[\left(\Delta_{LGA}\right)_{\max} - \left(\Delta_{3DFEA}\right)_{\max}\right]_{G3} - \left[\left(\Delta_{LGA}\right)_{\max} - \left(\Delta_{3DFEA}\right)_{\max}\right]_{G4}\right|}{w_g} \end{array}\right\} \tag{28}$$

$\left[\left(\Delta_{LGA}\right)_{\max} - \left(\Delta_{3DFEA}\right)_{\max}\right]_{G3}$ = difference between the maximum LGA and 3D FEA displacements for the girder closest to the mid-width of the bridge cross-section.

$\left[\left(\Delta_{LGA}\right)_{\max} - \left(\Delta_{3DFEA}\right)_{\max}\right]_{G1}$ = difference between the maximum LGA and 3D FEA displacements for fascia girder G1.

$\left[\left(\Delta_{LGA}\right)_{\max} - \left(\Delta_{3DFEA}\right)_{\max}\right]_{G3}$ = difference between the maximum LGA and 3D FEA displacements for the other fascia girder, which is labeled as G4 (irrespective of the total number of girders in the bridge cross-section).

w_g = width of the bridge between the fascia girders

Clearly, this measure relates to the difference between the LGA and 3D FEA girder vertical displacements and its variation across the bridge cross-section width. The limit of 0.001 on this measure can be related indirectly to a second deck smoothness tolerance provided in Section 400-15.2.5.5 of the FDOT Specifications (FDOT, 2019b):

"Ensure that the surface meets a ¼ inch in 10 feet straightedge check made transversely across the deck."

A transverse deviation of 1/4 inch per 10 feet translates to a limit of 1/480, which rounds to 1/500. Recognizing that cross-slopes are generally built across the deck from the median at the center of the bridge to the two transverse edges of the bridge, and considering an extension of the deck smoothness limit to vertical deviations along the length of the girders due to approximations from the structural analysis, a similar transverse "tolerance" on the deviation between the LGA and 3D FEA vertical displacements can be set as (w_g/2)/500 = w_g/1000, where w_g is the bridge framing width.

It should be noted that $|\varepsilon_{\max 3}| < 0.001$ is a more relaxed tolerance on deviations in the differential girder displacements across the bridge width compared to $|\varepsilon_{\max 2}| < 0.0005$ on the individual girder displacements relative to the span length.

4. Lastly, a maximum difference between LGA estimates of the girder layovers at the simply-supported ends of the bridge under the total dead load, including the consideration of the effects of steel dead load fit (SDLF) detailing of the cross-frames, and the corresponding 3D FEA values, ε_{max4}, less than or equal to 0.25 inches, where

$$\varepsilon_{\max 4} = \left|\left(\Delta_l\right)_{LGA} - \left(\Delta_l\right)_{3DFEA}\right| \tag{29}$$

$\left(\Delta_l\right)_{LGA}$ = total dead load layover displacement at the girder top flange predicted using FDOT recommended calculations and the major-axis bending displacements from LGA, including the consideration of the effects of steel dead load fit (SDLF) detailing of the cross-frames (girder steel dead load layovers taken equal to zero).

$\left(\Delta_l\right)_{3DFEA}$ = total dead load layover displacement at girder top flange obtained from 3D FEA solution, including the consideration of the effects of steel dead load fit (SDLF) detailing of the cross-frames (girder steel dead load layovers approximately equal to zero, based on 3D FEA calculations).

The rationale behind this measure is that the most meaningful parameter pertaining to girder layover is the physical layover itself, i.e., the lateral deflection at the top of the girders relative to the bearings at the simply-supported girder end bearing locations, and that 0.25 inches is a reasonable tolerance on this displacement coming from differences between LGA and 3D FEA solutions.

5.4 Summary of Parametric Study Bridges Satisfying and Not Satisfying the Requirements for Use of LGA

Tables 15 through 19 present a summary of the parametric study data for each of the five bridge categories discussed in Section 5.1. The first seven columns of these tables summarize key attributes of each of the bridges. The bridge number is highlighted in dark red with white text for bridges that exceed the specified I_s and θ limits for a given category. In addition, the I_s

and/or θ values that violate the specified limits for each of the categories are highlighted in dark red with white text.

The subsequent six columns of Tables 15 through 19 first summarize the largest ρ_{max} values for the following key design demands for each of the bridges:

1. The Strength I positive moment, $M_{u+.STRI}$, for all the girders of a given bridge,
2. The Strength I negative moment, $M_{u-.STRI}$, for all the girders of a given bridge (for the continuous-span bridges),
3. The Strength I shear forces, $V_{u.STRI}$, for all the girders of a given bridge,
4. The fascia girder HL-93 live load shear forces, V_{LL}, at the obtuse corners of the spans, both at abutments and at pier supports,
5. The fascia girder Strength I bearing reactions at the obtuse corners of the spans at the abutments, and at pier supports on the fascia girders in continuous-span bridges, $R_{u.STRI}$, and
6. The maximum fascia girder fatigue live load vertical shear ranges, ΔV_{FAT}, at the obtuse corners of the spans at the abutments or the pier supports.

As explained in Section 5.3, ρ_{max} values up to 1.11, indicating 10 % unconservatism of the LGA results, are recommended as being acceptable. Note that the reported ρ_{max} values in the tables are the largest of all the ρ_{max} values evaluated for the various girders in the study bridges. That is, only the least conservative ρ_{max} values are shown in these summary tables. In all cases, the modification factor recommended in Section 5.1.3 is applied in determining the ρ_{max} values for the reactions reported in these tables.

The cells in the tables for response quantities slightly violating the targeted limits are shaded light red. Note that also the bridge minimum offset divided by the corresponding flange width, O_{min}/b_f, is shaded light red when this value is less than 2.0. For bridges with $O_{min}/b_f < 2.0$, accurate LGA prediction of the total dead load vertical deflections tends to be significantly more difficult to obtain (discussed below). This parameter also appears to have some impact on the sufficiency of LGA for calculation of $V_{u.STRI}$, $R_{u.STRI}$, and ΔV_{FAT} in some bridges. Furthermore, small O_{min}/b_f also has implications regarding the cross-frame forces.

One can observe that with the exception of a few bridges that do not satisfy the Category 2 and 3 limits on θ and I_s, all the above design force demands can be determined accurately to conservatively by LGA. In addition, one can observe that θ is an important variable, in addition to I_s, for identifying when the geometry is starting to become too extreme for LGA to provide acceptable predictions. For a given value of I_s, bridges with larger skew angles, θ, tend to have larger skew effects.

As stated in Section 5.3, all of the above response quantities have a ρ_{max} less than or equal to 1.05 with the exception of an exterior girder reaction that is equal to 1.08 in one of the Category 1 bridges. Therefore, for the Category 1 and 2 bridges, the influence of the largest ρ_{max} values is approximately the same as the impact on the structural reliability by the variations in the load modifier η_i in Article 1.3.2.1 of AASHTO LRFD. One of the Category 3 bridges has a ρ_{max} equal to 1.16 for the Strength I shear on its fascia girders, indicating a somewhat larger impact on the structural reliability for this one bridge response quantity.

Table 15. Bridge properties and girder data for the Category 1 bridges (parallel skew, $\theta \leq 20^o$, and cross-frames oriented parallel to the bearing lines).†

Bridge	Characteristics	I_s	θ_{max}	$L_{s.min}$ (ft)	$L_{s.max}$ (ft)	w_g (ft)	O_{min}/b_f	$M_{u+.STRI}$ ρ_{max}	$M_{u-.STRI}$ ρ_{max}	$V_{u.STRI}$ ρ_{max}	V_{LL} ρ_{max}	$R_{u.STRI}$ ρ_{max}	ΔV_{FAT} exterior girders ρ_{max}	Δ_{TDL} $1/\varepsilon_{max\,2}$	Δ_{TDL} $1/\varepsilon_{max\,3}$	LGA - 3D FEA TDL (SDLF) Layover (in)	$f_{\ell max}$, LGA - 3D FEA, exterior girders (ksi)	$f_{\ell max}$, LGA - 3D FEA, interior girders (ksi)
21*	Contiguous CFs parallel to bearing line	0.15	16.2	NA	241	128	NA	0.90	NA	0.96	0.89	0.97	0.85	5905	3819	-0.02	-0.97	-0.69
26*	Contiguous CFs parallel to bearing line; solid-web diaphragms at abutments	0.15	10.0	79.4	92	67.5	NA	1.02	0.94	1.04	0.94	1.08	0.90	6421	5959	0.00	-2.68	-0.95

† Light shaded cells highlight properties and responses that marginally violate target requirements.

* This bridge meets, or nearly meets, the requirements for application of the recommended LGA-based procedures for bridge design.

Table 16. Bridge properties and girder data for the Category 2 bridges (parallel skew, $\theta \leq 50^o$, $I_s \leq 0.3$, cross-frames perpendicular to the girders) plus Bridge 25 with $\theta = 54.5^o$ and $I_s = 0.25$.†

Bridge	Characteristics	I_s	θ_{max}	$L_{s.min}$ (ft)	$L_{s.max}$ (ft)	w_g (ft)	O_{min}/b_f	$M_{u+.STRI}$ ρ_{max}	$M_{u-.STRI}$ ρ_{max}	$V_{u.STRI}$ ρ_{max}	V_{LL} ρ_{max}	$R_{u.STRI}$ ρ_{max}	ΔV_{FAT} exterior girders ρ_{max}	Δ_{TDL} $1/\varepsilon_{max\,2}$	Δ_{TDL} $1/\varepsilon_{max\,3}$	LGA - 3D FEA TDL (SDLF) Layover (in)	$f_{\ell max}$, LGA - 3D FEA, exterior girders (ksi)	$f_{\ell max}$, LGA - 3D FEA, interior girders (ksi)
8*	CFs normal to girders, staggered with small offsets	0.27	23.4	148	173	93.3	3.15	0.95	0.92	0.97	0.88	0.90	0.77	4345	3562	-0.02	9.93	1.04
11*	Contiguous CF lines normal to girders, framing into bearing lines	0.26	38.1	185	188	61.0	0.00	0.93	0.89	1.01	0.99	1.01	0.91	9031	3702	-0.03	9.54	8.10
17*	Contiguous CF lines normal to girders, small to large offsets at abutments	0.28	41.5	NA	202	63.0	2.15	0.94	NA	1.05	1.00	0.95	1.04	3534	1329	-0.10	2.05	13.0
18*	CFs normal to girders, ample offsets & staggers	0.20	39.7	NA	212	51.7	3.23	0.96	NA	1.01	0.98	0.94	1.03	6384	3519	-0.03	9.60	17.9
25	Contiguous CF lines normal to girders, framing into the pier bearing line and with no cross frames along the pier bearing line; small offsets relative to the abutment bearing lines	0.25	**54.5**	196	196	35.3	0.00	0.96	0.92	0.95	1.00	0.94	1.01	2374	**705**	-0.15	**-5.80**	-1.12

† Light red cells highlight properties and responses that marginally violate target requirements; dark shaded cells highlight properties and responses that significantly violate target requirements; the intermediate shade (green) cells highlight the bridges having offsets and staggers.

* This bridge meets, or nearly meets, the requirements for application of the recommended LGA-based procedures for bridge design.

Table 17. Bridge properties and girder data for the Category 3 bridges (parallel skew, $\theta \leq 50$ degrees with $0.30 < I_s \leq 0.40$, or $\theta \leq 30$ degrees with $0.40 < I_s \leq 0.45$) plus Bridges 1, 2, 9, 10, 23 and 24 with $I_s > 0.45$ or $\theta > 50^o$.†

Bridge	Characteristics	I_s	θ_{max}	$L_{s.min}$ (ft)	$L_{s.max}$ (ft)	w_g (ft)	O_{min}/b_f	$M_{u+.STRI}$ ρ_{max}	$M_{u-.STRI}$ ρ_{max}	$V_{u.STRI}$ ρ_{max}	V_{LL} ρ_{max}	$R_{u.STRI}$ ρ_{max}	ΔV_{FAT} exterior girders ρ_{max}	Δ_{TDL} $1/\varepsilon_{max\,2}$	Δ_{TDL} $1/\varepsilon_{max\,3}$	LGA - 3D FEA TDL (SDLF) Layover (in)	$f_{\ell max}$, LGA - 3D FEA, exterior girders (ksi)	$f_{\ell max}$, LGA - 3D FEA, interior girders (ksi)
1	Contiguous CF lines normal to girders, small to large offsets at abutments	**0.46**	49.4	NA	208	82.5	4.20	0.96	NA	**1.31**	**1.38**	**1.23**	**1.30**	2201	**518**	-0.15	2.26	8.47
2 (1 Alt)	CFs normal to girders, ample offsets & staggers	**0.46**	49.4	NA	208	82.5	4.00	0.99	NA	**1.21**	**1.32**	**1.13**	**1.24**	7313	1592	0.03	3.28	7.95
3*	Contiguous CF lines normal to girders, framing into bearing lines	0.39	38.2	185	185	91.0	0.00	0.96	0.93	0.96	0.84	0.93	0.69	1844	1185	-0.03	9.69	11.3
4* (3 Alt)	CFs normal to girders, ample offsets & staggers	0.39	38.2	185	185	91.0	4.00	1.01	0.96	0.98	0.86	0.90	0.75	2429	2321	-0.07	1.02	3.33
5*	Contiguous CF lines normal to girders, small to large offsets at abutments	0.42	29.4	NA	144	108	1.05	0.93	NA	1.00	0.91	0.93	0.86	3675	3471	-0.09	10.68	12.8
6	Contiguous CF lines normal to girders, small to large offsets at abutments	0.35	20.7	116	116	106	1.73	1.06	0.96	**1.16**	0.97	0.99	0.86	4267	17114	-0.01	9.57	14.3
7*	Contiguous diaphragms normal to girders, small to large offsets at abutments	0.33	35.5	NA	96	46.1	2.18	0.92	NA	0.95	0.84	0.91	0.86	1814	**666**	-0.06	7.32	10.8
9	Contiguous CF lines normal to girders, framing into the pier bearing line and with no cross frames along the pier bearing line	**0.47**	**57.2**	148	173	93.3	0.00	0.93	0.96	1.01	1.00	0.96	0.96	**1556**	**419**	-0.19	0.73	6.87
10 (9 Alt)	CFs normal to girders, ample offsets & staggers	**0.47**	**57.2**	148	173	93.3	4.00	0.92	0.93	0.92	0.80	0.85	0.86	2264	**656**	-0.11	9.54	3.40
22*+	CFs normal to girders, contiguous CF lines with offsets at bearing lines	0.31	36.1	195	204	85.5	2.63	0.91	0.91	1.02	0.99	0.95	0.86	3988	1636	-0.03	9.76	13.9
23	Contiguous CF lines normal to girders, framing into pier bearing line	0.37	**50.7**	252	252	76.6	0.00	0.94	0.95	1.00	0.97	0.95	0.82	**1437**	**458**	-0.24	9.18	9.65
24	Contiguous CF lines normal to girders, inadequate offsets at abutments	0.37	**52.7**	170	170	48.3	2.31	0.94	0.95	1.01	0.98	0.97	0.92	2579	**760**	-0.10	6.15	4.95

† Light shaded cells highlight properties and responses that marginally violate target requirements; dark shaded cells highlight properties and responses that significantly violate target requirements; the light shaded cells under "Characteristics" highlight that this bridge has ample offsets.

* This bridge meets, or nearly meets, the requirements for application of the recommended LGA-based procedures for bridge design.

+ Bridge 22 has a slight variation in the skew angle between its supports.

Table 18. Bridge properties and girder data for the Category 4 bridges (nonparallel skew).†

Bridge	Characteristics	I_s	θ_{max}	$L_{s.min}$ (ft)	$L_{s.max}$ (ft)	w_g (ft)	O_{min}/b_f	$M_{u+.STRI}$ ρ_{max}	$M_{u-.STRI}$ ρ_{max}	$V_{u.STRI}$ ρ_{max}	V_{LL} ρ_{max}	$R_{u.STRI}$ ρ_{max}	ΔV_{FAT} exterior girders ρ_{max}	Δ_{TDL} $1/\varepsilon_{max\,2}$	Δ_{TDL} $1/\varepsilon_{max\,3}$	LGA - 3D FEA TDL (SDLF) Layover (in)	$f_{\ell max}$, LGA - 3D FEA, exterior girders (ksi)	$f_{\ell max}$, LGA - 3D FEA, interior girders (ksi)
12	Contiguous CF lines normal to girders, small offsets at abutments, Intermed. CFs framing into bearings at piers, no CFs on bearing lines at piers	0.32	**58.7**	182	202	35.0	0.00	0.93	0.96	0.97	0.99	1.06	1.06	3100	**747**	-0.07	3.00	6.44
13	Contiguous CF lines normal to girders with offsets relative to pier bearing lines; zero skew at abutments	0.23	**50.1**	184	253	36.0	2.40	0.92	0.96	0.96	0.58	0.78	0.67	11575	1740	-0.01	3.93	6.36
14 (13 Alt)	CF lines normal to girders with ample staggers and offsets; zero skew at abutments	0.23	**50.1**	184	253	36.0	4.00	0.93	0.95	0.97	0.57	0.78	0.67	18806	2367	-0.01	-3.26	2.15
15	Contiguous CF lines normal to girders, small to ample offsets at abutments and piers; change in flange moment of inertia larger than a factor of two at flange transition	0.32	**53.4**	156	226	49.2	1.45	0.97	0.93	0.98	0.93	1.03	0.89	1848	**461**	-0.26	3.99	5.01
16 (15 Alt)	Contiguous CF lines normal to girders, ample offsets and staggers; change in flange moment of inertia larger than a factor of two at flange transition	0.32	**53.4**	156	226	49.2	4.00	0.98	0.94	0.97	0.90	1.02	0.84	1981	**533**	-0.21	-3.21	**-15.3**

† Light shaded cells highlight properties and responses that marginally violate target requirements; dark shaded cells highlight properties and responses that significantly violate target requirements.

Table 19. Bridge properties and girder data for the Category 5 bridges (splayed girder bridges).†

Bridge	Characteristics	I_s	θ_{max}	$L_{s.min}$ (ft)	$L_{s.max}$ (ft)	w_g (ft)	O_{min}/b_f	$M_{u+.STRI}$ ρ_{max}	$M_{u-.STRI}$ ρ_{max}	$V_{u.STRI}$ ρ_{max}	V_{LL} ρ_{max}	$R_{u.STRI}$ ρ_{max}	ΔV_{FAT} exterior girders ρ_{max}	Δ_{TDL} $1/\varepsilon_{max\,2}$	Δ_{TDL} $1/\varepsilon_{max\,3}$	LGA - 3D FEA TDL (SDLF) Layover (in)	$f_{\ell max}$, LGA - 3D FEA, exterior girders (ksi)	$f_{\ell max}$, LGA - 3D FEA, interior girders (ksi)
19	Contiguous CF lines normal to girders, small to ample offsets relative to abutment bearing lines	**0.45**	**52.2**	NA	196	55.5 to 66.2	2.30	1.07	NA	**1.23**	0.96	**1.17**	0.94	**1073**	**252**	-0.19	1.67	7.67
20 (19 Alt)	CF lines normal to girders with ample staggers and offsets	**0.45**	**52.2**	NA	196	55.5 to 66.2	4.00	0.96	NA	1.09	0.85	1.04	0.82	**1456**	**365**	-0.12	-0.50	1.03

† Dark shaded cells highlight properties and responses that significantly violate target requirements.

Bridge 6 is the Category 3 bridge having a ρ_{max} value of 1.16 for its Strength I exterior girder shear force. The other response quantities are predicted accurately to conservatively by LGA for this bridge. Therefore, Bridge 6 is marked as not meeting the requirements for application of the recommended LGA-based procedures in Table 17. However, since the requirements are violated by only this one response quantity, Bridge 6 might be considered as being acceptable for application of LGA in its design. This bridge is marked as being amenable for design based on LGA in the subsequent figures and tables.

The ρ_{max} values for the above six design force demands are followed by columns reporting $1/\varepsilon_{max2}$ and $1/\varepsilon_{max3}$, pertaining to the differences between the LGA and 3D FEA total dead load displacements, normalized by the girder lengths along the spans, and pertaining to the differential displacements across the bridge width, respectively. The recommended limit on ε_{max2} is 0.0005, or 1/2000, and the recommended limit on ε_{max3} is 0.001, or 1/1000. The inverse of these results, $1/\varepsilon_{max2}$ and $1/\varepsilon_{max3}$, is presented in the tables for ease of interpretation. The $1/\varepsilon_{max2}$ values should be larger than 1000 and the $1/\varepsilon_{max3}$ values should be larger than 2000 for the displacement results to be sufficient based on the suggested limits of Section 5.3.

The $1/\varepsilon_{max2}$ and $1/\varepsilon_{max3}$ columns show that the bridges violating the Category 2 or 3 limits on θ and I_s commonly have difficulty in predicting accurate bridge vertical displacements under the total dead load; hence, the girder LGA-based cambers can start to be significantly different from the true displacements that the cambers are aimed to offset. In addition, it can be observed that the Category 4 and 5 bridges generally have significant difficulty in predicting the total dead load displacements. This is believed to be due to the additional complexities regarding the influence of nonparallel skew and splay on the behavior, in combination with the fact that all of these bridges also violate the corresponding Category 2 or Category 3 limits.

Bridges 3 and 7 actually violate the targeted ε_{max2} requirements for use of LGA. However, the violation of these limits is by less than 10 %. Therefore, the corresponding cells in Table 17 are shaded light red. Furthermore, Bridge 7 violates the targeted requirements for ε_{max3} by more than 10 % and the corresponding cell for this bridge is shaded dark red in Table 17. However, these ε_{max3} limit might be considered to be the least consequential of the different limits, since it is a limit on differential displacements across the bridge width caused by the LGA approximations. Therefore, Bridges 3 and 7 are considered to "nearly meet" the requirements for application of the recommended LGA procedures.

Note that the responses for the splayed girder bridges are calculated using the assumption of equal distribution of the dead loads to all the girders employed throughout this research as discussed previously. For the distribution of the live loads, we are using the spacing at 2/3 of the span length as suggested in the AASHTO LRFD Article C4.6.2.2.1. Regarding the dead load effects, it was observed that switching to an alternative use of girder tributary widths at 2/3 of the span, etc. for these bridges does not have any significant influence on the LGA predictions. If the applied dead loads on the splayed exterior girder are calculated based on the tributary with at 2/3 of the span, the applied loads are increased by 5 % compared to the applied load based on the assumption of equal distribution of the dead loads. The applied dead loads on the first interior girder, also splayed, are approximately the same using tributary widths or equal distribution of the dead loads. However, the true total dead load (TDL) displacements, are equal to the sum of:

- The steel dead load (SDL) displacements with steel dead load fit (SLDF) detailing, where the girder response is effectively what is obtained by applying the tributary steel self-weight to the LGA model, and
- The concrete dead load (CDL) displacements, where the loads resisted by the girders are based on the relative stiffnesses and interactions within the three-dimensional bridge system.

It is apparent that the exterior fascia girder is attracting significantly more load than just its tributary applied load when the 3D FEA responses are inspected. In addition, if a larger portion of the applied load is being attracted by the exterior girder, the central interior girder is likely attracting a smaller fraction of the total load.

As can be observed from the tables, the dead load equal distribution rule performs reasonably well. However, it is also important to note that for the single splayed girder bridge studied in this research (Bridge 19), plus the version of this bridge with an alternative cross-frame framing arrangement (Bridge 20), the fascia girders have more than a 10 % difference in several of the girder noncomposite and short-term composite moments of inertia compared to the interior girders. Therefore, it can be argued that this bridge violates the AASHTO requirement of equal girder stiffness. All in all, to predict the 3D FEA total dead load displacements accurately for the splayed fascia girder, the corresponding applied load in the LGA model needs to be 1.29 and 1.17 times the load based on the equal distribution rule in Bridges 19 and 20 respectively. The situation is not as bad for Bridge 20 (19 Alt) due to the use of ample staggers and offsets of the cross-frames in this bridge. The conservatism of the live load predictions offsets the above unconservatism of the dead load predictions to some extent, but not enough to give sufficient predictions of the Bridge 19 Strength I vertical shear forces.

It is uncertain how much the splay and the unequal girder stiffnesses contribute to the above behavior of Bridges 19 and 20 versus the contributions from the large I_s and θ values for these bridges. Unfortunately, if it is desired to provide a limit on girder splay at which the LGA rules are viable, all that can be done is to make an educated guess. There are too many factors influencing the results for Bridges 19 and 20 for these bridges to contribute useful data to answer the splay question.

The next column of Tables 15 through 19 shows the maximum difference between the LGA and 3D FEA girder layovers at the abutments under the total dead load, including the influence of SDLF detailing of the cross-frames. The difference between the LGA predictions and 3D FEA layovers is less than or equal to 0.26 inches for all the bridges considered in this research. The maximum values of 0.26 inches is slightly larger than the suggested 0.25 inch tolerance in Section 2.3, but this is considered acceptable. It can be said that the FDOT mechanics-based estimation of the layover at the abutments gives excellent results (even though this estimate depends on vertical deflection estimates that may be outside of the recommended tolerances). It should be noted that the layovers for the splayed girders are calculated based on the specific angle between the girders and the skewed bearing lines.

Finally, the last two columns of Tables 15 through 19 show the maximum difference between the recommended estimates of the girder flange lateral bending stresses (involving simplification and extension of the current recommendations in the AASHTO LRFD Commentary), for use with LGA, versus the corresponding maximum flange lateral bending stress from 3D FEA for

the exterior girders and for the interior girders, respectively. These estimates are accurate to conservative for all the bridges, with the exception of Bridge 25, which violates the 50 degree limit on the skew angle, and Bridge 16, which contains a spike in the girder flange lateral bending stress at a section transition where the flange area is stepped by more than a factor of two.

Tables 20 through 24 show the Strength I 3D FEA maximum cross-frame member forces for the intermediate and end cross-frames of the bridges studied. The first seven columns in these tables are the same as in Tables 15 through 19, to convey the basic attributes of the bridges.

The following can be discerned from Tables 20 through 24:

- The bridges in Category 1 (Table 20) have slightly smaller maximum cross-frame member forces, highlighted in light green, than the bridges in Categories 2 and 3.
- The bridges in Category 2 (Table 21), barring the cases where the cross-frames are framed directly into a bearing, and where the bearing line also contains cross-frames, have slightly larger maximum cross-frame member forces than Category 1 and slightly smaller cross-frame member forces than Category 3. The cells corresponding to large bearing line cross-frame forces, due to framing of the intermediate cross-frames into the bearing line, are shaded light red.
- The dark-red shaded cells for the cross-frame member forces highlight situations where the forces are more than 10 % larger than the corresponding green shaded cells for a given bridge category.
- Bridge Category 3 (Table 22) tends to have the largest maximum cross-frame member forces, cells shaded green, compared to Categories 1 and 2 (although the maximum cross-frame diagonal and top chord forces are about the same in all three categories).
- Bridge Category 3 (Table 22) also has several cells corresponding to bridges where intermediate cross-frames are framed directly into bearings at bearing lines containing cross-frames, and the bearing line cross-frame forces are therefore relatively large. Again, these cells are shaded light red.
- Category 4 (Table 23) is nearly solid dark red. It is apparent that the cross-frames in nonparallel skew bridges can see substantial force demands, particularly when θ_{max} is greater than 50 degrees. The solid red cells in Table 21 correspond to cases where the cross-frame member forces are more than 10 % larger than the corresponding values in Tables 21 and 22.
- Table 24 suggests that Bridge 19 definitely has extreme characteristics (large I_s, large θ_{max}, unequal girder stiffness, and splay) that result in substantially larger maximum cross-frame forces. The cross-frame forces for Bridge 20 are significantly smaller due to the ample offsets and staggers employed.

The focus in Tables 20 through 24 on the maximum Strength I cross-frame bottom chord, diagonal and top chord member forces is useful for considering the potential impact on the design of these components. However, some type of normalization with respect to the cross-frame and bridge parameters is needed to generalize the data into useful design rules. This is because the magnitude of the cross-frame member forces can be influenced by the size (e.g., span length) of the bridge, the depth of the cross-frames, the inclination of the cross-frame diagonals (which is of course a function of the cross-frame depth), etc. Furthermore, the cross-

frame connections must be designed for the appropriate horizontal forces and shears transferred at the chord levels.

The maximum cross-frame shear forces correlate to some extent with the corresponding girder maximum shear forces, and the maximum cross-frame chord level connection forces correlate to some extent with the corresponding girder maximum moments. This allows the development of the generalized cross-frame force demands presented in Section 5.1.5.

Tables 25 through 27 show the cross-frame force ratios determined from 3D FEA corresponding to the Strength I load combination for the Category 1 through Category 3 parallel skew bridges from the parametric studies. The recommended Strength I design demands shown in these tables are obtained by rounding up the maximum values for a given cross-frame framing condition in these tables to the nearest percent, and by specifying a minimum values of 0.03 for the intermediate cross-frames, with the exception of the cross-frame top chord for composite loading conditions, and 0.02 for the bearing line cross-frames. These minimums correspond to representative torsional and lateral bracing strength requirements from Yura (2001).

Table 20. Bridge properties and STR I cross-frame forces for the Category 1 bridges (parallel skew, $\theta \leq 20^o$, and cross-frames oriented parallel to the bearing lines).†

Bridge	Characteristics	I_s	θ_{max}	$L_{s.min}$ (ft)	$L_{s.max}$ (ft)	w_g (ft)	O_{min}/b_f	Max $P_{u.STRI}$ intermed CF bottom chord (kips)	Max $P_{u.STRI}$ intermed CF diagonals (kips)	Max $P_{u.STRI}$ intermed CF top chord (kips)	Max $P_{u.STRI}$ bearing line CF bottom chord (kips)	Max $P_{u.STRI}$ bearing line CF diagonals (kips)	Max $P_{u.STRI}$ bearing line CF top chord (kips)
21*	Contiguous CFs parallel to bearing line	0.15	16.2	NA	241	128	NA	80	51	24	6	5	18
26*	Contiguous CFs parallel to bearing line; solid-web diaphragms at abutments	0.15	10.0	79.4	92	67.5	NA	65	25	33	NA	NA	NA

† Light shaded cells highlight the upper bound cross-frame forces for this category.

* This bridge meets, or nearly meets, the requirements for application of the recommended LGA-based procedures for bridge design.

Table 21. Bridge properties and STR I cross-frame forces for the Category 2 bridges (parallel skew, $\theta \leq 50^o$, $I_s \leq 0.3$, cross-frames perpendicular to the girders) plus Bridge 25 with $\theta = 54.5^o$ and $I_s = 0.25$.[†]

Bridge	Characteristics	I_s	θ_{max}	$L_{s.min}$ (ft)	$L_{s.max}$ (ft)	w_g (ft)	O_{min}/b_f	Max $P_{u.STRI}$ intermed CF bottom chord (kips)	Max $P_{u.STRI}$ intermed CF diagonals (kips)	Max $P_{u.STRI}$ intermed CF top chord (kips)	Max $P_{u.STRI}$ bearing line CF bottom chord (kips)	Max $P_{u.STRI}$ bearing line CF diagonals (kips)	Max $P_{u.STRI}$ bearing line CF top chord (kips)
8*	CFs normal to girders, staggered with small offsets	0.27	23.4	148	173	93.3	3.15	57	32	51	5	6	23
11*	Contiguous CF lines normal to girders, framing into bearing lines	0.26	38.1	185	188	61.0	0.00	117	51	31	128	38	17
17*	Contiguous CF lines normal to girders, small to large offsets at abutments	0.28	41.5	NA	202	63.0	2.15	113	62	29	13	10	38
18*	CFs normal to girders, ample offsets & staggers	0.20	39.7	NA	212	51.7	3.23	41	22	17	10	5	16
25	Contiguous CF lines normal to girders, framing into the pier bearing line and with no cross frames along the pier bearing line; small offsets relative to the abutment bearing lines	0.25	**54.5**	196	196	35.3	0.00	**151**	**124**	**93**	**33**	**28**	**43**

[†] The lightest shade (light red) cells highlight small cross-frame offset values and correspondingly large bearing line cross-frame forces; the dark shaded cells highlight properties and responses that significantly violate target requirements; the intermediate shade (green) cells highlight the upper bound cross-frame forces for this category.

[*] This bridge meets, or nearly meets, the requirements for application of the recommended LGA-based procedures for bridge design.

Table 22. Bridge properties and STR I cross-frame forces for the Category 3 bridges (parallel skew, $\theta \leq 50$ degrees with $0.30 < I_s \leq 0.40$, or $\theta \leq 30$ degrees with $0.40 < I_s \leq 0.45$) plus Bridges 1, 2, 9, 10, 23 and 24 with $I_s > 0.45$ or $\theta > 50^o$.†

Bridge	Characteristics	I_s	θ_{max}	$L_{s.min}$ (ft)	$L_{s.max}$ (ft)	w_g (ft)	O_{min}/b_f	Max $P_{u.STRI}$ intermed CF bottom chord (kips)	Max $P_{u.STRI}$ intermed CF diagonals (kips)	Max $P_{u.STRI}$ intermed CF top chord (kips)	Max $P_{u.STRI}$ bearing line CF bottom chord (kips)	Max $P_{u.STRI}$ bearing line CF diagonals (kips)	Max $P_{u.STRI}$ bearing line CF top chord (kips)
1	Contiguous CF lines normal to girders, small to large offsets at abutments	**0.46**	49.4	NA	208	82.5	4.20	**324**	**166**	**105**	17	25	23
2 (1 Alt)	CFs normal to girders, ample offsets & staggers	**0.46**	49.4	NA	208	82.5	4.00	**204**	**106**	**67**	21	14	26
3*	Contiguous CF lines normal to girders, framing into bearing lines	0.39	38.2	185	185	91.0	0.00	106	42	42	109	29	44
4* (3 Alt)	CFs normal to girders, ample offsets & staggers	0.39	38.2	185	185	91.0	4.00	75	33	50	38	18	40
5*	Contiguous CF lines normal to girders, small to large offsets at abutments	0.42	29.4	NA	144	108	1.05	115	38	37	6	9	29
6*	Contiguous CF lines normal to girders, small to large offsets at abutments	0.35	20.7	116	116	106	1.73	132	40	37	9	11	17
7*	Contiguous diaphragms normal to girders, small to large offsets at abutments	0.33	35.5	NA	96	46.1	2.18	NA	NA	NA	NA	NA	NA
9	Contiguous CF lines normal to girders, framing into the pier bearing line and with no cross frames along the pier bearing line	**0.47**	**57.2**	148	173	93.3	0.00	**214**	**85**	**62**	24	14	23
10 (9 Alt)	CFs normal to girders, ample offsets & staggers	**0.47**	**57.2**	148	173	93.3	4.00	147	**70**	39	36	21	22
22*+	CFs normal to girders, contiguous CF lines with offsets at bearing lines	0.31	36.1	195	204	85.5	2.63	137	50	39	23	32	34
23	Contiguous CF lines normal to girders, framing into pier bearing line	0.37	**50.7**	252	252	76.6	0.00	**261**	**147**	**145**	8	15	28
24	Contiguous CF lines normal to girders, inadequate offsets at abutments	0.37	**52.7**	170	170	48.3	2.31	117	45	30	20	23	53

† The lightest shade (light red) cells highlight small cross-frame offset values and correspondingly large bearing line cross-frame forces; the dark shaded cells highlight properties and responses that significantly violate target requirements; the intermediate shade (green) cells highlight the upper bound cross-frame forces for this category.

* This bridge meets, or nearly meets, the requirements for application of the recommended LGA-based procedures for bridge design.

+ Bridge 22 has a slight variation in the skew angle between its supports.

Table 23. Bridge properties and STR I cross-frame forces for Category 4 bridges (nonparallel skew).†

Bridge	Characteristics	I_s	θ_{max}	$L_{s.min}$ (ft)	$L_{s.max}$ (ft)	w_g (ft)	O_{min}/b_f	Max $P_{u.STRI}$ intermed CF bottom chord (kips)	Max $P_{u.STRI}$ intermed CF diagonals (kips)	Max $P_{u.STRI}$ intermed CF top chord (kips)	Max $P_{u.STRI}$ bearing line CF bottom chord (kips)	Max $P_{u.STRI}$ bearing line CF diagonals (kips)	Max $P_{u.STRI}$ bearing line CF top chord (kips)
12	Contiguous CF lines normal to girders, small offsets at abutments, Intermed. CFs framing into bearings at piers, no CFs on bearing lines at piers	0.32	**58.7**	182	202	35.0	0.00	**216**	**126**	**63**	**75**	**42**	30
13	Contiguous CF lines normal to girders with offsets relative to pier bearing lines; zero skew at abutments	0.23	**50.1**	184	253	36.0	2.40	**289**	**191**	**105**	**48**	**14**	20
14 (13 Alt)	CF lines normal to girders with ample staggers and offsets; zero skew at abutments	0.23	**50.1**	184	253	36.0	4.00	**318**	**209**	**94**	**48**	**15**	20
15	Contiguous CF lines normal to girders, small to ample offsets at abutments and piers; change in flange moment of inertia larger than a factor of two at flange transition	0.32	**53.4**	156	226	49.2	1.45	139	**98**	**71**	25	17	**62**
16 (15 Alt)	Contiguous CF lines normal to girders, ample offsets and staggers; change in flange moment of inertia larger than a factor of two at flange transition	0.32	**53.4**	156	226	49.2	4.00	**188**	**114**	**89**	22	20	**63**

† Light shaded cells highlight small cross-frame offset values and correspondingly large bearing line cross-frame forces; dark shaded cells highlight properties and responses that significantly violate target requirements.

Table 24. Bridge properties and STR I cross-frame forces for Category 5 bridges (splayed girder bridges).†

Bridge	Characteristics	I_s	θ_{max}	$L_{s.min}$ (ft)	$L_{s.max}$ (ft)	w_g (ft)	O_{min}/b_f	Max $P_{u.STRI}$ intermed CF bottom chord (kips)	Max $P_{u.STRI}$ intermed CF diagonals (kips)	Max $P_{u.STRI}$ intermed CF top chord (kips)	Max $P_{u.STRI}$ bearing line CF bottom chord (kips)	Max $P_{u.STRI}$ bearing line CF diagonals (kips)	Max $P_{u.STRI}$ bearing line CF top chord (kips)
19	Contiguous CF lines normal to girders, small to ample offsets relative to abutment bearing lines	**0.45**	**52.2**	NA	196	55.5 to 66.2	2.30	**212**	**123**	**80**	32	**41**	41
20 (19 Alt)	CF lines normal to girders with ample staggers and offsets	**0.45**	**52.2**	NA	196	55.5 to 66.2	4.00	114	**61**	42	21	26	38

† The dark shaded cells highlight properties and responses that significantly violate target requirements.

Table 25. Bridge properties and STR I cross-frame force ratios from 3D FEA for the Category 1 bridges (parallel skew, $\theta \leq 20^o$, and cross-frames oriented parallel to the bearing lines).

Bridge	Characteristics	I_s	θ_{max}	$L_{s.min}$ (ft)	$L_{s.max}$ (ft)	w_g (ft)	O_{min}/b_f	$V_{max.ICF}/V_{max.g}$	$B_{max.cn.ICF}/(M_{max}/h)_g$	$T_{max.cn.ICF}/(M_{max}/h)_g$	$B_{max.cn.ICF}\ h_{sc}/M_{max.g}$	$T_{max.cn.ICF}\ h_{sc}/M_{max.g}$	$V_{max.BCF}/V_{max.g}$	$B_{max.cn.BCF}\ h_{sc}/M_{max.g}$	$T_{max.cn.BCF}\ h_{sc}/M_{max.g}$
21*	Contiguous CFs parallel to bearing line	0.15	16.2	NA	241	128	NA	0.073	0.025	0.014	0.024	0.013	0.005	0.002	0.004
26*	Contiguous CFs parallel to bearing line; solid-web diaphragms at abutments	0.15	10.0	79.4	92	67.5	NA	0.045	0.069	0.026	0.074	0.028	NA	NA	NA

* This bridge meets, or nearly meets, the requirements for application of the recommended LGA-based procedures for bridge design.

Table 26. Bridge properties and STR I cross-frame force ratios from 3D FEA for the Category 2 bridges (parallel skew, $\theta \leq 50^o$, $I_s \leq 0.3$, and cross-frames perpendicular to the girders).†

Bridge	Characteristics	I_s	θ_{max}	$L_{s.min}$ (ft)	$L_{s.max}$ (ft)	w_g (ft)	O_{min}/b_f	$V_{max.ICF}/V_{max.g}$	$B_{max.cn.ICF}/(M_{max}/h)_g$	$T_{max.cn.ICF}/(M_{max}/h)_g$	$B_{max.cn.ICF}\ h_{sc}/M_{max.g}$	$T_{max.cn.ICF}\ h_{sc}/M_{max.g}$	$V_{max.BCF}/V_{max.g}$	$B_{max.cn.BCF}\ h_{sc}/M_{max.g}$	$T_{max.cn.BCF}\ h_{sc}/M_{max.g}$
8*	CFs normal to girders, staggered with small offsets	0.27	23.4	148	173	93.3	3.15	0.027	0.024	0.015	0.023	0.014	0.004	0.003	0.006
11*	Contiguous CF lines normal to girders, framing into bearing lines	0.26	38.1	185	188	61.0	0.00	0.063	0.042	0.024	0.042	0.024	0.037	0.044	0.017
17*	Contiguous CF lines normal to girders, small to large offsets at abutments	0.28	41.5	NA	202	63.0	2.15	0.087	0.033	0.020	0.034	0.020	0.012	0.006	0.011
18*	CFs normal to girders, ample offsets & staggers	0.20	39.7	NA	212	51.7	3.23	0.027	0.011	0.008	0.010	0.008	0.005	0.002	0.005
25	Contiguous CF lines normal to girders, framing into the pier bearing line and with no cross frames along the pier bearing line; small offsets relative to the abutment bearing lines	0.25	**54.5**	196	196	35.3	0.00	**0.122**	**0.064**	**0.025**	**0.062**	**0.024**	**0.019**	**0.015**	**0.011**

† The lighest shade (light red) cells highlight small cross-frame offset values and correspondingly large bearing line cross-frame forces; the dark shaded cells highlight properties and responses that significantly violate target requirements; the intermediate shade (green) cells highlight properties and results for bridges having offsets and staggers.

* This bridge meets, or nearly meets, the requirements for application of the recommended LGA-based procedures for bridge design.

Table 27. Bridge properties and STR I cross-frame force ratios from 3D FEA for the Category 3 bridges (parallel skew, θ ≤ 50 degrees with 0.30 < I_s ≤ 0.40, or θ ≤ 30 degrees with 0.40 < I_s ≤ 0.45).†

Bridge	Characteristics	I_s	θ_{max}	$L_{s.min}$ (ft)	$L_{s.max}$ (ft)	w_g (ft)	O_{min}/b_f	$B_{max.cn.ICF}/(M_{max}/h)_g$	$T_{max.cn.ICF}/(M_{max}/h)_g$	$B_{max.cn.ICF}\ h_{sc}/M_{max.g}$	$T_{max.cn.ICF}\ h_{sc}/M_{max.g}$	$V_{max.BCF}/V_{max.g}$	$B_{max.cn.BCF}/(M_{max}/h)_g$	$T_{max.cn.BCF}/(M_{max}/h)_g$	$B_{max.cn.BCF}\ h_{sc}/M_{max.g}$	$T_{max.cn.BCF}\ h_{sc}/M_{max.g}$
1	Contiguous CF lines normal to girders, small to large offsets at abutments	**0.46**	49.4	NA	208	82.5	4.20	**0.080**	**0.056**	**0.078**	**0.054**	**0.024**	**0.009**	**0.006**	**0.009**	**0.006**
2 (1 Alt)	CFs normal to girders, ample offsets & staggers	**0.46**	49.4	NA	208	82.5	4.00	**0.050**	**0.036**	**0.049**	**0.035**	**0.025**	**0.011**	**0.006**	**0.011**	**0.006**
3*	Contiguous CF lines normal to girders, framing into bearing lines	0.39	38.2	185	185	91.0	0.00	0.024	0.016	0.025	0.017	0.020	0.024	0.015	0.024	0.015
4* (3 Alt)	CFs normal to girders, ample offsets & staggers	0.39	38.2	185	185	91.0	4.00	0.017	0.017	0.018	0.018	0.012	0.008	0.012	0.008	0.012
5*	Contiguous CF lines normal to girders, small to large offsets at abutments	0.42	29.4	NA	144	108	1.05	0.045	0.023	0.044	0.022	0.010	0.005	0.011	0.005	0.011
6*	Contiguous CF lines normal to girders, small to large offsets at abutments	0.35	20.7	116	116	106	1.73	0.057	0.032	0.064	0.036	0.010	0.009	0.007	0.009	0.008
7*	Contiguous diaphragms normal to girders, small to large offsets at abutments	0.33	35.5	NA	96	46.1	2.18	NA	NA	NA	NA	NA	NA	NA	NA	NA
9	Contiguous CF lines normal to girders, framing into the pier bearing line and with no cross frames along the pier bearing line	**0.47**	**57.2**	148	173	93.3	0.00	**0.062**	**0.036**	**0.061**	**0.035**	**0.009**	**0.007**	**0.010**	**0.007**	**0.010**
10 (9 Alt)	CFs normal to girders, ample offsets & staggers	**0.47**	**57.2**	148	173	93.3	4.00	**0.043**	**0.026**	**0.042**	**0.025**	**0.014**	**0.010**	**0.012**	**0.010**	**0.012**
22*+	CFs normal to girders, contiguous CF lines with offsets at bearing lines	0.31	36.1	195	204	85.5	2.63	0.042	0.022	0.042	0.022	0.036	0.014	0.010	0.014	0.010
23	Contiguous CF lines normal to girders, framing into pier bearing line	0.37	**50.7**	252	252	76.6	0.00	**0.054**	**0.021**	**0.051**	**0.020**	**0.008**	**0.003**	**0.004**	**0.003**	**0.004**
24	Contiguous CF lines normal to girders, inadequate offsets at abutments	0.37	**52.7**	170	170	48.3	2.31	**0.045**	**0.022**	**0.045**	**0.023**	**0.026**	**0.015**	**0.020**	**0.015**	**0.021**

† The lightest shade (light red) cells highlight small cross-frame offset values and correspondingly large bearing line cross-frame forces; the dark shaded cells highlight properties and responses that significantly violate target requirements; the intermediate shade (green) cells highlight the upper bound cross-frame forces for this category.

* This bridge meets, or nearly meets, the requirements for application of the recommended LGA-based procedures for bridge design.

+ Bridge 22 has a slight variation in the skew angle between its supports.

5.5 Discussion of the Parametric Study Results

This section presents detailed comparisons of the LGA and 3D FEA solutions from the project parametric studies. The structural behavior of a skewed bridge is influenced heavily by a number of factors such as the bridge articulation (simple- or continuous-span), skew index, bridge width, type of skew (parallel or nonparallel skew), skew angle, and the cross-frame layout. The behavior of skewed bridges can be explained as that of an orthotropic plate stiffened by the girders in the longitudinal direction and by cross-frames and diaphragms in the transverse direction. Both the girders and the cross-frames and diaphragms participate with the bridge deck in delivering loads to the bearing lines.

In continuous-span bridges, the load distribution can be influenced by interaction between the spans, especially in bridges with unequal spans, based on compatibility of deformations of the continuous girders between the adjacent spans. Loads on one span can cause significant internal forces and changes in the displacements and bearing reactions in the other spans. The transverse stiffening from the cross-frames and diaphragms influences these interactions. Some cross-frame and/or diaphragm framing arrangements can develop significant continuity effects in the transverse direction at pier locations.

The longitudinal and transverse load paths within the bridge girders are influenced further by the nature of the skew, parallel or nonparallel. Figure 49 shows a set of two-span continuous bridges with similar characteristics except that one has parallel skew and the other has nonparallel skew. A key characteristic of parallel skew bridges is that all the girders have equal lengths within a span. The girders in a nonparallel skew bridge have unequal lengths within the span(s) having nonparallel skew. This affects the relative stiffness of the girders and influences the internal apportionment (distribution) of applied loads among the girders. The obtuse corners within a span in a nonparallel skew bridge may be located at opposite ends of the fascia girder on one side of the bridge, or they may be located at opposite sides of the overall bridge cross-section. Conversely, the bridge span in a bridge with parallel skew has a short and long diagonal direction. A relatively stiff transverse load path tends to form in the short diagonal direction. Bridge spans with nonparallel skew do not necessarily have this characteristic.

Splay of the girders can have further effects, complicating the loads and the load paths within the spans.

Based on the extent of the three-dimensional actions in a skewed bridge such as described in the above, the exterior, first interior, and the central interior girders are subjected to different internal forces compared to the loads calculated using the assumptions for LGA. Exterior girders directly receive the applied loads from overhangs and the components supported from overhangs. However, they interact with the other girders in the bridge cross-section via the interconnection of the girders via the cross-frames or diaphragms and the bridge deck, and the continuity of these components across the girders in the transverse direction. Hence, the assumption regarding the distribution of dead loads transversely among the girders can be a potential critical factor influencing the accuracy of LGA. The equal distribution assumption evaluated in this research is discussed in Section 2.5.1.

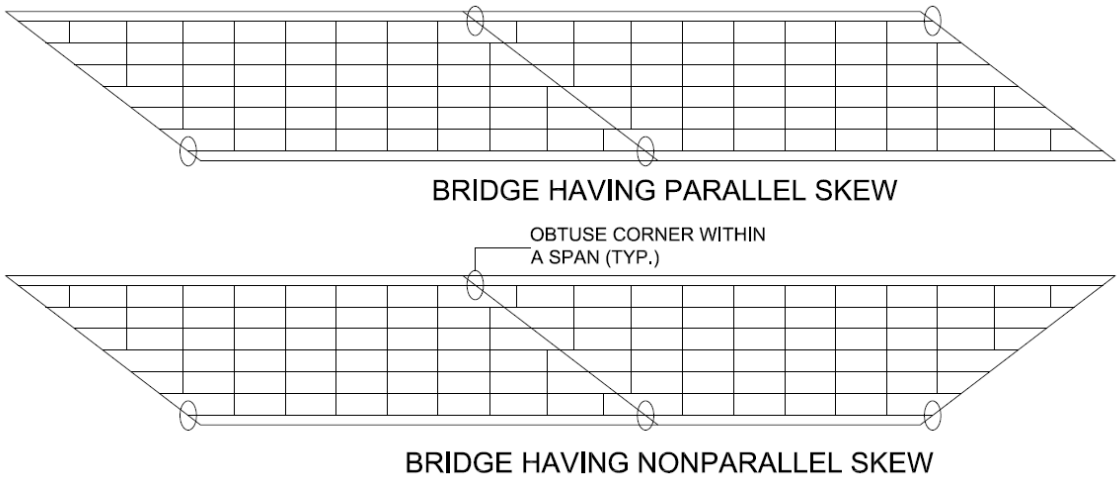

Figure 49. Obtuse corners within spans in a parallel and nonparallel skew bridge.

In this chapter, the results for exterior girders, first interior girders and the central interior girders are inspected and presented separately to ascertain the influence of the load distribution assumptions, both for the live load and for the dead load, on the LGA accuracy. The professional factor (ρ_{max}), defined by Equation 23, is employed as the primary summary measure of the differences between the 3D FEA and LGA calculations for the internal force quantities. The ρ_{max} values are useful in indicating the worst-case conservative and unconservative differences between the calculated responses, values larger than 1.0 indicating unconservative results and values less than 1.0 indicating conservative results. Differences in 3D FEA and LGA responses are tabulated in the individual bridge appendix sections in terms of normalized mean differences (ε_{mean}) and normalized differences of the maximums, ε_{max1}, defined in Equation 24. Equations 25 and 26 show the relationships between ε_{max1} and ρ_{max}.

The accuracy of the displacement predictions is quantified by the measures ε_{max2}, ε_{max3} and ε_{max4}. As discussed in Section 2.4, these measures provide a more meaningful evaluation of the differences between the LGA and 3D FEA displacements since they are measures normalized by the overall bridge span lengths and framing widths in the first two cases, and they are simple absolute measures of the displacement differences in the latter case.

The following key bridge responses pertaining to the design demands are presented in the following sections:

1. The girder positive and negative STR I major-axis bending moments.
2. The girder STR I vertical shear forces.
3. The girder HL-93 live load shear forces, focusing in particular on the live load shear forces at the obtuse corners of the bridge spans.
4. The girder STR I bearing reactions at the obtuse corners of simple spans, and at the fascia girders at the piers in continuous-span bridges.
5. The girder maximum total dead load vertical displacements, including consideration of the effects of steel dead load fit (SDLF) detailing of the cross-frames.

6. The girder concrete dead load maximum vertical displacements, considering both staged and unstaged deck placement.
7. The girder layovers under the total dead load, which for SDLF detailing of the cross-frames are equal to the girder layovers under the concrete dead load. This is because the layovers are approximately zero under the steel dead load when SDLF detailing is employed. (These responses are estimated indirectly from the LGA results using equations recommended by FDOT; since the calculations are relatively straightforward, simple, and based on mechanics, they are considered as a part of the LGA calculations.)
8. The girder fatigue live load vertical shear forces.
9. The girder fatigue live load flexural stresses.
10. Girder flange lateral bending stresses.
11. Cross-frame and diaphragm forces.
12. Fascia girder live load distribution factors (LLDFs), considering the conservatism of the lever rule and rigid cross-section analysis procedures.
13. Girder live load deflections.

5.5.1 Girder STR I Major-Axis Bending Moments

3D FEA and LGA girder responses are studied for noncomposite dead load, composite dead and live load cases in the parametric study. The responses from these basic load cases are combined to obtain the response for the STR I load combination. Section 15 of the individual appendix sections of each of the 26 bridges studied contains ε_{max1} values for all the load cases. The ρ_{max} values are calculated from the ε_{max1} values using Equation 26. Studying the ρ_{max} or ε_{max1} values for the major-axis bending moments for each bridge, it can be seen that 3D FEA solutions and LGA solutions have the largest difference for the rail load and live load cases. The rails are supported on the overhangs of the composite bridge deck, and typically the outer surface of the barrier rails are set flush with the outer edge of the overhang of the bridge deck. Rail loads are idealized as line loads acting at the center of gravity of the barrier rail in the 3D FEA. Distribution of the rail load among the bridge girders is complex, and is broadly dependent on the width of the bridge and number of girders in the bridge. In this research, the rail loads are distributed equally to all the girders in the bridge in the LGA calculations. This assumption introduces differences in the rail load responses obtained from 3D FEA and LGA.

LLDFs are used to calculate critical live load response envelopes in LGA. The primary AASHTO LRFD LLDFs used in LGA do not take into account the action of cross-frames in distributing the live load across the width of the bridge. This aspect is compensated for, when calculating the live load distribution to the fascia girders, via the rigid cross-section analysis requirement of AASHTO LRFD Article 4.6.2.2.2d. The approximations associated with these LGA tools introduce differences in the bending moments predicted by LGA and 3D FEA.

Steel dead load, steel dead load fit (SDLF) results from LGA and 3D FEA are in close agreement. Theoretically, SDL (SDLF) bending moments should be equal to LGA SDL bending moments. However, the self-weight of the intermediate cross-frames is totaled and applied as equal uniformly distributed load to all the girders in the bridge. Hence, this introduces differences in the LGA and 3D FEA girder bending moments. Fortunately, when the rail loads are sufficiently small, these differences are small compared to the other loading effects. The specific cross-frame and diaphragm self-weights tributary to each of the girders may be different

for the different girders, and these self-weights are applied as concentrated loads at their actual locations in the 3D FEA solutions. Therefore, the LGA dead load bending moments can be either conservative or unconservative compared to 3D FEA bending moments. ρ_{max} values greater than unity indicate that the LGA solutions are unconservative compared to 3D FEA solutions, and vice versa if ρ_{max} values are lesser than unity.

STR I bending moments were studied in detail and observations were presented in the project Task 3 report. These discussions are reiterated in this section for continuity of the discussions. The STR I load combination consists of noncomposite loads, loads applied long-term to the composite structure, and live loads applied as short-term transient loads to the composite structure. Live load is commonly the largest contributor to the STR I bending moments for the bridges studied in this research. The LGA procedures studied use the AASHTO LLDFs in the estimation of bending moments. The LGA estimates for live load bending moments tend to be conservative when compared to 3D FEA estimates. Hence, LGA values for the STR I bending moments tend to be conservative compared to 3D FEA in most cases. However, in some situations, the conservatism of the LGA live load calculations does not sufficiently compensate for unconservatism in the dead load calculations.

Table 28 summarizes the ρ_{max} values for the Strength I positive bending moments for the 26 bridges studied. In this table and in the subsequent presentations, girders G1 and G4 are the fascia girders on each side of the bridge. In many of the bridges, these girders are identical and the LGA solutions are the same for these girders. Minor deviations in the ρ_{max} values for G1 and G4 correspond to cases where there are some differences in the fascia girders. Girder G2 is the first interior girder, located at the top of the bridge plan in the plan sketches provided in Figures 16 through 41. Girder G3 is the central interior girder, located at or closest to the mid-width of the bridge cross-section.

Figures 50, 51 and 52 plot the ρ_{max} results for the exterior (fascia), first interior and central interior girders versus the bridge skew indices. The bridges for which the recommended LGA procedures, detailed in Section 5.1, provide sufficient accuracy as discussed in Section 5.4 are referred to as “LGA Amenable Bridges” in these plots and are represented by the solid diamond symbols. The other bridges are represented by the open diamond symbols. This notation is repeated in the subsequent sections of this chapter.

Table 29 and Figures 53 through 55 show comparable results to the above table and figures, but for the negative bending moments in the continuous-span bridges. The simple-span bridges are listed in Table 29, but show “NA” for “Not Applicable” with in the corresponding cells for ρ_{max}.

Observations regarding the differences between the LGA and 3D FEA results are as follows:

- A consistent trend in the differences between the LGA and 3D FEA STR I bending moments as a function of the bridge skew index is not observed. Clearly, there are numerous attributes that influence the accuracy of LGA for straight skewed bridges, the skew index only being one attribute.
- Only four of the study bridges have ρ_{max} larger than 1.0, and these bridges have $\rho_{max} > 1$ only for the exterior girders and for positive bending moments (see Figure 50).
- Considering Figure 50, the largest ρ_{maxG1} value (1.07) occurs for Bridge 19, which has I_s = 0.45, $\theta = 52.2^o$, splayed girders, and unequal girder stiffnesses, violating the requirements for Category 3 from Section 5.1.
- Interestingly, the positive moment ρ_{maxG4} for Bridge 19 is 0.75, which is one of the most conservative predictions for the exterior girders in the bridges studied.
- The other bridges with $\rho_{maxG1} > 1$ in Figure 50 are Bridges 4, 6 and 26. These bridges, having skew indices of 0.39, 0.35 and 0.15, are all amenable to LGA. Bridges 4 and 6 belong to Category 3 from Section 5.1, while Bridge 26 belongs to Category 1. Bridge 6 is a relatively wide bridge with 14 I-girders, and unequal spacing of the girders.
- All of the ρ_{max} values are smaller than the targeted maximum limit of 1.11 for both positive and negative bending moment.
- Both the positive moment ρ_{maxG1} and ρ_{maxG4} values are equal to 0.76 for Bridge 13, which has I_s = 0.23 and a maximum $\theta = 50.1^o$. This is a nonparallel skew continuous-span bridge.
- As a general trend the positive bending moment predictions become more conservative as we progress from the fascia girders to the first interior girders, and then to the central interior girders (see Figures 50, 51 and 52 respectively). One contributor to this trend is the under-prediction of the rail load moments on the fascia girders, and the over-prediction of these moments on the central interior girders, due to the use of the equal distribution rule.
- The negative bending moments exhibit the same general trend of higher conservatism as one moves from the fascia girders to the central interior girders (see Figures 53, 54 and 55).
- All of the negative bending moment ρ_{max} values are negative, i.e., the negative bending moments are predicted conservatively by the recommended LGA procedures for all of the continuous-span bridges considered in this research.
- The smallest ρ_{max} for all the positive and negative bending moments is the positive moment ρ_{maxG3} = 0.67 for Bridge 23 (Figure 52). This is a parallel skew bridge with I_s = 0.37 and $\theta = 50.7^o$, having two equal continuous spans. Since θ is larger than 50^o, this bridge slightly violates the limits for Category 3. Bridge 23 has intermediate cross-frames framing into the bearings at the intermediate pier in addition to having cross-frames along the bearing line at this location. The corresponding high transverse stiffness has a significant effect on the live load distribution among the various girders in the bridge. This is affirmed by the large differences in the maximum live load moments predicted by LGA and 3D FEA.

Table 28. ρ_{max} values for STR I positive bending moments.

Bridge	Skew Index	Width (ft)	CF Framing Arrangement Notes	ρ_{maxG1}	ρ_{maxG2}	ρ_{maxG3}	ρ_{maxG4}
1	0.46	87.1	Contiguous	0.96	0.93	0.83	0.96
2	0.46	87.1	Staggered	0.99	0.94	0.86	0.98
3*	0.39	102.1	Contiguous, CF framing into bearing line	0.96	0.94	0.88	0.96
4*	0.39	102.1	Staggered	1.01	0.95	0.92	1.01
5*	0.42	115.4	Contiguous	0.92	0.93	0.87	0.92
6*	0.35	112.2	Contiguous	1.06	0.94	0.84	1.06
7*	0.33	54.4	Contiguous	0.90	0.92	0.83	0.90
8*	0.27	101.1	Staggered	0.95	0.93	0.92	0.95
9	0.47	54.3	Contiguous, CF framing into bearing line	0.93	0.92	0.84	0.91
10	0.47	54.3	Staggered	0.91	0.90	0.85	0.92
11*	0.26	67.1	Contiguous, CF framing into bearing line	0.93	0.91	0.82	0.93
12	0.32	42.5	Contiguous, CF framing into bearing line	0.93	0.92	0.89	0.92
13	0.23	43.1	Contiguous	0.76	0.89	0.92	0.76
14	0.23	43.1	Staggered	0.76	0.89	0.93	0.77
15	0.33	60.2	Contiguous	0.97	0.87	0.74	0.92
16	0.33	60.2	Staggered	0.98	0.88	0.78	0.93
17*	0.28	71.1	Contiguous	0.90	0.94	0.84	0.90
18*	0.20	58.2	Staggered	0.95	0.96	0.89	0.95
19	0.45	67.6	Contiguous	1.07	0.76	0.80	0.75
20	0.45	67.6	Staggered	0.96	0.87	0.84	0.79
21*	0.15	135.1	Parallel to skew	0.90	0.80	0.79	0.90
22*	0.31	85.5	Contiguous	0.91	0.91	0.84	0.88
23	0.37	84.2	Contiguous, CF framing into bearing line	0.94	0.74	0.67	0.93
24	0.37	55.3	Contiguous, inadequate offsets near bearing line	0.94	0.94	0.79	0.94
25	0.25	43.1	Contiguous, CF framing into bearing line	0.91	0.96	0.96	0.91
26*	0.15	73.1	Parallel to skew	1.02	0.93	0.82	1.02

* This bridge meets, or nearly meets, the requirements for application of the recommended LGA-based procedures for the bridge design.

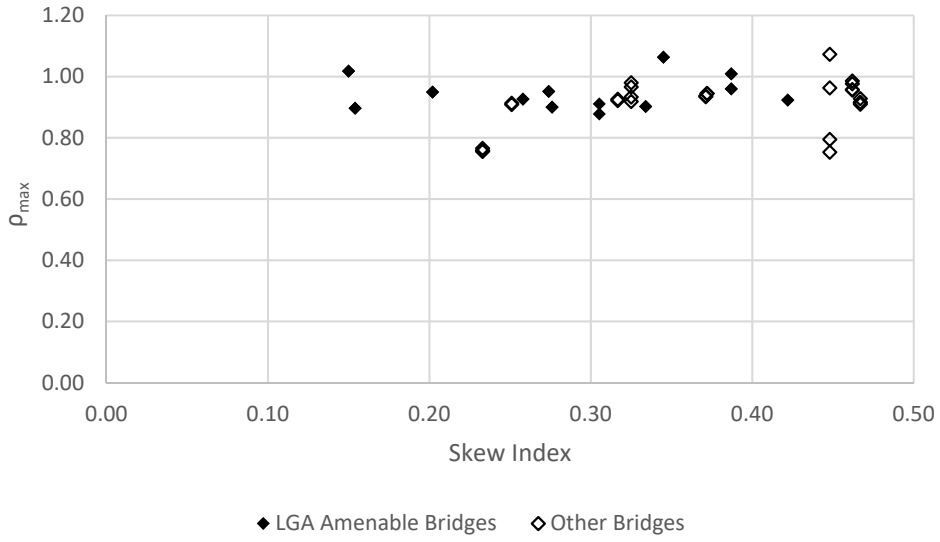

Figure 50. Comparison of ρ_{max} values for STR I positive bending moments for exterior girders.

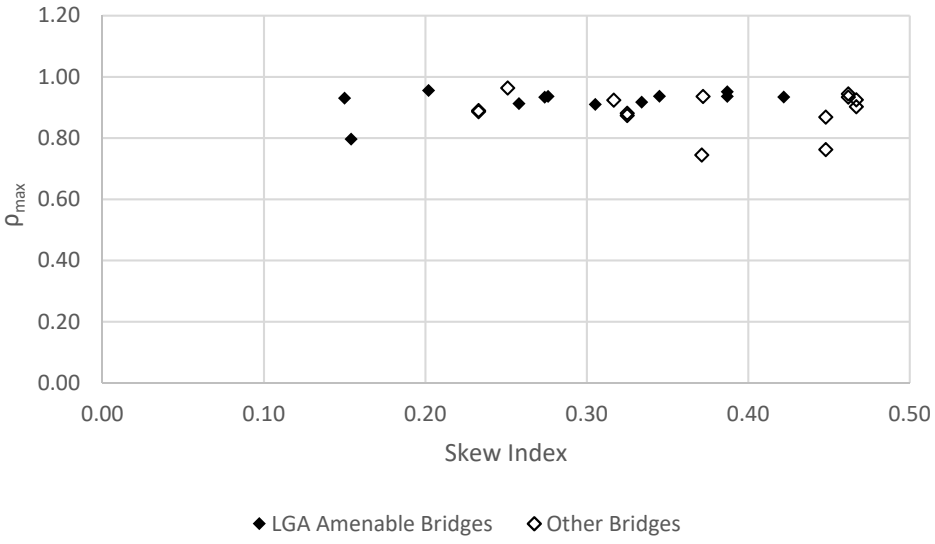

Figure 51. Comparison of ρ_{max} values for STR I positive bending moments for first interior girders.

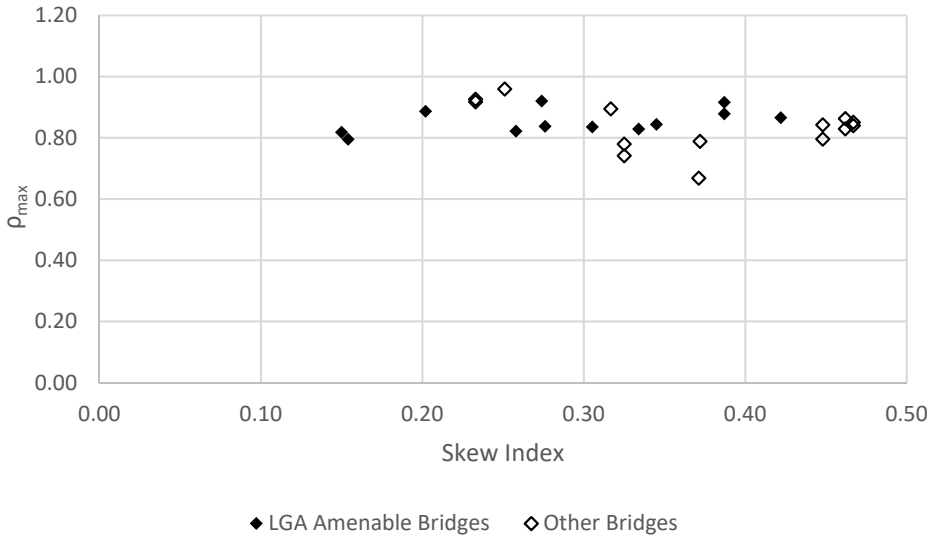

Figure 52. Comparison of ρ_{max} values for STR I positive bending moments for central interior girders.

Table 29. ρ_{max} values for STR I negative bending moments.

Bridge	Skew Index	Width (ft)	CF Framing Arrangement Notes	ρ_{maxG1}	ρ_{maxG2}	ρ_{maxG3}	ρ_{maxG4}
1	0.46	87.1	Contiguous	NA	NA	NA	NA
2	0.46	87.1	Staggered	NA	NA	NA	NA
3*	0.39	102.1	Contiguous, CF framing into bearing line	0.93	0.88	0.84	0.93
4*	0.39	102.1	Staggered	0.96	0.89	0.86	0.96
5*	0.42	115.4	Contiguous	NA	NA	NA	NA
6*	0.35	112.2	Contiguous	0.96	0.84	0.80	0.96
7*	0.33	54.4	Contiguous	NA	NA	NA	NA
8*	0.27	101.1	Staggered	0.92	0.88	0.88	0.92
9	0.47	54.3	Contiguous, CF framing into bearing line	0.96	0.86	0.79	0.87
10	0.47	54.3	Staggered	0.93	0.89	0.84	0.87
11*	0.26	67.1	Contiguous, CF framing into bearing line	0.89	0.89	0.83	0.89
12	0.32	42.5	Contiguous, CF framing into bearing line	0.96	0.89	0.90	0.85
13	0.23	43.1	Contiguous	0.80	0.95	0.96	0.80
14	0.23	43.1	Staggered	0.81	0.95	0.93	0.80
15	0.33	60.2	Contiguous	0.88	0.86	0.85	0.93
16	0.33	60.2	Staggered	0.91	0.86	0.84	0.94
17*	0.28	71.1	Contiguous	NA	NA	NA	NA
18*	0.20	58.2	Staggered	NA	NA	NA	NA
19	0.45	67.6	Contiguous	NA	NA	NA	NA
20	0.45	67.6	Staggered	NA	NA	NA	NA
21*	0.15	135.1	Parallel to skew	NA	NA	NA	NA
22*	0.31	85.5	Contiguous	0.89	0.86	0.86	0.91
23	0.37	84.2	Contiguous, CF framing into bearing line	0.95	0.78	0.78	0.95
24	0.37	55.3	Contiguous, inadequate offsets near bearing line	0.95	0.89	0.80	0.95
25	0.25	43.1	Contiguous, CF framing into bearing line	0.90	0.92	0.92	0.90
26*	0.15	73.1	Parallel to skew	0.94	0.82	0.77	0.94

* This bridge meets, or nearly meets, the requirements for application of the recommended LGA-based procedures for the bridge design.

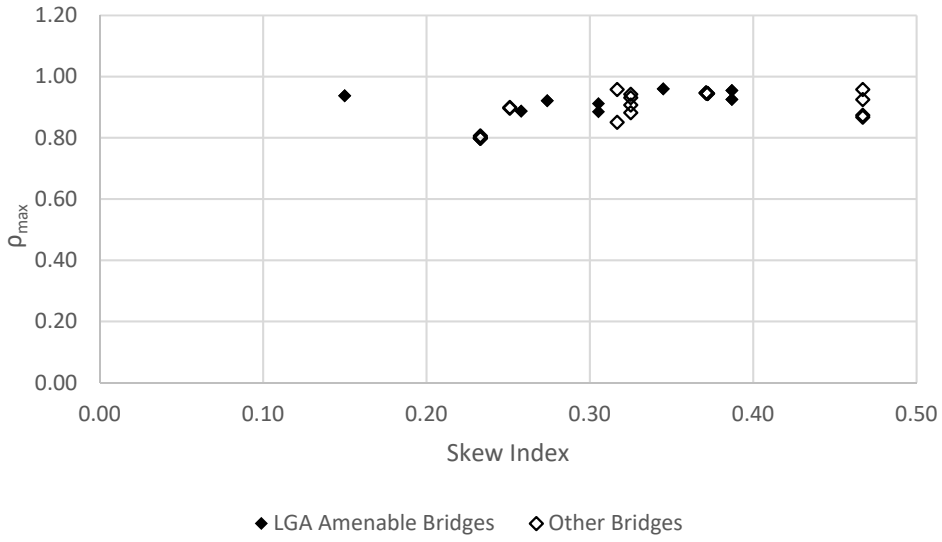

Figure 53. Comparison of ρ_{max} values for STR I negative bending moments for exterior girders.

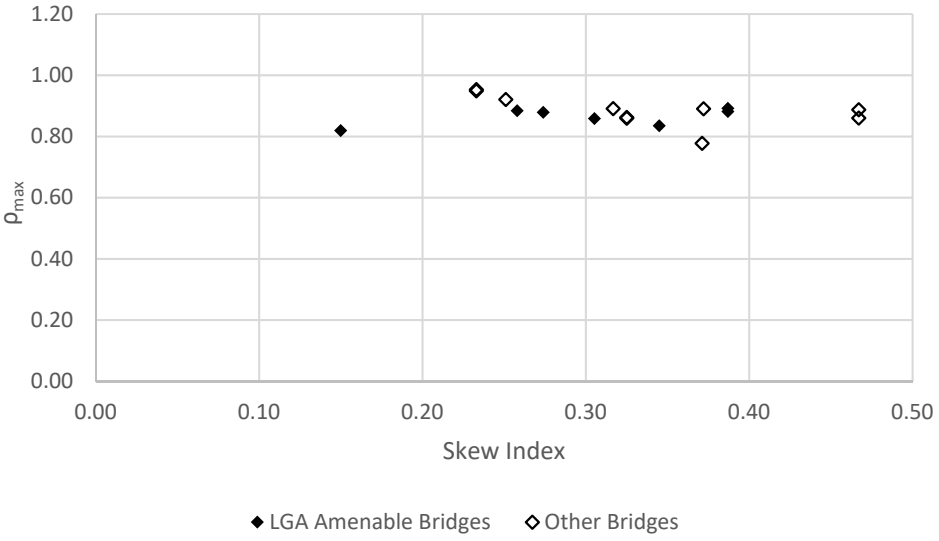

Figure 54. Comparison of ρ_{max} values for STR I negative bending moments for first interior girders.

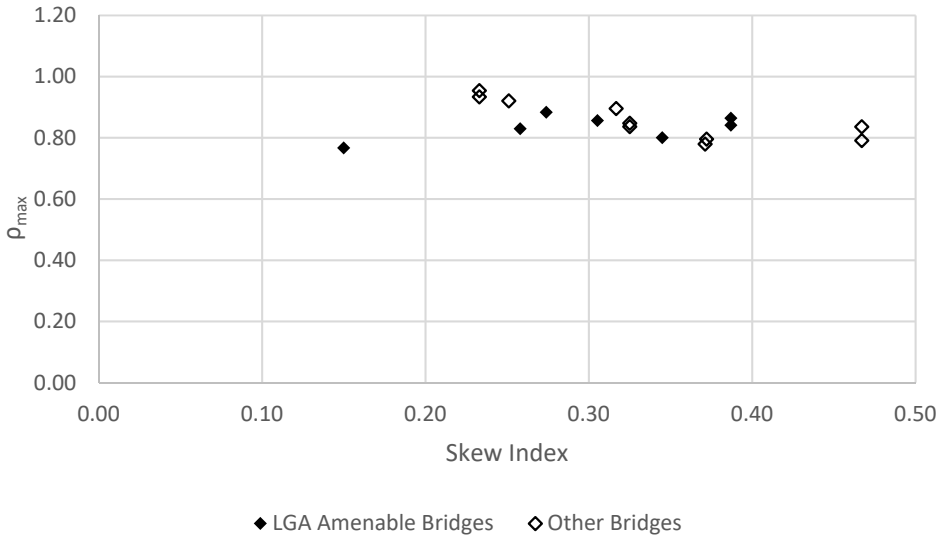

Figure 55. Comparison of ρ_{max} values for STR I negative bending moments for central interior girders.

- The most conservative prediction of the negative bending moments is $\rho_{maxG3} = 0.77$ for Bridge 26, belonging to Category 1 from Section 5.1. This is a parallel skew two-span continuous bridge with $I_s = 0.15$, $\theta = 10^o$, cross-frames oriented parallel to the skew and unbalanced spans. The next most conservative prediction of the negative moments is $\rho_{maxG3} = 0.78$ for Bridge 23.

Tables 30 through 32 and Figures 56 through 58 compare the LGA and 3D FEA predictions of the positive bending moments for the original (existing) FDOT bridges and the corresponding versions of these bridges configured with an alternative framing arrangement. Tables 33 through 35 and Figures 59 through 52 make the same comparisons for negative bending moments in the continuous-span bridges studied with an alternative cross-frame framing arrangement. The ρ_{max} values are conservative for all of these bridges. Marginal improvements are observed for the ρ_{max} values corresponding to the bridges with the alternative cross-frame framing arrangements. However, the largest improvement is only by an increment of 0.09 (for Bridges 19 and 20, see Table 30 and Figure 56. In several cases, the LGA predictions are slightly more conservative for the bridges having the alternative cross-frame framing arrangement.

Table 30. ρ_{max} values for STR I positive bending moments for exterior girders of bridges with original and alternative cross-frame arrangement.

Bridge	Skew Index	CF Arrangement	Characteristics of Bridge Geometry	ρ_{maxG1}	ρ_{maxG4}
1	0.46	Original	Simple span, parallel skew	0.96	0.96
2		Alternative		0.99	0.98
3*	0.39	Original	Two-span continuous, parallel skew	0.96	0.96
4*		Alternative		1.01	1.01
9	0.47	Original	Two-span continuous, parallel skew	0.93	0.91
10		Alternative		0.91	0.92
13	0.23	Original	Four-span continuous, nonparallel skew	0.76	0.76
14		Alternative		0.76	0.77
15	0.33	Original	Four-span continuous, nonparallel skew	0.97	0.92
16		Alternative		0.98	0.93
19	0.45	Original	Simple span, splayed girder, parallel skew	1.07	0.75
20		Alternative		0.96	0.79

* This bridge meets, or nearly meets, the requirements for application of the recommended LGA-based procedures for the bridge design.

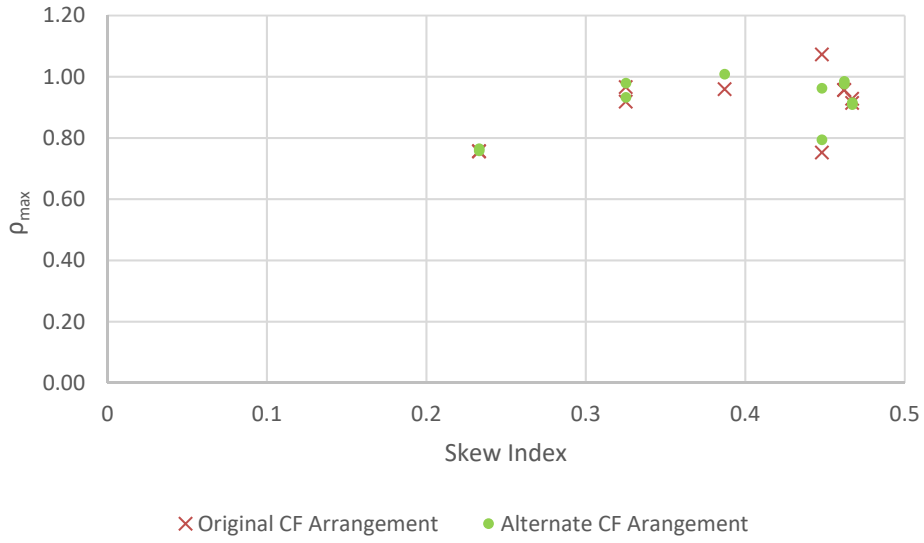

Figure 56. Comparison of ρ_{max} values for STR I positive bending moments for exterior girders in bridges with original and alternate cross-frame arrangements.

Table 31. ρ_{max} values for STR I positive bending moments for first interior girders of bridges with original and alternative cross-frame arrangements.

Bridge	Skew Index	CF Arrangement	Characteristics of Bridge Geometry	ρ_{maxG2}
1	0.46	Original	Simple span, parallel skew	0.93
2		Alternative		0.94
3*	0.39	Original	Two-span continuous, parallel skew	0.94
4*		Alternative		0.95
9	0.47	Original	Two-span continuous, parallel skew	0.92
10		Alternative		0.90
13	0.23	Original	Four-span continuous, nonparallel skew	0.89
				0.92
14		Alternative		0.89
				0.93
15	0.33	Original	Four-span continuous, nonparallel skew	0.87
16		Alternative		0.88
19	0.45	Original	Simple span, splayed girder, parallel skew	0.76
20		Alternative		0.87

* This bridge meets, or nearly meets, the requirements for application of the recommended LGA-based procedures for the bridge design.

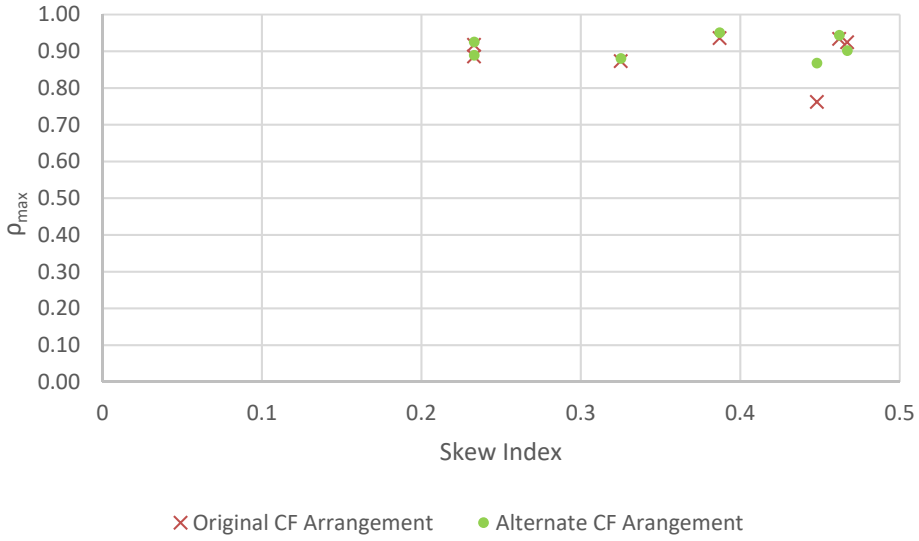

Figure 57. Comparison of ρ_{max} values for STR I positive bending moments for first interior girders in bridges with original and alternate cross-frame arrangements.

Table 32. ρ_{max} values for STR I positive bending moments for central interior girders of bridges with original and alternative cross-frame arrangements.

Bridge	Skew Index	CF Arrangement	Characteristics of Bridge Geometry	ρ_{maxG3}
1	0.46	Original	Simple span, parallel skew	0.83
2		Alternative		0.86
3	0.39	Original	Two-span continuous, parallel skew	0.88
4*		Alternative		0.92
9	0.47	Original	Two-span continuous, parallel skew	0.84
10		Alternative		0.85
15	0.33	Original	Four-span continuous, nonparallel skew	0.74
16		Alternative		0.78
19	0.45	Original	Simple span, splayed girder, parallel skew	0.80
20		Alternative		0.84

* This bridge meets, or nearly meets, the requirements for application of the recommended LGA-based procedures for the bridge design.

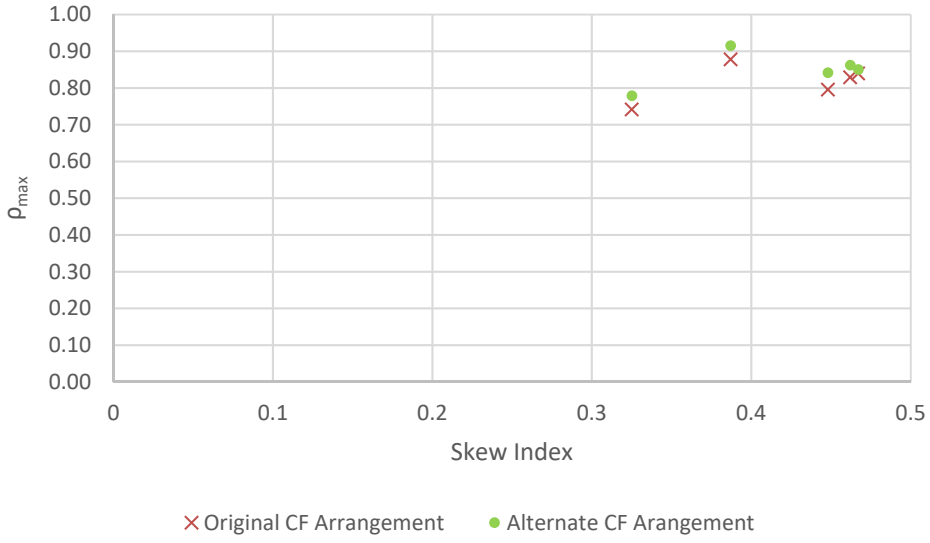

Figure 58. Comparison of ρ_{max} values for STR I positive bending moments for central interior girders in bridges with original and alternate cross-frame arrangements.

Table 33. ρ_{max} values for STR I negative bending moments for exterior girders of bridges with original and alternative cross-frame arrangements.

Bridge	Skew Index	CF Arrangement	Characteristics of Bridge Geometry	ρ_{maxG1}	ρ_{maxG4}
3*	0.39	Original	Two-span continuous, parallel skew	0.93	0.93
4*		Alternative		0.96	0.96
9	0.47	Original	Two-span continuous, parallel skew	0.96	0.87
10		Alternative		0.93	0.87
13	0.23	Original	Four-span continuous, nonparallel skew	0.80	0.80
14		Alternative		0.81	0.80
15	0.33	Original	Four-span continuous, nonparallel skew	0.88	0.93
16		Alternative		0.91	0.94

* This bridge meets, or nearly meets, the requirements for application of the recommended LGA-based procedures for the bridge design.

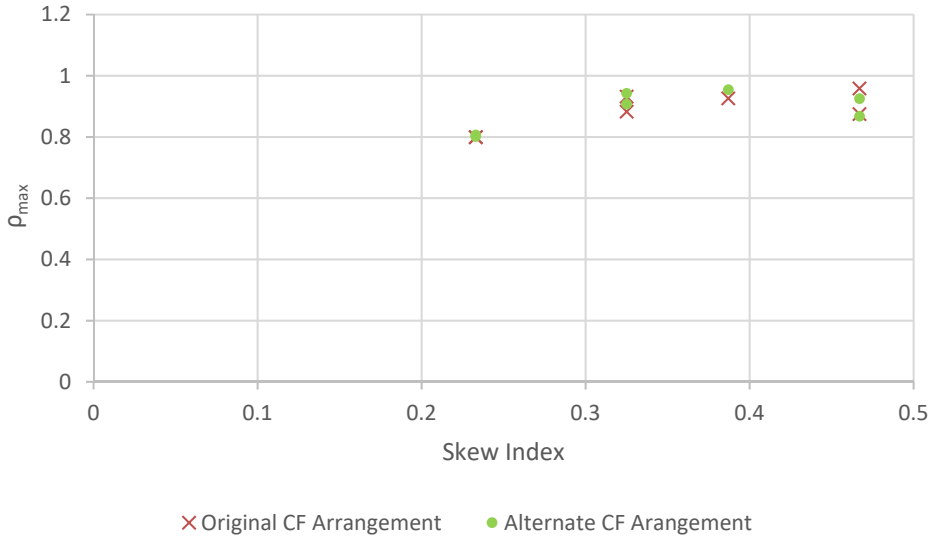

Figure 59. Comparison of ρ_{max} values for STR I negative bending moments for exterior girders in bridges with original and alternate cross-frame arrangements.

Table 34. ρ_{max} values for STR I negative bending moments for first interior girders of bridges with original and alternative cross-frame arrangements.

Bridge	Skew Index	CF Arrangement	Characteristics of Bridge Geometry	ρ_{maxG2}
3*	0.39	Original	Two-span continuous, parallel skew	0.88
4*		Alternative		0.89
9	0.47	Original	Two-span continuous, parallel skew	0.86
10		Alternative		0.89
13	0.23	Original	Four-span continuous, nonparallel skew	0.95
				0.96
14		Alternative		0.95
				0.93
15	0.33	Original	Four-span continuous, nonparallel skew	0.86
16		Alternative		0.86

* This bridge meets, or nearly meets, the requirements for application of the recommended LGA-based procedures for the bridge design.

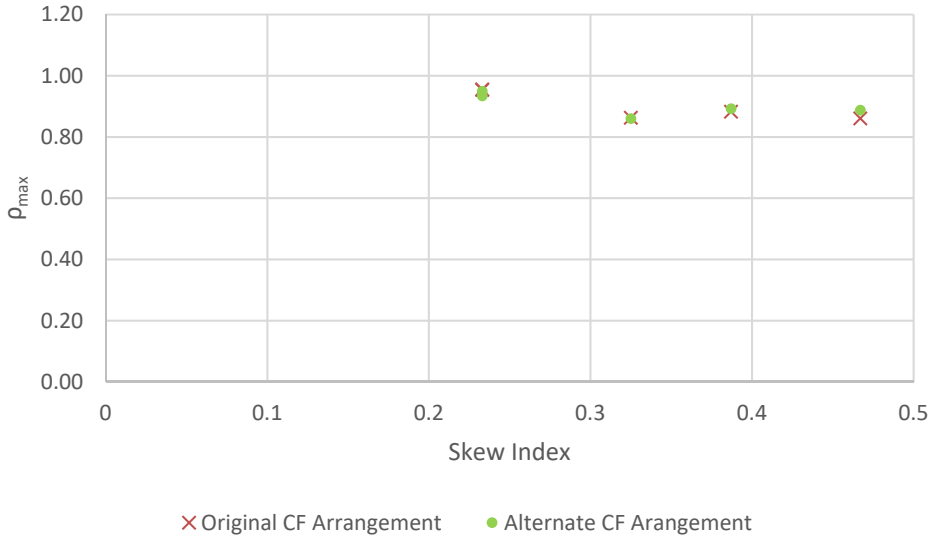

Figure 60. Comparison of ρ_{max} values for STR I negative bending moments for first interior girders in bridges with original and alternate cross-frame arrangements.

Table 35. ρ_{max} values for STR I negative bending moments for central interior girders of bridges with original and alternative cross-frame arrangements.

Bridge	Skew Index	CF Arrangement	Characteristics of Bridge Geometry	ρ_{maxG3}
3*	0.39	Original	Two-span continuous, parallel skew	0.84
4*		Alternative		0.86
9	0.47	Original	Two-span continuous, parallel skew	0.79
10		Alternative		0.84
15	0.33	Original	Four-span continuous, nonparallel skew	0.85
16		Alternative		0.84

* This bridge meets, or nearly meets, the requirements for application of the recommended LGA-based procedures for the bridge design.

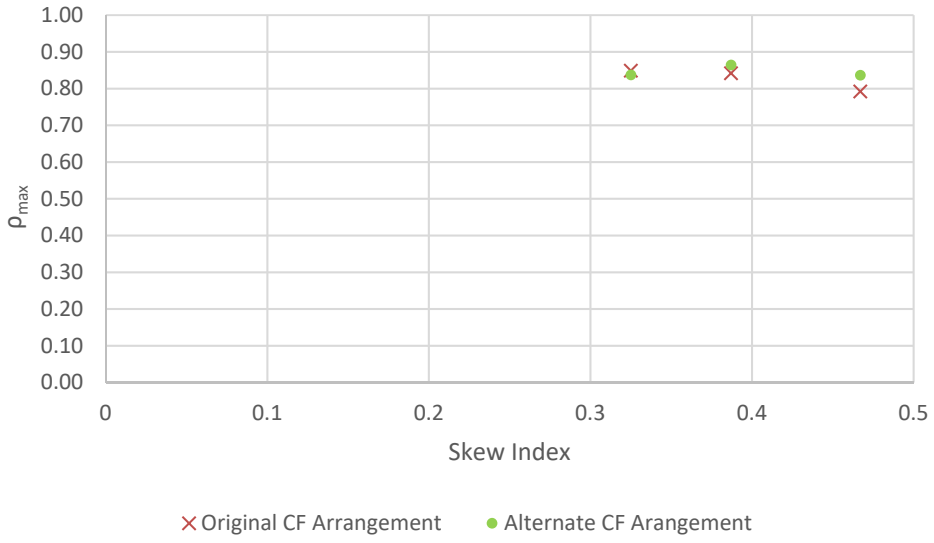

Figure 61. Comparison of ρ_{max} values for STR I negative bending moments for central interior girders in bridges with original and alternate cross-frame arrangements.

5.5.2 Girder STR I Vertical Shear Forces

In a skewed bridge, the intermediate cross-frames act to transfer shear forces to the girders at the connecting points. Hence, the shear force diagrams are discontinuous at the locations where the cross-frames connect to the girders. The deck, after hardening, also transfers forces due to its in-plane rigidity. Additionally, in spans having parallel skew, there is a tendency to form a transverse load path between the obtuse corners. Furthermore, the bearing line cross-frames aligned along the skew tend to twist the girders to maintain compatibility of displacements, thus developing a torsional moment that tends to increase the load transferred at the obtuse corners, and decrease loads at the acute corners. These effects drive additional shear forces at the ends of girders near the obtuse corners. Hence, larger ρ_{max} values are observed for STR I shear forces compared to STR I bending moments. Furthermore, a larger number of discrete changes may be observed in the shear force diagrams when a staggered cross-frame arrangement is used, since stagger can increase the number of points along the girders at which cross-frames are connected in some cases. The discrete changes in shear at these connection points are not modeled in the recommended LGA procedures, adding to the differences observed in 3D FEA and LGA solutions.

Table 36 summarizes the ρ_{max} values for the Strength I vertical shear forces for the 26 bridges studied, and Figures 62 through 64 plot the corresponding results for the exterior girders, the first interior girders, and the central interior girders, respectively.

Observations regarding the differences between the LGA and 3D FEA results are as follows:

- There is a clear spike in the ρ_{maxG1} and ρ_{maxG4} values corresponding to the fascia girders for a number of bridges with I_s close to the largest values considered (see Figure 62). Aside from this spike, there is no consistent trend between the LGA and 3D FEA STR I bending moments as a function of the bridge skew index.
- Bridge 1, with $I_s = 0.46$, has ρ_{maxG1} and ρ_{maxG4} values of 1.31 and 1.30. Bridge 1 also has a contiguous cross-frame arrangement. Hence, a very stiff transverse load path develops between the obtuse corners of the bridge, introducing large differences between the LGA and 3D FEA vertical shear estimates. Bridge 2, which is the same bridge with an alternative cross-frame framing arrangement, has a substantial reduction in the corresponding ρ_{maxG1} and ρ_{maxG4} values to 1.16 and 1.21. This clearly demonstrates the benefits of softening the transverse load path via the alternative arrangement. The I_s value of 0.46 slightly violates the limits for Category 3, while the θ value or 49.4° falls just under the maximum limit for this category.
- Bridge 6, with $I_s = 0.35$, has ρ_{maxG1} and ρ_{maxG4} values of 1.16. Bridge 6 is 112.2 ft wide and the spacing between girders is not constant throughout the width. Bridge 6 has contiguous cross-frame framing arrangement. The large width, combined with the non-constant spacing between the girders, reduces the beneficial effect of transverse load sharing between the girders.
- Bridges 19 and 20 exhibit a similar trend. These are the splayed girder bridges discussed previously, having $I_s = 0.45$ and $\theta = 52.2°$, and a splayed exterior girder that has noncomposite and composite moments of inertia that are more than 10 % larger than the interior girders. Therefore, these bridges do not meet the targeted requirements for application of LGA. Bridge 19 has ρ_{maxG1} and ρ_{maxG4} values of 1.19 and 1.23, whereas the

corresponding values for Bridge 20, having the alternative cross-frame framing arrangement, are 1.06 and 1.09.

Table 36. ρ_{max} values for STR I vertical shear forces.

Bridge	Skew Index	Width (ft)	CF Framing Arrangement Notes	ρ_{maxG1}	ρ_{maxG2}	ρ_{maxG3}	ρ_{maxG4}
1	0.46	87.1	Contiguous	1.31	0.87	0.81	1.30
2	0.46	87.1	Staggered	1.16	0.84	0.88	1.21
3*	0.39	102.1	Contiguous, CF framing into bearing line	0.96	0.82	0.86	0.96
4*	0.39	102.1	Staggered	0.98	0.85	0.88	0.98
5*	0.42	115.4	Contiguous	1.00	0.86	0.86	1.00
6*	0.35	112.2	Contiguous	1.16	0.81	0.81	1.16
7*	0.33	54.4	Contiguous	0.95	0.74	0.77	0.95
8*	0.27	101.1	Staggered	0.97	0.86	0.87	0.97
9	0.47	54.3	Contiguous, CF framing into bearing line	1.01	0.82	0.85	0.95
10	0.47	54.3	Staggered	0.92	0.84	0.86	0.85
11*	0.26	67.1	Contiguous, CF framing into bearing line	1.01	0.84	0.87	1.01
12	0.32	42.5	Contiguous, CF framing into bearing line	0.95	0.82	0.97	0.97
13	0.23	43.1	Contiguous	0.82	0.96	0.96	0.82
14	0.23	43.1	Staggered	0.83	0.97	0.94	0.82
15	0.33	60.2	Contiguous	0.88	0.81	0.92	0.98
16	0.33	60.2	Staggered	0.90	0.82	0.89	0.97
17*	0.28	71.1	Contiguous	1.05	0.78	0.82	1.05
18*	0.20	58.2	Staggered	1.01	0.85	0.81	1.01
19	0.45	67.6	Contiguous	1.19	0.83	0.79	1.23
20	0.45	67.6	Staggered	1.06	0.89	0.84	1.09
21*	0.15	135.1	Parallel to skew	0.96	0.86	0.85	0.96
22*	0.31	85.5	Contiguous	0.99	0.80	0.85	1.02
23	0.37	84.2	Contiguous, CF framing into bearing line	0.99	0.89	0.94	1.00
24	0.37	55.3	Contiguous, inadequate offsets near bearing line	1.01	0.83	0.90	1.01
25	0.25	43.1	Contiguous, CF framing into bearing line	0.95	0.90	0.91	0.94
26*	0.15	73.1	Parallel to skew	1.04	0.85	0.81	1.04

* This bridge meets, or nearly meets, the requirements for application of the recommended LGA-based procedures for the bridge design.

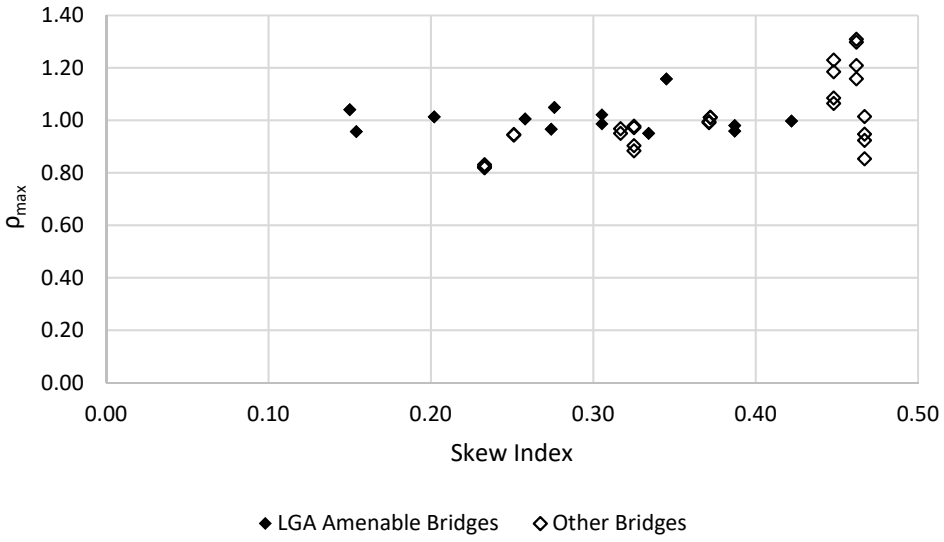

Figure 62. Comparison of ρ_{max} values for STR I vertical shear forces for exterior girders.

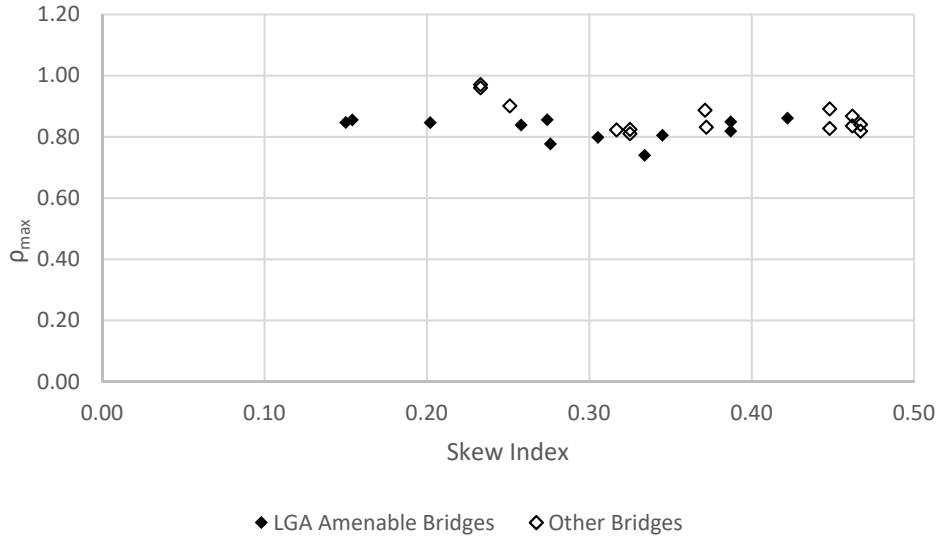

Figure 63. Comparison of ρ_{max} values for STR I vertical shear forces for first interior girders.

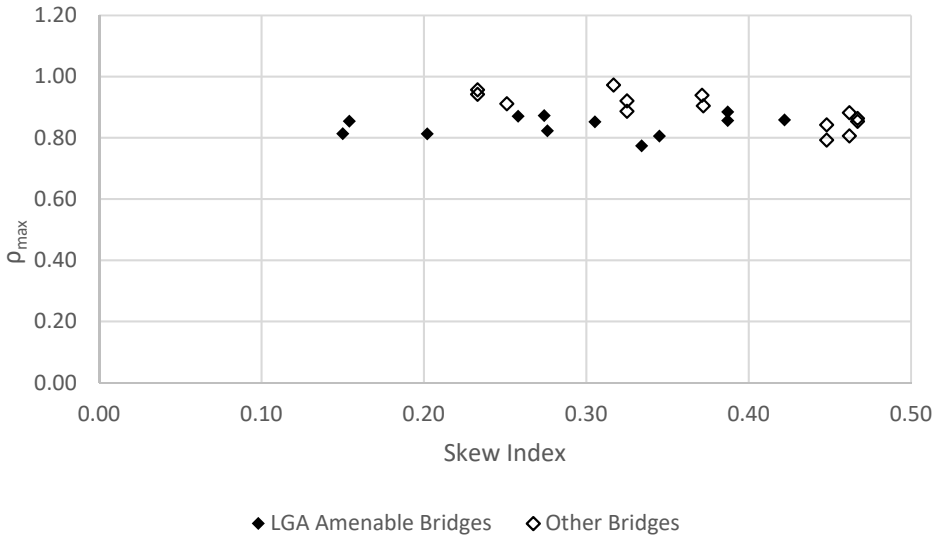

Figure 64. Comparison of ρ_{max} values for STR I vertical shear forces for central interior girders.

- All of the other bridges studied have vertical shear ρ_{max} values smaller than 1.11.
- Bridges 6, 9, 18, 24 and 26 have exterior girder vertical shear ρ_{max} values larger than 1.0 (see Table 36 and Figure 62). These bridges range across all three of the categories for application of the recommended LGA procedures. Bridge 9 violates the maximum limits for application of LGA in Category 3, given its I_s of 0.47 and its $\theta = 57.2^o$.
- Similar to the trend in the moment ρ_{max} values, the predictions generally tend to become more conservative as we progress from the fascia girders to the first interior girders, and then to the central interior girders (see Figures 62, 63 and 64 respectively).
- All of the ρ_{max} values are less than 1.0 for the first interior and central interior girders.
- The most conservative shear predictions are for the first interior girder of Bridge 7 (ρ_{maxG2} = 0.74). This is a relatively small bridge having a limited number of intermediate cross-frames. It is classified as nearly meeting the targeted limits on the differences between LGA and 3D FEA. The next most conservative shear prediction is $\rho_{maxG2} = 0.78$ for Bridge 17. Bridge 17 is a simple span bridge having a contiguous cross-frame arrangement.

Tables 37 through 39 and Figures 65 through 67 highlight the differences between the LGA and 3D FEA predictions of the girder shears for the original (existing) FDOT bridges and the corresponding versions of these bridges configured with an alternative cross-frame framing arrangement. The most significant improvements in the LGA predictions occur for Bridges 1 and 2 and 19 and 20, which have been discussed in the above. Considering Bridges 9 and 10, the LGA predictions are less accurate for the fascia girders in Bridge 10, having the alternative arrangement (1.01 to 0.92 for ρ_{maxG1} and 0.95 to 0.85 for ρ_{maxG4}). It is believed that these results relate to the complexities of these continuous-span bridges, which have unbalanced spans. The other changes in the ρ_{max} values due to the consideration of an alternative framing arrangement are relatively small.

Table 37. ρ_{max} values for STR I vertical shear forces for exterior girders of bridges with original and alternative cross-frame arrangements.†

Bridge	Skew Index	CF Arrangement	Characteristics of Bridge Geometry	ρ_{maxG1}	ρ_{maxG4}
1	0.46	Original	Simple span, parallel skew	1.31	1.30
2		Alternative		1.16	1.21
3*	0.39	Original	Two-span continuous, parallel skew	0.96	0.96
4*		Alternative		0.98	0.98
9	0.47	Original	Two-span continuous, parallel skew	1.01	0.95
10		Alternative		0.92	0.85
13	0.23	Original	Four-span continuous, nonparallel skew	0.82	0.82
14		Alternative		0.83	0.82
15	0.33	Original	Four-span continuous, nonparallel skew	0.88	0.98
16		Alternative		0.90	0.97
19	0.45	Original	Simple span, splayed girder, parallel skew	1.19	1.23
20		Alternative		1.06	1.09

† The shaded cells indicate ρ_{max} values that exceed the targeted limits for applicability of LGA.
* This bridge meets, or nearly meets, the requirements for application of the recommended LGA-based procedures for the bridge design.

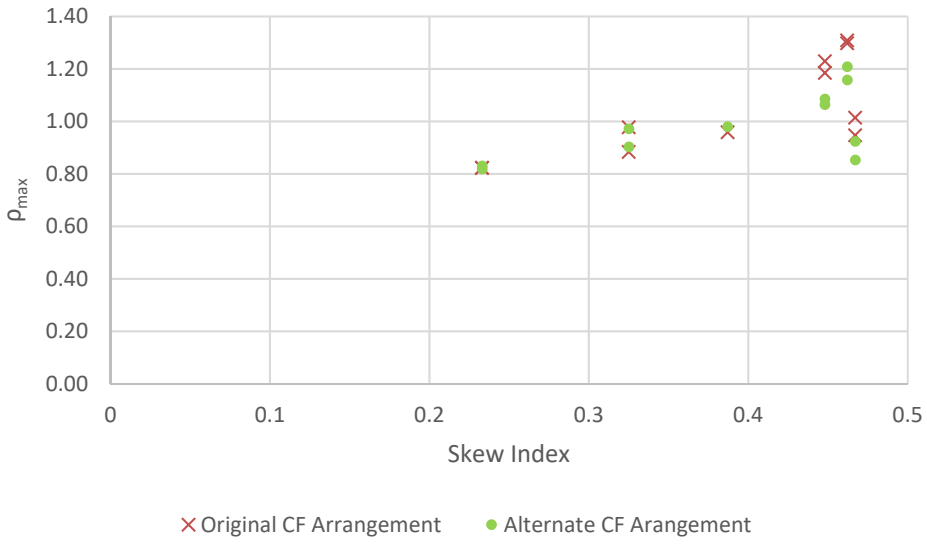

Figure 65. Comparison of ρ_{max} values for STR I vertical shear forces for exterior girders in bridges with original and alternate cross-frame arrangements.

Table 38. ρ_{max} values for STR I vertical shear forces for first interior girders of bridges with original and alternative cross-frame arrangements.

Bridge	Skew Index	CF Arrangement	Characteristics of Bridge Geometry	ρ_{maxG2}
1	0.46	Original	Simple span, parallel skew	0.87
2		Alternative		0.84
3*	0.39	Original	Two-span continuous, parallel skew	0.82
4*		Alternative		0.85
9	0.47	Original	Two-span continuous, parallel skew	0.82
10		Alternative		0.84
13	0.23	Original	Four-span continuous, nonparallel skew	0.96
				0.96
14		Alternative		0.97
				0.94
15	0.33	Original	Four-span continuous, nonparallel skew	0.81
16		Alternative		0.82
19	0.45	Original	Simple span, splayed girder, parallel skew	0.83
20		Alternative		0.89

* This bridge meets, or nearly meets, the requirements for application of the recommended LGA-based procedures for the bridge design.

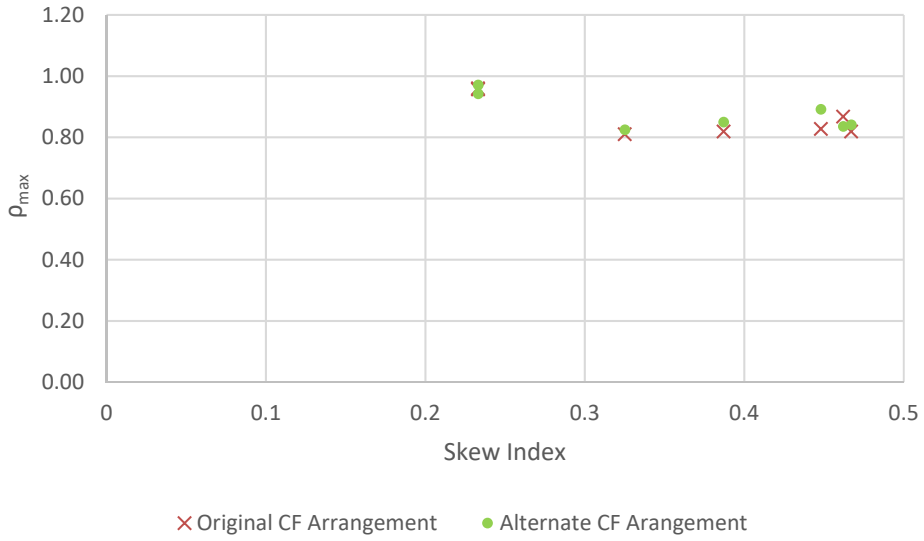

Figure 66. Comparison of ρ_{max} values for STR I vertical shear forces for first interior girders in bridges with original and alternate cross-frame arrangements.

Table 39. ρ_{max} values for STR I vertical shear forces for central interior girders of bridges with original and alternative cross-frame arrangements.

Bridge	Skew Index	CF Arrangement	Characteristics of Bridge Geometry	ρ_{maxG3}
1	0.46	Original	Simple span, parallel skew	0.81
2		Alternative		0.88
3*	0.39	Original	Two-span continuous, parallel skew	0.86
4*		Alternative		0.88
9	0.47	Original	Two-span continuous, parallel skew	0.85
10		Alternative		0.85
15	0.33	Original	Four-span continuous, nonparallel skew	0.92
16		Alternative		0.89
19	0.45	Original	Simple span, splayed girder, parallel skew	0.79
20		Alternative		0.84

* This bridge meets, or nearly meets, the requirements for application of the recommended LGA-based procedures for the bridge design.

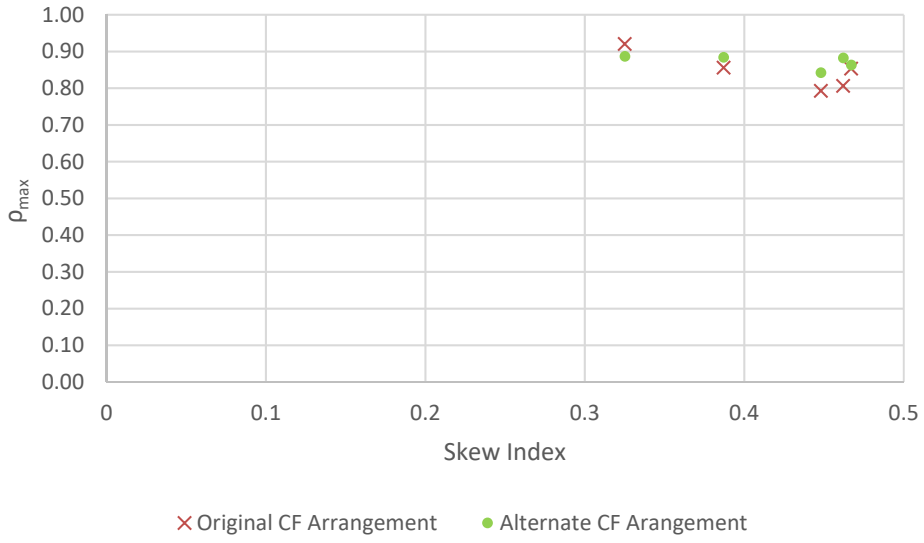

Figure 67. Comparison of ρ_{max} values for STR I vertical shear forces for central interior girders in bridges with original and alternate cross-frame arrangements.

5.5.3 Girder Live Load Shear Forces

Predicting the response of highway bridges to vehicular live load is key to designing for strength and serviceability requirements. 3D FEA solutions calculate maximum and minimum envelopes for response quantities at all locations throughout the structure, algorithmically finding the critical location of the live loads on the bridge deck causing the maximum or minimum response at each location. Hence, the problem of estimating live loads is a complex one that involves significant computational demands. Live load distribution factors (LLDFs) provide a coarse approximation of the transverse distribution of the live loads across the bridge deck. In combination with the use of influence lines to determine the longitudinal positioning of the live loads to cause the largest maximum and minimum effects, they greatly simplify the live load calculations. The AASHTO LLDFs have been developed to be typically conservative when compared to 3D FEA solutions (AASHTO, 2017).

In the parametric studies, the behavior of the 26 bridges is studied using the AASHTO HL-93 live load model. As a part of the study, LLDFs using the 3D FEA solutions are calculated and documented in each of the individual bridge appendix sections. SIMON provides LGA live load envelopes of bending moments and vertical shears at every tenth point in the spans. If these envelope values are divided by the AASHTO live load distribution factor (LLDF) corresponding to the quantity under consideration, an envelope of values corresponding to a LLDF = 1.0 is obtained. The 3D FEA LLDF is defined as the ratio of the 3D FEA live load envelope values at the tenth points to the corresponding LGA values for LLDF = 1.0. These factors are calculated for the live load girder major-axis bending moments and vertical shear forces and are presented in Appendix 3.

The LLDF thus calculated can be compared to the distribution factors calculated using the AASHTO recommended procedures. These comparisons provide insight into the accuracy of LGA with respect to 3D FEA. Such comparisons are presented in Section 5.5.12.

It is known that the local effects of skew near the bearing lines and the stiff transverse load path that develops between the obtuse corners in a parallel skew bridge span causes larger shear forces at the ends of girders near the obtuse corners. This section focuses on the accuracy of the AASHTO LRFD prediction of these shear forces. It should be noted that the skew correction factor is included in the calculation of the AASHTO LLDFs being considered. In a number of cases, the professional factor, ρ_{max}, for the live load shear forces at obtuse corners of bridge spans is observed to be greater than unity. The ρ_{max} values represent multipliers that can be applied to the AASHTO LLDFs to obtain 3D FEA estimates.

Table 40 and Figure 68 present the ρ_{max} values for the AASHTO LRFD calculation of the fascia girder shear forces at the obtuse corners of the bridge spans at the end abutments for all the bridges studied, both simple- and continuous-span. Table 41 and Figure 69 show these results for the fascia girder corresponding to the span having the obtuse corner at intermediate pier locations in continuous- span bridges.

Table 40. ρ_{max} values for the HL-93 live load shear forces for exterior girders at the obtuse corners of the span at end abutments.†

Bridge	Skew Index	CF Arrangement Notes	ρ_{maxG1}	ρ_{maxG4}
1	0.46	Contiguous	1.38	1.37
2	0.46	Staggered	1.23	1.32
3*	0.39	Contiguous, CF framing into bearing line	0.84	0.84
4*	0.39	Staggered	0.86	0.86
5*	0.42	Contiguous	0.91	0.91
6*	0.35	Contiguous	0.97	0.97
7*	0.33	Contiguous	0.84	0.84
8*	0.27	Staggered	0.88	0.88
9	0.47	Contiguous, CF framing into bearing line	0.92	1.00
10	0.47	Staggered	0.73	0.80
11*	0.26	Contiguous	0.99	0.99
12	0.32	Contiguous, CF framing into bearing line	0.99	0.99
13	0.23	Contiguous	0.58	0.58
14	0.23	Staggered	0.57	0.57
15	0.33	Contiguous	0.93	0.61
16	0.33	Staggered	0.90	0.63
17*	0.28	Contiguous	1.00	1.00
18*	0.20	Staggered	0.98	0.98
19	0.45	Contiguous	0.89	0.96
20	0.45	Staggered	0.77	0.85
21*	0.15	Parallel to skew	0.89	0.89
22*	0.31	Contiguous	0.99	0.91
23	0.37	Contiguous, CF framing into bearing line	0.97	0.97
24	0.37	Contiguous, inadequate offsets near bearing line	0.98	0.98
25	0.25	Contiguous, CF framing into bearing line	1.00	1.00
26*	0.15	Parallel to skew	0.94	0.94

† The shaded cells indicate ρ_{max} values that exceed the targeted limits for applicability of LGA.

* This bridge meets, or nearly meets, the requirements for application of the recommended LGA-based procedures for the bridge design.

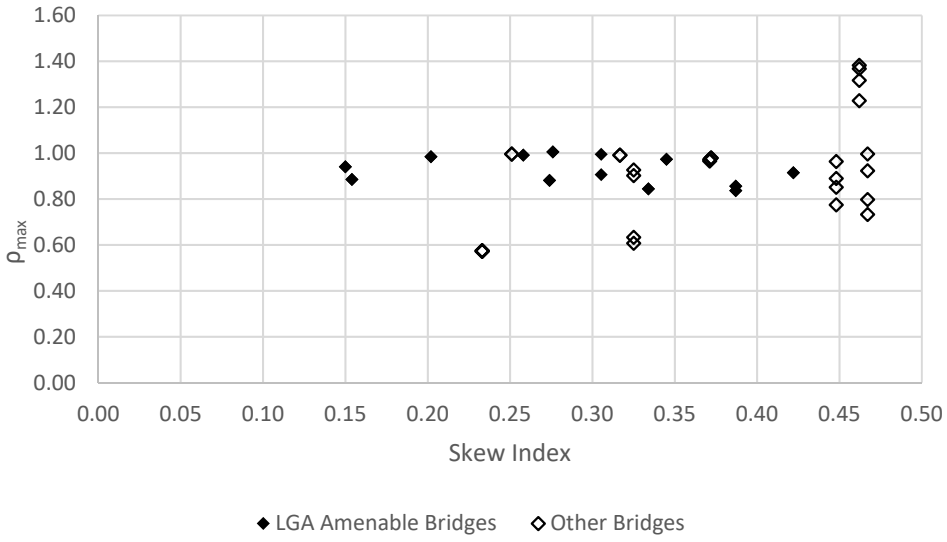

Figure 68. ρ_{max} values for the HL-93 live load shear forces for exterior girders at the obtuse corners of the span at end abutments.

Table 41. ρ_{max} values for the HL-93 live load shear forces for exterior girders at obtuse corners of the spans at intermediate piers of continuous-span bridges.

Bridge	Skew Index	CF Arrangement Notes	ρ_{maxG1}	ρ_{maxG4}
1	0.46	Contiguous	NA	NA
2	0.46	Staggered	NA	NA
3*	0.387	Contiguous, CF framing into bearing line	0.84	0.84
4*	0.387	Staggered	0.85	0.85
5*	0.42	Contiguous	NA	NA
6*	0.345	Contiguous	0.99	0.99
7*	0.33	Contiguous	NA	NA
8*	0.274	Staggered	0.93	0.93
9	0.467	Contiguous, CF framing into bearing line	0.97	0.87
10	0.467	Staggered	0.81	0.68
11*	0.258	Contiguous	0.98	0.98
12	0.3167	Contiguous, CF framing into bearing line	0.90	0.89
13	0.233	Contiguous	0.72	0.72
14	0.233	Staggered	0.72	0.68
15	0.325	Contiguous	0.85	0.90
16	0.325	Staggered	0.82	0.86
17*	0.28	Contiguous	NA	NA
18*	0.20	Staggered	NA	NA
19	0.45	Contiguous	NA	NA
20	0.45	Staggered	NA	NA
21*	0.15	Parallel to skew	NA	NA
22*	0.3053	Contiguous	0.94	0.98
23	0.3712	Contiguous, CF framing into bearing line	0.96	0.97
24	0.372	Contiguous, inadequate offsets near bearing line	0.95	0.95
25	0.251	Contiguous, CF framing into bearing line	0.90	0.89
26*	0.15	Parallel to skew	0.97	0.97

* This bridge meets, or nearly meets, the requirements for application of the recommended LGA-based procedures for the bridge design.

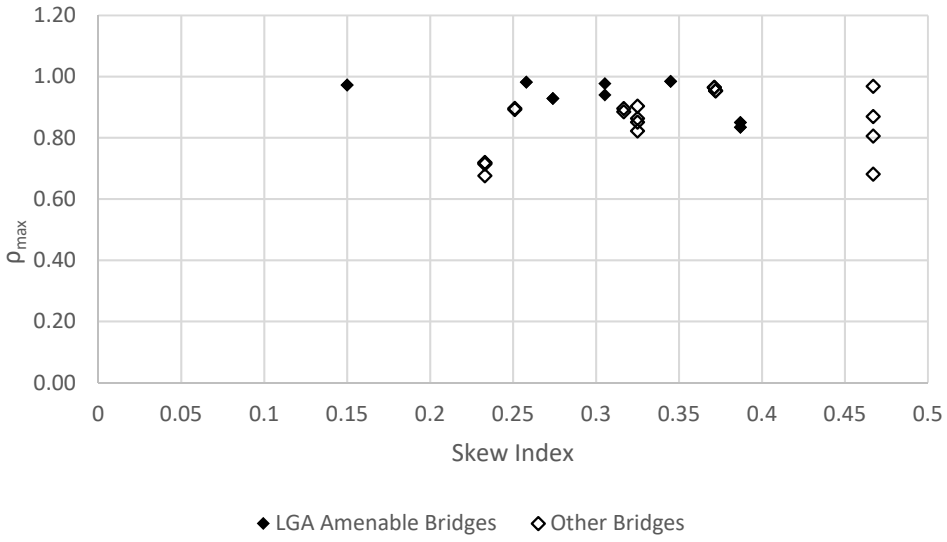

Figure 69. ρ_{max} values for the HL-93 live load shear forces for exterior girders at the obtuse corners of the spans at intermediate piers of continuous-span bridges.

Cells of these tables that have a ρ_{max} value larger than 1.11, the tolerance on ρ_{max} discussed in Section 5.3, are shaded. It should be noted that the ρ_{max} values for interior girders (not shown in the tables) are all smaller than 1.0, indicating that the LGA estimates are uniformly conservative compared to the 3D FEA values for the interior girders. Considering Table 40, the exterior girders of Bridges 1 and 2 have ρ_{max} values greater than 1.2. The LGA estimates are accurate to conservative for the exterior girders of the other simple-span bridges studied. Regarding the LGA estimated shear values at the span obtuse corners at pier locations in continuous-span bridges, Table 41 and Figure 69 show that all the ρ_{max} values corresponding to these locations show that the AASHTO LGA calculations are accurate to conservative.

5.5.4 Girder Strength I Bearing Reactions

The bearing reactions include the contributions from the girders through girder shear forces as well as from bearing line cross-frames through cross-frame shear forces. Some of the study bridges do not have cross-frames at intermediate pier bearing lines, but have intermediate cross-frames framing into the pier bearings. In such cases, the bearing reactions include contributions from the intermediate cross-frames framing into the bearing. Similar to the Strength I (STR I) girder shear forces, the ρ_{max} values for the STR I bearing reactions at the obtuse corners at end abutments, and the bearing reactions at the fascia girders at pier locations in the continuous-span bridges, are observed to be greater than unity in some cases. As noted previously, ρ_{max} values greater than unity can be considered as a correction factor to be applied to the LGA reaction to accurately estimate the 3D FEA values.

Table 42 and Figures 70 and 71 show the bearing reaction ρ_{max} results from the parametric studies. Cells that do not satisfy the tolerance on ρ_{max} of 1.11 recommended in Section 5.3 are highlighted in the table. Bridges 1, 2 and 19 have ρ_{max} values larger than 1.15 at their abutments. This is due to the combination of their large I_s and θ values (I_s = 0.46 and θ = 49.4° for Bridges 1 and 2, and I_s = 0.45 and θ = 52.2° for Bridge 19). The large ρ_{max} of 1.35 in Bridge 1 is mitigated by the alternative cross-frame framing arrangement in Bridge 2, but the updated value of 1.24 is still larger than the recommended tolerance. The large ρ_{max} of 1.17 in Bridge 19 is mitigated successfully to 1.04 by the alternative cross-frame framing arrangement in Bridge 20. The largest ρ_{max} for the pier reactions is 1.11 for Bridge 11, which is equal to the recommended tolerance on ρ_{max}. In addition, a few Category 3 bridges have ρ_{max} for the pier reactions close to 1.10.

The multiplicative modification factor of 1.10 recommended in Section 5.1.3 for the Category 2 and 3 bridges is based on the above results. By multiplying the calculated bearing reactions on the fascia girders at the obtuse corners at end abutments by 1.10, the ρ_{max} values for the reactions are made less than the tolerance of 1.11 in all cases. The reported ρ_{max} values in Tables 17, 18 and 19 in Section 5.4 reflect the use of this modification factor.

The smallest ρ_{max} values in Table 42 correspond to the bearings on the fascia girders at the end abutments in Bridges 13 and 14 (ρ_{max} = 0.72 for both cases). Bridges 13 and 14 are nonparallel skew continuous-span bridges and their end abutments are actually not skewed.

It should be noted that while the ρ_{max} values for the STR I bearing reactions are the largest at the fascia girders, the magnitude of the LGA reaction at the interior girders adjacent to these obtuse corners may actually be larger than the fascia girder reaction, depending on the characteristics of the bridge. Additionally, it should be noted that the sum of the STR I bearing reactions from LGA is not equal to the corresponding sum of the 3D FEA reactions because the live load reaction values are envelope values.

Table 42. ρ_{max} values for STR I bearing reactions at obtuse corners at end abutments and at the fascia girders at the piers in continuous-span bridges (shaded cells indicate ρ_{max} values that exceed the targeted limits for applicability of LGA).†

Bridge	Skew Index	ρ_{max} at Abutments	ρ_{max} at Intermediate Piers
1	0.46	1.35	NA
2	0.46	1.24	NA
3*	0.39	1.02	0.87
4*	0.39	0.99	0.99
5*	0.42	1.02	NA
6*	0.35	1.09	1.06
7*	0.33	1.00	NA
8*	0.27	0.97	0.99
9	0.47	0.83	1.06
10	0.47	0.81	0.94
11*	0.26	1.04	1.11
12	0.32	0.86	1.06
13	0.23	0.72	0.78
14	0.23	0.72	0.78
15	0.33	1.03	1.03
16	0.33	1.00	1.02
17*	0.28	1.04	NA
18*	0.20	1.03	NA
19	0.45	1.17	NA
20	0.45	1.04	NA
21*	0.15	0.97	NA
22*	0.31	1.05	1.01
23	0.37	1.04	1.04
24	0.37	0.91	1.07
25	0.25	0.86	1.03
26*	0.15	1.07	1.08

† The shaded cells indicate values that exceed the targeted limits for applicability of LGA.

* This bridge meets, or nearly meets, the requirements for application of the recommended LGA-based procedures for the bridge design.

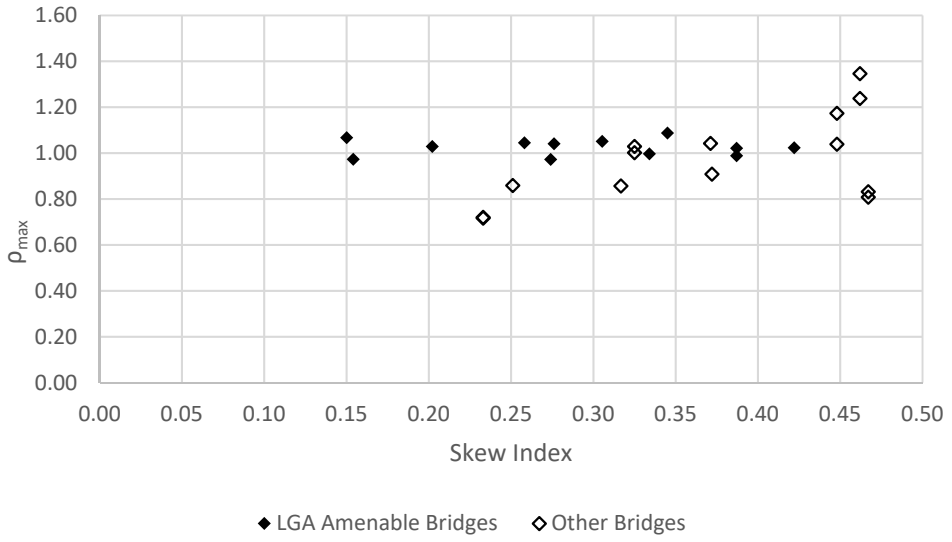

Figure 70. ρ_{max} values for STR I bearing reactions at obtuse corners at end abutments.

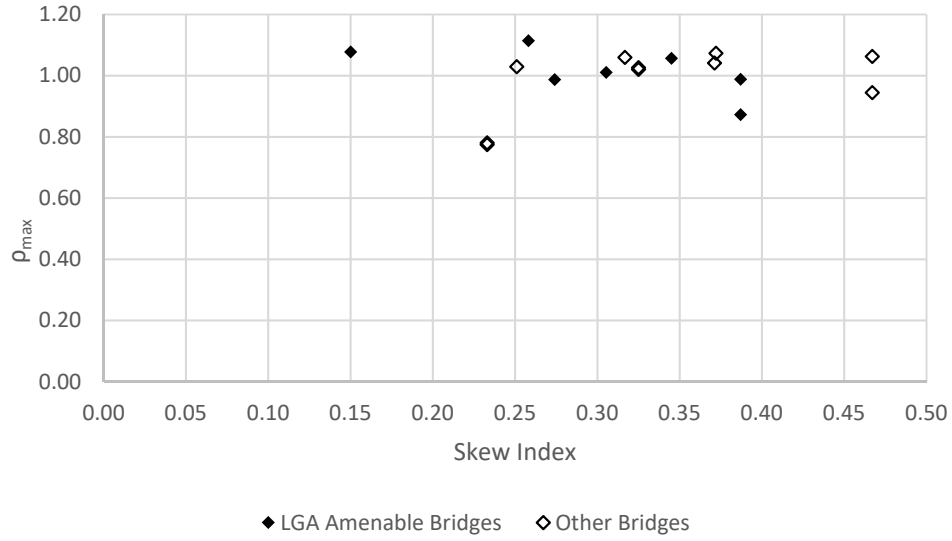

Figure 71. ρ_{max} values for STR I bearing reactions at the fascia girders at the piers in continuous-span bridges.

For the 26 bridges studied, uplift is not observed under the STR I loading combination in any of the bridges. Uplift can potentially occur at the acute corners of the bridge spans at the end abutments as the skewed geometry becomes more and more severe. The 3D FEA reactions are typically smaller than the LGA reactions at the acute corners of the spans and at the end abutments, using the STR I uplift load combination and using the minimum envelope values for the live load reactions from the 3D FEA (i.e., greater tendency for uplift in the 3D FEA calculations). The differences are due to the use of conservative AASHTO LLDFs. This is why Article C4.6.2.2.3c suggests "A supplementary investigation of uplift should be considered using the correction factor from Table 4.6.2.2.3c-1, i.e., the terms other than 1.0, taken as negative for the exterior beam on the acute corner." The results of the parametric studies indicate that, for all the bridges considered, this check would not be needed.

5.5.5 Girder Total Dead Load Vertical Displacements, Considering the Effects of SDLF Detailing of the Cross-Frames

In a skewed bridge, intermediate cross-frames that are perpendicular to the girders connect to the girders at different longitudinal positions within the span. At such cross-frames, the girders do not deflect by the same amount vertically. Cross-frames employed in the 26 bridges studied are primarily V or inverted V shaped truss-like assemblies. All the cross-frames considered in the studies have a top chord. Such cross-frames have a high in-plane stiffness. Hence, the cross-frames tend to twist the girders such that they essentially have an equal layover at the cross-frame ends due to the differential displacements in the girders. This interaction between the cross-frames and girders influences the overall vertical displacement profile of girders in the bridges. After the concrete deck hardens, a similar participation of the deck is observed in maintaining overall compatibility of deformations between the bridge deck, cross-frames and girders. Additionally, as discussed at the beginning of Chapter 5, the spans may interact in continuous-span bridges, especially in bridges with unequal spans, due to compatibility of deformations between the continuous girders within adjacent spans. In the recommended LGA calculations considered in this research, the concrete deck loads, barrier rail loads and wearing surface and utilities loads are distributed equally to the girders in the bridge under consideration. However, the complex 3D interaction in skewed bridges do not necessarily match well with the assumption of equal distribution of the dead loads. Hence, large differences can observed in the vertical displacements for all the dead load cases with the exception of the steel dead load (SDLF) load case. As discussed in Section 2.4, given steel dead load fit (SDLF) detailing of the cross-frames, the girders essentially respond as predicted in by the LGA under the steel dead loads.

Figure 72 shows a comparative plot of the LGA and 3D FEA displacements for Girder 1 in the nonparallel skew four-span continuous Bridge 13. The 3D FEA vertical displacements in Span 3 are larger than the LGA vertical displacements. On the other hand, the 3D FEA vertical displacements in Span 4 are smaller than the LGA vertical displacements. These results are influenced by the interaction with adjacent girders in each of the spans, as well as the interaction between the span in resisting the total dead loads.

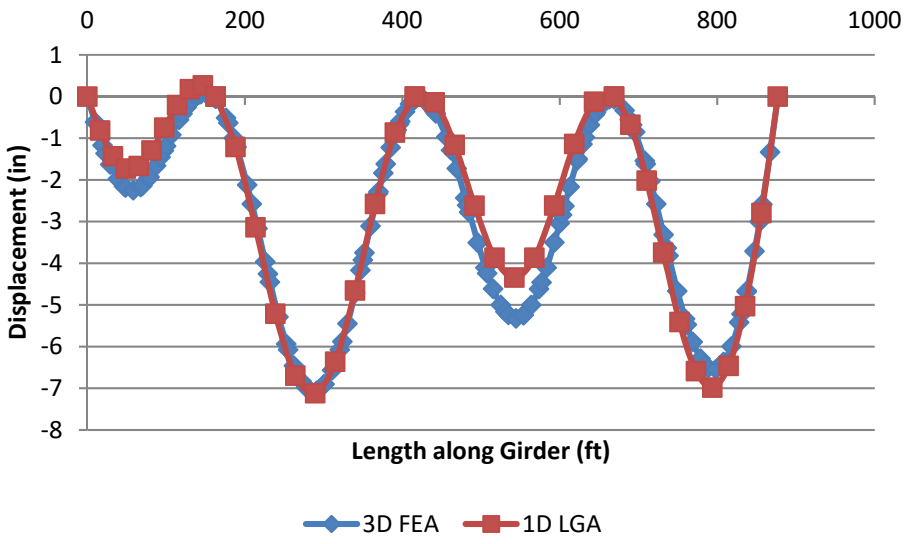

Figure 72. TDL (SDLF) vertical displacements for Girder 1 of Bridge 13.

The LGA - 3D FEA difference measures ε_{max2} and ε_{max3} (see Section 5.3) are used for evaluation of the accuracy of the LGA vertical displacement predictions in this research. These difference measures are applied to the maximum TDL (SDLF) vertical displacement calculations, as indicated in Equations 27 and 28 respectively.

Table 43 shows the differences in the maximum TDL (SDLF) displacements between the LGA and 3D FEA values for the various girders of the bridges studied. Cells that do not satisfy the tolerances recommended in Section 5.3 are highlighted in the tables. It is clear that many of the bridges considered in the parametric studies have difficulty in satisfying the recommended tolerances. This issue should be expected since (1) the total dead load displacement estimates do not have the benefit of offsetting conservative live load estimates, which is the case in evaluating the Strength I force quantities discussed in the previous sections of this chapter, and (2) conservative displacement estimates can be as difficult of a problem as unconservative displacement estimates. Conservative total dead load displacement estimates can result in over-cambering of the girders while unconservative total dead load displacement estimates can result in under-cambering of the girders. However, once the bridges from the parametric study are distributed to their respective Categories 1, 2 and 3 (see Section 5.1), it can be observed that the bridges that satisfy the limits on I_s and θ for the respective categories tend to have acceptable LGA predictions of their total dead load (SDLF) displacements.

Figures 73 and 74 plot the results for ε_{max2} and ε_{max3} respectively for all of the study bridges versus the skew index. One can observe that there is significant scatter in the results. However, with the exception of ε_{max3} for Bridge 7, all of the bridges that satisfy the requirements for application of LGA for their respective categories have ε_{max2} and ε_{max3} values that are within 10 % of the recommended respective tolerance values of 0.0005 = 1/2000 and 0.001 = 1/1000. Furthermore, one can observe that the maximum values obtained for ε_{max2} and ε_{max3} vary approximately as a linear function of the skew index.

Table 43. Maximum TDL (SDLF) differences in maximum displacements (inches) between LGA and 3D FEA.†

Bridge	Skew Index	Width (ft)	Span Length (ft)	CF Framing Arrangement Notes	$[\Delta_{LGAmax} - \Delta_{3DFEAmax}]_{G1}$ (in)	$[\Delta_{LGAmax} - \Delta_{3DFEAmax}]_{G2}$ (in)	$[\Delta_{LGAmax} - \Delta_{3DFEAmax}]_{G3}$ (in)	$[\Delta_{LGAmax} - \Delta_{3DFEAmax}]_{G4}$ (in)	ε_{max3} w_g (in)	ε_{max2}	ε_{max3}
1	0.46	87.1	208	Contiguous	-1.14	-0.66	0.88	-1.10	2.02	0.00045	0.00193
2	0.46	87.1	208	Staggered	-0.31	-0.10	0.34	-0.25	0.66	0.00014	0.00063
3*	0.39	102.1	185	Contiguous, CF framing into bearing line	-1.20	-0.63	-0.17	-1.20	1.03	0.00054	0.00084
4*	0.39	102.1	185	Staggered	-0.91	-0.42	-0.39	-0.91	0.53	0.00041	0.00043
5*	0.42	115.4	144	Contiguous	-0.47	-0.29	-0.07	-0.47	0.40	0.00027	0.00029
6*	0.35	112.2	116	Contiguous	-0.33	-0.24	-0.25	-0.33	0.08	0.00023	0.00006
7*	0.33	54.4	96	Contiguous	-0.64	0.08	0.34	-0.64	0.98	0.00055	0.00150
8*	0.27	84.2	173	Staggered	-0.19	-0.34	-0.48	-0.19	0.28	0.00023	0.00028
9	0.47	54.3	202	Contiguous, CF framing into bearing line	-1.56	-0.71	0.00	-0.19	1.56	0.00064	0.00239
10	0.47	54.3	202	Staggered	-1.07	-0.46	-0.08	-0.53	0.99	0.00044	0.00152
11*	0.26	67.1	188	Contiguous, CF framing into bearing line	-0.25	-0.12	-0.03	-0.25	0.22	0.00011	0.00027
12	0.32	42.5	202	Contiguous, CF framing into bearing line	-0.78	-0.01	-0.10	-0.78	0.68	0.00032	0.00134
13	0.23	43.1	253	Contiguous	0.06	0.09	-0.03	0.26	0.30	0.00009	0.00057
14	0.23	43.1	253	Staggered	-0.15	0.04	-0.06	0.16	0.22	0.00005	0.00042
15	0.33	60.2	188	Contiguous	-1.03	0.32	0.34	-1.22	1.57	0.00054	0.00217
16	0.33	60.2	188	Staggered	-1.04	0.30	0.22	-1.14	1.36	0.00050	0.00188
17*	0.28	71.1	202	Contiguous	-0.69	-0.39	-0.04	-0.69	0.64	0.00028	0.00075
18*	0.20	58.2	212	Staggered	-0.40	-0.29	-0.20	-0.40	0.20	0.00016	0.00028
19	0.45	67.6	196	Contiguous	-2.19	0.16	1.13	-1.67	3.32	0.00093	0.00409
20	0.45	67.6	196	Staggered	-1.61	0.32	0.61	-1.55	2.22	0.00069	0.00274
21*	0.15	135.1	241	Parallel to skew	-0.07	-0.27	-0.49	-0.07	0.42	0.00017	0.00026
22*	0.31	85.5	204	Contiguous	-0.28	-0.14	0.01	-0.61	0.63	0.00025	0.00061
23	0.37	84.2	252	Contiguous, CF framing into bearing line	-2.09	-1.11	0.12	-2.10	2.20	0.00070	0.00218
24	0.37	55.3	170	Contiguous, inadequate offsets near bearing line	-0.79	-0.38	0.08	-0.79	0.87	0.00039	0.00132
25	0.25	43.1	196	Contiguous, CF framing into bearing line	-0.99	-0.26	-0.26	-0.99	0.73	0.00042	0.00142
26*	0.15	73.1	92	Parallel to skew	-0.17	-0.09	-0.02	-0.17	0.15	0.00016	0.00017

† The shaded cells indicate values that exceed the targeted limits for applicability of LGA.

* This bridge meets, or nearly meets, the requirements for application of the recommended LGA-based procedures for the bridge design.

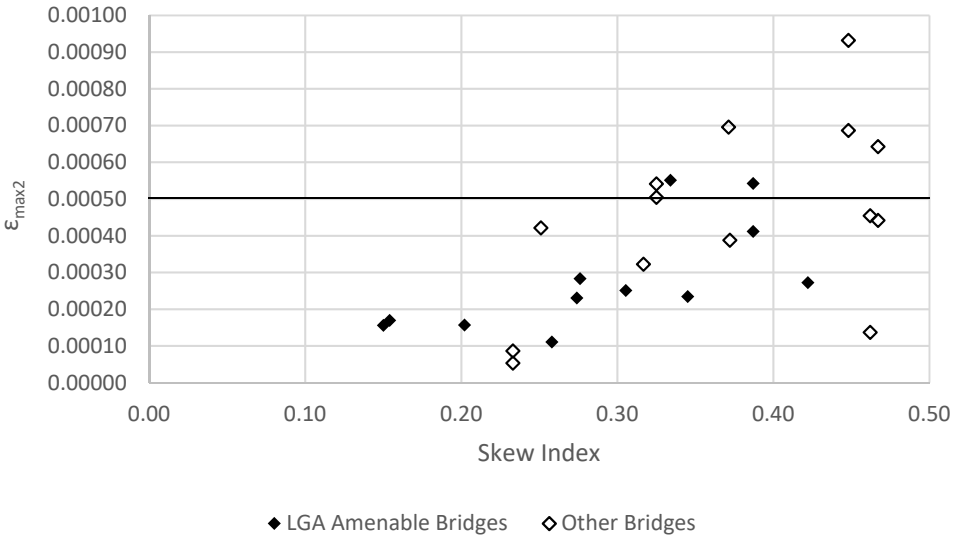

Figure 73. ε_{max2} values for TDL (SDLF) vertical displacements.

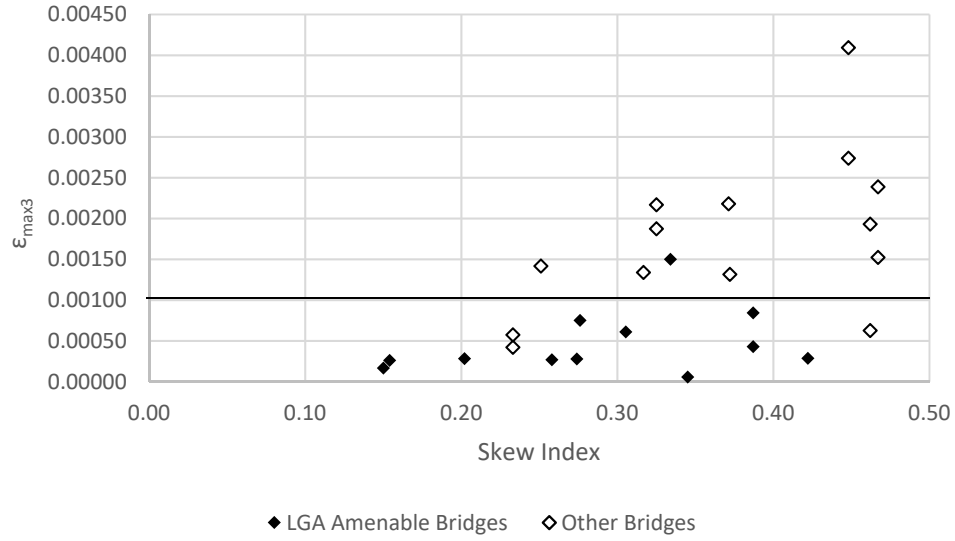

Figure 74. ε_{max3} values for TDL (SDLF) vertical displacements.

5.5.6 Girder Concrete Dead Load Vertical Displacements, Considering the Effects of Staged and Unstaged Deck Placement

The simplest analysis for concrete dead load effects is to assume that the deck is placed in one casting sequence, and that the entire concrete deck is placed prior to any setup of the concrete. Therefore, the bare steel structure consisting of the I-girders and cross-frames or diaphragms resists its own self-weight and the weight of the wet concrete deck slab, deck forms and construction equipment. The deck becomes composite with the steel I-girders once the deck hardens.

Depending on the length of the bridge, casting of the deck in stages may be required. If the deck is cast in stages, some portions of the deck become composite with the girders before other portions. As a result, the behavior of the bridge changes during the staged deck placement. For continuous-span bridges, the deck in the positive moment regions is typically placed before the negative moment regions over the intermediate supports in order to minimize cracking of the deck within the negative moment regions (Grubb et al., 2010). A typical result is that the downward vertical displacements will be larger in the spans where the concrete is placed first. Once the concrete deck sets up in these spans, the composite girders have larger stiffness in resisting additional deformations from the loads applied during the subsequent stages. Hence the total displacements in the spans that are placed first will tend to be larger at the end of the staged deck placement.

Staged deck placement was studied for four bridges in this research – the two-span continuous Bridges 3 and 4, the three-span continuous Bridge 11 and the four-span continuous Bridge 15. Bridges 3, 4 and 11 have parallel skew whereas Bridge 15 has nonparallel skew. Tables 44 through 46 show the concrete dead load (CDL) maximum displacements for staged and unstaged deck placement, for the exterior, first interior and central interior girders, respectively, and show the results for the corresponding ε_{max2} values. Table 44 shows the ε_{max2} results for both fascia girders. These results are different for the fascia girders in Bridge 15. The differences in the bending moments due to staged and unstaged deck placement are relatively small. However, the differences between the unstaged and staged deck placement vertical displacements are measureable. The staged deck placement displacements are larger due to the reason explained above.

LRFD Simon (NSBA, 2019) provides LGA capabilities that allow for the consideration of staged deck placement. These solutions are compared to the 3D FEA solutions for staged deck placement from CSiBridge (CSi, 2019). For the exterior girders, the ε_{max2} values for Bridges 3, 4 and 15 are smaller for staged deck placement compared to the corresponding values for unstaged deck placement. The ε_{max2} values change significantly from -1/22,000 to 1/2,850 for the exterior girders of Bridge 11. The LGA maximum displacement is measurably larger than the corresponding 3D FEA displacement for all the girders of this bridge for the staged construction case. This appears to be due to stiffening due to a significant transverse load path from contiguous cross-frames framed across the pier bearing lines, and significant three-dimensional interactions between the end and middle spans in this three-span continuous bridge during the initial stage of the staged deck placement. This initial stage involves the placement of the concrete deck in one of the end spans. The LGA solution misses these interactions since it only focuses on the individual girders and does not consider any transverse load path effects from the

cross-frames. In all cases with the exception of the staged construction case for the central interior girder of Bridge 11, the ε_{max2} values are smaller than the recommended tolerance from Section 5.3. The central interior girder has substantially larger vertical stiffness in resisting the loads from the placement of the concrete on the end spans than predicted by the LGA model.

Table 47 shows the differences between the staged and unstaged maximum displacements from the 3D FEA solutions for each of the above bridges, normalized by the corresponding span lengths. It is observed that the changes in the maximum vertical displacements due to staged deck placement are also smaller than the corresponding tolerance on ε_{max2} for all the bridges considered here. In many of the cases shown, the above differences between the LGA and 3D FEA solutions are the same order of magnitude as the changes in the vertical displacements due to staged versus unstaged placement of the concrete deck.

Additional detailed results are presented for CDL displacements corresponding to staged placement of the concrete decks for Bridges 3, 4, 11 and 15 in Appendix 4.

Table 44. Comparison of CDL displacements for staged and unstaged deck placement for exterior girders.

Bridge	L_s (ft)	Deck Placement	LGA (in)	3D FEA (in)	LGA - 3D FEA (in)	ε_{max2G1}	ε_{max2G4}
3*	185	Unstaged	4.87	5.76	-0.89	-1/2,490	-1/2,490
		Staged	5.40	5.83	-0.43	-1/5,160	-1/5,160
4*	185	Unstaged	4.87	5.33	-0.46	-1/4,830	-1/4,830
		Staged	5.36	5.73	-0.37	-1/6,000	-1/6,000
11*	185	Unstaged	6.08	6.49	-0.41	-1/22,000	-1/22,000
		Staged	7.86	6.89	0.97	1/2,850	1/2,850
15	226	Unstaged	6.50	7.35	-0.85	-1/3,190	-1/2,780
		Staged	6.83	7.61	-0.78	-1/3,480	-1/4,960

* This bridge meets, or nearly meets, the requirements for application of the recommended LGA-based procedures for the bridge design.

Table 45. Comparison of CDL displacements for staged and unstaged deck placement for first interior girders.

Bridge	L_s (ft)	Deck Placement	LGA (in)	3D FEA (in)	LGA - 3D FEA (in)	ε_{max2G2}
3*	185	Unstaged	4.87	5.35	-0.48	-1/4,620
		Staged	5.41	5.64	-0.23	-1/9,650
4*	185	Unstaged	4.87	5.14	-0.27	-1/8,220
		Staged	5.37	5.69	-0.32	-1/6,940
11*	185	Unstaged	6.08	6.28	-0.20	-1/11,100
		Staged	7.82	6.72	1.10	1/2,020
15	226	Unstaged	7.59	7.17	0.42	1/6,460
		Staged	8.10	7.53	0.57	1/4,760

* This bridge meets, or nearly meets, the requirements for application of the recommended LGA-based procedures for the bridge design.

Table 46. Comparison of CDL displacements for staged and unstaged deck placement for central interior girders.

Bridge	L_s (ft)	Deck Placement	LGA (in)	3D FEA (in)	LGA - 3D FEA (in)	ε_{max2G3}
3*	185	Unstaged	4.87	5.06	-0.19	-1/11,700
		Staged	5.41	5.63	-0.22	-1/10,100
4*	185	Unstaged	4.87	5.35	-0.48	-1/4,620
		Staged	5.37	5.97	-0.60	-1/3,700
11*	185	Unstaged	6.08	6.09	-0.01	-1/222,000
		Staged	8.19	6.54	1.65	1/1,350
15	226	Unstaged	7.62	7.24	0.38	1/7,140
		Staged	8.27	7.67	0.60	1/4,520

* This bridge meets, or nearly meets, the requirements for application of the recommended LGA-based procedures for the bridge design.

Table 47. Difference between the CDL maximum vertical displacements determined from 3D FEA for Bridges 3, 4, 11 and 15.

Bridge	L_s (ft)	Displacement Difference, Staged - Unstaged (in)			Displacement Difference / L_s		
		Exterior Girders	First Interior Girders	Central Interior Girders	Exterior Girders	First Interior Girders	Central Interior Girders
3*	185	0.07	0.29	0.57	1/31,700	1/7,660	1/3,900
4*	185	0.40	0.55	0.62	1/5,550	1/4,040	1/3,580
11*	185	0.40	0.44	0.45	1/5,550	1/5,050	1/4,940
15	226	0.26	0.36	0.43	1/8,540	1/6,167	1/5,160

* This bridge meets, or nearly meets, the requirements for application of the recommended LGA-based procedures for the bridge design.

5.5.7 Girder Layover under Total Dead Load (SDLF)

At skewed bearing lines, the cross-frames connect to the girders along the skew angle. The girders cannot displace vertically, but can rotate at the bearings. The cross-frames typically have a high in-plane stiffness compared to the torsional stiffness of the girders. To maintain compatibility with the girder major-axis bending rotations, the skewed bearing line cross-frames twist the girders. In parallel skew bridges, the girders twist in opposite directions at the two ends of the bridge. In this research, the twist at the bridge ends are reported as a twist rotation of the girders in radians and additionally as the layover displacement of the top flange relative to the bottom flange.

Girder layovers, calculated by the FDOT recommended procedure described in Section 5.1.2, are considered to be essentially an LGA response estimate, since the corresponding equations are based on fundamental compatibility of displacements (given the assumption that the cross-frame in-plane deformations are negligible).

Table 48 lists the girder total dead load layovers predicted at the abutment bearing lines located at the left end of the plan view of the bridges for all of the bridges studied. The data is listed in the order of increasing skew angle of the bearing line. Figure 75 plots the corresponding LGA and 3D FEA layovers, and their differences, as the girder twist rotation in radians as well as the layover displacement of the top flange of the girders relative to their bottom flange at the abutments. One can observe that all the girder layovers are predicted with good accuracy in all cases. The largest difference in the layover displacement between the LGA estimate and the 3D FEA calculation is 0.2599 inches, corresponding to Bridge 15. This bridge has a nonparallel skew geometry, intermediate cross-frames framing into the girders at offsets close to the bearing line being considered, and one of the largest skew angles of the bridges studied (53.4^{o}). This introduces significant forces in and some deformation of the end cross-frames in the bridge, resulting in the larger differences between the LGA and 3D FEA layover estimates. The fact that layover differences are smaller for the bridges having alternative cross-frame arrangements reinforces this observation.

The results show that the FDOT recommended procedure, which suggests that the girder layover is proportional to the tangent of the skew angle, gives an accurate estimate of the 3D FEA layovers. This accuracy is achieved although the displacements employed in predicting the layover have trouble satisfying the tolerances on ε_{max2} and ε_{max3} for many of the bridges studied. (It should be noted, however, that only two of the bridges satisfying the Category 1-3 accuracy requirements violate the ε_{max2} and ε_{max3} tolerances. These are bridges 3 and 7.)

Table 48. Maximum differences in LGA and 3D FEA CDL girder layovers at the abutment located on the left end of the plan view of the bridges.

Bridge	Skew Index	Skew Angle	Web Depth	Girder	LGA (rad)	3D FEA (rad)	LGA - 3D FEA (rad)	LGA (in)	3D FEA (in)	LGA - 3D FEA (in)
13	0.23	0.0	96.0	4	0.000000	0.000117	-0.000117	0.0000	0.0112	-0.0112
14	0.23	0.0	96.0	4	0.000000	0.000118	-0.000118	0.0000	0.0114	-0.0114
26*	0.15	10.0	34.0	1	0.000421	0.000306	0.000115	0.0143	0.0104	0.0039
21*	0.15	16.2	102.0	3	0.002948	0.003143	-0.000195	0.3007	0.3206	-0.0199
6*	0.35	20.7	39.0	3	0.003427	0.003770	-0.000343	0.1336	0.1470	-0.0134
8*	0.27	23.4	72.0	3	0.001772	0.002045	-0.000273	0.1276	0.1472	-0.0197
22*	0.31	28.4	86.0	4	0.005859	0.006227	-0.000368	0.5039	0.5355	-0.0316
5*	0.42	29.4	60.0	3	0.003920	0.005373	-0.001454	0.2353	0.3226	-0.0873
7*	0.33	35.5	39.4	1	0.008314	0.009957	-0.001642	0.3273	0.3920	-0.0647
11*	0.26	38.1	74.0	1	0.008489	0.008882	-0.000393	0.6282	0.6573	-0.0290
3*	0.39	38.2	79.0	1	0.007135	0.007550	-0.000414	0.5637	0.5964	-0.0327
4*	0.39	38.2	79.0	3	0.007127	0.007957	-0.000830	0.5630	0.6286	-0.0655
18*	0.20	39.7	84.3	3	0.009587	0.009954	-0.000368	0.8077	0.8387	-0.0310
17*	0.28	41.5	90.0	1	0.009357	0.010504	-0.001147	0.8421	0.9454	-0.1033
15	0.33	45.3	102.4	4	0.011759	0.014298	-0.002539	1.2037	1.4636	-0.2599
16	0.33	45.3	102.4	4	0.011762	0.013818	-0.002056	1.2040	1.4144	-0.2105
1	0.46	49.4	62.0	1	0.018375	0.020852	-0.002477	1.1392	1.2928	-0.1536
2	0.46	49.4	62.0	4	0.018564	0.018141	0.000423	1.1510	1.1247	0.0262
23	0.37	50.7	94.0	4	0.012361	0.014922	-0.002561	1.1619	1.4026	-0.2407
19	0.45	52.2	78.0	4	0.016427	0.018906	-0.002479	1.2813	1.4747	-0.1934
20	0.45	52.2	78.0	4	0.013176	0.014745	-0.001569	1.0278	1.1501	-0.1223
24	0.37	52.7	70.0	1	0.007758	0.009182	-0.001424	0.5430	0.6427	-0.0997
25	0.25	54.5	90.0	1	0.011427	0.013086	-0.001660	1.0284	1.1778	-0.1494
9	0.47	57.2	71.0	1	0.014765	0.017414	-0.002649	1.0483	1.2364	-0.1881
10	0.47	57.2	71.0	1	0.014775	0.016393	-0.001618	1.0491	1.1639	-0.1149
12	0.32	58.7	71.0	4	0.011198	0.012201	-0.001003	0.7951	0.8663	-0.0712

* This bridge meets, or nearly meets, the requirements for application of the recommended LGA-based procedures for the bridge design.

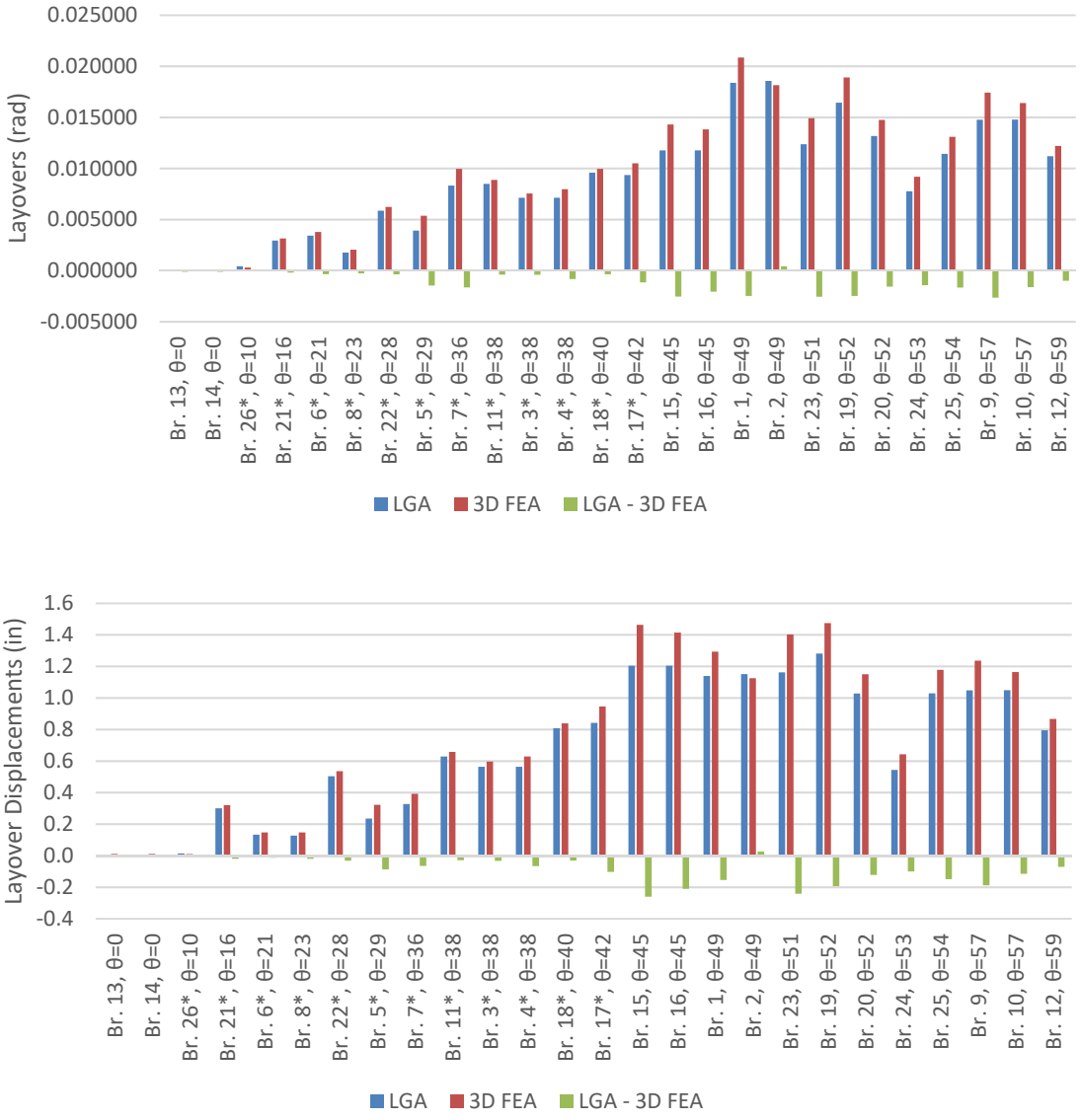

* This bridge meets, or nearly meets, the requirements for application of the recommended LGA-based procedures for the bridge design.

Figure 75. Maximum differences in LGA and 3D FEA CDL girder layovers at the abutment located on the left end of the plan view of the bridges.

5.5.8 Girder Fatigue Live Load Vertical Shear Forces

Design of bridge girder shear connectors is typically governed by fatigue. The corresponding demand quantity is the range of the girder vertical shear force. The recommended LGA procedures utilize the single-lane live load distribution factors (LLDFs) calculated from the AASHTO (2017) Article 4.6.2.2.3 provisions along with the maximum and minimum girder shear envelopes determined from the LGA for calculation of the girder vertical shear force range from the AASHTO Article 3.6.1.4 fatigue truck loading. Interestingly, the corresponding 3D FEA LLDFs can be determined by: (1) taking the difference between the maximum and minimum 3D FEA fatigue shear envelope values at a point of interest, (2) calculating the difference between the maximum and minimum LGA fatigue shear envelope values at this point from LGA using a LLDF of 1.0, and (3) dividing the result from (1) by the result from (2). Generally, the LLDFs determined in this way will be different from the LLDFs calculated using the HL-93 live load model. Therefore, accurate calculation of the LGA HL-93 live load shear forces does not necessarily ensure accurate calculation of the fatigue live load shear force range. In addition, the "true" LLDFs calculated from 3D FEA in general vary along the length of the bridge girders, both for the HL-93 and for the fatigue truck loadings.

In Appendix 3, the 3D FEA "true" LLDFs are calculated for the HL-93 moments and shears, and for the AASHTO fatigue truck loading moment and shear ranges. These distribution factors are calculated and presented at each tenth point of the spans and are compared to the AASHTO LRFD moment and shear LLDFs.

It should be noted that, in the 3D FEA solutions, the back-calculated distribution factors for the maximum shear envelope values, the minimum shear envelope values, and the shear range values are generally all different. The 3D FEA LLDFs for the live load shear range are calculated by dividing the shear range obtained from the 3D FEA solution by the shear range obtained from LGA using a LLDF of 1.0. In the LGA solutions, the LLDFs from AASHTO Article 4.6.2.2.3 are employed.

Table 49 and Figure 76 focus on a more direct evaluation of the LGA accuracy in determining the fatigue shear range in the bridge girders for all the bridges studied. They present the ρ_{max} values for the fatigue live load shear force range corresponding to the fascia girders at the obtuse corners at the end abutments of the study bridges. Table 50 and Figure 77 show comparable results to the above for the fatigue live load shear force ranges in the fascia girders at the obtuse corners of the spans and at pier locations in the continuous-span bridges studied. The largest differences between the LGA and 3D FEA results for the fatigue force range commonly occur at these locations. The ρ_{max} values for the fatigue shear range at the obtuse corners of bridge spans are observed to be greater than unity for a number of bridges. It should be noted that the ρ_{max} values for the interior girders are found generally to be less than 1.0.

As noted previously, the ρ_{max} values represent multipliers that need to be applied to the AASHTO LGA estimates to obtain the 3D FEA values. The cells of Tables 49 and 50 that have a ρ_{max} value larger than 1.11, the tolerance on ρ_{max} discussed in Section 5.3, are shaded. The ρ_{max} values are larger than 1.11 for at the abutments for Bridges 1 and 2. These parallel skew bridges have an I_s of 0.46, slightly violating the limits for application of the recommended LGA procedures to the Category 3 bridges discussed in Section 5.1, and a θ of 49.4°, close to the

maximum limit on the skew angle for the Category 3 bridges. Four other bridges have ρ_{max} values larger than 1.0 corresponding to the end abutments but smaller than the 1.11 limit. These are Bridges 12, 17, 18, and 25. Of these bridges, Bridges 12 and 25 violate the Category 2 and 3 limits for application of the recommended LGA procedures, while Bridges 17 and 18 qualify for application of these procedures. All of the other results shown in Table 49 and Figure 76 are accurate to conservative. The most conservative LGA shear live load range calculation corresponds to Girder G4 of Bridge 15. Bridge 15 is a nonparallel skew bridge that does not qualify for the recommended LGA calculations.

The largest ρ_{max} values for the fatigue live load shear force range occur for Bridge 13 at the obtuse corners of the spans at the piers on both fascia girders G1 and G4 (ρ_{maxG1} and ρ_{maxG4} = 1.10). The largest ρ_{max} values for the fatigue live load shear force range in Category 3 bridge occur for Bridges 9 and 24 at the obtuse corners of the spans at the piers fascia girders G1 and/or G4 (ρ_{maxG1} and ρ_{maxG4} = 1.07 for Bridge 24 and ρ_{maxG1} = 1.07 for Bridge 9). Six additional bridges have ρ_{max} values larger than 1.0 in Table 50. Bridge 11, with ρ_{max} = 1.03, is the only one of these bridges that meets the requirements for application of the recommended LGA procedures. This bridge is classified in Category 2.

Table 49. ρ_{max} values for fatigue live load shear force ranges for exterior girders at the obtuse corners at end abutments.†

Bridge	Skew Index	CF Arrangement Notes	ρ_{maxG1}	ρ_{maxG4}
1	0.46	Contiguous	1.30	1.29
2	0.46	Staggered	1.16	1.24
3*	0.39	Contiguous, CF framing into bearing line	0.69	0.69
4*	0.39	Staggered	0.75	0.75
5*	0.42	Contiguous	0.86	0.86
6*	0.35	Contiguous	0.86	0.86
7*	0.33	Contiguous	0.86	0.86
8*	0.27	Staggered	0.77	0.77
9	0.47	Contiguous, CF framing into bearing line	0.76	0.96
10	0.47	Staggered	0.78	0.86
11*	0.26	Contiguous	0.91	0.91
12	0.32	Contiguous, CF framing into bearing line	1.06	0.91
13	0.23	Contiguous	0.67	0.67
14	0.23	Staggered	0.67	0.67
15	0.33	Contiguous	0.89	0.54
16	0.33	Staggered	0.84	0.57
17*	0.28	Contiguous	1.04	1.04
18*	0.20	Staggered	1.03	1.03
19	0.45	Contiguous	0.86	0.94
20	0.45	Staggered	0.73	0.82
21*	0.15	Parallel to skew	0.85	0.85
22*	0.31	Contiguous	0.86	0.78
23	0.37	Contiguous, CF framing into bearing line	0.81	0.82
24	0.37	Contiguous, inadequate offsets near bearing line	0.92	0.92
25	0.25	Contiguous, CF framing into bearing line	1.01	1.01
26*	0.15	Parallel to skew	0.90	0.90

† The shaded cells indicate ρ_{max} values that exceed the targeted limits for applicability of LGA.

* This bridge meets, or nearly meets, the requirements for application of the recommended LGA-based procedures for the bridge design.

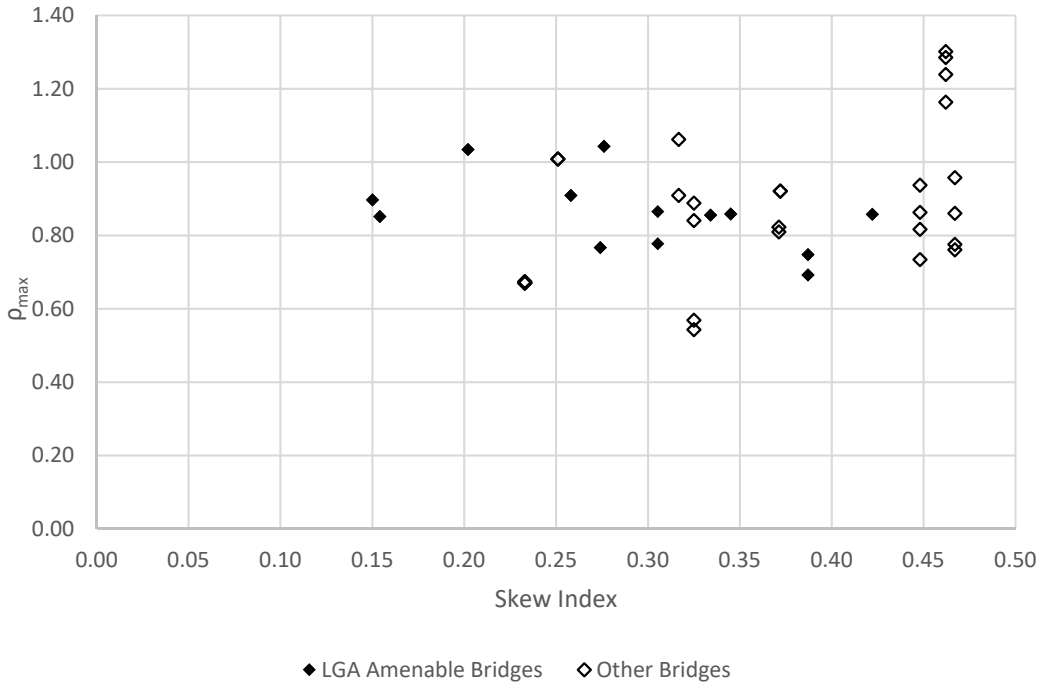

Figure 76. ρ_{max} values for fatigue live load shear force ranges for exterior girders at the obtuse corners at end abutments.

Table 50. ρ_{max} values for fatigue live load shear force ranges for exterior girders at the obtuse corners of the spans at piers of continuous-span bridges.†

Bridge	Skew Index	CF Arrangement Notes	ρ_{maxG1}	ρ_{maxG4}
1	0.46	Contiguous	NA	NA
2	0.46	Staggered	NA	NA
3*	0.39	Contiguous, CF framing into bearing line	0.81	0.81
4*	0.39	Staggered	0.84	0.84
5*	0.42	Contiguous	NA	NA
6*	0.35	Contiguous	0.97	0.97
7*	0.33	Contiguous	NA	NA
8*	0.27	Staggered	0.88	0.88
9	0.47	Contiguous, CF framing into bearing line	1.07	0.95
10	0.47	Staggered	1.01	0.91
11*	0.26	Contiguous	1.03	1.03
12	0.32	Contiguous, CF framing into bearing line	1.07	1.00
13	0.23	Contiguous	1.10	1.10
14	0.23	Staggered	1.08	1.01
15	0.33	Contiguous	0.90	0.96
16	0.33	Staggered	0.81	0.88
17*	0.28	Contiguous	NA	NA
18*	0.20	Staggered	NA	NA
19	0.45	Contiguous	NA	NA
20	0.45	Staggered	NA	NA
21*	0.15	Parallel to skew	NA	NA
22*	0.31	Contiguous	0.97	0.99
23	0.37	Contiguous, CF framing into bearing line	1.01	1.01
24	0.37	Contiguous, inadequate offsets near bearing line	1.07	1.07
25	0.25	Contiguous, CF framing into bearing line	1.04	1.04
26*	0.15	Parallel to skew	0.98	0.98

† The shaded cells indicate ρ_{max} values that exceed the targeted limits for applicability of LGA.

* This bridge meets, or nearly meets, the requirements for application of the recommended LGA-based procedures for the bridge design.

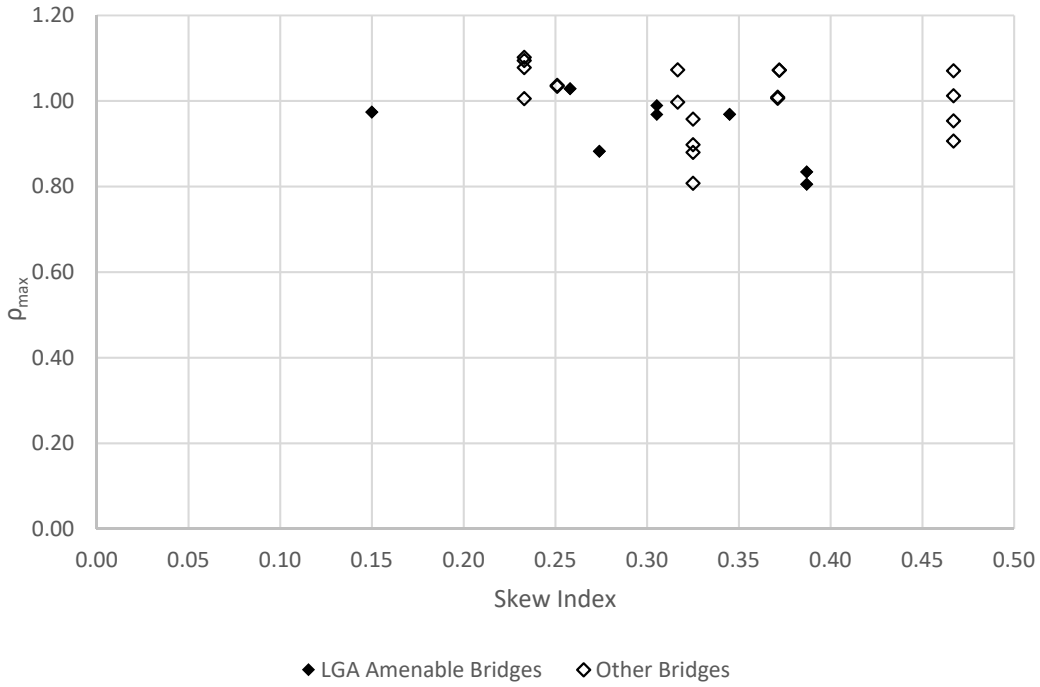

Figure 77. ρ_{max} values for fatigue live load shear force ranges for exterior girders at the obtuse corners of the spans at the piers in continuous-span bridges.

5.5.9 Girder Fatigue Live Load Flexural Stresses

The fatigue flexural stress range can be critical in the design of girder connection plates in certain cases. The 3D FEA and LGA methods used in the parametric study do not provide the fatigue live load flexural stresses directly. Maximum and minimum envelopes for fatigue live load bending moment can be obtained from both the 3D FEA and the LGA solutions. By convention, the maximum envelope provides an estimate of the maximum positive bending moment and the minimum envelope provides an estimate of the maximum negative bending moment. Flexural stresses are calculated from the bending moment envelopes given the girder composite cross-section properties. Although the girder flexural stresses could be obtained directly from the 3D FEA model, it is considered more reliable to work with the girder moments reported by the 3D FEA software.

For continuous-span bridges, the corresponding LGA estimates are typically conservative compared to the 3D FEA estimates. However, larger differences are observed between the LGA and 3D FEA estimates for simple-span bridges. The LGA procedures employ a line element idealization for the analysis. On the other hand, the 3D FEA procedures involve modeling of the girders, cross-frames, diaphragms, bridge deck, bearings and other structural components at their specific locations in three-dimensional space. For a girder of a simple-span bridge, the LGA idealizations are not capable of capturing girder negative bending moment effects from the live load on the skewed bridge. The negative bending effects are captured by 3D FEA. Section 1a of the appendices for the 26 bridges show comparative plots of fatigue live load bending moment envelopes. Representative plots for the exterior girder of Bridge 17 are shown in Figures 78 and 79.

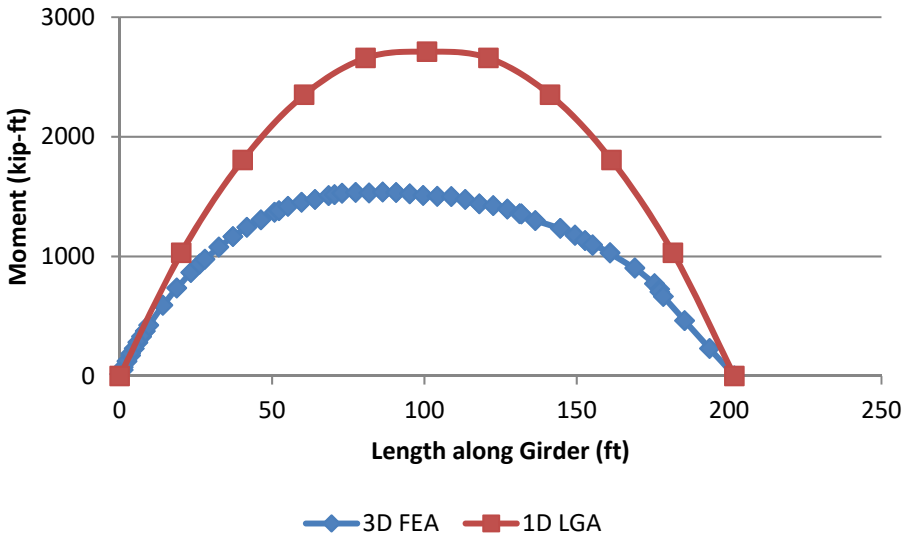

Figure 78. Envelope of maximum major-axis bending moments due to fatigue live loads in Girder 1 of Bridge 17.

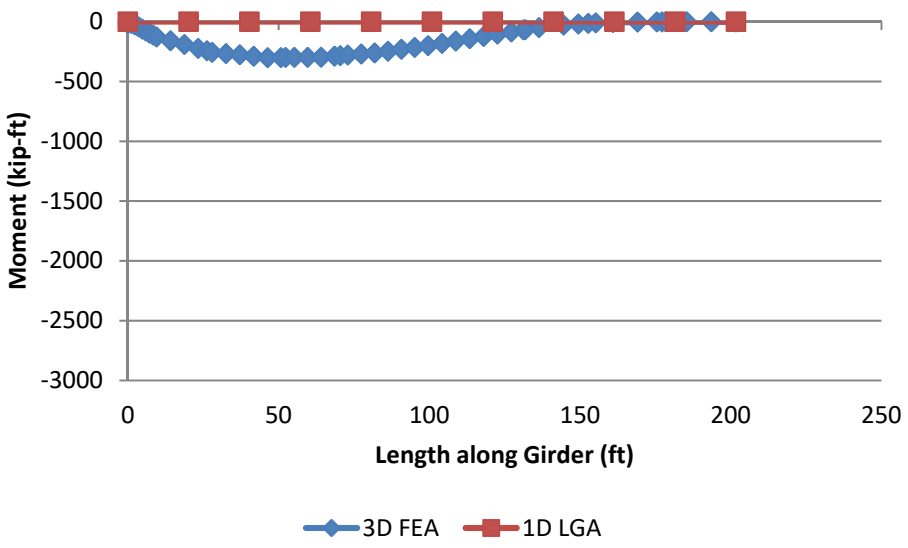

Figure 79. Envelope of minimum major-axis bending moments due to fatigue live loads in Girder 1 of Bridge 17.

Figure 78 indicates that LGA estimates for the maximum envelope of the major-bending moments are quite conservative compared to the 3D FEA estimates. Furthermore, measurable negative moment estimates obtained from 3D FEA are generated in exterior girders near the obtuse corners of simple-span skewed bridges, and are reflected in Figure 79. The flexural stress ranges for the top and bottom flanges are calculated using the maximum and minimum envelopes of the bending moments from the above figures. Figure 80 shows the major-axis bending stress range due to fatigue live load calculated for the top flange of Girder 1 of Bridge 17. Figure 81 shows the major-axis bending stress range due to fatigue live load calculated for the bottom flange of Girder 1 of Bridge 17. The 3D FEA estimates of the stress ranges are larger than the LGA estimates, until approximately the mid-span of the girder. This is because of the significant negative bending moment due to skew effects near the obtuse corner. A similar increase in fatigue stress range for the top flange of the exterior girder is observed in Girder 1 of Bridge 18.

Fatigue design of components and details are required if the components or details are subjected to a net tensile stress. Figure 80 indicates that LGA under-predicts the fatigue stress range for the top flange by a maximum of 1 ksi. However, the top flange is subjected to compression under the dead load cases for this simple-span bridge. Hence, it is highly improbable that the top flange is subjected to a net tensile stress. The bottom flange, on the other hand, is subjected to tensile stresses under dead load. Figure 81 indicates that the under-prediction by LGA is in the range of 0.2 to 0.5 ksi, which is relatively small to be significant in the fatigue design of the bottom flange and its connections for this bridge. These results are representative of the worst-case unconservative predictions of the fatigue flexural stresses upon inspection of the results for the different study bridges in Appendix 3.

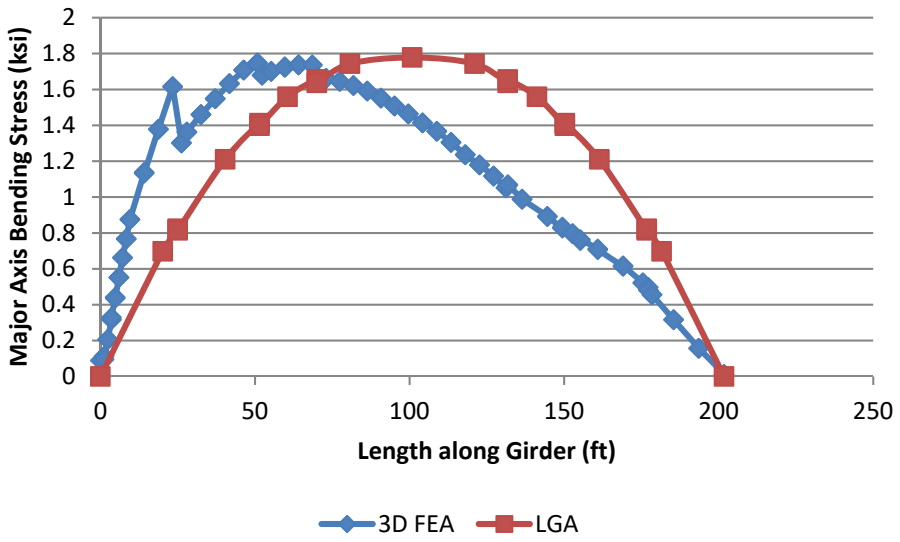

Figure 80. Major-axis bending stress range due to fatigue live loads in the top flange of Girder 1 of Bridge 17.

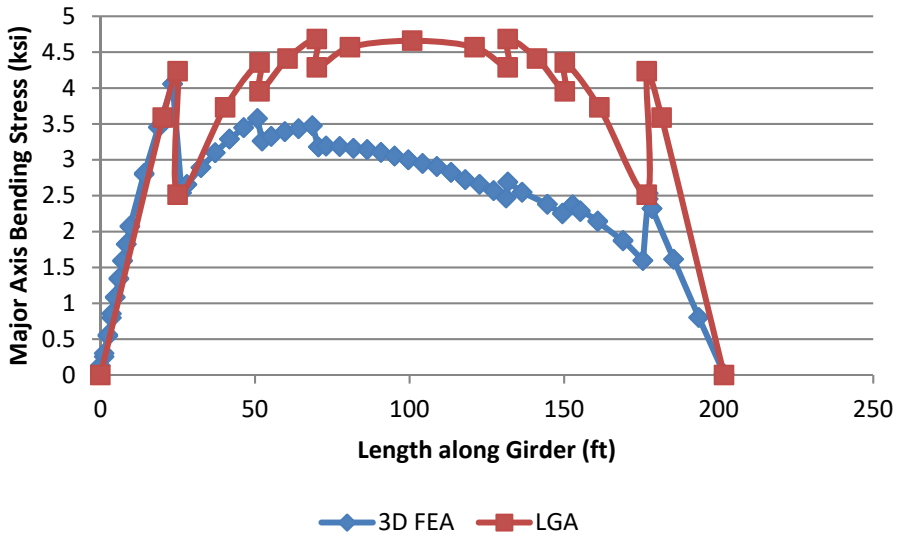

Figure 81. Major-axis bending stress range due to fatigue live loads in the bottom flange of Girder 1 of Bridge 17.

5.5.10 Girder Flange Lateral Bending Stresses

As explained in Section 5.1.4, twisting of the girders to maintain compatibility of the girder and cross-frame displacements and rotations produces girder flange lateral bending stresses. The stresses developed are influenced by the wide variety of cross-frame framing arrangements that have been employed in practice: contiguous and parallel to the skew, contiguous and perpendicular to the girders, staggered and perpendicular to the girders, and with various offsets between the cross-frames and between the cross-frames and the supports, and other arrangements involving local discontinuation of the cross-frame lines, etc. AASHTO LRFD Article C6.10.1 recognizes this and suggests estimates for the flange lateral bending stresses based on the cross-frame framing arrangement. Generous offsets near the skewed bearing lines are required to mitigate the effects of a stiff transverse load path and reduce the girder flange lateral bending stresses.

The 3D FEA solutions employed in the parametric studies account for flange lateral bending stresses due to overhang bracket loads on the exterior girder in a simple fashion. The CSiBridge models are set up to provide basic estimates of flange lateral bending stresses due to overhang bracket loads on the exterior girder, neglecting the elastic rebounding of the deck and girders when the brackets are removed. CSiBridge simulates the torsion from the overhang bracket loads on the exterior girders by applying equivalent equal and opposite uniformly distributed loads at the top and bottom flange-web junctures. Flange lateral bending stresses due to overhang loads on exterior girders are calculated consistently for LGA using AASHTO (2017) Equation C6.10.3.4.1-2 and the load factor of 1.25 for concrete dead loads is applied to the recommended LGA estimates for the flange lateral bending due to skew from Section 5.1.4.

Table 51 compares the recommended maximum girder flange lateral bending estimates for use with LGA, defined in Section 5.1.4, to the maximum STR I bottom flange f_ℓ values obtained from 3D FEA for all the girders considered in all the parametric study bridges. To focus predominantly on the accuracy associated with the estimation of the bridge skewed geometry effects, the fascia girder stresses from AASHTO (2017) Equation C6.10.3.4.1-2 are subtracted from the 3D FEA values obtained from CSiBridge. The difference between the corresponding f_ℓ values are shown in the table. Negative difference values, where the LGA estimate under-predicts the 3D FEA calculation (minus the f_ℓ values from Equation C6.10.3.4.1-2 on the fascia girders), are highlighted by shading of the cells. The following observations are noted:

- The recommended f_ℓ estimates are accurate to conservative for all the bridges with the exception of Bridge 16, which has a dramatic spike in the flange lateral bending of one of its girders due to a sharp section transition where the flange lateral moment of inertia changes by more than a factor of 2.0. An unusually large f_ℓ of 31.32 ksi is observed from the 3D FEA model in the central interior girder of Bridge 16 at this location, which is highlighted in Figure 82. The bottom flange lateral section modulus reduces by a factor of about 10 at this position. Such an abrupt transition is not recommended by AASHTO (2017) and is not common practice

- For Bridges 21 and 26, where the cross-frame lines are contiguous and oriented parallel to the skew, the estimated f_ℓ values are 0.0. Clearly, any flange lateral bending calculated in the 3D FEA models will result in a negative difference value for these cases. The negative difference values are as large as -2.68 ksi on the exterior girders and -0.95 ksi on the interior girders. AASHTO LRFD Article C6.10.1 clearly endorses the practical consideration that flange lateral bending stresses of these magnitudes may be taken as zero. (The -2.68 ksi value on the exterior girders includes a contribution between the LGA estimate of the overhang eccentric loading effects on the fascia girders from Equation C6.10.3.4.1-2 and the corresponding values determined in CSiBridge calculation procedures.
- It should be noted that the Bridge 8 central interior girder LGA – 3D FEA value of +1.04 is obtained only after applying the modification to the AASHTO LRFD Article C6.10.1 rules discussed in Section 5.1.4. The f_ℓ values determined using the Article C6.10.1 recommendations are underestimated for the central interior girder in Bridge 8. The cross-frame arrangement of Bridge 8 is staggered throughout its spans. However, the staggers do not satisfy the recommended offset of at least $4b_f$. The central girder of a bridge with this type of arrangement attracts the largest lateral bending due to the stiff path developing between the obtuse corners of the span causing the maximum internal transverse bending moment at the middle of the bridge span and at the middle of the bridge width. The location of the maximum f_ℓ in Bridge 8 is highlighted in Figure 83.
- The flange lateral bending stresses are under-estimated for all four of the girders shown for Bridge 25. Bridge 25 uses a contiguous cross-frame framing arrangement. However, the offsets near the abutment bearing lines do not satisfy AASHTO (2017) recommendations of $4b_f$. As a result, the maximum f_ℓ for the girders is observed in the vicinity of the obtuse corners. The locations of maximum f_ℓ for all the girders of Bridge 25 are shown in Figure 84. It should be noted that Bridge 25 has a skew angle of $\theta = 54.5^o$. This violates the maximum limits associated with the Category 3 bridges discussed in Section 5.1.

It can be observed that most of the LGA - 3D FEA values for f_ℓ in Table 51 are significantly positive. Excluding Bridges 16 and 25 for the reasons stated above, the average and standard deviation for the exterior girder f_ℓ values are 4.91 ksi and 4.34 ksi respectively. The average and standard deviation for the interior girder f_ℓ values are 8.27 ksi and 4.84 ksi. It should be noted that when these estimates are applied in the context of the AASHTO 1/3 rule, the corresponding stress effect on the major-axis bending resistance is 1/3 of the above values. Furthermore, the above data analysis focuses only on the largest flange lateral bending stresses in the girders. The suggested procedure in Section 5.1.4 allows for the use of smaller f_ℓ estimates within the exterior girders at locations other than the cross-frame adjacent to the supports, and within the interior girders at locations adjacent to the supports. Therefore, it is concluded that the corresponding conservatism in the AASHTO flexural resistance calculations is reasonable and acceptable.

Table 51. Comparison of maximum STR I 3D FEA bottom flange lateral bending stress to recommended LGA estimates.†

			STR I Bottom Flange f_ℓ											
			Left Exterior Girder			Right Exterior Girder			First Interior Girder			Central Interior Girder		
Bridge	Skew Index	CF Arrangement Notes	LGA (ksi)	3D FEA (ksi)	LGA - 3D FEA	LGA (ksi)	3D FEA (ksi)	LGA - 3D FEA	LGA (ksi)	3D FEA (ksi)	LGA - 3D FEA	LGA (ksi)	3D FEA (ksi)	LGA - 3D FEA
1	0.462	Contiguous	6.40	4.14	2.26	6.40	4.11	2.29	16.00	6.78	9.22	16.00	7.53	8.47
2	0.462	Staggered	6.40	3.12	3.28	6.40	5.28	1.12	16.00	5.52	10.48	16.00	8.05	7.95
3*	0.387	Contiguous, CF framing into bearing line	12.80	3.11	9.69	12.80	3.11	9.69	16.00	4.56	11.44	16.00	4.67	11.33
4*	0.387	Staggered	6.40	5.38	1.02	6.40	5.38	1.02	16.00	7.47	8.53	16.00	12.67	3.33
5*	0.422	Contiguous	12.80	2.12	10.68	12.80	2.12	10.68	16.00	3.20	12.80	16.00	3.21	12.79
6*	0.345	Contiguous	12.80	3.23	9.57	12.80	3.23	9.57	16.00	1.71	14.29	16.00	1.62	14.38
7*	0.334	Contiguous	12.80	5.48	7.32	12.80	5.48	7.32	16.00	2.22	13.78	16.00	5.16	10.84
8*	0.274	Staggered	12.80	2.87	9.93	12.80	2.87	9.93	24.00	12.35	11.65	24.00	22.96	1.04
9	0.467	Contiguous, CF framing into bearing line	12.80	3.35	9.45	6.40	5.67	0.73	16.00	8.22	7.78	16.00	9.13	6.87
10	0.467	Staggered	6.40	5.67	0.73	6.40	4.59	1.81	16.00	8.55	7.45	16.00	12.60	3.40
11*	0.258	Contiguous	12.80	3.26	9.54	12.80	3.26	9.54	16.00	6.92	9.08	16.00	7.90	8.10
12	0.3167	Contiguous, CF framing into bearing line	12.80	9.19	3.61	12.80	9.80	3.00	16.00	9.11	6.89	16.00	9.56	6.44
13	0.233	Contiguous	12.80	8.87	3.93	12.80	8.64	4.16	16.00	9.40	6.60	16.00	9.64	6.36
14	0.233	Staggered	6.40	9.66	-3.26	6.40	5.42	0.98	16.00	13.60	2.40	16.00	13.85	2.15
15	0.325	Contiguous	12.80	8.81	3.99	12.80	8.60	4.20	16.00	10.25	5.75	16.00	10.99	5.01
16	0.325	Staggered	6.40	9.61	-3.21	6.40	9.58	-3.18	16.00	12.41	3.59	16.00	31.32	-15.32
17*	0.276	Contiguous	12.80	10.75	2.05	12.80	10.75	2.05	16.00	2.32	13.68	16.00	3.05	12.95
18*	0.202	Staggered	12.80	3.20	9.60	12.80	3.20	9.60	24.00	5.56	18.44	24.00	6.12	17.88
19	0.448	Contiguous	12.80	5.54	7.26	12.80	11.13	1.67	16.00	5.95	10.05	16.00	8.33	7.67
20	0.448	Staggered	6.40	3.73	2.67	6.40	6.90	-0.50	16.00	7.23	8.77	16.00	14.97	1.03
21*	0.154	Parallel to skew	0.00	0.97	-0.97	0.00	0.97	-0.97	0.00	0.69	-0.69	0.00	0.48	-0.48
22*	0.3053	Contiguous	12.80	3.04	9.76	12.80	2.49	10.31	16.00	2.14	13.86	16.00	1.43	14.57
23	0.3712	Contiguous, CF framing into bearing line	12.80	3.62	9.18	12.80	3.62	9.18	16.00	6.35	9.65	16.00	3.26	12.74
24	0.372	Contiguous, inadequate offsets near bearing line	12.80	6.65	6.15	12.80	6.65	6.15	16.00	9.06	6.94	16.00	11.05	4.95
25	0.251	Contiguous, CF framing into bearing line	12.80	18.51	-5.71	12.80	18.60	-5.80	16.00	16.75	-0.75	16.00	17.12	-1.12
26*	0.15	Parallel to skew	0.00	2.68	-2.68	0.00	2.68	-2.68	0.00	0.95	-0.95	0.00	0.61	-0.61

† Negative difference values, where the LGA estimate under-predicts the 3D FEA calculation (minus the values from Equation C6.10.3.4.1-2 on the fascia girders), are highlighted by shading the cells.

* This bridge meets, or nearly meets, the requirements for application of the recommended LGA-based procedures for the bridge design.

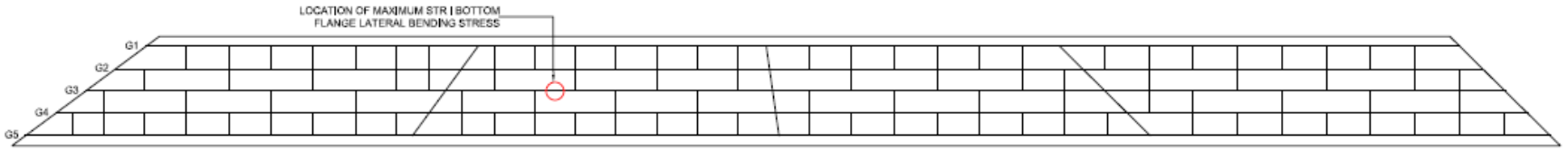

Figure 82. Maximum STR I bottom flange f_ℓ in Girder 3 of Bridge16.

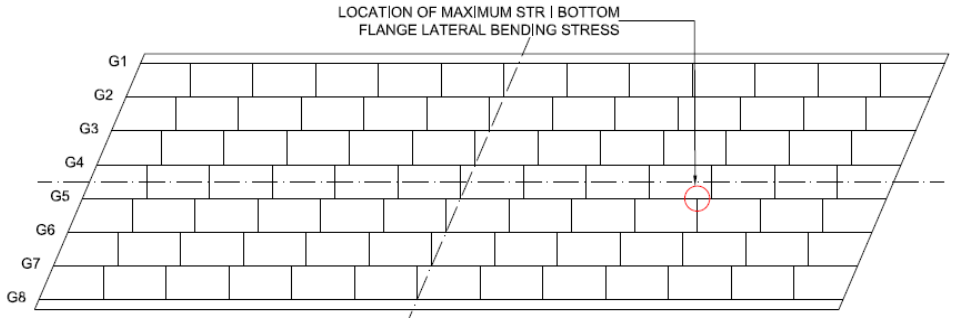

Figure 83. Maximum STR I bottom flange f_ℓ in Girder 3 of Bridge 8.

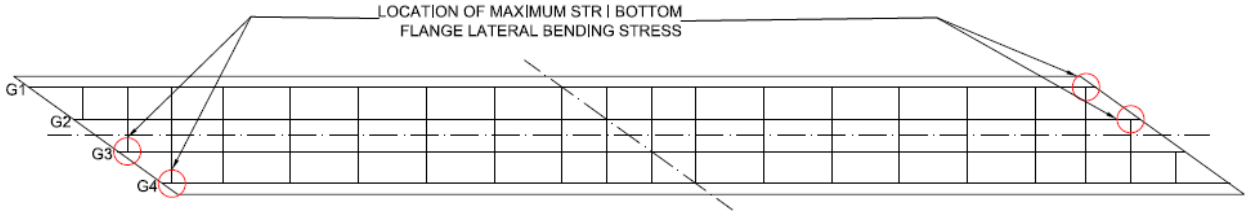

Figure 84. Maximum STR I bottom flange f_ℓ in girders of Bridge 25.

5.5.11 Cross-Frame and Diaphragm Forces

Cross-frames and solid-web diaphragms provide bracing to the bridge girders. In addition, they also distribute the dead and live loads within the superstructure. They participate with the bridge deck in transferring loads in the transverse direction of the bridge. The behavior of a skewed bridge is complex, and the forces in the cross-frames and diaphragms are influenced by a number of factors including the skew index, their framing arrangement, offsets near the skewed bearing lines and the types of cross-frames or diaphragms employed.

End cross-frames or diaphragms in a skewed bridge are typically provided along the skew. Intermediate cross-frames are usually oriented perpendicular to the longitudinal axes of the girders for bridges that have a skew angle greater than 20°. For bridges that have a skew angle less than 20°, the cross-frames may be oriented parallel to the skew according to the AASHTO (2017) provisions. In the parametric studies, Bridges 21 and 26 have skew angles less than 20° and have intermediate cross-frames oriented parallel to the skew. In all the other bridges studied, the intermediate cross-frames are oriented perpendicular to the longitudinal axis of girders. The end bearing line members in Bridge 7, and the end and intermediate pier bearing line members in Bridge 26 are solid-web diaphragms. Bridge 21 has X-type intermediate cross-frames. All other cross-frames in the bridges studied are V or inverted V assemblies.

The existing Bridges 8 and 18 of the 26 bridges studied in have a staggered cross-frame arrangement throughout their spans. In these bridges, the staggers are such that, if one connects a line between common ends of the nearest adjacent cross-frames across the bridge width, the line thus formed is parallel to the skew. This is illustrated in Figure 85, where the dotted lines connecting the left-upper ends of the cross-frames in the plan view are oriented parallel to the skew. In this particular bridge, this approach results in relatively small offsets that do not satisfy AASHTO (2017) Article C6.7.4.2, i.e., $L_b \geq 4b_f$, where b_f is the larger flange width within the unbraced lengths adjacent to a given cross-frame. The relatively moderate skew angle of 39.7º is not sufficient to accommodate this particular arrangement. AASHTO (2017) Article C6.7.4.2 recommends another potential approach that involves placing the intermediate cross-frames at a constant spacing along portions of the span length to satisfy the flange bracing requirements, but then omitting every other cross-frame in the interior bays between the girders. Bridge 4 (see Figure 19 in Chapter 3) uses this type of framing arrangement. Figure 86 shows this framing arrangement applied to Bridge 18. A key consideration in this arrangement is to ensure that the longer unbraced lengths, due to the skewed geometry effects, are less than or equal to than a maximum acceptable value, while ensuring that the shorter unbraced lengths are larger than the $4b_f$ requirement. The design in Figure 86 satisfies the $4b_f$ requirement of 4(32 in.) = 128 in = 10.7 ft on this bridge, while also not exceeding L_b = 25 ft in any unbraced length along the bridge span. (Note that Figure 86 is shown only for illustration purposes; the application of this framing arrangement specifically to Bridge 18 has not been studied in this work.)

The “optimum” framing arrangement is typically one in which the offsets or staggers between all the intermediate cross-frames, and the intermediate cross-frames and the bearing lines, are greater than or equal to $4b_f$ while satisfying girder lateral bracing requirements. The girders need to be braced to provide sufficient lateral-torsional buckling strength for noncomposite construction conditions within the maximum positive moment regions, and sufficient lateral-torsional buckling strength for noncomposite construction conditions and final

constructed composite conditions in negative moment regions. In addition, cross-frames need to be spaced at close enough intervals along the length of the fascia girders to maintain their torsional deformations due to eccentric bracket loads to acceptable limits, and to ensure adequate strength of these girders. The use of liberal offsets and staggers ($\geq 4b_f$) tends to soften the transverse load paths in the bridge, resulting in smaller cross-frame forces. In addition, framing arrangements where roughly every other cross-frame is omitted in certain interior bays between the girders (i.e., Bridges 2, 4 and 10 from the parametric studies, and the hypothetical example in Figure 86) can lead to the elimination of a significant number of cross-frames within the bridge. This tends to satisfy both the "optimum" aspects of reducing the cross-frame forces, potentially allowing for the use of smaller cross-frame members, as well as reducing the cost by reducing the number of cross-frames within a bridge. Bridges 14 and 16 (see Figures 29 and 31 in Chapter 3) also utilize this type of scheme, but on more complex geometries involving nonparallel skew. Bridge 20 (see Figure 35 in Chapter 3) applies this type of scheme on a simple-span bridge with splayed girders.

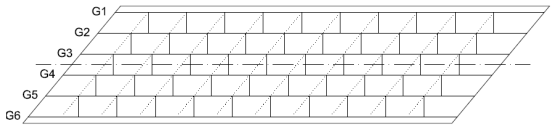

Figure 85. Staggered cross-frame arrangement of Bridge 18.

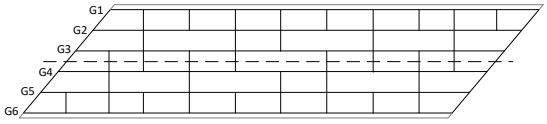

Figure 86. Modified staggered cross-frame arrangement of Bridge 18 satisfying AASHTO LRFD C6.7.4.2 recommendations.

All of the other bridges studied (Bridges 1, 3, 5-7, 9, 11-13, 15, 17, 19, and 22-25, shown in the corresponding figures in Chapter 3), utilize some form of a contiguous framing arrangement. This is a common traditional approach for nonskewed and skewed I-girder bridges. The cross-frames are all perpendicular to the girders in these bridges, since their skew angle is greater than 20°. Various schemes have been utilized within bridge design practice as an attempt to mitigate the development of large cross-frame forces, due to the unwanted or "nuisance" transverse stiffness of the cross-frame arrangements. These include: (1) providing an offset of the intermediate cross-frame lines relative to the skewed bearing lines, (2) leaving the cross-frames out of the bearing lines at the bridge piers and framing the intermediate cross-frames directly into the bearings instead (see Bridges 9, 11, 12 and 25), and (3) selectively removing certain cross-frames from the framing arrangement. However, it is common to encounter straight skewed bridges in which contiguous intermediate cross-frames are framed into or very close to the abutment or pier bearing lines that also contain bearing line cross-frames. Bridges 3, 5-7, 9, 11-13, 15, 17, 19, and 22-25 all have examples of this type of framing. A common practice for straight non-skewed I-girder bridges is to utilize contiguous cross-frame lines across the full bridge width (although this practice is unnecessary; alternate cross-frames can be omitted in certain interior bays in straight non-skewed bridges as well, resulting in fewer cross-frames and smaller cross-frame forces in these bridges as well). The practice of using contiguous cross-

frame lines across the full bridge width often has been extended to skewed I-girder bridges, with many different decisions having been made about the offset of the intermediate cross-frame lines relative to the bearing lines.

It should be noted that Bridges 2, 4, 10, 14, 16 and 20 involve the design and application of alterative cross-frame arrangements to the six existing Bridges, 1, 3, 9, 13, 15 and 19 respectively. The alternative cross-frame framing arrangements are developed using the following recommendations of AASHTO LRFD Article C6.7.4.2:

1. Cross-frames should be placed along the skewed bearing lines at the abutments, and at the piers in continuous-span bridges.
2. The intermediate cross-frames or diaphragms closest to the bearing lines should be offset by a minimum of $4b_f$ from the supports, where b_f is the largest girder flange width within the unbraced lengths on either side of the cross-frame or diaphragm under consideration.
3. Use a staggered cross-frame arrangement within the bridge spans in which all girder unbraced lengths between intermediate diaphragms or cross-frame locations are greater than or equal to $4b_f$, where b_f is the largest girder flange width within the unbraced length. This may be achieved by various schemes, such as those discussed above, or combinations of these schemes.
4. If the above offset requirement relative to the support results in an excessive unbraced length on the fascia girder at an acute corner, frame a cross-frame with top and bottom chords and no diagonal members from the first interior girder to the fascia girder at a small or zero offset relative to the interior support.

Figure 86 shows a result of applying this procedure to Bridge 18. As stated above, the bridge in Figure 86 is provided as an illustration, but has not been studied specifically in this research.

One aspect of the above engineering of the cross-frame framing arrangements should be clear from the above discussions - the cross-frame framing arrangements encountered in skewed I-girder bridge design practice can vary widely. This is true even when using the above current guidance, and it is even truer when bridges are considered that have been designed with various traditional practices. The challenge when applying Line Girder Analysis (LGA) to these bridges is the appropriate sizing of cross-frames designed with these many different framing arrangements. The developments discussed below address the requirements presented in Section 5.1.5 by providing reasonable upper-bound estimates for the force demands on the cross-frames as a function the skewed geometry and different framing arrangement effects for bridges having low to moderate skew.

Tables 52 through 54 list the maximum Strength I tension and compression axial forces determined in the bottom chord, diagonal and top chord cross-frame members from 3D FEA considering all the intermediate cross-frames of the 26 bridges studied. Figures 66 through 71 plot these forces versus the skew indices of the bridges.

Tables 55 through 57 and Figures 93 through 98 show these results for the bearing line cross-frames in all of the study bridges. Detailed plots of all the forces in all the members of all the cross-frames in all of the bridges are provided in Appendix 3.

In the above tables, the bridges where the recommended LGA procedures would be permitted are marked by the asterisk "*". The following observations are relevant to these tables and figures:

- The different cross-frame members are often subjected both to substantial tension and substantial compression considering all the cross-frames within a given bridge.
- Some of the cell entries in the tables list a value of 0.0 for the tension or compression force. In these cases, the member is subjected only to tension or compression, corresponding to the nonzero reported maximum value.
- The figures highlight the bridges that satisfy the requirements from Categories 1, 2 or 3 of Section 5.1 for design using the recommended LGA procedures as "LGA Amenable Bridges" and show the data points for these bridges by solid black diamond symbols.
- The Category 4 and 5 bridges, which have nonparallel skew and splay respectively, and been shown in the summary discussions of Section 5.4 to all have skew index and skew angle values that violate the Category 1 through 3 limits, are highlighted by shaded open diamond symbols and labeled as "Case 4 or 5 bridges" in the plots.
- The data for the other bridges considered in the discussions of Categories 1 through 3 in Section 5.4, but which have skew indices and/or skew angles that violate the requirements for application of the recommended LGA procedures, are shown as open white diamond symbols.
- In general, the force levels in the intermediate cross-frames of the "LGA Amenable Bridges" are relatively small in magnitude compared to the "Case 4 or 5 Bridges" and to the "Other Bridges."
- The magnitude of the axial forces in the bearing line cross-frames are relatively small in most situations. However, there are some exceptions. As identified in Section 5.4, these are cases where intermediate cross-frames frame into the girders at or close to bearing lines that also contain cross-frames.

A detailed assessment of the cross-frame forces indicates that some of their largest contributions are from live load applied to the composite bridge system. In these cases, the cross-frames tend to work compositely with the bridge deck. The deck is capable of working in effect as a large top chord of the cross-frames, or as a large top flange in developing composite transverse bending actions along with the cross-frame members (or the solid-web diaphragms). As such, it is observed that the steel cross-frames or solid-web diaphragms, when isolated as free-body diagram not including the concrete slab, are subjected to significant net axial force in addition to shear forces and bending moments. Detailed plots showing the variation of the bottom chord, diagonal and top chord cross-frame forces throughout bridge structural system are shown for each of the study bridges in Appendix 3 of the main project report. It can be observed in many of the cases that both the top and bottom chords of the cross-frames can be subjected to the same sign of axial force, tension or compression, within certain regions of the bridge geometry. For instance, the composite transverse bending at the mid-span and mid-width of the bridges can often result in both chords being placed in axial tension. The axial forces in the top chords of course tend to be smaller than the axial forces in the bottom chords. This is due to the action of the deck as the predominant composite top chord "member" of the cross-frames.

Table 52. Maximum STR I tension and compression forces in bottom chords of intermediate cross-frames.

Bridge	Skew Index	STR I Max Tension (kip)	STR I Max Compression (kip)
1	0.46	324	171
2	0.46	204	158
3*	0.39	102	106
4*	0.39	55	75
5*	0.42	114	77
6*	0.35	132	83
7*	0.33	NA**	NA**
8*	0.27	57	45
9	0.47	112	214
10	0.47	66	147
11*	0.26	110	117
12	0.32	104	216
13	0.23	62	289
14	0.23	76	318
15	0.32	83	139
16	0.32	58	188
17*	0.28	113	84
18*	0.20	41	37
19	0.45	212	119
20	0.45	102	114
21*	0.15	80	15
22*	0.31	137	121
23	0.37	180	261
24	0.37	71	117
25	0.25	58	151
26*	0.15	65	41

* This bridge meets, or nearly meets, the requirements for application of the recommended LGA-based procedures for the bridge design.

** This bridge has solid-web diaphragms rather than cross-frames.

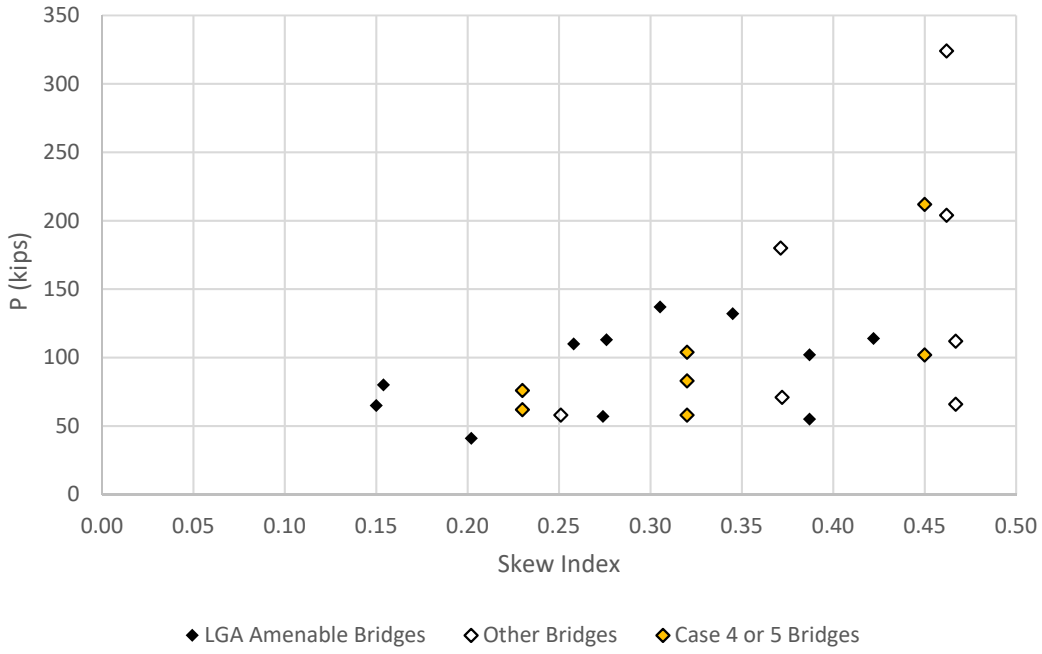

Figure 87. Maximum STR I tension forces in bottom chords of intermediate cross-frames.

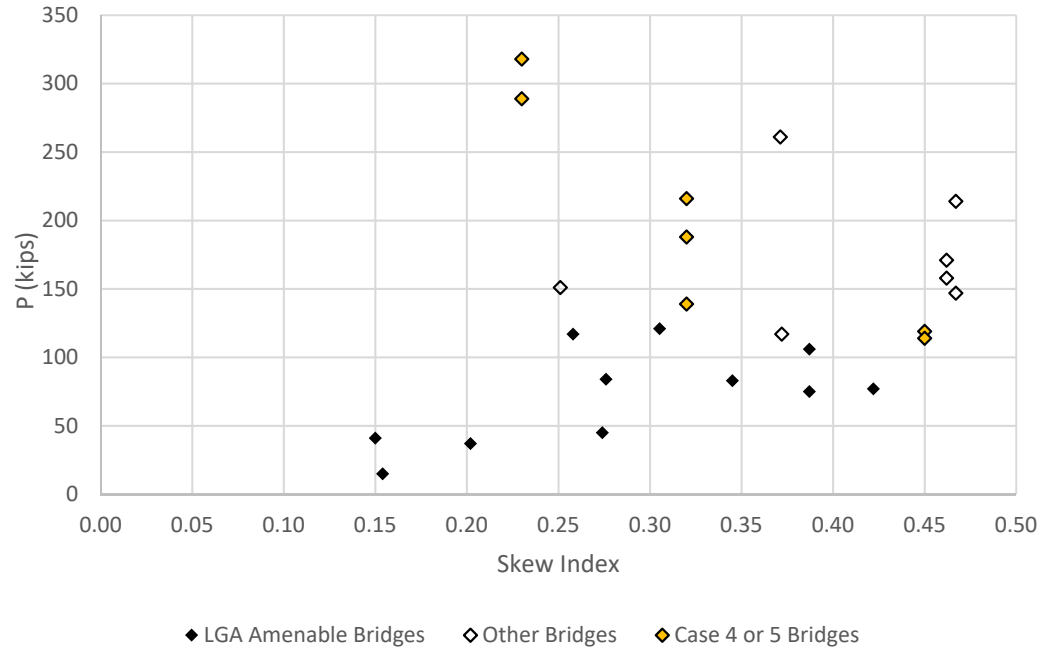

Figure 88. Maximum compression forces in bottom chords of intermediate cross-frames.

Table 53. Maximum STR I tension and compression forces in diagonals of intermediate cross-frames.

Bridge	Skew Index	STR I Max Tension (kip)	STR I Max Compression (kip)
1	0.46	166	166
2	0.46	106	106
3*	0.39	42	41
4*	0.39	33	33
5*	0.42	38	38
6*	0.35	40	40
7*	0.33	NA**	NA**
8*	0.27	32	31
9	0.47	85	85
10	0.47	70	70
11*	0.26	51	50
12	0.32	126	126
13	0.23	191	191
14	0.23	209	209
15	0.32	98	98
16	0.32	114	114
17*	0.28	62	62
18*	0.20	22	22
19	0.45	123	123
20	0.45	61	61
21*	0.15	51	31
22*	0.31	50	49
23	0.37	146	147
24	0.37	45	45
25	0.25	124	124
26*	0.15	25	24

* This bridge meets, or nearly meets, the requirements for application of the recommended LGA-based procedures for the bridge design.

** This bridge has solid-web diaphragms rather than cross-frames.

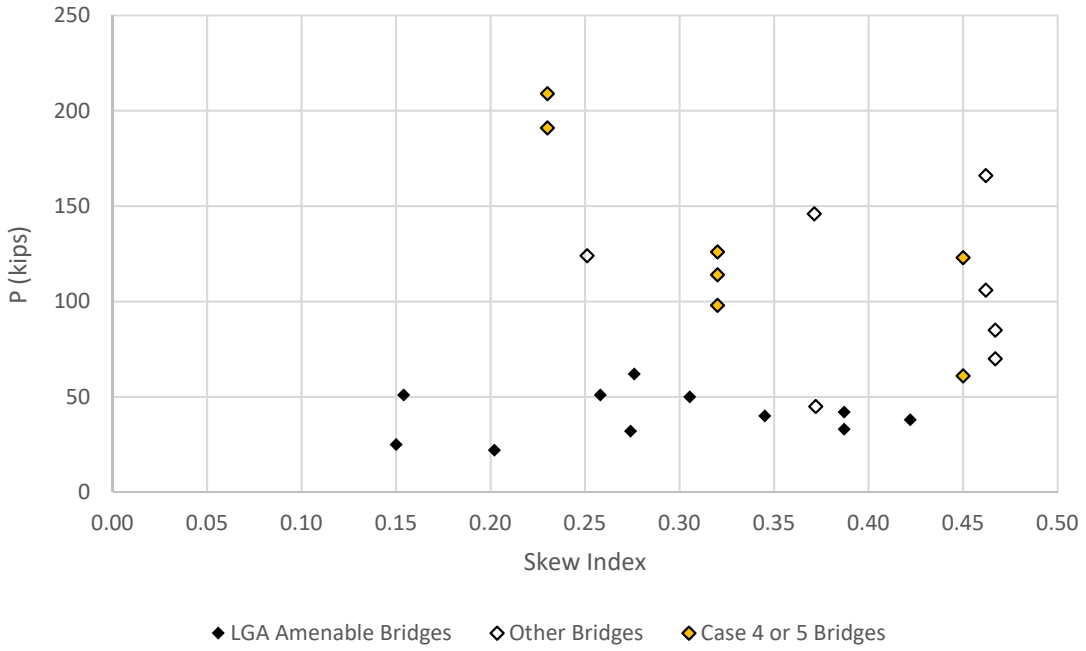

Figure 89. Maximum STR I tension forces in diagonals of intermediate cross-frames.

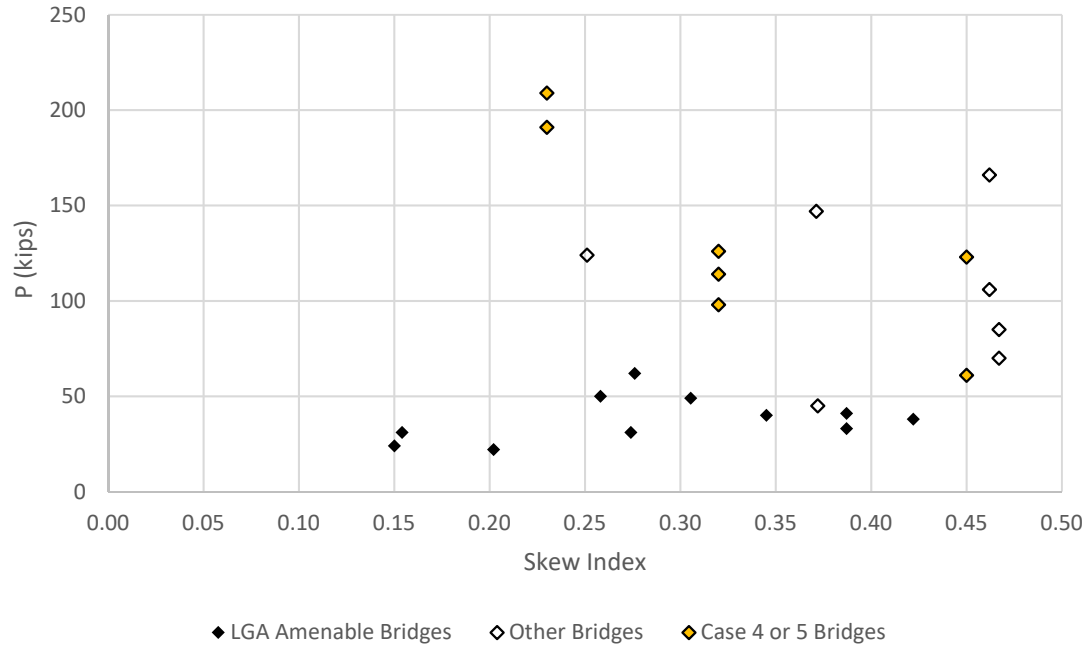

Figure 90. Maximum STR I compression forces in diagonals of intermediate cross-frames.

Table 54. Maximum STR I tension and compression forces in top chords of intermediate cross-frames.

Bridge	Skew Index	STR I Max Tension (kip)	STR I Max Compression (kip)
1	0.46	22	105
2	0.46	51	67
3*	0.39	37	42
4*	0.39	50	32
5*	0.42	15	28
6*	0.35	29	37
7*	0.33	NA**	NA**
8*	0.27	51	45
9	0.47	62	38
10	0.47	39	37
11*	0.26	31	30
12	0.32	63	21
13	0.23	105	23
14	0.23	94	34
15	0.32	68	71
16	0.32	82	89
17*	0.28	10	29
18*	0.20	0	17
19	0.45	30	80
20	0.45	25	42
21*	0.15	0	24
22*	0.31	26	39
23	0.37	145	95
24	0.37	30	25
25	0.25	93	84
26*	0.15	33	22

* This bridge meets, or nearly meets, the requirements for application of the recommended LGA-based procedures for the bridge design.

** This bridge has solid-web diaphragms rather than cross-frames.

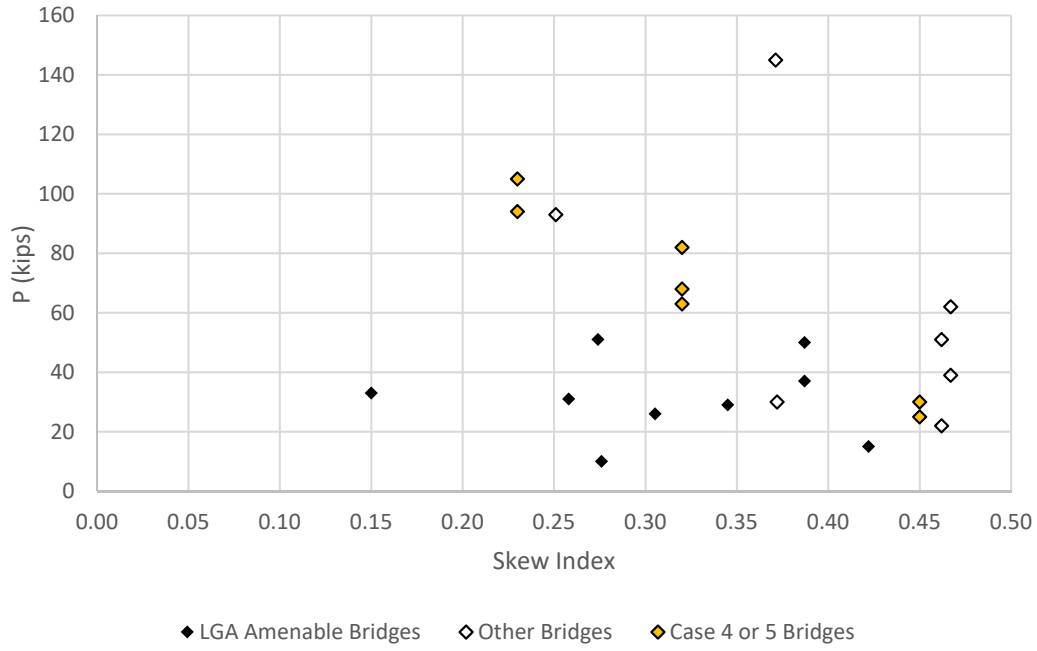

Figure 91. Maximum STR I tension forces in top chords of intermediate cross-frames.

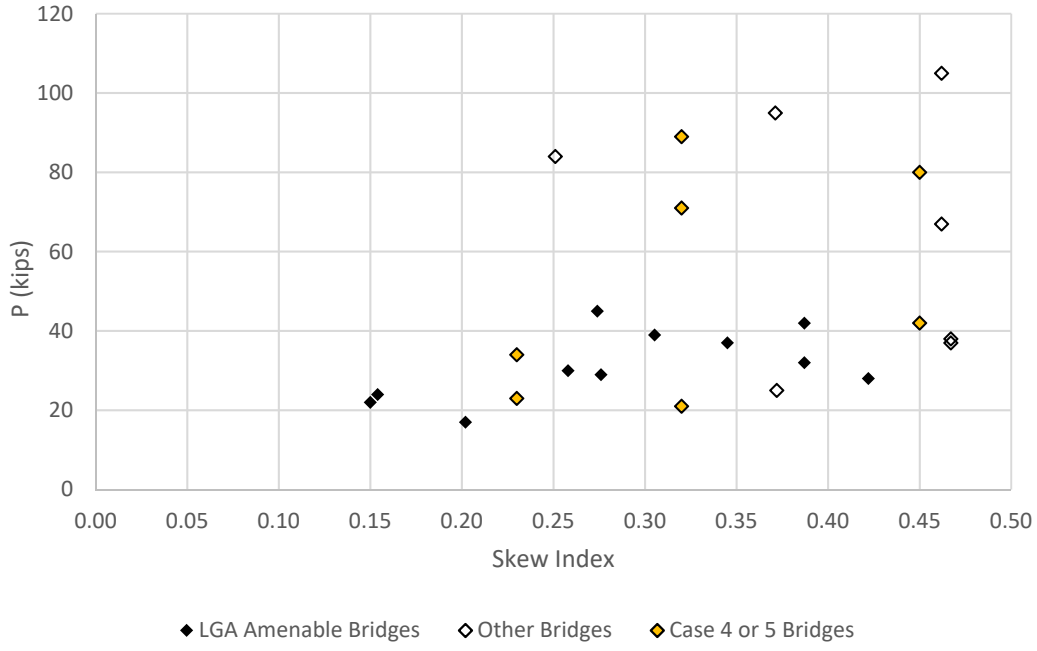

Figure 92. Maximum STR I compression forces in top chords of intermediate cross-frames.

Table 55. Maximum STR I tension and compression forces in bottom chords bearing line cross-frames at abutments and intermediate piers.

Bridge	Skew Index	STR I Max Tension (kip)	STR I Max Compression (kip)
1	0.46	5	17
2	0.46	21	16
3*	0.39	66	109
4*	0.39	38	35
5*	0.42	6	4
6*	0.35	8	9
7*	0.33	NA**	NA**
8*	0.27	5	3
9	0.47	7	24
10	0.47	36	33
11*	0.26	53	128
12	0.32	27	75
13	0.23	48	39
14	0.23	48	31
15	0.32	23	25
16	0.32	19	22
17*	0.28	0	13
18*	0.20	4	10
19	0.45	0	32
20	0.45	11	21
21*	0.15	6	3
22*	0.31	23	9
23	0.37	8	7
24	0.37	20	15
25	0.25	8	33
26*	0.15	NA	NA

* This bridge meets, or nearly meets, the requirements for application of the recommended LGA-based procedures for the bridge design.

** This bridge has solid-web diaphragms rather than cross-frames.

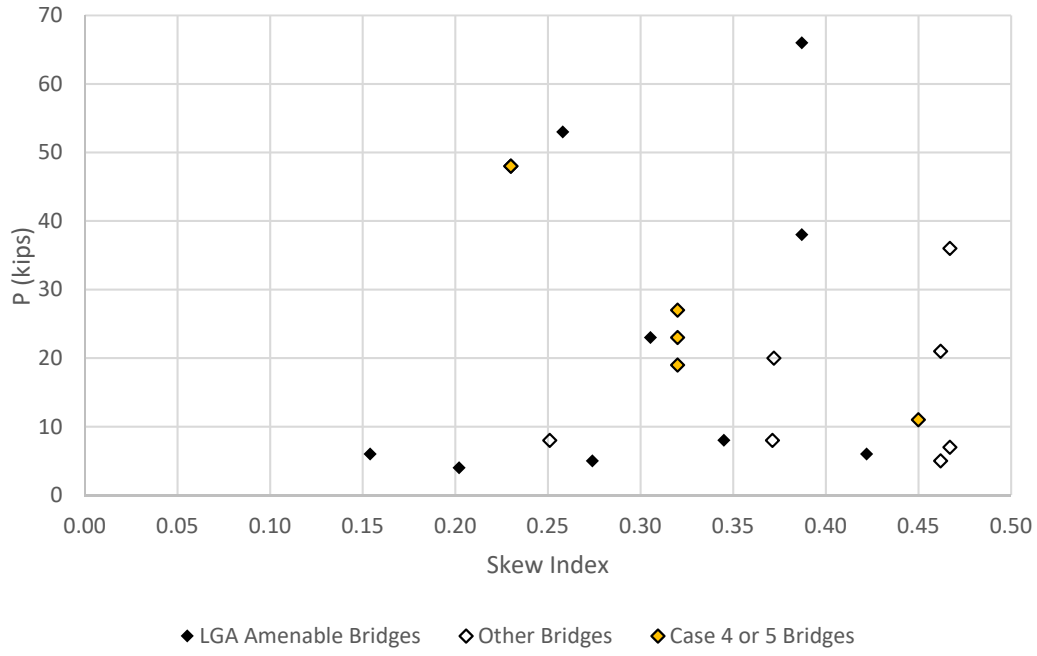

Figure 93. Maximum STR I tension forces in bottom chords of bearing line cross-frames at abutments and intermediate piers.

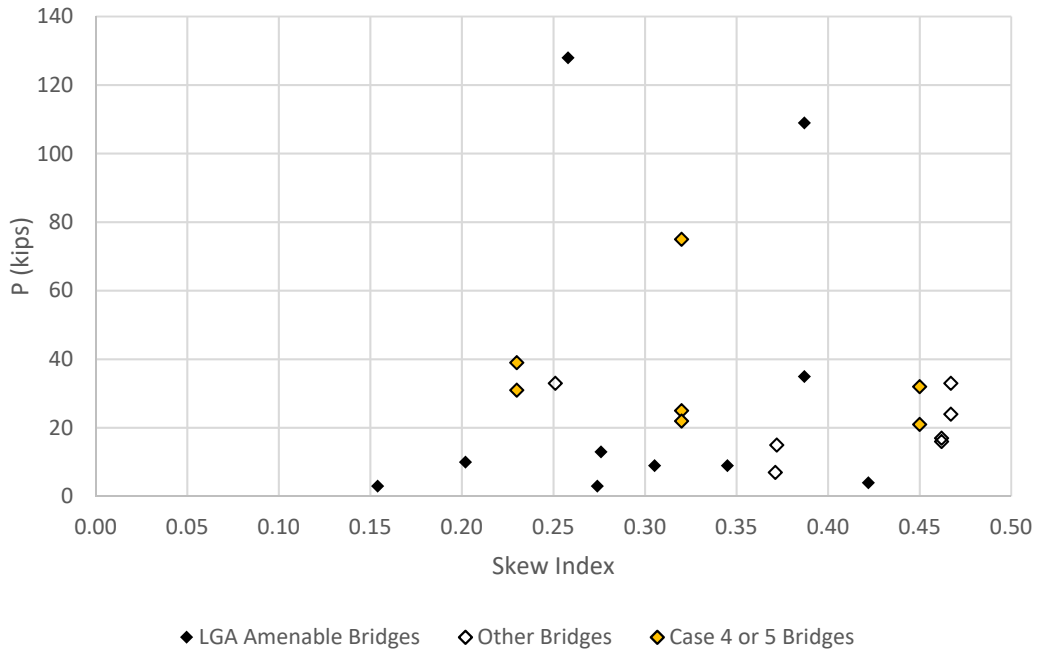

Figure 94. Maximum STR I compression forces in bottom chords of bearing line cross-frames at abutments and intermediate piers.

Table 56. Maximum tension and compression forces in diagonals of end and intermediate-pier cross-frames.

Bridge	Skew Index	STR I Max Tension (kip)	STR I Max Compression (kip)
1	0.46	22	25
2	0.46	23	26
3*	0.39	26	29
4*	0.39	15	18
5*	0.42	5	9
6*	0.35	10	11
7*	0.33	NA**	NA**
8*	0.27	4	6
9	0.47	13	14
10	0.47	21	21
11*	0.26	31	38
12	0.32	41	42
13	0.23	14	14
14	0.23	15	15
15	0.32	17	17
16	0.32	20	20
17*	0.28	0	0
18*	0.20	5	5
19	0.45	37	41
20	0.45	24	26
21*	0.15	4	5
22*	0.31	30	32
23	0.37	12	15
24	0.37	22	23
25	0.25	28	28
26*	0.15	NA**	NA**

* This bridge meets, or nearly meets, the requirements for application of the recommended LGA-based procedures for the bridge design.

** This bridge has solid-web diaphragms rather than cross-frames.

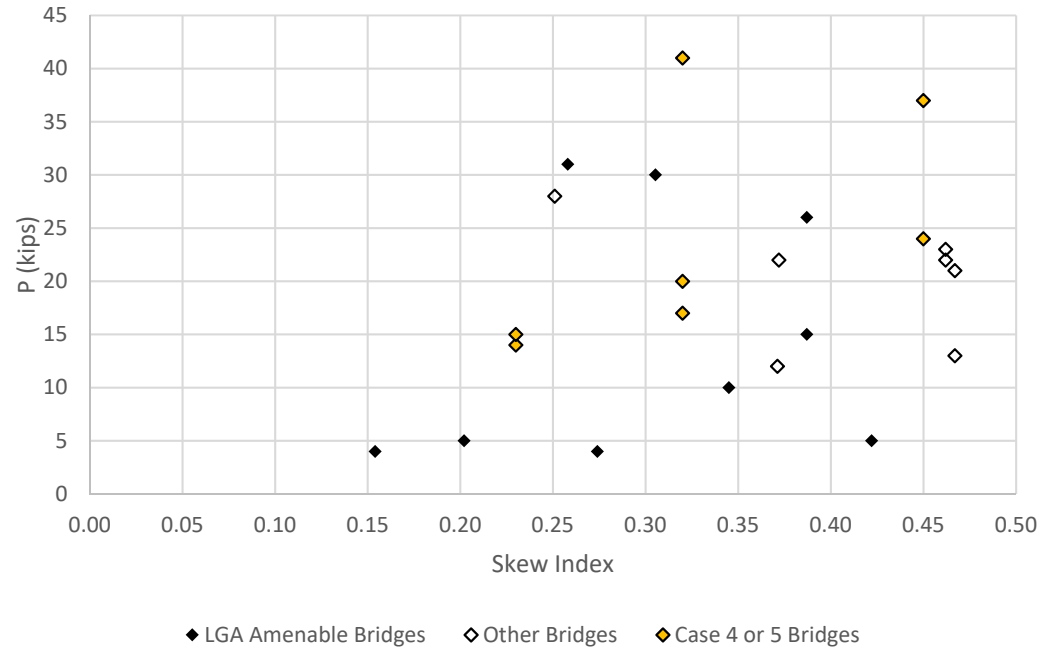

Figure 95. Maximum STR I tension forces in diagonals of end and intermediate-pier cross-frames.

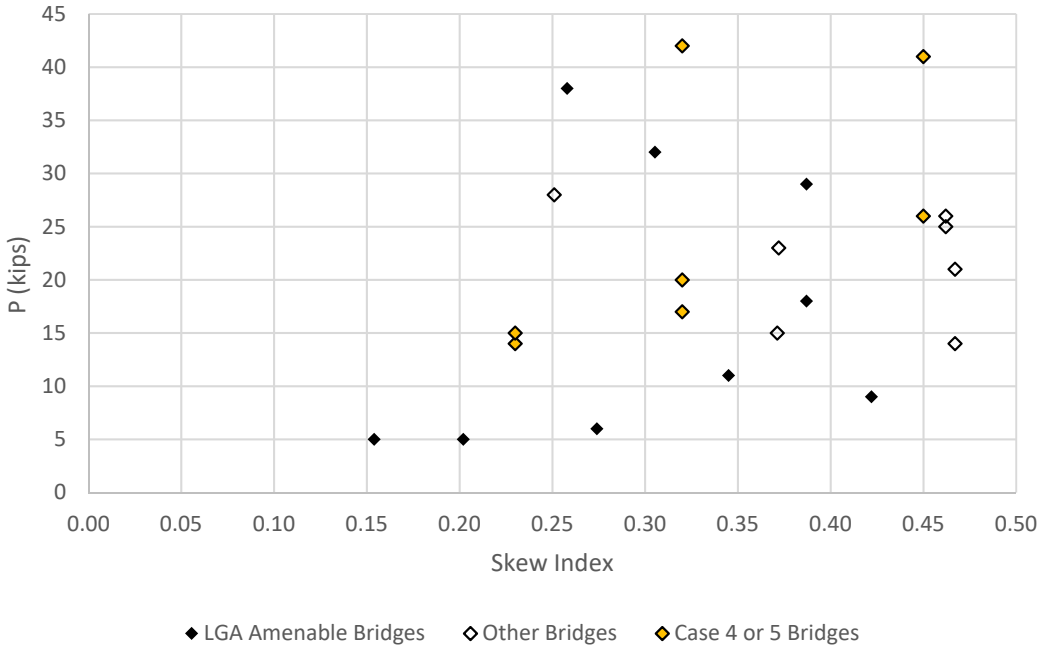

Figure 96. Maximum STR I compression forces in diagonals of end and intermediate-pier cross-frames.

Table 57. Maximum STR I tension and compression forces in top chords of end and intermediate-pier cross-frames.

Bridge	Skew Index	STR I Max Tension (kip)	STR I Max Compression (kip)
1	0.46	23	20
2	0.46	26	20
3*	0.39	29	44
4*	0.39	27	40
5*	0.42	29	26
6*	0.35	15	17
7*	0.33	NA**	NA**
8*	0.27	23	15
9	0.47	0	23
10	0.47	22	17
11*	0.26	17	17
12	0.32	15	30
13	0.23	18	20
14	0.23	19	20
15	0.32	34	62
16	0.32	34	63
17*	0.28	19	38
18*	0.20	16	15
19	0.45	38	41
20	0.45	22	38
21*	0.15	18	16
22*	0.31	34	27
23	0.37	24	28
24	0.37	38	53
25	0.25	30	43
26*	0.15	NA**	NA**

* This bridge meets, or nearly meets, the requirements for application of the recommended LGA-based procedures for the bridge design.

** This bridge has solid-web diaphragms rather than cross-frames.

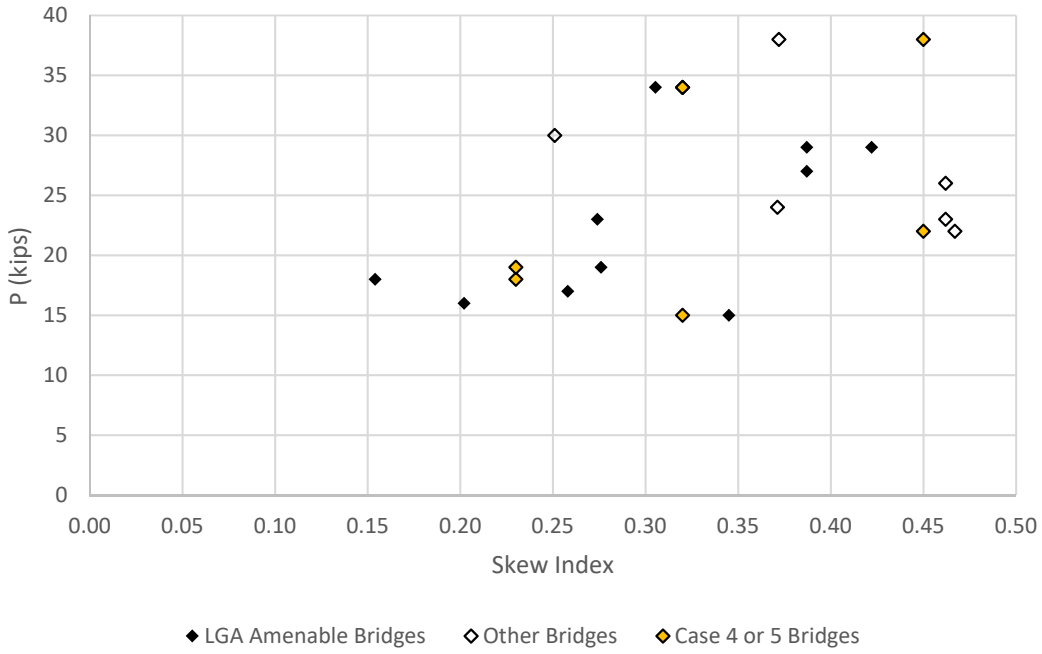

Figure 97. Maximum STR I tension forces in top chords of end and intermediate-pier cross-frames.

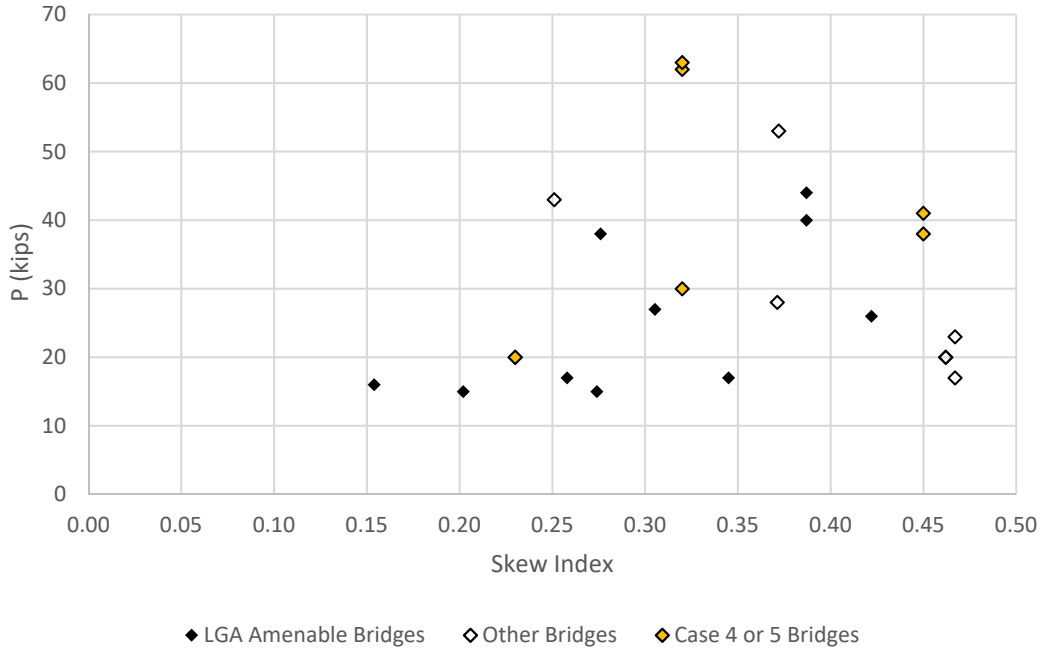

Figure 98. Maximum STR I compression forces in top chords of end and intermediate-pier cross-frames.

As noted in Section 5.4, some type of normalization with respect to the cross-frame and bridge parameters is needed to generalize the above data into useful design rules. Fortunately, the maximum cross-frame shear forces correlate to some extent with the corresponding girder maximum shear forces, and the maximum cross-frame chord level connection forces correlate to some extent with the corresponding girder maximum moments.

Table 58 and Figures 99 through 104 illustrate the correlation of the above Strength I cross-frame forces with the corresponding LGA girder maximum shears and moments for the intermediate cross-frame Cases 1i and 2i and the bearing line cross-frame Cases 1b and 2b listed in Table 14 of Section 5.1.5, and for cross-frame Cases 3i and 3b corresponding to the parallel skew bridges that do not satisfy the I_s and/or θ requirements for application of the recommended LGA procedures. The cross-frame case numbers 1, 2 and 3 are listed in the first column of the table. The data for the intermediate and the bearing line cross-frames are provided in the six rightmost columns of the table. The nonparallel skew and splayed girder bridges are discussed previously and are not considered in this data analysis, since none of the nonparallel skew and splayed girder bridges considered in this research would qualify for the recommended LGA calculations.

Figures 99 through 101 emphasize the fact that the bridges with Cross Frame Case 1i, where the intermediate cross-frames are framed with offsets and staggers greater than or equal to $4b_f$ throughout the span, generally have smaller cross-frame forces than the bridges with Cross Frame Case 2i, which use either contiguous intermediate cross-frames or offsets less than $4b_f$ within the span. Bridges 4, 8 and 18 are considered conservatively as having Case 1i arrangements, although the minimum offsets in Bridges 8 and 18 are actually only 3.15 and $3.23b_f$. Bridges 21, 26, 11, 17, 3, 5, 6 and 22 are considered as the bridges with Case 2i arrangements. Additional observations are as follows:

- The cross-frame force ratios for Cases 1i show larger scatter when plotted versus the skew index.
- The Case 1i arrangements are sufficiently bounded by maximum force ratios of 0.03 for the shear and the bottom chord level connection forces, and they are sufficiently bounded by the maximum ratio of 0.02 for the top chord level connection forces.
- The Case 2i arrangements are sufficiently bounded by maximum force ratios of 0.09 for the shear, 0.08 for the bottom chord level connections, and 0.04 for the top chord level connections.
- The cross-frame maximum force ratios generally have the most scatter, and the largest values for the calculated bounds for these ratios, for the Case 3 cross-frame framing arrangements. Again, these cases correspond to the parallel skew bridges that do not satisfy the I_s and/or θ requirements for application of the recommended LGA procedures.

Similar results are observed for the bearing line cross-frame force ratios with the exception that the bearing line cross-frame force ratios tend to be smaller. Fortunately, the bridges that have the Case 1i and 2i cross-frame framing arrangements also correspond to the 1b and 2b arrangements, with the exception of Bridge 21, which has a Case 1b arrangement for its bearing line cross-frames. This allows the presentation of all the data in the single Table 58. Tables for the other load cases and the SER II load combination are provided in Appendix 6.

Table 58. Bridge characteristics and STR I cross-frame force ratios for the parallel skew bridges studied.[†, §]

CF Case	Bridge Cat.	Bridge	I_s	$V_{max.g}$ (kip)	$M_{max.g}$ (kip-in)	$h_{cf.i}$ (in)	$h_{cf.b}$ (in)	Intermediate CFs			Bearing Line CFs		
								V Ratio	BC Ratio	TC Ratio	V ratio	BC Ratio	TC Ratio
1	2	8	0.27	692	250162	70.2	68.2	0.027	0.023	0.014	0.004	0.003	0.006
		18	0.2	584	326717	76.3	79.4	0.027	0.010	0.008	0.005	0.002	0.005
	3	4	0.39	776	353794	82.8	77	0.029	0.018	0.018	0.012	0.008	0.012
2	1	21	0.15	701	505223	97.8	97.8	0.073	0.024	0.013	0.005*	0.002*	0.004*
		26	0.15	273	42742	36.6	NA	0.045	0.074	0.028	NA	NA	NA
	2	11	0.26	590	205924	74.5	71	0.063	0.042	0.024	0.037	0.044	0.017
		17	0.28	556	305651	92.4	92.4	0.087	0.034	0.020	0.012	0.006	0.011
	3	3	0.39	778	354800	82.8	77	0.036	0.025	0.017	0.020	0.024	0.015
		5	0.42	404	152580	58.9	55.7	0.059	0.044	0.022	0.010	0.005	0.011
		6	0.35	351	90179	43.8	42.2	0.043	0.064	0.036	0.010	0.009	0.008
		22	0.31	615	277538	84.4	85.1	0.062	0.042	0.022	0.036	0.014	0.010
3	2	25	0.25	749	330473	86.2	86.2	0.122	0.062	0.024	0.019	0.015	0.011
	3	1	0.46	509	251174	60.2	62	0.222	0.078	0.054	0.024	0.009	0.006
		9	0.47	662	245100	69.5	69.5	0.088	0.061	0.035	0.009	0.007	0.010
		23	0.37	974	638636	88.2	95.8	0.104	0.051	0.020	0.008	0.003	0.004
		24	0.37	509	183740	71.1	72.4	0.067	0.045	0.023	0.026	0.015	0.021
		2	0.46	506	250566	60.2	62	0.143	0.049	0.035	0.025	0.011	0.006
		10	0.47	661	244508	69.5	69.5	0.073	0.042	0.025	0.014	0.010	0.012

† $V_{max.g}$ and $M_{max.g}$ are the maximum LGA STR I shears and moments, $h_{cf.i}$ and $h_{cf.b}$ are the distances between the mid-thickness of the bridge deck and the centroid of the cross-frame bottom chord for the intermediate and bearing line cross-frames, respectively, the V ratios are cross-frame force ratios corresponding to the shear, $V_{max.ICF}/V_{max.g}$ and $V_{.max.BCF}/V_{max.g}$, the BC ratios are the bottom chord level connections cross-frame force ratios $B_{max.cn.ICF}/(M_{.max.g}/h_{cf})$ and $B_{max.cn.BCF}/(M_{.max.g}/h_{cf})$, and the TC ratios are the top chord level connection force ratios ($T_{max.cn.ICF}/(M_{.max.g}/h_{cf})$ and $T_{max.cn.BCF}/(M_{.max.g}/h_{cf})$.

§ Bridge 7 is not included in Table 58 since it used all diaphragms than cross-frames.

* The bearing line cross-frames for Bridge 21 actually belong to Cross-Frame Case 1.

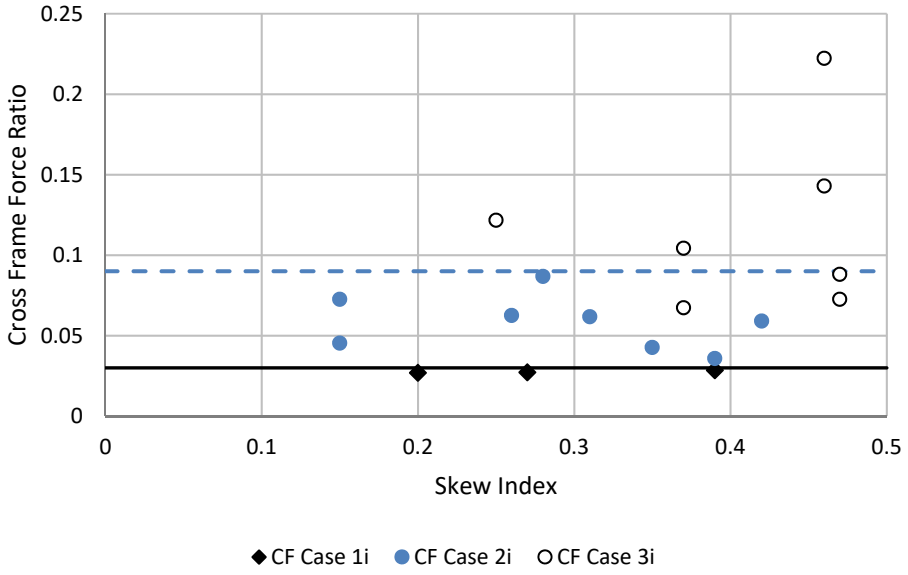

Figure 99. STR I shear force ratio $V_{max.ICF}/V_{max.g}$ for the intermediate cross-frames of the parallel skew bridges for cross-frame Cases 1i, 2i, and 3i versus the skew index.

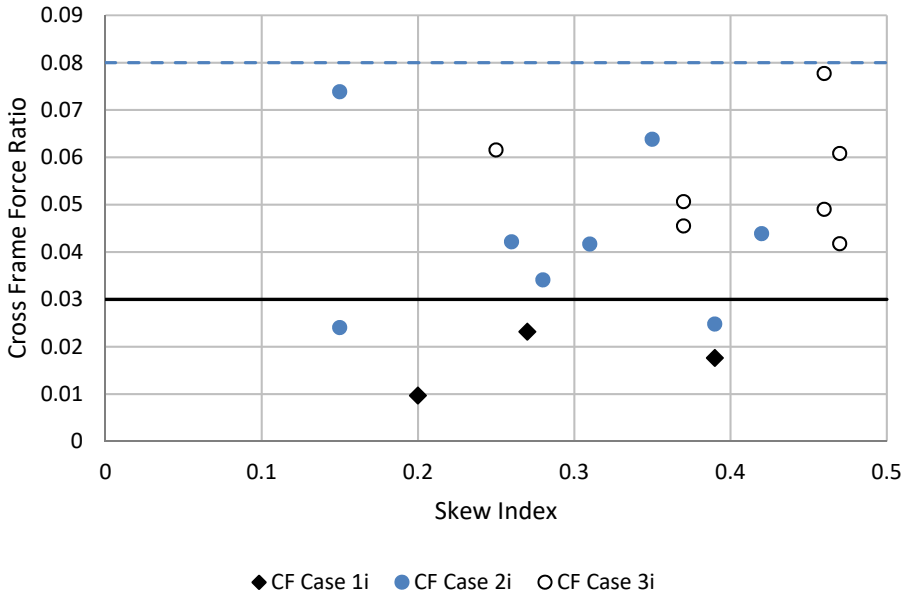

Figure 100. STR I bottom chord connection horizontal force ratio $B_{max.cn,ICF}/(M_{max.g}/h_{cf})$ for the intermediate cross-frames of the parallel skew bridges for cross-frame Cases 1i, 2i, and 3i versus the skew index.

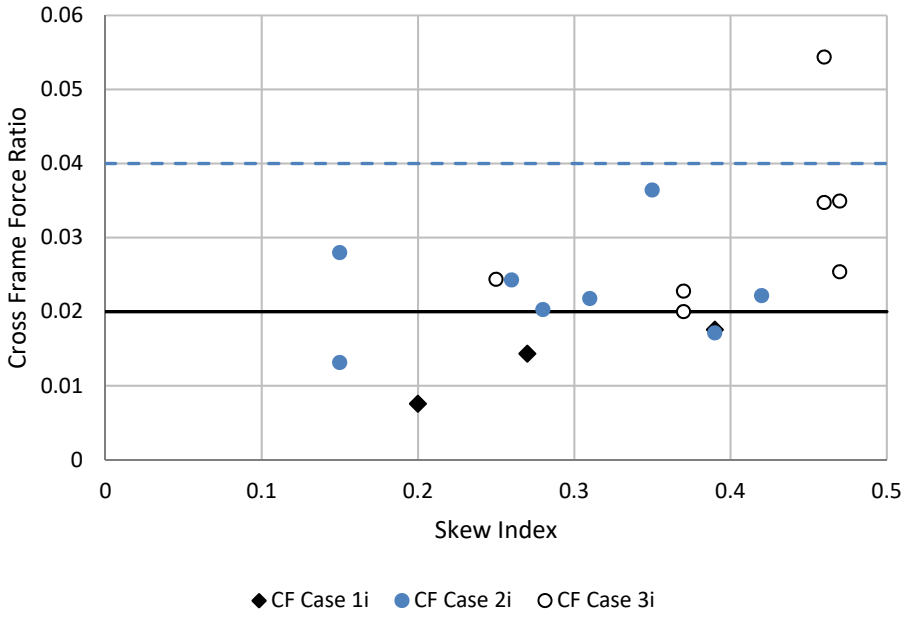

Figure 101. STR I top chord connection horizontal force ratio $T_{max.cn,ICF}/(M_{max.g}/h_{cf})$ for the intermediate cross-frames of the parallel skew bridges for cross-frame Cases 1i, 2i, and 3i versus the skew index.

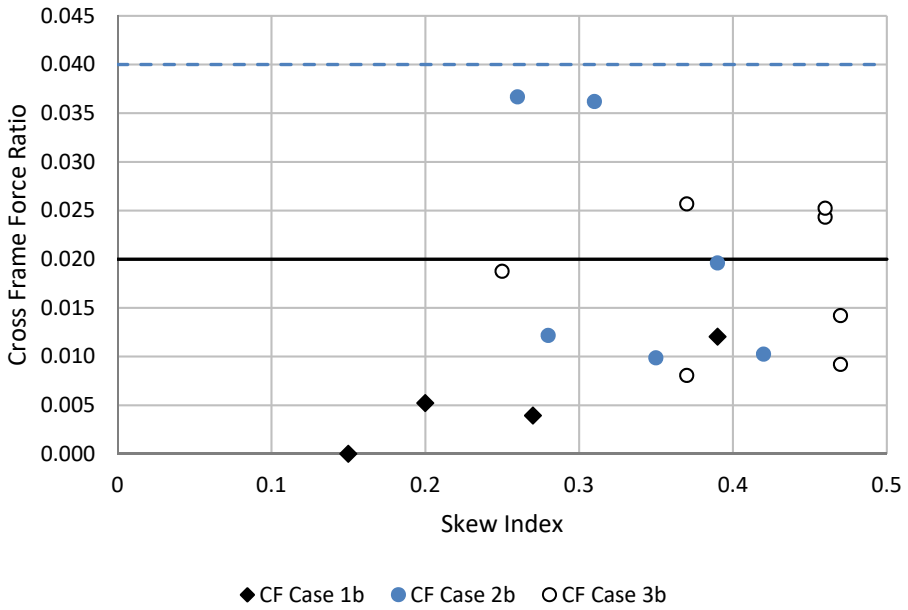

Figure 102. STR I shear force ratio $V_{max.BCF}/V_{max.g}$ for the bearing line cross-frames of the parallel skew bridges for cross-frame Cases 1b, 2b, and 3b versus the skew index.

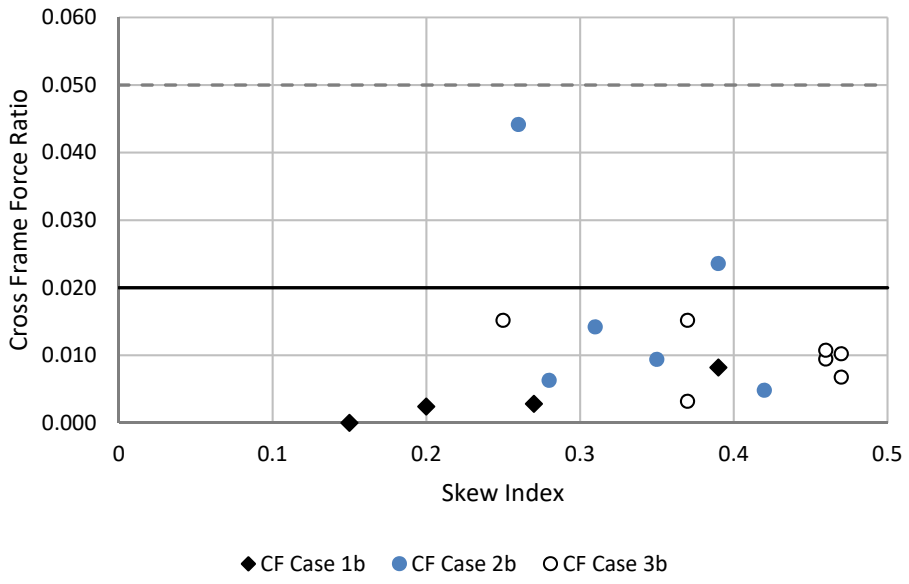

Figure 103. STR I bottom chord connection horizontal force ratio $B_{max.cn,BCF}/(M_{max.g}/h_{cf})$ for the bearing line cross-frames of the parallel skew bridges for cross-frame Cases 1b, 2b, and 3b versus the skew index.

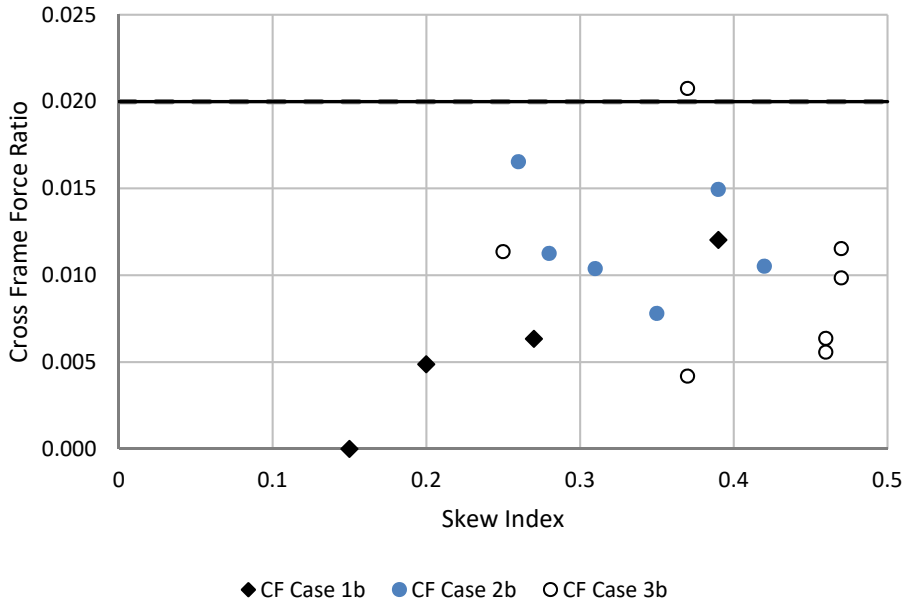

Figure 104. STR I top chord connection horizontal force ratio $T_{max.cn,BCF}/(M_{max.g}/h_{cf})$ for the bearing line cross-frames of the parallel skew bridges for cross-frame Cases 1b, 2b, and 3b versus the skew index.

All of the bounds on the Case 1i, 2i, 1b and 2b cross-frame forces, which are plotted as the horizontal lines in Figures 99 through 104, are reflected as the values in the STR I column of Table 14 in Section 5.1.5. Similar data analyses are performed for the DC1 (i.e., steel dead load and noncomposite concrete dead load), DC2 (rail load), DW (future wearing surface), HL-93 live load maximum and minimum force envelopes, and the fatigue live load range cross-frame forces and force ratios. These data are reflected in the other columns of Table 14 in Section 5.1.5. Tables containing the cross-frame force ratios, similar to Table 57, are shown in Appendix 6.

It should be noted that the cross-frame fatigue force ranges determined in this study are based on the full application of the AASHTO fatigue live load model to the bridge system. AASHTO (2017) Article C6.6.1.2.1 indicates that for cross-frames and diaphragms, "… the effect of positioning the fatigue truck in two different transverse positions located directly over the adjacent connected girders… usually creates the largest range of stress or torque in these bracing members. There is an extremely low probability of the truck being located in these two critical relative transverse positions over millions of cycles. Also, field observation has not indicated a significant problem with the details on these members caused by load-induced fatigue or fatigue due to cross-section distortion. Therefore, it is recommended that the fatigue truck be positioned to determine the maximum range of stress or torque, as applicable, in these members as specified in Article 3.6.1.4.3a, with the truck confined to one critical transverse position per each longitudinal position throughout the length of the bridge in the analysis." In other words, AASHTO (2017) Article C6.6.1.2.1 recommends that the fatigue truck should be considered only at one position transversely, specifically the position that maximizes the fatigue shear force range at a given cross-frame member, for every longitudinal position of the truck along the bridge. This recommendation requires postprocessing of the full fatigue live load data from the 3D FEA that is not readily accessible at the current time in CSiBridge (CSi, 2019). Furthermore, NCHRP 12-113 (NCHRP, 2019) is currently in progress with an intent to scientifically determine the specific cross-frame member force ranges that should be employed in design for fatigue. It is recommended that the results of NHCRP 12-113 should be evaluated regarding cross-frame member fatigue design criteria when this information becomes available.

5.5.12 Evaluation of AASHTO Fascia Girder Live Load Distribution Factors Considering Potential Conservatism of the Lever Rule and Rigid Cross-section Analysis Calculations

A rigid cross-section analysis (RCA) is required in the AASHTO (2017) procedures for the determination of fascia girder live load distribution factor (LLDF), with an intent to avoid potential unconservative LLDF estimates in cases where the bridge girders are "well connected" by cross-frames across the bridge width. Furthermore, for single-lane live load cases, AASHTO (2017) uses the lever rule for calculation of the base moment and shear LLDF on the exterior girders along with also performing the RCA. AASHTO requires that the larger of the lever rule and RCA values should be used in designing for single-lane loadings, such as the fatigue loading case. In addition, when considering the general HL-93 moment and shear demands on the exterior girders, the maximum of the single- and multiple-lane LLDF is employed for design since the bridge must conceptually accommodate both single- and multiple-lane loading.

Figure 105 shows the results for the fascia girder fatigue moment LLDF obtained from the single lane lever rule (no multiple presence factor), and the rigid cross-section analysis (RCA).

These results are presented as $1/\rho_{max}$ values, that is, the LGA results divided by the 3D FEA LLDF results. As noted above, for the single-lane case, AASHTO LRFD requires the use of the lever rule for the base exterior girder moment LLDF calculation. The lever rule tends give a conservative representation of the true live load distribution to the exterior girders. This is due to the assumption that the deck is simply supported at the first interior girder, that is, the assumption there is no continuity of the deck over the top of the first interior girder. As such, the lever rule often governs relative to RCA. It should be noted that $1/\rho_{max}$ values larger than 1.0 in Figure 105 indicate that LGA results are accurate to conservative relative to the 3D FEA calculations. In Figure 105, the $1/\rho_{max}$ values are increased due to the inclusion of the RCA solution only for Bridges 13 and 14, meaning the RCA solution governs only for these bridges. The reason Bridges 13 and 14 have a more critical RCA result is because their bridge cross-sections are relatively narrow, making them more sensitive to overall torsional "overturning" moments due to off-center positioning of the live load.

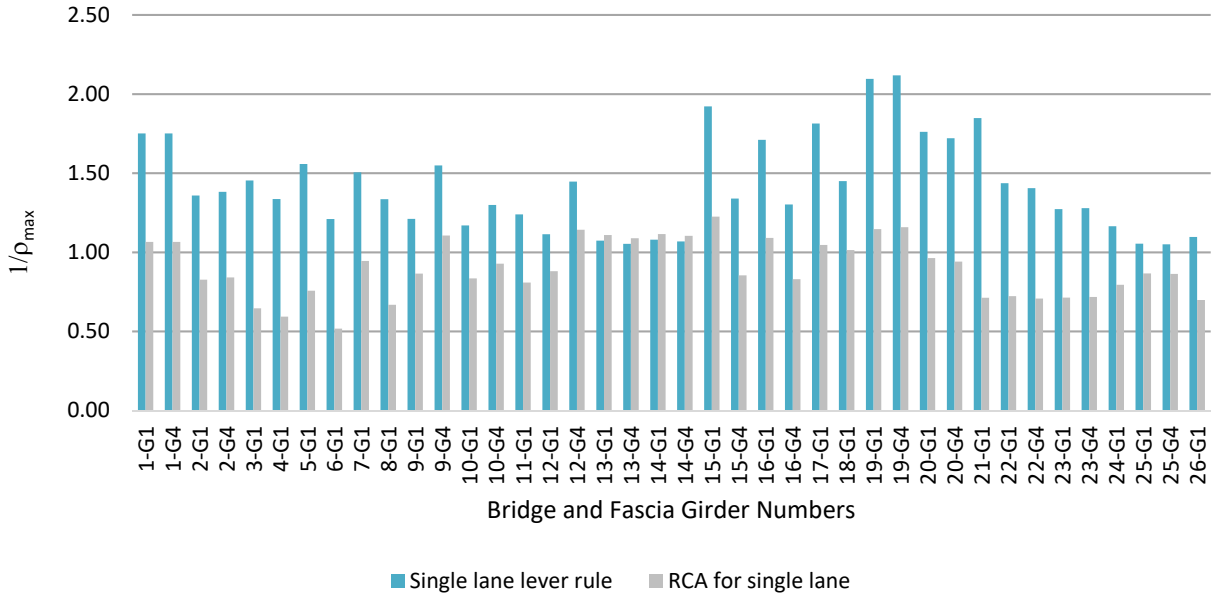

Figure 105. Ratios of the LGA results for the fatigue moment LLDF for the fascia girders from the single-lane lever rule (no multiple presence factor), and rigid cross-section analysis to the fatigue moment LLDF value determined from 3D FEA.

It should be noted that the 3D FEA moment LLDF is taken as the fraction of the AASHTO HL-93 load that needs to be applied to the LGA model to match the maximum positive 3D FEA live load moment envelope value for the simple-span bridges, and it is taken as the fraction of the AASHTO HL-93 load that needs to be applied to the LGA model to match the maximum negative 3D FEA live load moment envelope value for the continuous-span bridges. The actual 3D FEA moment LLDF varies along the span. This is one of the complexities of addressing "true" versus estimated LLDFs. Detailed plots of bridge girder LLDFs from the 3D FEA calculations are provided in Appendix 3.

The conservatism associated with the single lane lever rule LLDF calculations can be seen from the fact that the average $1/\rho_{max}$ value associated with the calculations is 1.417. The $1/\rho_{max}$

values range from 1.050 to 2.096 and the coefficient of variation is 0.205. It may be possible to modify the lever rule procedure to reduce the conservatism of the exterior girder LLDFs for these cases. However, modification of the AASHTO LLDF procedures is beyond the scope of this research.

Figure 106 shows the results for the governing single or multiple-lane moment LLDF for the fascia girders for the bridges studied in this research, which includes the multiple presence factor. The governing LLDF is considered as the maximum of the single- and multiple-lane LLDF obtained from: 1) the empirical equation for multiple lanes, 2) the single lane lever rule and, 3) the larger of single and multiple-lane RCA results. Figure 106 presents separate results for the three LLDFs described above as $1/\rho_{max}$ values, that is, the LGA divided by the 3D FEA result. The 3D FEA LLDF are calculated as discussed above.

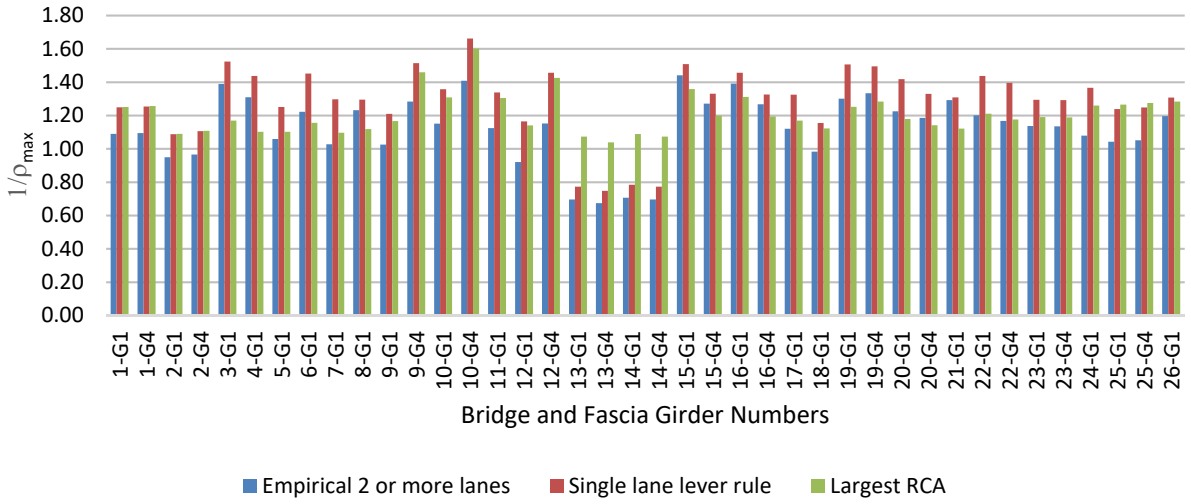

Figure 106. Ratios of the LGA results for the moment LLDF for the fascia girders from the AASHTO empirical equations (multiple lane, including the multiple presence factor), the single-lane lever rule, and rigid cross-section analysis to the corresponding moment LLDF value determined from 3D FEA.

One can observe that the $1/\rho_{max}$ values for the single lane lever rule in Figure 106 are the largest for most of the bridges. RCA is observed to govern for the fascia girders of Bridges 13, 14 and 25. The LLDF values obtained from the empirical equation and the single lane lever rule calculations are unconservative for Bridges 13 and 14, whereas the RCA values are accurate to conservative. Bridges 13 and 14 are relatively narrow nonparallel skew bridges. Bridge 25 is a relatively narrow parallel skew bridge. In this case, although the RCA and the single lane lever rule LLFDs are larger than the LLDF obtained from the empirical equation, the empirical LLDF is the most accurate.

Figure 107 shows the $1/\rho_{max}$ result for the fascia girder fatigue shear LLDF obtained from the single lane lever rule (no multiple presence factor, and including the AASHTO skew correction factor), and RCA. It should be noted that the 3D FEA multiple-lane HL-93 live load calculation includes the consideration of a single lane up the maximum number of lanes that can be placed on a given bridge, with the lanes shifted as necessary to produce the maximum load effects as

explained in Section 4.2.5. One can observe from this figure that the $1/\rho_{max}$ values are reduced relative to Figure 105 for a large number of the bridges, and that the RCA results govern relative to lever rule application for a single lane for Bridges 13 and 14. Bridges 13 and 14, as explained earlier, are relatively narrow nonparallel skew bridges, where the worst-case positioning of the live load is not particularly damning according to the lever rule. It can be observed that the RCA result is still necessary to ensure adequate conservatism of the LGA calculations for the narrow nonparallel skew Bridges 13 and 14.

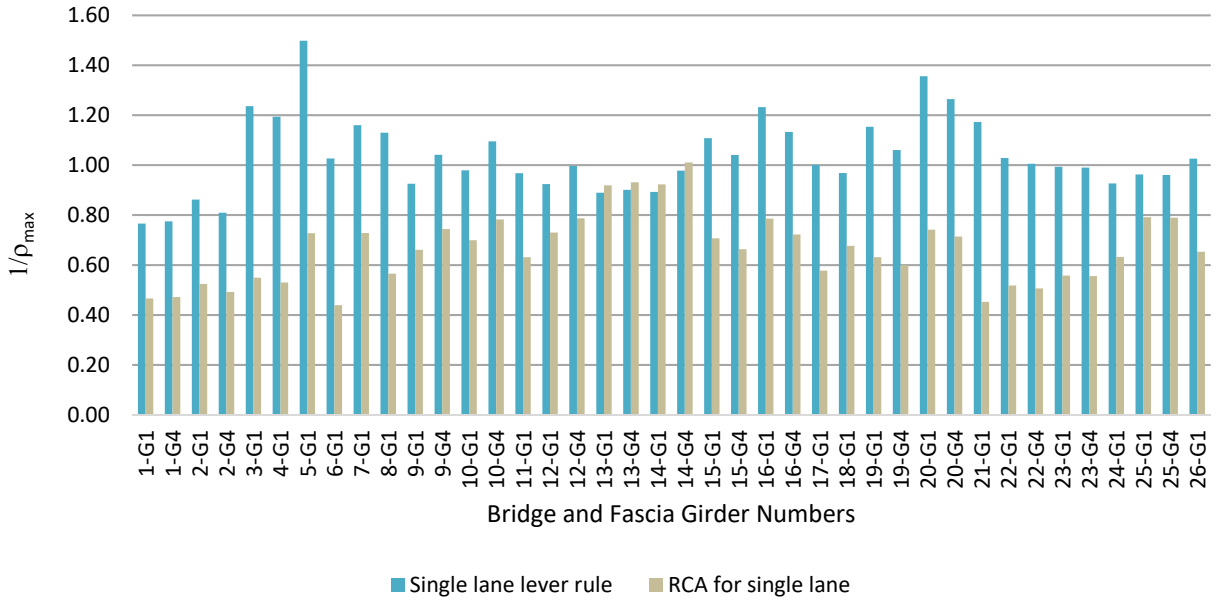

Figure 107**. Ratios of the LGA results for the fatigue shear LLDF for the fascia girders from the single-lane lever rule (no multiple presence factor, and including the AASHTO LGA skew correction factor), and rigid cross-section analysis to the fatigue shear LLDF value determined from 3D FEA.**

Similar to the 3D FEA moment LLDF, the 3D FEA shear LLDF is taken as the fraction of the live load (the fatigue live load in the case of Figure 108) that needs to be applied to the LGA model to match the maximum (absolute value) 3D FEA live load shear envelope value for both simple-span and continuous-span bridges. The actual 3D FEA shear LLDF varies along the span. Furthermore, it should be noted that the AASHTO LLDF estimates are taken from the span corresponding to the maximum 3D FEA live load shear envelope value. Also, it should be noted that the AASHTO LLDF estimates shown here include the AASHTO skew correction factor. Detailed plots of bridge girder LLDFs from the 3D FEA calculations are provided in Appendix 3.

It can be observed that a number of the $1/\rho_{max}$ values obtained from the single lane lever rule calculations in Figure 107 are larger than 1.0. The $1/\rho_{max}$ value range from 0.77 to 1.502 with a mean of 1.04 and the co-efficient for variation is 0.146. The $1/\rho_{max}$ values are unconservative for the fascia girders of Bridges 1, 2, 9, 10, 11, 12, 13, 14, 18, 23, 24 and 25. While many of the bridges where this is the case either violate the requirements for bridge Categories 1 through 3 defined in Section 5.1, or are nonparallel skew or splayed girder bridges (Categories 4 and 5

defined in Section 5.1), Bridges 11, 18 and 25 belong to Category 2. RCA is more unconservative compared to the single lane lever rule calculations for the fatigue shear LLDF. The $1/\rho_{max}$ value range from 0.441 to 1.015 with a mean of 0.667 and the co-efficient for variation is 0.213. Therefore, the AASHTO shear LLDF procedures are unconservative relative to 3D FEA for a large number of the bridges studied, it appears that some other factor would have to be included to provide for sufficiently accurate LLDF values.

Similar to Figure 106, Figure 108 shows the results for the governing single or multiple-lane shear LLDF for the fascia girders for the bridges studied in this research, which includes the multiple presence factor but does not include the skew correction factor. The governing LLDF is considered as the maximum of the single- and multiple-lane LLDF obtained from: 1) the empirical equation for multiple lanes, 2) the single lane lever rule and, 3) the larger of single and multiple-lane RCA. Figure 108 presents separate results for the three LLDFs described above as $1/\rho_{max}$ values, that is, the LGA divided by the 3D FEA result.

Again, one can observe that the $1/\rho_{max}$ values for the single lane lever rule in **Error! Reference source not found.** are the largest for most of the bridges. RCA is the largest for the fascia girders of Bridges 13, 14 and 25. However, the single lane lever rule are more accurate than RCA for Bridges 13 and 14, whereas RCA is accurate to conservative for the fascia girders of Bridge 12.

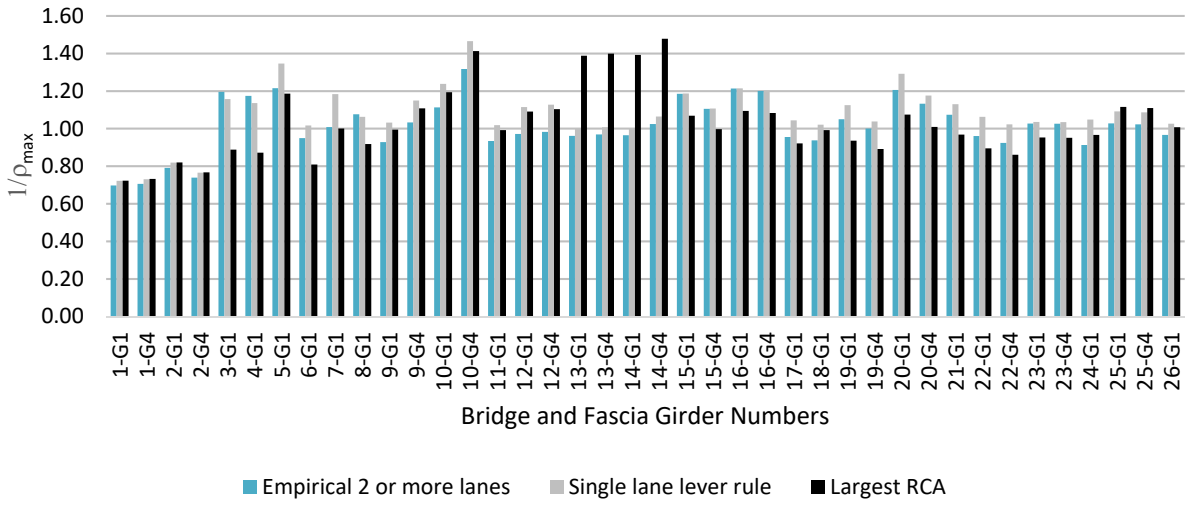

Figure 108. Ratios of the LGA results for the shear LLDF for the fascia girders from the AASHTO empirical equations (multiple lane, including the multiple presence factor, but not including the AASHTO LGA skew correction factor for shear), the single-lane lever rule, and rigid cross-section analysis to the corresponding shear LLDF value determined from 3D FEA.

Although Figures 106 and 108 show evidence of significant potential for removing the repetitive and tedious calculations associated with the RCA, while making the multiple-lane LLDF less conservative, modification of the AASHTO LLDF calculations is outside of the scope of this research. It should be noted that the AASHTO moment LLDF values are already

significantly less conservative than the values obtained from the overly-simple LLDF equation in the Standard Specifications (AASHTO, 2002). The RCA solution is necessary to avoid significant unconservative error due to the large torsional "overturning" effects on the narrow nonparallel skew Bridges 13 and 14.

All of the $1/\rho_{max}$ values obtained from the three different LLDF calculations for the fascia girders of Bridges 1 and 2 in Figures 106 and 108 are less than 1.0. It should be noted that Bridges 1 and 2 have a combination of both large I_s values that violate the targeted limits for Case 3 as well as large θ values that nearly violate the targeted limits for Case 3. It is apparent that once we are reaching these extremes of the skew, the LGA procedures can be limited in their ability to capture the live load shear forces generated at the obtuse corners of the spans.

There is indeed potential for improvement of the AASHTO shear LLDF procedures. However, the conservatism of these LLDFs is not unreasonable for many of the bridges considered. Furthermore, the solutions rely on the conservatism of the LLDFs to compensate for moderate unconservatism in the LGA calculation of the dead load responses within the overall LGA recommendations from this research. None of the current AASHTO (2017) calculations are sufficient to predict the large 3D FEA LLDF determined at the obtuse corners of the spans for the more severely skewed Bridge 1 and 2 geometries.

5.5.13 Girder Live Load Deflections

For optional live load deflection evaluation, AASHTO LRFD Specification (AASHTO, 2017) Article 3.6.1.3.2 states:

"If the owner invokes the optional live load deflection criteria specified in Article 2.5.6.2, the deflection should be taken as the larger of:

1. That resulting from the design truck alone, or
2. That resulting from 25% of the design truck taken together with the design lane load"

Further, the AASHTO LRFD Specification (AASHTO, 2017) Article 2.5.2.6.2 states:

1. "… the vehicular load shall include the dynamic allowance."
2. "When investigating the maximum absolute deflection for straight girder systems, all design lanes should be loaded, and all supporting components should be assumed to deflect equally."
3. "For composite design, the stiffness of the design cross-section used for the determination of deflection should include the entire width of the roadway and the structurally continuous portion of the railings, sidewalks and median barriers." (It is assumed that none of these components are structurally continuous in this research.)
4. "For straight girder systems, the composite bending stiffness may be taken as the stiffness determined as specified above, divided by the number of girders."
5. "The live load portion of Load Combination Service I of Table 3.4.1-1 should be used including the dynamic load allowance, IM." Basically a live load multiplier of 1.0 times 1.33 should be used. In addition, the reference to Table 3.4.1-1 indirectly brings in the

consideration of the multiple presence factor, since Article 3.4.1 requires the use of the multiple presence factor along with the factors in Table 3.4.1-1.

6. "The live load shall be taken from Article 3.6.1.3.2." This brings in the above requirement of 25 % of the HL-93 truck with the lane load, or the HL-93 truck alone.

In summary, all of the above, combined strictly with the assumption of equal stiffnesses of the bridge girders, results in an effective live load distribution factor (LLDF) of:

$$DF_{\Delta(LGA)} = m\left(\frac{N_L}{N_g}\right) \tag{30}$$

applied with 25 % of the HL-93 truck plus the lane load, or the HL-93 truck alone, since these loads are specified to be applied in all of the lanes on the bridge, where

m is the multiple presence factor,

N_L is the maximum number of lanes that can be accommodated on the bridge, and

N_g is the number of girders in the bridge.

Therefore, the base LGA live load displacements calculated in this work are obtained as the larger of the displacements from the application of 25 % of the HL-93 truck plus the lane load, and the HL-93 truck alone, using the above LLDF.

It can be argued that for curved and/or skewed bridges, the above idealizations may not be appropriate (Grubb et al., 2010). This is because of the differential displacements that occur across the width of the bridge structure under the live load. Given these differential displacements, the deflections associated with conditions where less than all the lanes are loaded on the bridge may be appropriate to consider.

In the 3D FEA solutions conducted in this research, the live load displacements envelopes are obtained by positioning the above live loads in one, two, three, up through the total number of lanes accommodated by the bridge.

Table 59 summarizes the various underlying values and calculations pertaining to the calculation of maximum girder live load displacements by the above LGA procedures and by 3D FEA, leading to the calculation of ρ_{max} from the above LGA procedures, and ρ_{maxrec} for a recommended modification to these procedures observed to be more appropriate for skewed I-girder bridges.

Upon comparison to the maximum LGA displacements obtained using the above assumptions that all the lanes are loaded, all the girders have equal stiffness, and the loads are distributed equally to all the girders, the maximum 3D FEA live load displacements are always greater than the maximum LGA displacements. This is because of the sensitivities of skewed bridges to loadings that are not necessarily centered on the bridge cross-section. The variable DF_{3DFEA} in Table 59 represents a distribution factor calculated from the 3D FEA solution for the

maximum displacements. This distribution factor is compared to AASHTO LLDF for bending moment, $DF_{M(LGA)}$ and to the above distribution factor from Equation 30.

Figure 109 plots the ρ_{max} values for all the bridges studied versus their skew index. The ρ_{max} values range from 1.04 to 1.93. Figure 110 shows ρ_{maxrec} versus the bridge skew indices. These values range from 0.74 to 1.05 for the full suite of bridges considered in this research. For the LGA amenable bridges, ρ_{maxrec} varies from 0.80 to 1.05. The AASHTO LLDF for bending moment gives an accurate to conservative prediction of the 3D FEA displacements, and provides a closer correlation with the 3D FEA results than the distribution factor $DF_{\Delta(LGA)}$.

Table 59. Comparison of maximum live load displacements obtained from LGA and 3D FEA for exterior girders of bridges having parallel or near-parallel skew.

Bridge	Skew Index	Girder	N_L	N_g	m	$DF_{\Delta(LGA)}$	Δ_{3DFEA}	Δ_{LGA}	$\Delta_{LGA}/\Delta_{3DFEA}$	ρ_{max}	$DF_{\Delta(3DFEA)}$	$DF_{M(LGA)}$	ρ_{maxrec}
1	0.46	G1	7	11	0.65	0.41	2.40	2.31	0.96	1.04	0.43	0.58	0.74
1	0.46	G4	7	11	0.65	0.41	2.40	2.04	0.85	1.18	0.49	0.58	0.84
2	0.46	G1	7	11	0.65	0.41	2.71	2.36	0.87	1.15	0.47	0.58	0.81
2	0.46	G4	7	11	0.65	0.41	2.70	2.08	0.77	1.30	0.54	0.58	0.92
3*	0.39	G1	8	8	0.65	0.65	1.50	1.07	0.71	1.40	0.91	1.11	0.82
4*	0.39	G1	8	8	0.65	0.65	1.60	1.07	0.67	1.50	0.97	1.11	0.88
5*	0.42	G1	9	12	0.65	0.49	1.45	0.99	0.68	1.47	0.72	0.83	0.86
6*	0.35	G1	9	14	0.65	0.42	1.63	1.06	0.65	1.54	0.64	0.68	0.95
7*	0.33	G1	9	12	0.65	0.49	1.28	0.68	0.53	1.90	0.93	0.94	0.98
8*	0.27	G1	8	8	0.65	0.65	1.77	1.28	0.72	1.39	0.90	0.96	0.94
9	0.47	G1	4	6	0.65	0.43	1.94	1.25	0.64	1.56	0.67	0.80	0.84
9	0.47	G4	4	6	0.65	0.43	1.76	1.25	0.71	1.41	0.61	0.80	0.76
10	0.47	G1	4	6	0.65	0.43	1.88	1.25	0.67	1.50	0.65	0.80	0.81
10	0.47	G4	4	6	0.65	0.43	1.77	1.25	0.71	1.42	0.61	0.80	0.77
11*	0.26	G1	5	7	0.65	0.46	1.78	1.24	0.70	1.44	0.67	0.79	0.85
17*	0.28	G1	5	7	0.65	0.46	1.71	1.08	0.63	1.58	0.74	0.91	0.80
18*	0.20	G1	4	6	0.65	0.43	2.10	1.21	0.57	1.74	0.75	0.82	0.92
21*	0.15	G1	11	12	0.65	0.60	1.92	1.58	0.83	1.21	0.72	0.89	0.81
22*	0.31	G1	7	10	0.65	0.46	1.57	1.07	0.68	1.46	0.67	0.78	0.85
22*	0.31	G4	7	10	0.65	0.46	1.77	1.25	0.71	1.41	0.64	0.78	0.83
23	0.37	G1	6	7	0.65	0.56	2.45	1.88	0.77	1.30	0.73	0.95	0.77
23	0.37	G4	6	7	0.65	0.56	2.45	1.88	0.77	1.30	0.73	0.95	0.77
24	0.37	G1	4	7	0.65	0.37	1.47	0.86	0.59	1.70	0.63	0.75	0.85
25	0.25	G1	3	4	0.85	0.64	1.74	1.38	0.79	1.26	0.81	0.94	0.86
25	0.25	G4	3	4	0.85	0.64	1.71	1.38	0.81	1.24	0.79	0.94	0.84
26*	0.15	G1	5	10	0.65	0.33	0.96	0.50	0.52	1.93	0.63	0.60	1.05

* This bridge meets, or nearly meets, the requirements for application of the recommended LGA-based procedures for the bridge design.

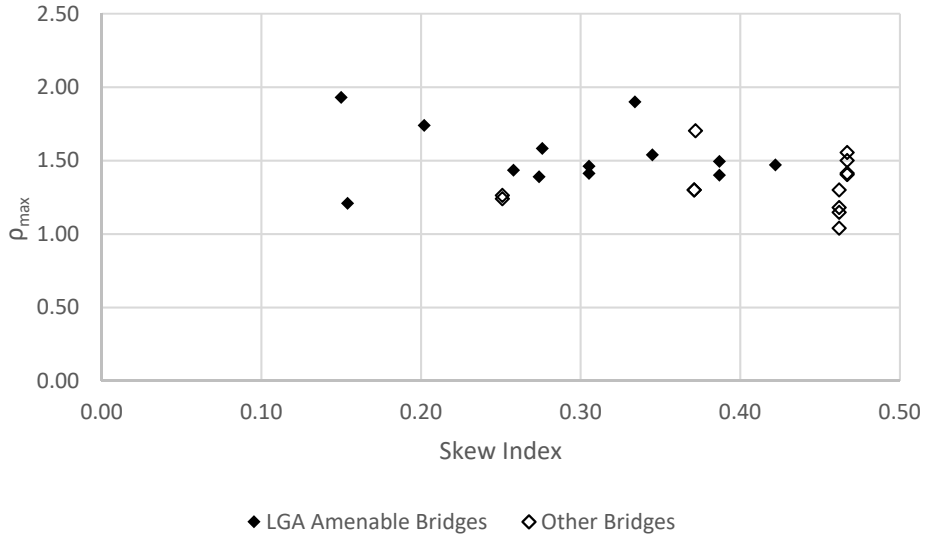

Figure 109. ρ_{max} values for live load vertical displacements for bridges having parallel or near-parallel skew, using AASHTO recommended distribution factor.

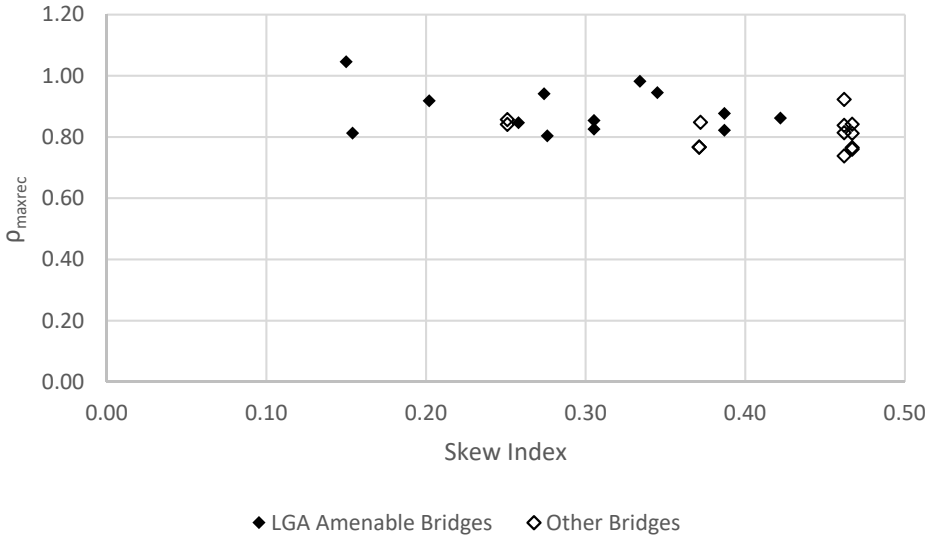

Figure 110. ρ_{max} values for live load vertical displacements for bridges having parallel or near-parallel skew, using recommended application of the bending moment LLDF.

6. CONCLUSIONS

6.1 Satisfaction of Research Objectives

The objective of this research is to understand more fully the behavior of steel I-girder bridges with skew indices approaching 0.3, and to determine when, for skewed bridges having skew indices approaching 0.3, Line Girder Analysis (LGA) will yield results that are very similar to those obtained from more complex modeling. To achieve this, a parametric study was carried out for 26 bridges. Twenty of the bridges studied were selected from 57 bridges screened by FDOT from their inventory. Six bridges out of the 20 bridges that were expected to exhibit the largest skew effects were identified and selected for study using an alternative cross-frame arrangement aimed at minimizing transverse load path effects.

Section 5.1 summarizes the resulting recommended LGA-based calculation procedures for straight skewed I-girder bridges with small to moderate skew. The LGA-based calculations involve equal distribution of dead loads and use of the AASHTO live load distribution factors (LLDF) for calculation of live load effects. Streamlined estimates are provided for coarse upper-bound girder flange lateral bending stresses and cross-frame and diaphragm forces that allow for the consideration of these force requirements when LGA is employed for the design of the girders.

The assumed load distribution to the girders influences the accuracy of the LGA. Additionally, the behavior of skewed bridges is influenced by numerous structural attributes. A few of the most pertinent qualitative aspects of straight skewed girder bridge structural behavior are as follows:

1. The Strength I (STR I) bending moments predicted by LGA are accurate to conservative for all girders of all bridges compared to 3D FEA. This is because of the conservatism associated with the AASHTO LLDFs used in LGA. Hence, although LGA under-predicts the CDL bending moments somewhat in some girders for a number of bridges (due to the assumption of equal dead load distribution to the girders), the CDL moments typically being the largest contributor to the dead load effects, the overall STR I bending moment predictions are conservative compared to 3D FEA.
2. The presence of cross-frames in skewed bridges tends to engage all the girders and thus the CDL and DW internal load effects tend to be approximately equal on all the girders in parallel skew bridges. Hence, the assumption of equal distribution of CDL and DW loads to all the girders in the bridge cross-section is observed to be a reasonable one. However, for barrier rails, the exterior girders attract most of the load. In very wide bridges, the barrier rail load tends to induce an upward load effect on the central interior girders. Fortunately, typical barrier rail loads are not large enough to where this behavior needs to be addressed explicitly in the design. The bridge studies conducted in this research assumed 36 inch single-slope rails weighing 430 plf at the edges of the bridge deck. In the judgment of the research team, the equal distribution assumption should be sufficient with concentrated loads up to 625 plf, representing somewhat larger barrier rails.
3. The accuracy of LGA estimates of the TDL (SDLF) displacements depends critically on the accuracy of LGA for prediction of the dead load responses. Significant differences between

the LGA and 3D FEA predictions are observed in a number of bridges. The maximum differences are observed in the exterior girders.

4. The cross-frame framing arrangement significantly influences the behavior of straight skewed bridges. Some of the observed qualitative effects are:
   a) Comparison of a contiguous and an alternative staggered cross-frame arrangement shows that exterior girders attract more load when the cross-frame framing arrangement is contiguous.
   b) For contiguous cross-frame framing arrangements in parallel skew bridges with the cross-frames framed perpendicular to the girders, the maximum flange lateral bending stress is generally found to occur at the intermediate cross-frame locations closest to the bearing lines. This lateral bending is associated with the transfer of torsion in the associated girder from the position on the cross-frame line closest to the end bearings to the end bearing line. On the other hand, if a staggered cross-frame framing arrangement is employed, the maximum flange lateral bending stress in typically observed in the central interior girder near the center of the bridge span. This behavior is due to "breaking up" of the load path associated with the beam action along the short diagonal direction in a parallel skew bridge, requiring transfer of these bending actions from cross-frame to cross-frame via flange lateral bending in the girders near the mid-spans and mid-width of the bridge.
   c) The mitigation of a stiff transverse load path achieved by using a staggered cross-frame framing arrangement reduces the transfer of load to the obtuse corners, in turn reducing the vertical reactions and girder end shears at these locations.
5. Nonparallel skew bridges typically behave very differently from parallel skew bridges; the range of behaviors for these types of bridges can vary widely as a function of the differences in magnitude and sign of the skew angles at the ends of the spans.

Hence, it can be concluded that the key variables affecting the behavior of straight I-girder skewed bridges are:

1. The skew index,
2. The nature of the skew (parallel or nonparallel skew),
3. The actual skew angle at the bearing lines, and
4. The framing arrangement of the cross-frames.

It is concluded that LGA is not applicable for the nonparallel skewed and splayed girder bridges considered in this study. This is believed to be related in part to the fact that the skew index and skew angles for these nonparallel skew and splayed girder bridges exceed the identified limits of applicability of the recommended LGA procedures for parallel skew bridges. Additional complications are introduced in the behavior of nonparallel skewed and splayed girder bridges that are difficult to capture by LGA. However, recommendations are provided to allow for application of the recommended LGA procedures to bridges having only minor deviations from parallel skew and/or constant width and/or parallel girders. More restrictive limits on the skew index and the skew angles would appear to be necessary to allow LGA for more severe nonparallel skew and splayed girder geometries.

A useful way to consider the LGA and design of parallel skewed bridges is to classify them broadly into three categories:

1. Bridges having a skew angle $\theta \leq 20°$ and contiguous cross-frame lines oriented parallel to the skew.
2. Bridges having skew index $I_s \leq 0.3$ and skew angle $\theta \leq 50°$ with cross-frames oriented normal to the girders. The bridges in this category may have a contiguous or a staggered cross-frame arrangement, or combinations thereof.
3. Bridges having skew index $0.3 < I_s \leq 0.40$ with a skew angle $\theta \leq 50°$, or $0.40 < I_s \leq 0.45$ with a skew angle $\theta \leq 30^o$, with cross-frames oriented normal to the girders. The bridges in this category may have a contiguous or staggered cross-frame arrangement or combinations thereof. Several multiplicative adjustment factors are required on a few of the LGA calculations for bridges that fall within this category.

For each category, the research has identified design guidance for the effective use of LGA to design bridges that meet the geometrical and structural limits of the category.

In conclusion, the synthesized results from this research provide detailed insights into the various structural attributes influencing the behavior of straight skewed I-girder bridges. Based on the understanding of the overall behavior, recommended guidelines for application of LGA to the design of skewed I-girder bridges have been developed.

6.2 Recommendations for Implementation

Given the findings from this research, it is apparent that LGA can be utilized as a sufficient tool for design of straight skewed I-girder bridges up to skew angles of 50^o and skew indices up to 0.45 subject to the above qualifications. Therefore, it is recommended that the FDOT (2019a) Structures Design Guidelines may be modified to extend the allowable use of LGA within these limits.

6.3 Recommendations for Future Research

The current research has shed light on numerous aspects pertaining to the design of straight skewed I-girder bridges that can benefit from further focused research studies. A number of the most important of these aspects are as follows:

- It is clear that equal dead load distribution to the girders is a poor approximation when it comes to line-type concentrated loads along the bridge length, such as barrier rails, walls, sidewalks, etc. It should be feasible to develop a reasonable simplified approximate analysis model for the distribution of these types of loads. Such a model can potentially extend the limits of LGA to a more complete range of situations, as long as the magnitudes of these loads are not large enough to require significantly different sizes and stiffnesses for the girders within the vicinity of these loads.

- It is clear that the AASHTO LRFD Article 4.2.2 LLDF procedures are not simple by the broadest stretch of the word when it comes to their application to practical steel I-girder bridge design, which involves the use of I-girders typically having non-prismatic (stepped) geometries along their length and continuous spans. Given that even the use of a minimal number of cross-frames with ample staggers and offsets would decrease the effective ratio K_g/Lt_s^3 (by the cross-frames providing some assistance to the transverse bending stiffness of

the bridge deck), possibly a simpler way of characterizing these relative stiffness effects can be devised that does not require such an elaborate amount of work for such a coarse approximation. For exterior girders, based on comparison to 3D FEA solutions, it is clear that the rigid cross-section analysis (RCA) may serve as an important minimum limit on the value of the LLDF for relatively narrow girder bridges. It may be possible to provide broad guidance that excludes the need for RCA for bridges beyond a certain minimum width. For exterior girders, it is clear that current usage of the lever rule for the consideration of single-lane loading often controls over the LLDF for multiple-lane cases. It should be possible to develop a coarse but better "lever rule-type" approximation that accounts for the influence of the continuity of the bridge deck over the top of the first interior girders. With the development of such a revised rule, the single-lane LLDF may be found to generally not govern relative to the multiple-lane LLDF when calculating the LLDF for the exterior girders (with the exception of narrow bridges governed by the RCA).

It is suggested that the appropriate mantra with respect to the potential improvement of the steel I-girder bridge LLDFs would be greater simplicity of design without any further significant sacrifices in conservatism. If accuracy can be improved somewhat for certain situations, that would be an additional benefit. However, the current AASHTO LRFD LLDF procedures already provide a significant improvement relative to traditional design.

- It would be useful to study the design and analysis of additional straight skewed I-girder bridges designed at the limits of the three categories recommended for LGA in this research. This would shed more light on nuances that may occur as the limits are approached, and provide further demonstration of the efficacy of the recommendations from this research. This would include further investigation of the impact of relatively minor estimated girder flange lateral bending stresses on the girder designs, and the impact of estimated cross-frame and diaphragm forces on cross-frame and diaphragm designs.

- Additional studies should be conducted to investigate and compare the cost and performance characteristics of staggered cross-frame arrangements versus the general system lean-on bracing design of cross-frames discussed in Section 2.3. It is commonly recognized that cross-frames are one of the most expensive components in a steel I-girder bridge on a dollar per pound basis for the fabricated and erected structure. Therefore, reducing the overall number of cross-frames within a given bridge design can be very beneficial to the competitiveness of steel I-girder bridges versus comparable bridge designs using other structural configurations and/or materials. Reducing the number of cross-frames has a direct impact on the speed of the steel fabrication and erection. Representative cost functions should be developed, in consultation with steel fabricators and erectors, to gage the cost of "Chord Only" (CO) cross-frames used extensively in lean-on designs versus welded single-piece cross-frames having diagonal members.

  The impact of staggered and lean-on cross-frame designs on the cost and performance should be considered more broadly than just skewed I-girder bridges. The investigations should be applied to straight non-skewed I-girder bridges as well. It appears that the use of contiguous cross-frames across the full bridge width is common practice for straight non-skewed steel I-girder bridges among many consultants and owners. Effective bracing against lateral torsional buckling can be achieved without the use of these extensive cross-frame systems.

Use of stagger patterns for the internal intermediate cross-frames in non-skewed or in skewed Category 1 bridges should yield similar benefits to those observed in this research for Category 2 and 3 bridges, i.e., reductions in cross-frame forces while at the same time using a smaller overall number of cross-frames. This is expected to be particularly true on wider bridges.

As discussed in Section 5.1.5, current stability bracing design guidance focusses fundamentally on idealized analysis models in which the first-order internal bracing forces are zero and the strength requirements are derived solely from second-order amplification of initial geometric imperfections. 3D FEA of straight skewed I-girder bridge systems shows clearly that significant first-order cross-frame and diaphragm forces exist within the cross-frame and diaphragm systems in general. Significant cross-frame forces can be induced by the interaction of the cross-frames with the composite bridge slab in final constructed conditions. Further research is needed to better understand the second-order amplification of the displacements and internal forces caused by skew and other effects in general bridge structural systems.

Application of structural optimization principles may be very beneficial to reducing the overall cost of cross-frames in both staggered and lean-on cross-frame system designs. For example, a number of published lean-on cross-frame system designs have used relatively small offsets relative to pier and abutment bearing lines. It is expected that the intermediate cross-frames having diagonals in these designs will "fight" with the bearing line cross-frames regarding the compatibility of deformations of the bridge structural system subjected to gravity loads. The use of larger minimum offsets in lean-on cross-frame system designs should be beneficial to these designs.

Speed of fabrication and erection may be the greatest factor in terms of cross-frame cost. Careful scrutiny of common cross-frame fabrication and connection details may be very beneficial in this regard. For instance TxDOT commonly employs a single erection bolt detail, followed by field welding, for their cross-frame to girder connections (Farris, 2018). This type of detail potentially can be very effective for straight skewed I-girder bridges.

The use of staggered and/or lean-on cross-frame system designs generally implies that the bridge deck is serving a greater role in distributing loads between the girders in the composite structure as well as in "connecting" the girders in the overall three-dimensional structural system in which the bridge deck can be conceptualized as a plate, or flat shell, with the steel girders, cross-frames and diaphragms serving as relatively large longitudinal and transverse stiffening ribs. Based on the 3D FEA studies conducted in this research, the additional structural demands on the deck by minimizing the number of cross-frames in the structural system is expected to be minor. However, a more thorough investigation of the structural demands on the bridge deck, and how those are influenced by the framing arrangement of the cross-frames and diaphragms would be worthwhile to ensure that all the bases are covered.

- The fatigue design demands on cross-frame members need to be better understood. As discussed in Section 5.5.11 of this report, NCHRP 12-113 (NCHRP, 2019) is a large multi-

year project that aims to provide greater clarity on the true fatigue design demands on these components.

- The cost savings gained by application of 3D FEA to I-girder bridges identified as being amenable for LGA should be better understood. Use of 3D FEA can result in less conservatism in terms of the application of LLDF for design of the girders, and the application of coarse conservative estimates for girder flange lateral bending stresses and cross-frame and diaphragm forces. However, it is commonly known that minor changes in plate and members sizes due to better resolution of the structural analysis often have a minor effect on the final bottom line in terms of structural cost. Speed and ease of the design, and speed and ease of the fabrication and construction are often more paramount to cost savings.

  It is anticipated that the benefits of design by 2D grid and/or plate eccentric beam models, compared to 3D FEA models, are becoming smaller and smaller as the sophistication of graphical user interfaces for design using 3D FEA models continues to improve. The inherent approximations associated with 2D grid and/or plate eccentric beam models, in some cases, may actually lead to a degradation in design performance (White et al., 2012). Therefore, a focus on the broader use of 3D FEA models, when refined analysis is performed, may be a more productive route in terms of overall advancement in the structural design of I-girder bridges with moderately complex or more highly complex geometries.

  Continuing improvements to 3D FEA design software should be pursued aggressively. Further improvement to user interfaces that allow for graphical comparison of girder and other component structural demands versus structural capacities is needed. Innovations in presenting the structural demands versus capacities for the various bridge design limit states from 3D FEA is needed to lessen the "black box" nature of the design checks, or the need for substantial processing to realize simple meaningful design checks, that often occurs with 3D FEA. Only with the further development of these software capabilities, combine with greater and greater computing horsepower, can 3D FEA actually compete with LGA on a basis of simplicity of the design.

- The extension of Category 1 type designs to skew angles larger than 20º should be considered, both with and without the use of continuous cross-frame framing arrangements. One of the considerations that may be a limiting factor on the skew angles with some traditional connection details to the girders is the fact that the fatigue performance of these details may degrade with increases in the skew angle. This consideration relates to the fatigue performance of transversely-welded versus longitudinally-welded attachments such as in Sections 4.1 and 6.1 of Table 6.6.1.2.3-1 of AASHTO (2017). The use of split-pipe stiffeners for the connection of skewed cross-frames, as investigated by Quadrato (2010), may be a very beneficial solution that avoids these issues. It is important to avoid bent-plate type details for intermediate cross-frames that may soften the cross-frame stiffnesses such that geometry control of the bridge is lost during construction.

- The limits of applicability of routine LGA procedures for nonparallel skew I-girder bridge design should be investigated in greater detail. Unfortunately, the range of geometries becomes wider with these designs. Therefore, this effort would likely require a substantial study. Furthermore, the limits of applicability of routine LGA procedures for bridges

involving girder splay, and unequal girder stiffness, should be investigated at greater resolution. The bridges studied in this research predominantly have girder stiffnesses that are equal or nearly equal.

- In all the 3D FEA studies conducted in this research, the bearings were assumed to be designed and detailed such that bearing horizontal forces are negligible under gravity loads. Particularly as skewed geometries become more severe, the design of bearing details to allow for minor lateral displacements under gravity loads (via tolerances, etc.) while providing for sufficient lateral restraint under extreme loads becomes more difficult. These aspects of the bearing design details, such as captured within AASHTO/NSBA (2004) need to be better understood.

REFERENCES

AASHTO (2002). *Standard Specifications for Highway Bridges*, 17th Edition, American Association of State Highway and Transportation Officials, Washington, D.C.

AASHTO/NSBA (2004). *Steel Bridge Bearing Design and Detailing Guidelines*, G9.1, AASHTO/NSBA Steel Bridge Collaboration, American Association of State Highway and Transportation Officials, Washington, D.C. and National Steel Bridge Alliance, Chicago, IL.

AASHTO (2015). *AASHTO LRFD Bridge Design Specifications*, 7th Edition with 2015 Interims, American Association of State Highway and Transportation Officials, Washington, DC.

AASHTO (2017). *AASHTO LRFD Bridge Design Specifications*, 8th Edition, American Association of State Highway and Transportation Officials, Washington, DC.

ANSYS (2019). ANSYS Structures, ANSYS Inc., Canonsburg, PA.

AWS (2019). *AWS D1.5 Bridge Welding Code*, American Welding Society.

CSi (2019). CSiBridge Version 21.0.2, Computers and Structures, Inc., Berkeley, CA.

Farris, J.F. (2018). "Lean-On Bracing for Steel I-Shaped Girders," AISC Live Webinar, American Institute of Steel Construction, Chicago, IL.

FDOT (2017). *Straight Steel I-Girder Bridges with Skew Index Approaching 0.3*, RFP-DOT-17/18-90350CA, Florida Department of Transportation, Tallahassee, FL.

FDOT (2018). "Simplified Method to Determine Girder Layover at Simply Supported Girder Ends," private communication from the project steering group, Florida Department of Transportation, Tallahassee, FL.

FDOT (2019a). "Structures Design Guidelines," *Structures Manual*, Volume 1, Florida Department of Transportation, Tallahassee, FL, January.

FDOT (2019b). *Standard Specifications for Road and Bridge Construction*, Florida Department of Transportation, Tallahassee, FL, July.

GDOT (2019). *Bridge and Structures Design Manual*, Georgia Department of Transportation, Atlanta, GA.

Grubb, M.A., Wilson, K.E., White, C.D, and Nickas, W.N. (2015). *Load and Resistance Factor Design (LRFD) for Highway Bridge Superstructures – Reference Manual*, NHI Course No. 130081, 130081A, and 130081B, Publication No. FHWA-NHI-15-047, National Highway Institute, Federal Highway Administration, 1,698 pp.

Grubb, M.A., Hall, D.H., Yadlosky, J.M., Wilson, K.E. and Volle, L.E. (2010). *Analysis and Design of Skewed and Curved Steel Bridges with LRFD – Reference Manual*, NHI Course No.

130095, Publication No. FHWA-NHI-10-087, National Highway Institute, Federal Highway Administration, 1,476 pp.

Gull, J.H. and Azizinamini, A., (2014a). *Steel Plate Girder Diaphragm and Cross Bracing Loads*, FDOT Contract No. BDK80-977-20 Final Report, Florida Department of Transportation, Tallahassee, FL.

Gull, J.H. and Azizinamini, A., (2014b). *Steel Framing Strategies for Highly Skewed Bridges to Reduce/Eliminate Distortion near Skewed Supports*, FDOT Contract No. BDK80-977-21 Final Report, Florida Department of Transportation, Tallahassee, FL.

Helwig, T.A. and Yura, J.A. (2015). "Bracing System Design," *Steel Bridge Design Handbook*, Publication No. FHWA-HIF-16-002 - Vol. 13, December. 91 pp.

IOWA DOT (2018). *LRFD Bridge Design Manual*, Iowa Department of Transportation, Ames, IA.

Kupricka, G., and Poellot, B. (1993). "Nuisance Stiffness," *Bridgeline*, HDR Engineering, Inc., 4(1), 3 pp.

NCHRP (2019). "Proposed Modification to AASHTO Cross-Frame Analysis and Design," National Cooperative Highway Research Program, Active Project, https://apps.trb.org/cmsfeed/TRBNetProjectDisplay.asp?ProjectID=4194, Accessed 12/31/19.

NSBA (2019). LRFD Simon, Version 10.3 (AASHTO 8th edition), National Steel Bridge Alliance, Chicago, IL.

NSBA (2016). *Skewed and Curved Steel I-Girder Bridge Fit*, NSBA Technical Subcommittee Fit Task Force, Guide Document, National Steel Bridge Alliance, Chicago, IL, November 2015.

ODOT (2007). *Bridge Design Manual*, Ohio Department of Transportation, Columbus, OH.

PennDOT (2015). *Design Manual*, Part 4, Pennsylvania Department of Transportation, Harrisburg, PA

Quadrato, C.E. (2010). *Stability of Skewed I-Shaped Girder Bridges using Bent Plate Connections*, Ph.D. dissertation, University of Texas at Austin, Austin, TX.

Romage, M.L. (2008). *Field Measurements on Lean-On-Bracing for Steel Girder Bridges with Skewed Supports*, M.S. thesis, University of Texas, Austin, TX.

Sanchez, T.A. (2011). *Influence of Bracing Systems on the Behavior of Steel Curved and/or Skewed I-Girder Bridges during Construction*, Ph.D. Dissertation, School of Civil and Environmental Engineering, Georgia Institute of Technology, Atlanta, GA, 335 pp.

Sumner, E.A., Rizkall, S., Fisher, S.T., Whisenhunt, T.W., Paoinchantara, N. (2006). *Development of a Simplified Procedure to Predict Dead Load Deflections of Skewed and Non-*

skewed Steel Plate Girder Bridges, NCSU-CFL Report No. RD-06-05, NCDOT Report No. FHWA/NC/2006-13, North Carolina DOT, Raleigh, NC.

Wang, L. and Helwig, T.A. (2008). "Stability Bracing Requirements for Steel Bridge Girders with Skewed Supports," *Journal of Bridge Engineering*, ASCE, 13(2), 149-157.

White, D.W., Coletti, D., Chavel, B.W., Sanchez, A., Ozgur, C., Jimenez Chong, J.M., Leon, R.T., Medlock, R.D., Cisneros, R.A., Galambos, T.V., Yadlosky, J.M., Gatti, W.J., and Kowatch, G.T. (2012). *Guidelines for Analytical Methods and Construction Engineering of Curved and Skewed Steel Girder Bridges*, NCHRP Report 725, Transportation Research Board, National Research Council, Washington, D.C.

White, D.W., Nguyen, T.V., Coletti, D.A., Chavel, B.W., Grubb, M.A., and Boring, C.G. (2015). *Guidelines for Reliable Fit-Up of Steel I-Girder Bridges*, NCHRP 20-07/Task 355, Transportation Research Board, National Research Council, Washington, D.C.

WisDOT (2019). "Chapter 24-Steel Girder Structures," *Bridge Manual*, Wisconsin Department of Transportation, Madison, WI.

Yura, J.A. (2001). "Fundamentals of Beam Bracing," *Engineering Journal*, AISC, 38(1), 11-26.

Zhou, C. (2006). *Utilizing Lean-On Cross-Frame Bracing for Steel Bridges*, Ph.D. dissertation, University of Houston, Houston, TX.

Zhou, J., Bennett, C., Matamoros, A., Li, J., (2017). *Skewed Steel Bridges, Part II: Cross-Frame and Connection Design to Ensure Brace Effectiveness*, Report No. K-TRAN: KU-13-7, Kansas Department of Transportation, Topeka, KS.

Zokaie, T., Osterkamp, T.A., Imbsen, R.A., (1991). *Distribution of Wheel Loads on Highway Bridges*, NCHRP Report 12-26, Transportation Research Board, National Research Council, Washington, D.C.

APPENDIX 1. DATA SUMMARY OF 57 SELECTED BRIDGES

Tables 60 to 63 summarize the cross-frame details of all bridges, in the order of increasing number of spans. Similarly, Tables 64 to 67 summarize the deck superstructure details of all bridges, and Tables 68 to 71 summarize the bearing details of all bridges in the order of increasing number of spans. Tables 72 to 75 show the span length-to-web depth, *L*/*D*, of the different bridges.

Table 60. Cross-frame details of simple-span bridges.

	Bearing Cross Frame			Intermediate Cross Frame			
Bridge	**Type**	**Connection to Girder**	**Remarks**	**Type**	**Connection to Girder**	**Remarks**	**Fit Condition**
F1	Inverted V	Skewed Connection Plate	Staggered	V	Perpendicular Connection Plate	Contiguous	Not Available
F2	Inverted V	Alternate Bent Connection Plate	Contiguous	V	Perpendicular Connection Plate	Contiguous	Total Dead Load Fit
F3	V	One side Skewed Connection Plate and other side Alternate Bent Connection Plate	Staggered	V	Perpendicular Connection Plate	Staggered	Total Dead Load Fit
F4	V	One side Skewed Connection Plate and other side Alternate Bent Connection Plate	Staggered	V	Perpendicular Connection Plate	Staggered	Total Dead Load Fit
F5	Inverted V	Alternate Bent Connection Plate	Contiguous (half width)	V	Perpendicular Connection Plate	Contiguous	Not Available
F6	Inverted V	Not Available	Contiguous (half width)	V	Not Available	Contiguous	Not Available
F7	Inverted V	Not Available	Contiguous (half width)	V	Not Available	Contiguous	Not Available
F8	Inverted V	Skewed Connection Plate	Staggered	V	Perpendicular Connection Plate	Contiguous	Not Available
F9	Welded Plate Girder Diaphragm	Skewed Connection Plate	Staggered	V	Perpendicular Connection Plate	Contiguous	Not Available
F10	Inverted V	Bent Gusset Plate	Contiguous (parallel to skew)	X	Bent Gusset Plate	Contiguous (parallel to skew)	Not Available
F11	Welded Plate Girder Diaphragm	Bent Gusset Plate	Contiguous (spanning into bearing cross frame)	Alternate Inverted V (No gusset plate)	Perpendicular Connection Plate	Contiguous	Not Available
F12	Alternate V (No gusset plate)	Skewed Connection Plate	Contiguous	Alternate V (No gusset plate)	Perpendicular Connection Plate	Contiguous	Not Available
F13	Alternate Inverted V (No gusset plate)	Skewed Connection Plate	Contiguous (half-width)	Alternate V (No gusset plate)	Perpendicular Connection Plate	Contiguous	Not Available
F14	Alternate V (No gusset plate)	Not Available	Contiguous	V	Perpendicular Connection Plate	Contiguous	Erected Fit

Table 60 (contd.). Cross-frame details of simple-span bridges.

	Bearing Cross Frame			Intermediate Cross Frame			
Bridge	**Type**	**Connection to Girder**	**Remarks**	**Type**	**Connection to Girder**	**Remarks**	**Fit Condition**
F15	Welded Plate Girder Diaphragm	Skewed Connection Plate	Contiguous	V	Perpendicular Connection Plate	Contiguous	Not Available
F16	Welded Plate Girder Diaphragm	Skewed Connection Plate	Contiguous	V	Perpendicular Connection Plate	Contiguous	Not Available
F17	Inverted V	Alternate Bent Connection Plate	Staggered	V	Perpendicular Connection Plate	Contiguous	Not Available
F18	Inverted V	Alternate Bent Connection Plate	Staggered	V	Perpendicular Connection Plate	Contiguous	Not Available
F19	Welded Plate Girder Diaphragm	Skewed Connection Plate	Contiguous (half-width)	V	Perpendicular Connection Plate	Contiguous	Not Available
F20	Welded Plate Girder Diaphragm	Skewed Connection Plate	Contiguous (half-width)	V	Perpendicular Connection Plate	Contiguous	Not Available
F21	V	One side Perpendicular Connection Plate and other side Alternate	Staggered	V	Perpendicular Connection Plate	Contiguous	Erected Fit
F22	V	One side Perpendicular Connection Plate and other side Alternate	Staggered	V	Perpendicular Connection Plate	Contiguous	Erected Fit
F23	Diaphragm MC Section	Alternate Bent Connection Plate	Staggered	Diaphragm MC Section	Perpendicular Connection Plate	Contiguous	Not Available
F24	Inverted V	Alternate Bent Connection Plate	Staggered	V	Perpendicular Connection Plate	Contiguous	Erected Fit
F25	Inverted V	Alternate Bent Connection Plate	Staggered	V	Perpendicular Connection Plate	Contiguous	Not Available
F26	Alternate Inverted V (No Gusset Plates)	Skewed Connection Plate	Contiguous	Alternate Inverted V (No Gusset	Perpendicular Connection Plate	Contiguous	Not Available

Table 61. Cross-frame details of two-span continuous bridges.

	Bearing Cross Frame			Intermediate Cross Frame			
Bridge	**Type**	**Connection to Girder**	**Remarks**	**Type**	**Connection to Girder**	**Remarks**	**Fit Condition**
F27	Inverted V	Bent Gusset Plate @ pier, Alternate Bent Connection Plate @ End Bents	Staggered	V	Perpendicular Connection Plate	Contiguous	Erected Fit
F28	Inverted V	Alternate Bent Connection Plate	Staggered	X	Perpendicular Connection Plate	Contiguous	Total Dead Load Fit
F29	Welded Plate Girder Diaphragm	Skewed Connection Plate	Contiguous	V	Perpendicular Connection Plate	Contiguous	Not Available
F30	Inverted V (only @ end bents), No cf along intermediate pier	Alternate Bent Connection Plate @ end bents, Perpendicular connection plate for intermediate cf framing into intermediate pier bearing line	Staggered near End Bents, Contiguous @ intemediate pier (Intermediate Cf framing into Bearing line @ intermediate pier)	Inverted V	Perpendicular Connection Plate	Contiguous	Not Available
F31	Inverted V (only @ end bents), No cf along intermediate pier	Alternate Bent Connection Plate @ end bents, Perpendicular connection plate for intermediate cf framing into intermediate pier bearing line	Contiguous (Intermediate Cf framing into Bearing line @ intermediate pier)	Inverted V	Perpendicular Connection Plate	Contiguous	Not Available
F32	Inverted V (only @ end bents), No cf along intermediate pier	Alternate Bent Connection Plate @ end bents, Perpendicular connection plate for intermediate cf framing into intermediate pier bearing line	Contiguous (Intermediate Cf framing into Bearing line @ intermediate pier)	Inverted V	Perpendicular Connection Plate	Contiguous	Not Available
F33	Inverted V (only @ end bents), No cf along intermediate pier	Skewed Connection Plate	Staggered	Inverted V	Perpendicular Connection Plate	Staggered	Not Available
F34	Not Available	Not Available	Contiguous	Not Available	Perpendicular Connection Plate	Contiguous	Not Available
F35	Eccentric V	Skewed Connection Plate	Contiguous (for half-width)	Alternate Eccentric V (without gusset plates), Alternate V between girders S3 & S4 (without	Perpendicular Connection Plate	Contiguous	Not Available
F36	Alternate V (No Gusset Plates)	Skewed Connection Plate	Contiguous	Alternate V (No Gusset Plates)	Perpendicular Connection Plate	Contiguous	Not Available
F37	Alternate V (No Gusset Plates)	Skewed Connection Plate	Contiguous	Alternate V (No Gusset Plates)	Perpendicular Connection Plate	Contiguous	Not Available
F38	Alternate V (No Gusset Plates)	Skewed Connection Plate	Contiguous	Alternate V (No Gusset Plates)	Perpendicular Connection Plate	Contiguous	Not Available
F39	Inverted V (2 cf framing into end bearing line)	Alternate Bent Connection Plate	Staggered	V	Perpendicular Connection Plate	Contiguous	Total Dead Load Fit
F40	Inverted V (2 cf framing into end bearing line)	Alternate Bent Connection Plate	Staggered	V	Perpendicular Connection Plate	Contiguous	Total Dead Load Fit

Table 61 (contd.). Cross-frame details of two-span continuous bridges.

	Bearing Cross Frame			Intermediate Cross Frame			
Bridge	**Type**	**Connection to Girder**	**Remarks**	**Type**	**Connection to Girder**	**Remarks**	**Fit Condition**
F41	Alternate V (No Gusset Plates)	Skewed Connection Plate	Contiguous	Alternate V (No Gusset Plates)	Perpendicular Connection Plate	Contiguous	Erected Fit
F42	Inverted V	Alternate Bent Connection Plate	Staggered	Alternate V (No Gusset Plates)	Perpendicular Connection Plate	Contiguous	Not Available
F43	Inverted V (only @ end bents), No cf along intermediate pier	Alternate Bent Connection Plate	Contiguous (Intermediate Cf framing into Bearing line @ both end abutments and intermediate pier)	Inverted V	Perpendicular Connection Plate	Contiguous	Erected Fit
F44	Not Available	Not Available	Staggered near End Abutments, Contiguous (Intermediate Cf framing into Bearing line @ intermediate pier)	V	Perpendicular Connection Plate	Contiguous	Total Dead Load Fit
F45	Welded Plate Girder Diaphragm	Alternate Bent Connection Plate	Staggered near End Abutments, Contiguous (Intermediate Cf framing into Bearing line @ intermediate pier)	Alternate V (No Gusset Plates)	Perpendicular Connection Plate	Contiguous	Not Available
F46	Alternate V (No Gusset Plates for Top Channel)	Not Available	Staggered near End Bents &@ intermediate pier	V	Perpendicular Connection Plate	Contiguous	Erected Fit
F47	Alternate V (No Gusset Plates for Top Channel)	Not Available	Staggered near End Bents &@ intermediate pier	V	Perpendicular Connection Plate	Contiguous	Erected Fit
F48	Alternate V (No gusset plate)	Bent Gusset Plate, intermediate cross-frame also connected on the same connection plate	Contiguous (Intermediate Cf framing into Bearing line @ intermediate pier from both side)	Alternate V (No gusset plate for the bottom chord)	Perpendicular Connection Plate	Contiguous	Not Available
F49	Inverted V	Alternate Bent Connection Plate	Contiguous	Alternate V (No Gusset Plates)	Perpendicular Connection Plate	Contiguous	Not Available
F50	Inverted V	Alternate Bent Connection Plate	Contiguous (half-width)	Alternate V (No Gusset Plates)	Perpendicular Connection Plate	Contiguous	Not Available
F51	Inverted V	Alternate Bent Connection Plate	Contiguous (half-width)	Alternate V (No Gusset Plates)	Perpendicular Connection Plate	Contiguous	Not Available
F52	Inverted V	Bent Gusset Plate	Contiguous (half-width)	V (Alternate V for closure pour)	Perpendicular Connection Plate	Contiguous	Not Available
F53	W Section Diaphragm	Skewed Connection Plate	Contiguous (parallel to skew)	Inverted V	Skewed Connection Plate	Contiguous (parallel to skew)	Not Available

Table 62. Cross-frame details of three-span continuous bridges.

	Bearing Cross Frame			Intermediate Cross Frame			
Bridge	**Type**	**Connection to Girder**	**Remarks**	**Type**	**Connection to Girder**	**Remarks**	**Fit Condition**
F54	Inverted V @ left end, Double Inverted V @ right end	Alternate Bent Connection Plate	Contiguous (for half-width), Intermediate Cf framing into Bearing line @ intermediate pier from both side	V	Perpendicular Connection Plate	Contiguous	Total Dead Load Fit
F55	V	Bent Web Plate	Staggered	Alternate V (No gusset plate)	Perpendicular Connection Plate	Contiguous	Not Available

Table 63. Cross-frame details of three-span continuous bridges.

	Bearing Cross Frame			Intermediate Cross Frame			
Bridge	**Type**	**Connection to Girder**	**Remarks**	**Type**	**Connection to Girder**	**Remarks**	**Fit Condition**
F56	V	Alternate Bent Connection Plate	Staggered	V	Perpendicular Connection Plate	Contiguous	Not Available
F57	Inverted V	Alternate Bent Connection Plate	Staggered	Inverted V	Perpendicular Connection Plate	Contiguous	Total Dead Load Fit

Table 64. Deck superstructure details of simple-span bridges.

Bridge	Grade of Concrete	Width of Deck	Structural Thickness	Type of Deck Form	Casting Sequence		Remarks
					# of Phases	# of Stages	
F1	4.5 ksi	71 ft 1 in	8 in	SIP Metal Deck	3	1	Replacement of an existing bridge, Each phase shall be completed in a single pour.
F2	4.5 ksi	30 ft 1 in	9 in	SIP Metal Deck	1	1	Deck Casting to start from the right end of the bridge, 9 in thick deck includes 0.5 in sacrificial thickness
F3	31 MPa	17.75 m	215 mm	Not Available	Not Available	Not Available	
F4	31 MPa	17.75 m	215 mm	Not Available	Not Available	Not Available	
F5	Not Available	Not Available	Not Available	Not Available	Not Available	Not Available	
F6	4.5 ksi	59 ft 1 in	9 in	Not Available	3 (including closure pour)	Not Available	
F7	4.5 ksi	59 ft 1 in	9 in	Not Available	3 (including closure pour)	Not Available	
F8	31 MPa	12.641 m	200 mm	SIP Metal Deck	Not Available	Not Available	
F9	4.5 ksi	123 ft 1 in	8 in	SIP Metal Deck	5 (including closure pours)	Not Available	Existing 2 bridges to be replaced by 1 single wide bridge
F10	4.5 ksi	135 ft 1 in	8.5 in	SIP Metal Deck	5 (including closure pours)	1	Existing 2 bridges to be replaced by 1 single wide bridge
F11	Not Available	43 ft 1 in	8.75 in	SIP Metal Deck	1	1	
F12	4.5 ksi	43 ft 1 in	8.5 in	SIP Metal Deck	Not Available	Not Available	Scope for future expansion
F13	31 MPa	35.160 m	200 mm	SIP Metal Deck	5 (including closure pours)	Not Available	Existing 2 bridges to be replaced by 1 single wide bridge

Table 64 (contd.). Deck superstructure details of simple-span bridges.

Bridge	Grade of Concrete	Width of Deck	Structural Thickness	Type of Deck Form	Casting Sequence		Remarks
					# of Phases	# of Stages	
F14	4.5 ksi	64 ft 8 in	9.25 in	SIP Metal Deck	Not Available	Not Available	
F15	4.5 ksi	43 ft 1 in	8 in	SIP Metal Deck	Not Available	Not Available	
F16	4.5 ksi	30 ft 1 in	8 in	SIP Metal Deck	Not Available	Not Available	
F17	4.5 ksi	43 ft 1 in	9 in	SIP Metal Deck	Not Available	Not Available	9 in thick deck includes 0.5 in sacrificial thickness
F18	4.5 ksi	43 ft 1 in	9 in	SIP Metal Deck	Not Available	Not Available	9 in thick deck includes 0.5 in sacrificial thickness
F19	31 MPa	19.3 m	200 mm	SIP Metal Deck	1	1	
F20	31 MPa	22.885 m	200 mm	SIP Metal Deck	3 (including closure pour)	1	
F21	31 MPa	12.95 m	210 mm	SIP Metal Deck	Not Available	Not Available	
F22	31 MPa	16.55 m	210 mm	SIP Metal Deck	Not Available	Not Available	
F23	31 MPa	16.772 m	8.5 in	SIP Metal Deck	1	1	
F24	Not Available	73 ft	8.5 in	SIP Metal Deck	1	1	Deck Casting to start from the right end of the bridge, maximum width reported for the splayed girder bridge
F25	Not Available	87 ft 1 in	8.5 in	SIP Metal Deck	1	2	Deck Casting from both ends of the bridge
F26	4.5 ksi	55 ft 1 in	8 in	SIP Metal Deck	Not Available	Not Available	

Table 65. Deck superstructure details of two-span continuous bridges.

Bridge	Grade of Concrete	Width of Deck	Structural Thickness	Type of Deck Form	Casting Sequence		Remarks
					# of Phases	# of Stages	
F27	4.5 ksi	91 ft 11 in	8.5 in	SIP Metal Deck	1	5	
F28	4.5 ksi	43 ft 1 in	8.5 in	SIP Metal Deck	1	3	
F29	Not Available	50 ft 2 in	9 in	SIP Metal Deck	1	1	Continuous concrete placement from left end abutment to right end abutment (revised)
F30	4.5 ksi	65 ft	8.5 in	SIP Metal Deck	1	3	
F31	4.5 ksi	59 ft	9 in	SIP Metal Deck	1	3	
F32	4.5 ksi	84 ft 2 in	9 in	SIP Metal Deck	1	3	
F33	4.5 ksi	101 ft 1 in	9 in	SIP Metal Deck	1	1	Deck to be cast all at once with no construction joint
F34	5.5 ksi	47 ft 1 in	8.5 in	SIP Metal Deck	1	3	
F35	31 MPa	27.66 m	200 mm	SIP Metal Deck	3 (including closure pour)	3	
F36	Not Available	30 ft 1 in	9 in	SIP Metal Deck	1	3	
F37	Not Available	55 ft 1 in	9 in	SIP Metal Deck	1	3	
F38	Not Available	51 ft 1 in	9 in	SIP Metal Deck	1	3	
F39	Not Available	71 ft 1 in	9 in	SIP Metal Deck	1	3	
F40	Not Available	59 ft 1 in	9 in	SIP Metal Deck	1	3	Deck thickness includes 0.5 in sacrificial thickness

Table 65 (contd.). Deck superstructure details of two-span continuous bridges.

Bridge	Grade of Concrete	Width of Deck	Structural Thickness	Type of Deck Form	Casting Sequence		Remarks
					# of Phases	# of Stages	
F41	4.5 ksi	35 ft 1 in	8.5 in	SIP Metal Deck	3 (including closure pour)	3	
F42	4.5 ksi	55 ft 3 in	8.5 in	SIP Metal Deck	3 (including closure pour)	3	
F43	4.5 ksi	43 ft 1 in	9 in	SIP Metal Deck	1	3	Deck pour transverse direction perpendicular to girders
F44	4.5 ksi	54 ft	8.5 in	SIP Metal Deck	Not Available	Not Available	
F45	4.5 ksi	37 ft 1 in	8.5 in	SIP Metal Deck	1	3	
F46	Not Available	56 ft 1 in	9 in	SIP Metal Deck	1	3	
F47	Not Available	67 ft 1 in	9 in	SIP Metal Deck	1	3	
F48	4.5 ksi	102 ft 1 in	9.5 in	SIP Metal Deck	1	5	
F49	31 MPa	9.05 m	200 mm	SIP Metal Deck	1	3	
F50	31 MPa	29.75 m	200 mm	SIP Metal Deck	3 (including closure pour)	3	
F51	31 MPa	9.05 m	200 mm	SIP Metal Deck	1	3	
F52	4.5 ksi	112 ft 2 in	8 in	SIP Metal Deck	5 (including closure pour)	2	Staged construction begins from the two ends of the bridge
F53	4.5 ksi	73 ft 1 in	8 in	SIP Metal Deck	Not Available	Not Available	

Table 66. Deck superstructure details of three-span continuous bridges.

Bridge	Grade of Concrete	Width of Deck	Structural Thickness	Type of Deck Form	Casting Sequence		Remarks
					# of Phases	# of Stages	
F54	4.5 ksi	42 ft 5.5 in	8.5 in	SIP Metal Deck	Not Available	Not Available	
F55	4.5 ksi	67 ft 1 in	8 in	SIP Metal Deck	1	5	2 pairs of stages identical

Table 67. Deck superstructure details of four-span continuous bridges.

Bridge	Grade of Concrete	Width of Deck	Structural Thickness	Type of Deck Form	Casting Sequence	
					# of Phases	# of Stages
F56	4.5 ksi	43 ft 1 in	9.5 in	SIP Metal Deck	1	7
F57	Not Available	18.35 m	220 mm	SIP Metal Deck	1	7

Table 68. Bearing details of simple-span bridges.

	Bearing Articulation			
Bridge	**Left End**	**Right End**	**Type of Bearing**	**Remarks**
F1	Expansion	Fixed	Elastomeric: Composite Neoprene Pads	Slotted Holes in Longitudinal direction at expansion end with seismic bars
F2	Fixed	Expansion	Elastomeric: Composite Neoprene Pads	Slotted Holes in Longitudinal direction at expansion end with anchor bolts
F3	Expansion	Fixed	Elastomeric: Composite Neoprene Pads	Slotted Holes in Longitudinal direction at expansion end with anchor bolts
F4	Fixed	Fixed	Elastomeric: Composite Neoprene Pads	Slotted Holes in Longitudinal direction at expansion end with anchor bolts
F5	Expansion	Fixed	Not Available	
F6	Expansion	Expansion	Not Available	
F7	Expansion	Expansion	Not Available	
F8	Fixed	Expansion	Elastomeric: Composite Neoprene Pads	Slotted Holes in Longitudinal direction at expansion end with anchor bolts
F9	Expansion	Fixed	Elastomeric: Composite Neoprene Pads	Slotted Holes in Longitudinal direction at expansion end with anchor bolts
F10	Expansion	Expansion	Elastomeric: Composite Neoprene Pads	Slotted Holes in Longitudinal direction at expansion end with anchor bolts
F11	Expansion	Expansion	Elastomeric: Composite Neoprene Pads	Slotted Holes in Longitudinal direction at expansion end with anchor bolts
F12	Expansion	Fixed	Elastomeric: Composite Neoprene Pads	Slotted Holes in Longitudinal direction at expansion end with anchor bolts
F13	Expansion	Fixed	Elastomeric: Composite Neoprene Pads	Slotted Holes in Longitudinal direction at expansion end with anchor bolts
F14	Expansion	Expansion	Elastomeric: Composite Neoprene Pads	Slotted Holes in Longitudinal direction at expansion end with anchor bolts

Table 68 (contd.). Bearing details of simple-span bridges.

	Bearing Articulation			
Bridge	**Left End**	**Right End**	**Type of Bearing**	**Remarks**
F15	Expansion	Fixed	Elastomeric: Composite Neoprene Pads	Slotted Holes in Longitudinal direction at expansion end with anchor bolts
F16	Fixed	Expansion	Elastomeric: Composite Neoprene Pads	Slotted Holes in Longitudinal direction at expansion end with anchor bolts
F17	Expansion	Expansion	Elastomeric: Composite Neoprene Pads	Slotted Holes in Longitudinal direction at expansion end with anchor bolts
F18	Expansion	Expansion	Elastomeric: Composite Neoprene Pads	Slotted Holes in Longitudinal direction at expansion end with anchor bolts
F19	Fixed	Expansion	Elastomeric: Composite Neoprene Pads	Slotted Holes in Longitudinal direction at expansion end with anchor bolts
F20	Fixed	Expansion	Elastomeric: Composite Neoprene Pads	Slotted Holes in Longitudinal direction at expansion end with anchor bolts
F21	Expansion	Expansion	Elastomeric: Composite Neoprene Pads	Slotted Holes in Longitudinal direction at expansion end with anchor bolts
F22	Expansion	Expansion	Elastomeric: Composite Neoprene Pads	Slotted Holes in Longitudinal direction at expansion end with anchor bolts
F23	Expansion	Fixed	Elastomeric: Composite Neoprene Pads	
F24	Expansion	Fixed	Elastomeric: Composite Neoprene Pads	Slotted Holes in Longitudinal direction at expansion end with anchor bolts
F25	Fixed	Expansion	Elastomeric: Composite Neoprene Pads	Slotted Holes in Longitudinal direction at expansion end with anchor bolts
F26	Fixed	Expansion	Elastomeric: Composite Neoprene Pads	Slotted Holes in Longitudinal direction at expansion end with anchor bolts

Table 69. Bearing details of two-span continuous bridges.

	Bearing Articulation				
Bridge	**Left End**	**Intermediate Pier**	**Right End**	**Type of Bearing**	**Remarks**
F27	Expansion	Fixed	Expansion	Elastomeric: Composite Neoprene Pads	Slotted Holes in Longitudinal direction (actual) at expansion end with anchor bolts
F28	Uni-directional Pot Bearing	Fixed Pot Bearing	Uni-directional Pot Bearing	Pot Bearing	Masonry Plate with Swedged Anchor Bolt
F29	Expansion	Fixed	Expansion	Elastomeric: Composite Neoprene Pads	Slotted Holes in Longitudinal direction at expansion end with anchor bolts
F30	Uni-directional Pot Bearing	Fixed Pot Bearing	Uni-directional Pot Bearing	Pot Bearing	Swedged anchor bolt with longitudinal slotted holes at end bents 1 & 3
F31	Uni-directional Pot Bearing	Fixed Pot Bearing	Uni-directional Pot Bearing	Pot Bearing	Swedged anchor bolt with longitudinal slotted holes at end bents 1 & 3
F32	Uni-directional Pot Bearing	Fixed Pot Bearing	Uni-directional Pot Bearing	Pot Bearing	Swedged anchor bolt with longitudinal slotted holes at end bents 1 & 3
F33	Uni-directional Pot Bearing	Fixed Pot Bearing	Uni-directional Pot Bearing	Pot Bearing	Swedged anchor bolts at 4 corners with longitudinal slotted holes at end bents 1 & 3
F34	Expansion	Fixed	Expansion	Not Available	
F35	Expansion	Fixed	Expansion	Elastomeric: Composite Neoprene Pads	Slotted Holes in Longitudinal direction at expansion end with anchor bolts
F36	Expansion	Fixed	Expansion	Elastomeric: Composite Neoprene Pads	Slotted Holes in Longitudinal direction at expansion end with swedged anchor rods
F37	Expansion	Fixed	Expansion	Elastomeric: Composite Neoprene Pads	Slotted Holes in Longitudinal direction at expansion end with swedged anchor rods
F38	Expansion	Fixed	Expansion	Elastomeric: Composite Neoprene Pads	Slotted Holes in Longitudinal direction at expansion end with swedged anchor rods
F39	Expansion	Fixed	Expansion	Elastomeric: Composite Neoprene Pads	Slotted Holes in Longitudinal direction at expansion end with swedged anchor rods
F40	Expansion	Fixed	Expansion	Elastomeric: Composite Neoprene Pads	Slotted Holes in Longitudinal direction at expansion end with swedged anchor rods

Table 69 (contd.). Bearing details of two-span continuous bridges.

	Bearing Articulation				
Bridge	**Left End**	**Right End**	**Type of Bearing**	**Remarks**	
F41	Expansion	Fixed	Expansion	Elastomeric: Composite Neoprene Pads	Slotted Holes in (actual) Longitudinal direction at expansion end with swedged anchor rods
F42	Expansion	Fixed	Expansion	Elastomeric: Composite Neoprene Pads	Slotted Holes in Longitudinal direction at expansion end with anchor bolts
F43	Expansion	Fixed	Expansion	Elastomeric: Composite Neoprene Pads	Slotted Holes in Longitudinal direction at expansion end with swedged anchor rods
F44	Expansion	Fixed	Expansion	Not Available	Not Available
F45	Expansion	Fixed	Expansion	Elastomeric: Composite Neoprene Pads	Slotted Holes in Longitudinal direction at expansion end with swedged anchor rods
F46	Expansion	Fixed	Expansion	Elastomeric: Composite Neoprene Pads	Slotted Holes in (actual) Longitudinal direction at expansion end with swedged anchor rods
F47	Expansion	Fixed	Expansion	Elastomeric: Composite Neoprene Pads	Slotted Holes in (actual) Longitudinal direction at expansion end with swedged anchor rods
F48	Expansion	Fixed	Expansion	Multirotational Pot Bearing	Swedge anchor bolt
F49	Expansion	Fixed	Expansion	Elastomeric: Composite Neoprene Pads	Not Available
F50	Expansion	Fixed	Expansion	Elastomeric: Composite Neoprene Pads	
F51	Expansion	Fixed	Expansion	Elastomeric: Composite Neoprene Pads	
F52	Expansion	Fixed	Expansion	Elastomeric: Composite Neoprene Pads	Slotted Holes in Longitudinal direction at expansion end with swedged anchor rods
F53	Expansion	Fixed	Expansion	Elastomeric: Composite Neoprene Pads	Slotted Holes in Longitudinal direction at expansion end with anchor bolts

Table 70. Bearing details of three-span continuous bridges.

	Bearing Articulation					
Bridge	**Left End**	**Left Intermediate**	**Right Intermediate**	**Right End**	**Type of Bearing**	**Remarks**
F54	Expansion	Expansion	Fixed	Expansion	Not Available	
F55	Expansion	Expansion	Expansion	Expansion	Elastomeric: Composite Neoprene Pads	Slotted Holes in Longitudinal direction at expansion end with swedge anchor bolts

Table 71. Bearing details of four-span continuous bridges.

	Bearing Articulation						
Bridge	**Left End**	**Left Intermediate**	**Center**	**Right Intermediate**	**Right End**	**Type of Bearing**	**Remarks**
F56	Expansion	Expansion	Fixed	Expansion	Expansion	Elastomeric: Composite Neoprene Pads	Slotted Holes in Longitudinal direction at expansion end with swedge anchor bolts
F57	Expansion	Expansion	Fixed	Expansion	Expansion	Elastomeric: Composite Neoprene Pads	Slotted Holes in Longitudinal direction at expansion end

Table 72. Maximum span length-to-web depth, *L*/*D*, for girders of simple-span bridges.

Bridge	Max L/D^*
F1	26.90
F2	27.82
F3	28.72
F4	30.26
F5	28.79
F6	29.41
F7	29.41
F8	27.13
F9	27.55
F10	28.34
F11	25.84
F12	24.30
F13	29.51
F14	24.36
F15	27.92
F16	27.52
F17	28.39
F18	25.47
F19	28.34
F20	28.34
F21	28.04
F22	28.04
F23	29.39
F24	30.08
F25	40.33
F26	25.76

* L is taken as the maximum span length between centerline of bearings

Table 73. Maximum span length-to-web depth, *L*/*D*, for girders of two-span continuous bridges.

Bridge	Max *L*/*D*
F27	29.04
F28	26.99
F29	27.07
F30	33.35
F31	32.50
F32	32.14
F33	28.79
F34	27.78
F35	30.29
F36	35.46
F37	35.46
F38	35.46
F39	33.68
F40	33.68
F41	36.16
F42	29.11
F43	26.19
F44	34.48
F45	24.68
F46	30.79
F47	30.55
F48	28.13
F49	31.11
F50	29.09
F51	28.54
F52	35.64
F53	32.32
F54	34.19
F55	30.43

* *L* is taken as the maximum span length between centerline of bearings

Table 74. Maximum span length-to-web depth, *L*/*D*, for girders of three-span continuous bridges.

Bridge	Max *L*/*D*
F54	34.19
F55	30.43

* *L* is taken as the maximum span length between centerline of bearings

Table 75. Maximum span length-to-web depth, *L*/*D*, for girders of four-span continuous bridges.

Bridge	Max *L*/*D*
F56	29.66
F57	28.31

* *L* is taken as the maximum span length between centerline of bearings

APPENDIX 2. SIMPLE-SPAN AND TWO-SPAN CONTINUOUS BRIDGES NOT SELECTED FOR FURTHER STUDY

This appendix shows the plan geometry of the bridges that were not selected for the parametric study.

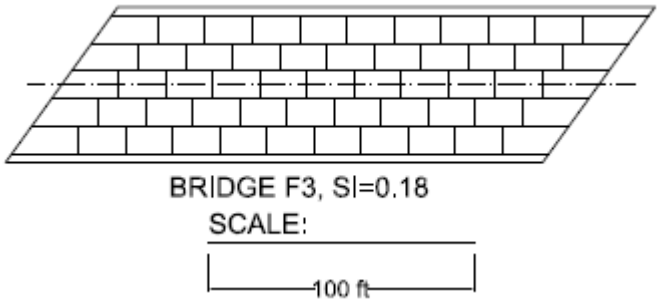

Figure 111. Other simple-span bridges with staggered cross-frame arrangement.

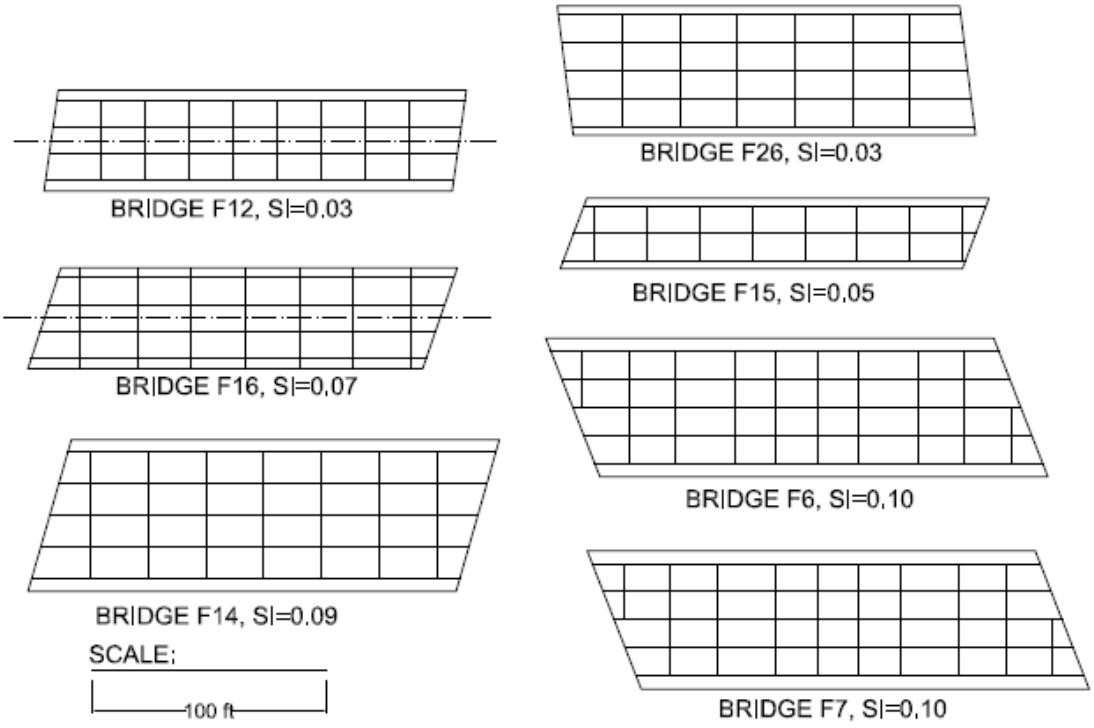

Figure 112. Other simple-span bridges with contiguous cross-frame arrangement.

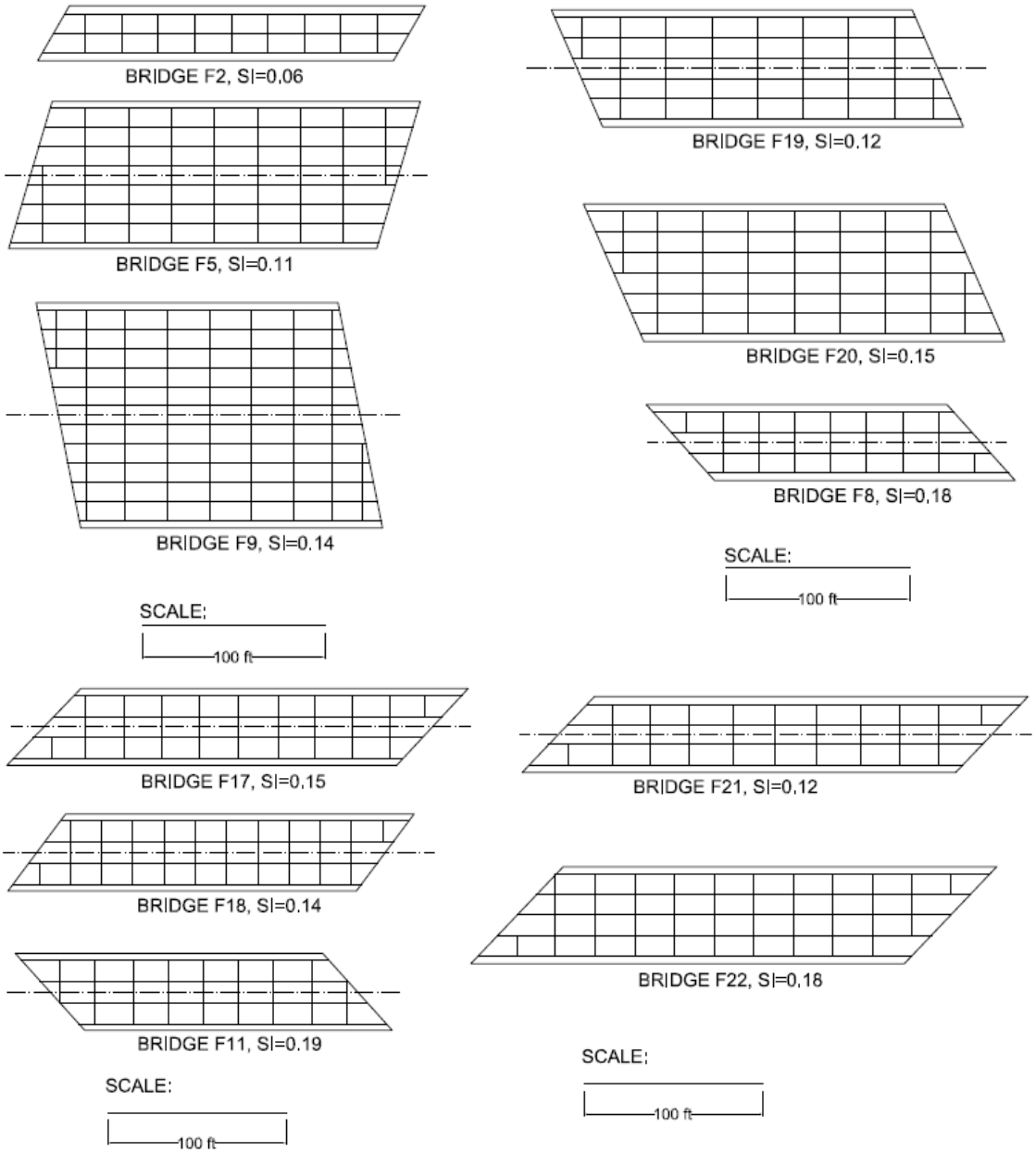

Figure 112 (contd.). Other simple-span bridges having contiguous cross-frame arrangement.

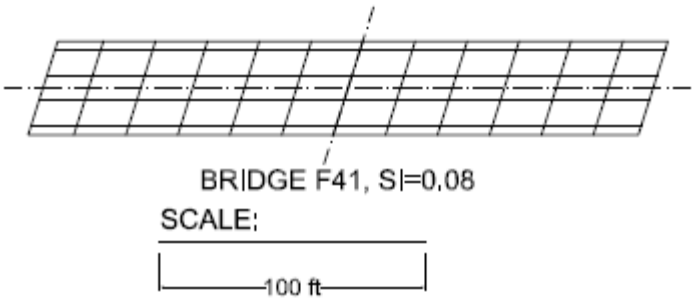

Figure 113. Other two-span continuous bridges having cross-frames parallel to skew.

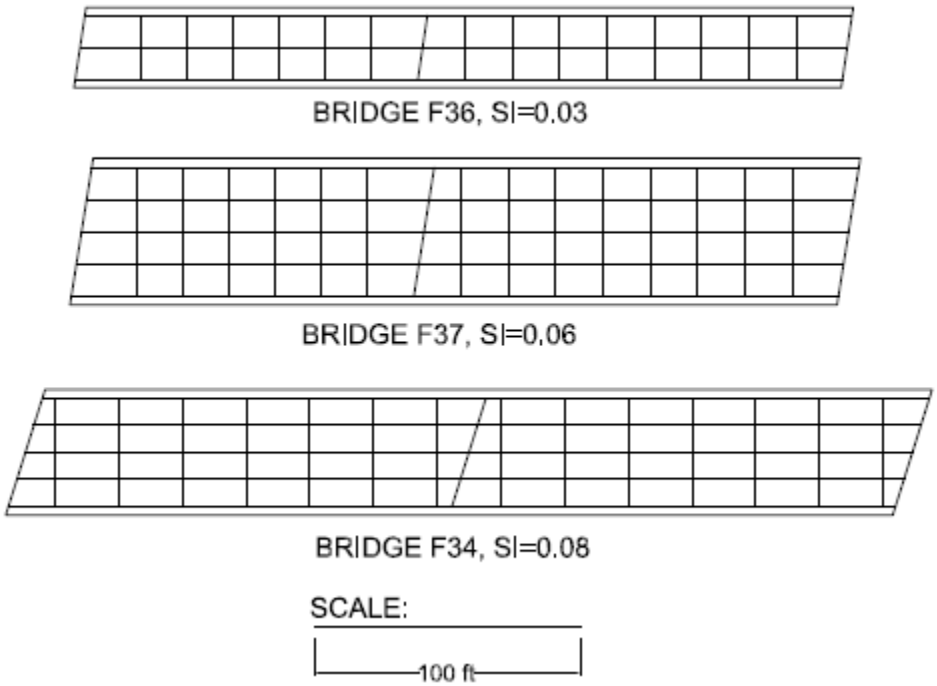

Figure 114. Other two-span continuous bridges having contiguous cross-frame arrangement.

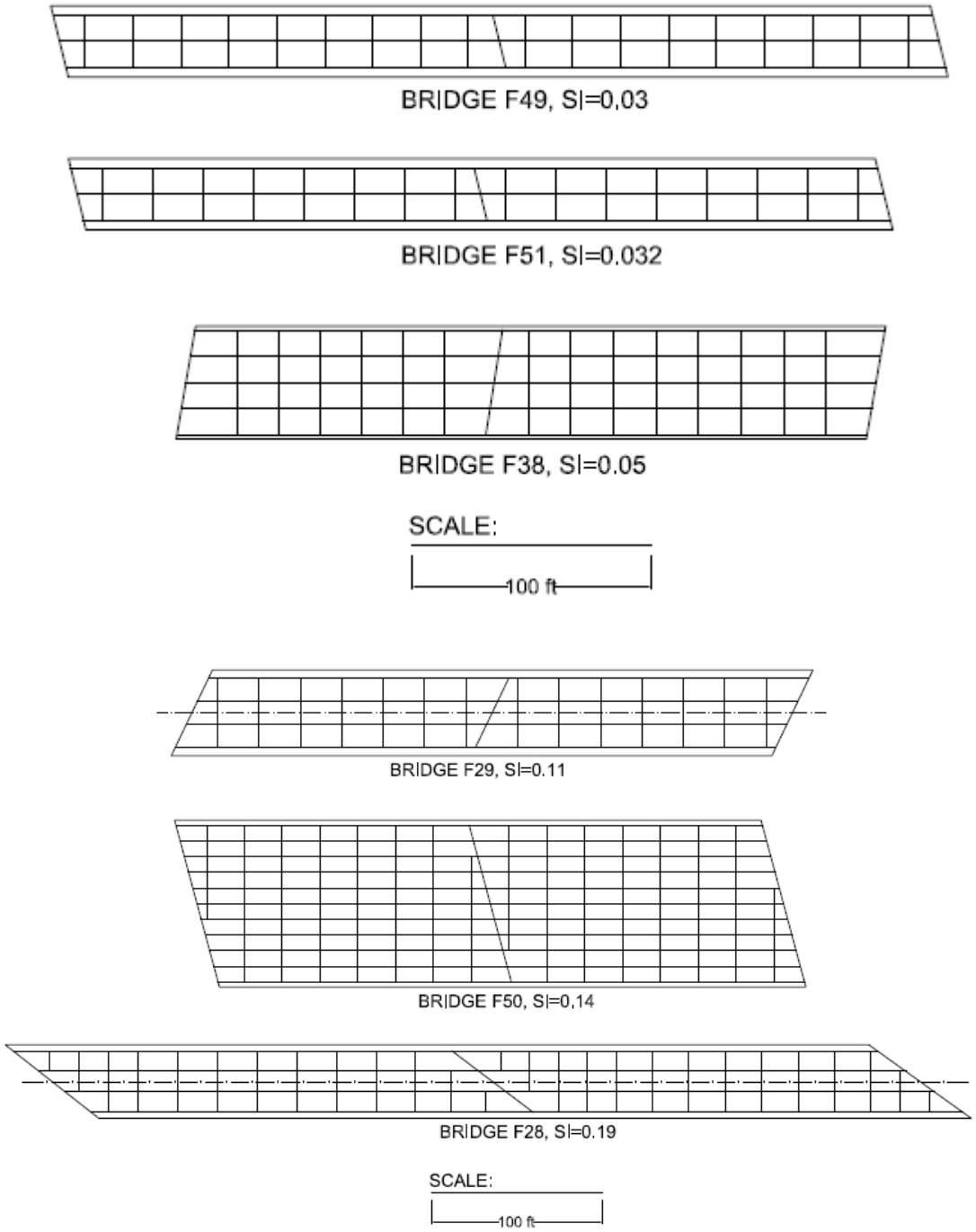

Figure 114 (contd.). Other two-span continuous bridges having contiguous cross-frame arrangement.

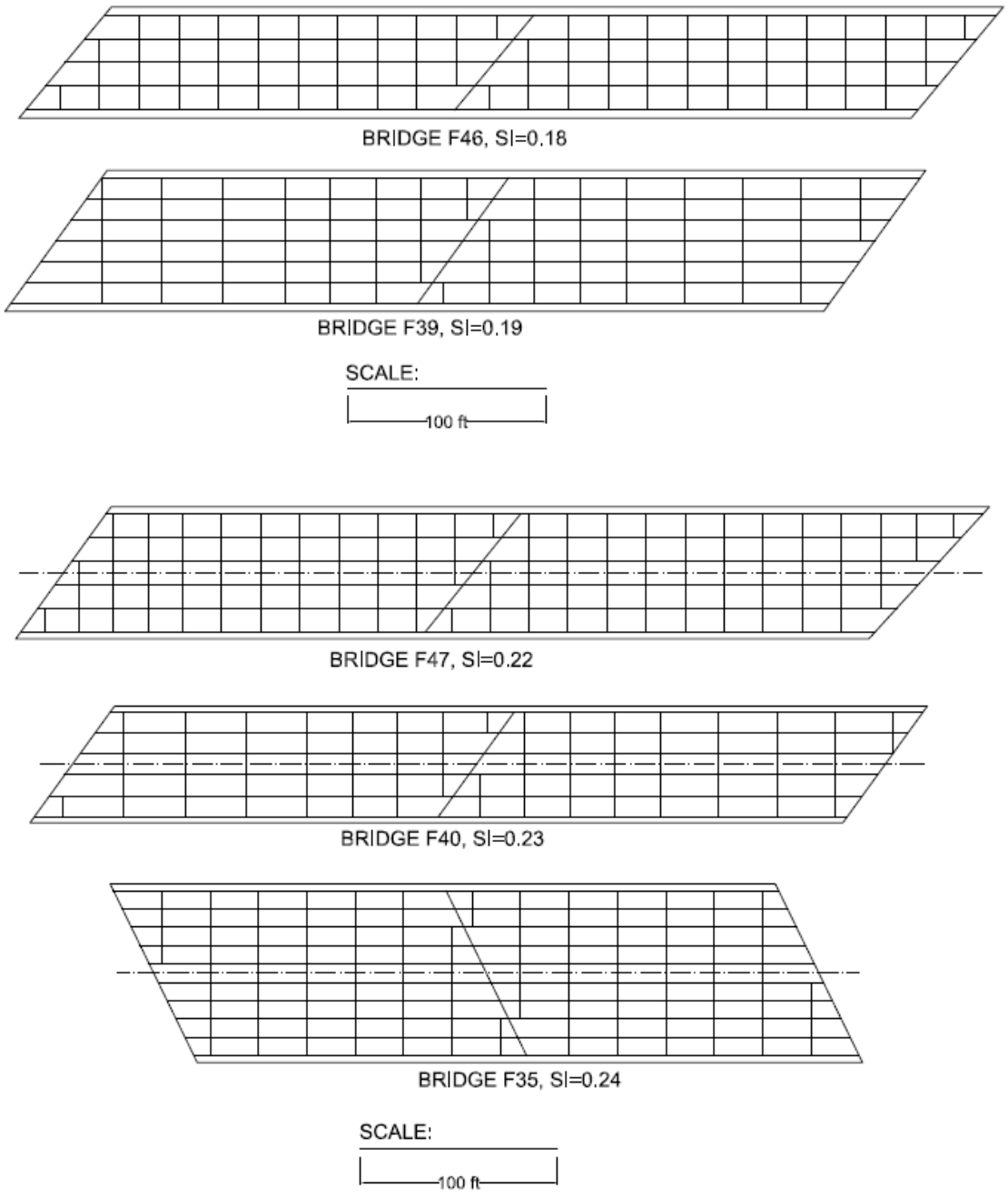

Figure 114 (contd.). Other two-span continuous bridges having contiguous cross-frame arrangement.